NATIONAL CENTER FOR EARTHQUAKE
ENGINEERING RESEARCH
State University of New York at Buffalo

Seismic Resistance of Reinforced Concrete Frame Structures Designed Only for Gravity Loads:

Part II — Experimental Performance of Subassemblages

by

L.E. Aycardi, J.B. Mander and A.M. Reinhorn
State University of New York at Buffalo
Department of Civil Engineering
Buffalo, New York 14260

Technical Report NCEER-92-0028

December 1, 1992

This research was conducted at the State University of New York at Buffalo and was partially supported by the National Science Foundation under Grant No. BCS 90-25010 and the New York State Science and Technology Foundation under Grant No. NEC-91029.

NOTICE

This report was prepared by the State University of New York at Buffalo as a result of research sponsored by the National Center for Earthquake Engineering Research (NCEER) through grants from the National Science Foundation, the New York State Science and Technology Foundation, and other sponsors. Neither NCEER, associates of NCEER, its sponsors, the State University of New York at Buffalo, nor any person acting on their behalf:

a. makes any warranty, express or implied, with respect to the use of any information, apparatus, method, or process disclosed in this report or that such use may not infringe upon privately owned rights; or

b. assumes any liabilities of whatsoever kind with respect to the use of, or the damage resulting from the use of, any information, apparatus, method or process disclosed in this report.

Any opinions, findings, and conclusions or recommendations expressed in this publication are those of the author(s) and do not necessarily reflect the views of the National Science Foundation, the New York State Science and Technology Foundation, or other sponsors.

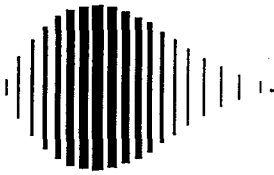

PB94-104510

Seismic Resistance of Reinforced Concrete Frame Structures Designed Only for Gravity Loads:

Part II - Experimental Performance of Subassemblages

by

L.E. Aycardi[1], J.B. Mander[2] and A.M. Reinhorn[3]

December 1, 1992

Technical Report NCEER-92-0028

NCEER Project Numbers 89-1001A, 90-1001A and 91-3111B

NSF Master Contract Number BCS 90-25010
and
NYSSTF Grant Number NEC-91029

1 Graduate Research Assistant, Department of Civil Engineering, State University of New York at Buffalo
2 Assistant Professor, Department of Civil Engineering, State University of New York at Buffalo
3 Professor, Department of Civil Engineering, State University of New York at Buffalo

NATIONAL CENTER FOR EARTHQUAKE ENGINEERING RESEARCH
State University of New York at Buffalo
Red Jacket Quadrangle, Buffalo, NY 14261

PREFACE

The National Center for Earthquake Engineering Research (NCEER) was established to expand and disseminate knowledge about earthquakes, improve earthquake-resistant design, and implement seismic hazard mitigation procedures to minimize loss of lives and property. The emphasis is on structures in the eastern and central United States and lifelines throughout the country that are found in zones of low, moderate, and high seismicity.

NCEER's research and implementation plan in years six through ten (1991-1996) comprises four interlocked elements, as shown in the figure below. Element I, Basic Research, is carried out to support projects in the Applied Research area. Element II, Applied Research, is the major focus of work for years six through ten. Element III, Demonstration Projects, have been planned to support Applied Research projects, and will be either case studies or regional studies. Element IV, Implementation, will result from activity in the four Applied Research projects, and from Demonstration Projects.

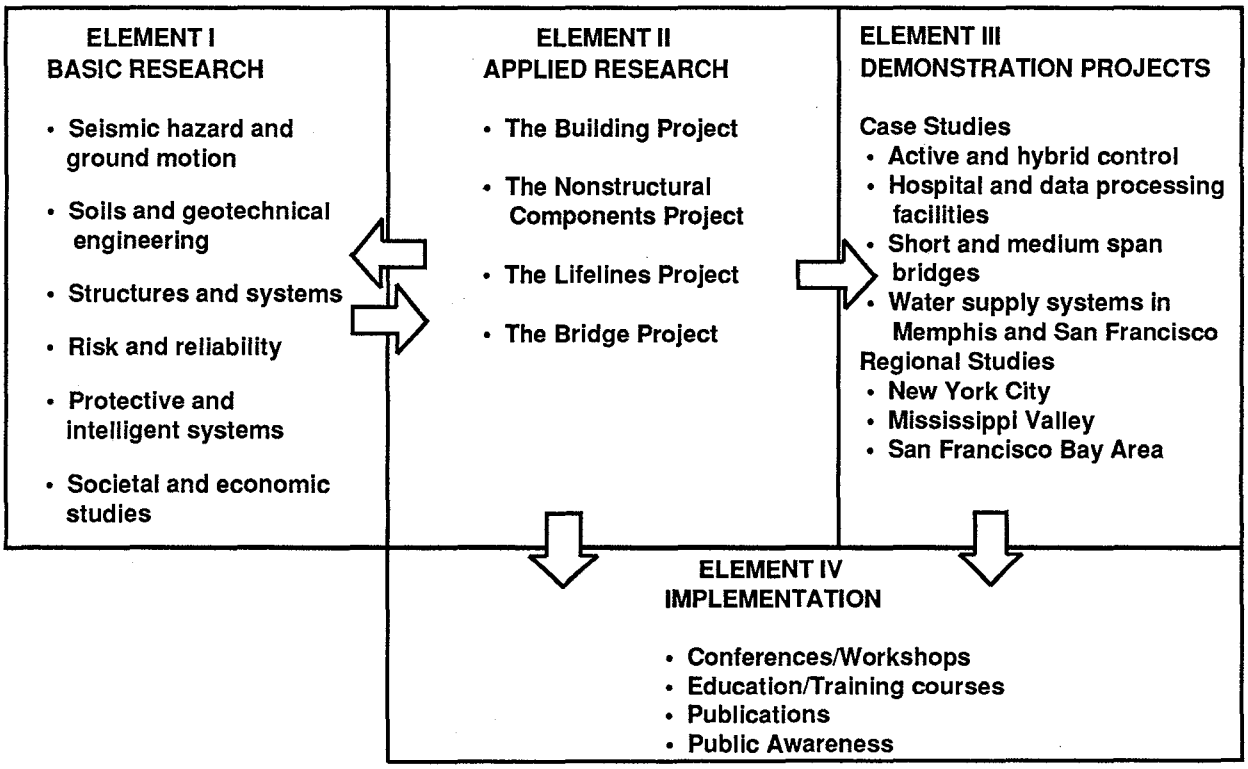

Research in the **Building Project** focuses on the evaluation and retrofit of buildings in regions of moderate seismicity. Emphasis is on lightly reinforced concrete buildings, steel semi-rigid frames, and masonry walls or infills. The research involves small- and medium-scale shake table tests and full-scale component tests at several institutions. In a parallel effort, analytical models and computer programs are being developed to aid in the prediction of the response of these buildings to various types of ground motion.

Two of the short-term products of the **Building Project** will be a monograph on the evaluation of lightly reinforced concrete buildings and a state-of-the-art report on unreinforced masonry.

The **structures and systems program** constitutes one of the important areas of research in the **Building Project**. Current tasks include the following:

1. Continued testing of lightly reinforced concrete external joints.
2. Continued development of analytical tools, such as system identification, idealization, and computer programs.
3. Perform parametric studies of building response.
4. Retrofit of lightly reinforced concrete frames, flat plates and unreinforced masonry.
5. Enhancement of the IDARC (inelastic damage analysis of reinforced concrete) computer program.
6. Research infilled frames, including the development of an experimental program, development of analytical models and response simulation.
7. Investigate the torsional response of symmetrical buildings.

One of the key accomplishments in the development of evaluation methods for existing buildings was the design and shake-table testing of three-story gravity-load designed buildings at the University at Buffalo and at Cornell University. These tests followed extensive preparatory full and reduced-scale component tests and the development of computer models.

This is the second in a series of three reports summarizing the test program at the University at Buffalo. It contains a detailed description of a series component and subassemblage tests that were used in the development of analytical models and in the study of detailing performance for the building model.

ABSTRACT

This report is Part II of a three part series on the *evaluation of seismic resistance of reinforced concrete frame structures designed only for gravity loads*. It is concerned with the experimental behavior of gravity load designed reinforced concrete columns and subassemblages under reversed cyclic lateral load.

This report presents the study of four column specimens (with and without lap splice), and two beam-column (exterior and interior) subassemblages of a one-third scale model of a prototype designed for gravity loads according to ACI 318 non-seismic detailing were subjected to axial load and cyclic lateral displacements. Part I of this evaluation series of reports presents the design of the prototype, model construction, shaking table testing program, and the experimental identification of structural characteristics from minor base motions. Finally, the experimental and analytical performance of the one-third scale model during moderate and severe ground motions is presented in Part III of this evaluation series.

Column failure was flexurally dominated, resulting either from buckling of the longitudinal steel or from low cycle fatigue of the longitudinal bars.

The exterior subassemblage experienced a weak beam-strong column failure mechanism whereas the interior subassemblage developed a weak column-strong beam mechanism. Thus a hybrid mechanism is likely to occur in a complete structural frame.

Conclusions are drawn regarding the appropriateness of hoop spacing in the columns, length and location of lap splices, joint reinforcement, equivalent plastic hinge lengths, and desirable failure mechanism for an entire frame.

The results presented in this report were used to identify member characteristics to develop analytical models to predict the seismic response of the one-third scale model building. The comparison between the experimental performance of the building and the predicted behavior using the results from component tests is presented in Part III of this evaluation report series.

ACKNOWLEDGEMENTS

This research was carried out at the Department of Civil Engineering at the State University of New York at Buffalo. Financial support is gratefully acknowledged from the National Center for Earthquake Engineering Research under contract numbers NCEER 89-1001A, 90-1001A, and 913111B.

The authors wish to thank Messrs. M. Pittman, P. Patarroyo, D. Walch, and R. Cizdziel for their assistance towards the construction and testing of the specimens.

TABLE OF CONTENTS

TABLE OF CONTENTS (Cont'd)

LIST OF ILLUSTRATIONS

LIST OF ILLUSTRATIONS (Cont'd)

LIST OF ILLUSTRATIONS (Cont'd)

LIST OF ILLUSTRATIONS (Cont'd)

LIST OF TABLES

SECTION 1

INTRODUCTION

1.1 Research Context

The study presented herein is part of a comprehensive research program sponsored by the National Center for Earthquake Engineering (NCEER) to assess seismic damage potential and evaluate the performance of buildings subjected to earthquakes in low to medium seismic zones, such as in the eastern and central United States. Buildings in these zones are typically designed only for gravity loads (U=1.4D+1.7L) according to the non-seismic detailing provisions of the code. These buildings are also referred to as lightly reinforced concrete (LRC) structures throughout this report. Although such structures are designed without consideration of lateral loads, they still possess an inherent lateral strength which may be capable of resisting some minor and moderate earthquakes. However, the deficient detailing of members can lead to inadequate structural performance during major seismic activity.

The research program, entitled **seismic performance of gravity load designed reinforced concrete frame buildings,** was developed and carried out according to the plan outlined in Fig. 1.1.

Based on a survey of typical building construction practices in the eastern and central United States (Lao 1990 and El-Attar et.al., 1991a and 1991b), a one-third scale model was constructed and tested on the shaking table in the State University of New York (SUNY) at Buffalo Earthquake Simulation Laboratory. The prototype design, model construction and similitude, initial dynamic characteristics, shaking table testing program along with the simulated ground motions, and the elastic response of the model from minor base motions are presented in Part I of the evaluation report series (Bracci et.al. 1992a). Based on that report analytical models were developed and used to predict the inelastic response of the model building during more severe earthquakes.

The present report presents the results of the experimental investigation of the companion columns and beam-column components of the one-third scale model building. The components were tested under quasi-static reversed cyclic loading and tests were conducted prior to testing of the model building. The results of the component tests were used to identify the behavior of

localized members and subassemblages of the structure and the member properties were used to predict the overall response of the model building with analytical tools.

The experimental and analytical performance of the model building during moderate and severe ground shaking is presented in Part III of the evaluation report series (Bracci et.al. 1992b). The analytical predictions of the model building during these earthquakes are presented based on member behavior developed from engineering approximations and component tests. Some of the conclusions of this study are that the response of the model is governed by weak column-strong beam behavior and large story drifts develop under moderate and severe earthquakes. A one-eighth scale model of the same prototype building was also constructed and tested at Cornell University by El-Attar et.al. (1991b) as part of a collaborative study with SUNY/Buffalo. A comparison of the response behavior between the two scale models is also presented in Part III of the evaluation report series (Bracci et.al. 1992b).

A continuing research program was conducted on various **seismic retrofit techniques for reinforced concrete frame structures** typically constructed in low seismicity zones. Based on the seismic behavior of the one-third scale model from the evaluation study, a series of retrofit schemes were proposed for improved seismic resistance and presented in Part II of the retrofit report series (Bracci et.al. 1992c). Retrofit using the concrete jacketing technique was selected and first performed on companion components as described in Part I of the retrofit report series (Choudhuri et.al. 1992). The retrofitted components were tested under quasi-static reversed cyclic loading and used to identify the behavior of the individual members. Retrofit of the components was also performed to verify the constructability of the retrofit technique for the model building.

In Part II of the retrofit report series by Bracci et.al. (1992c), the member properties from these component tests using the concrete jacketing technique were used to predict the response of the overall retrofitted model building with analytical tools. Based on analytical estimates, a global seismic retrofit for the one-third scale model building was proposed and constructed. An experimental and analytical shaking table study of the retrofitted model building was then conducted and the response behavior is presented. The main conclusions from this study are that seismic retrofit of gravity load designed R/C frame buildings: (i) can be designed to successfully enforce strong column-weak beam behavior; and (ii) is a viable economic and structural alternative as compared to demolition and reconstruction of another building.

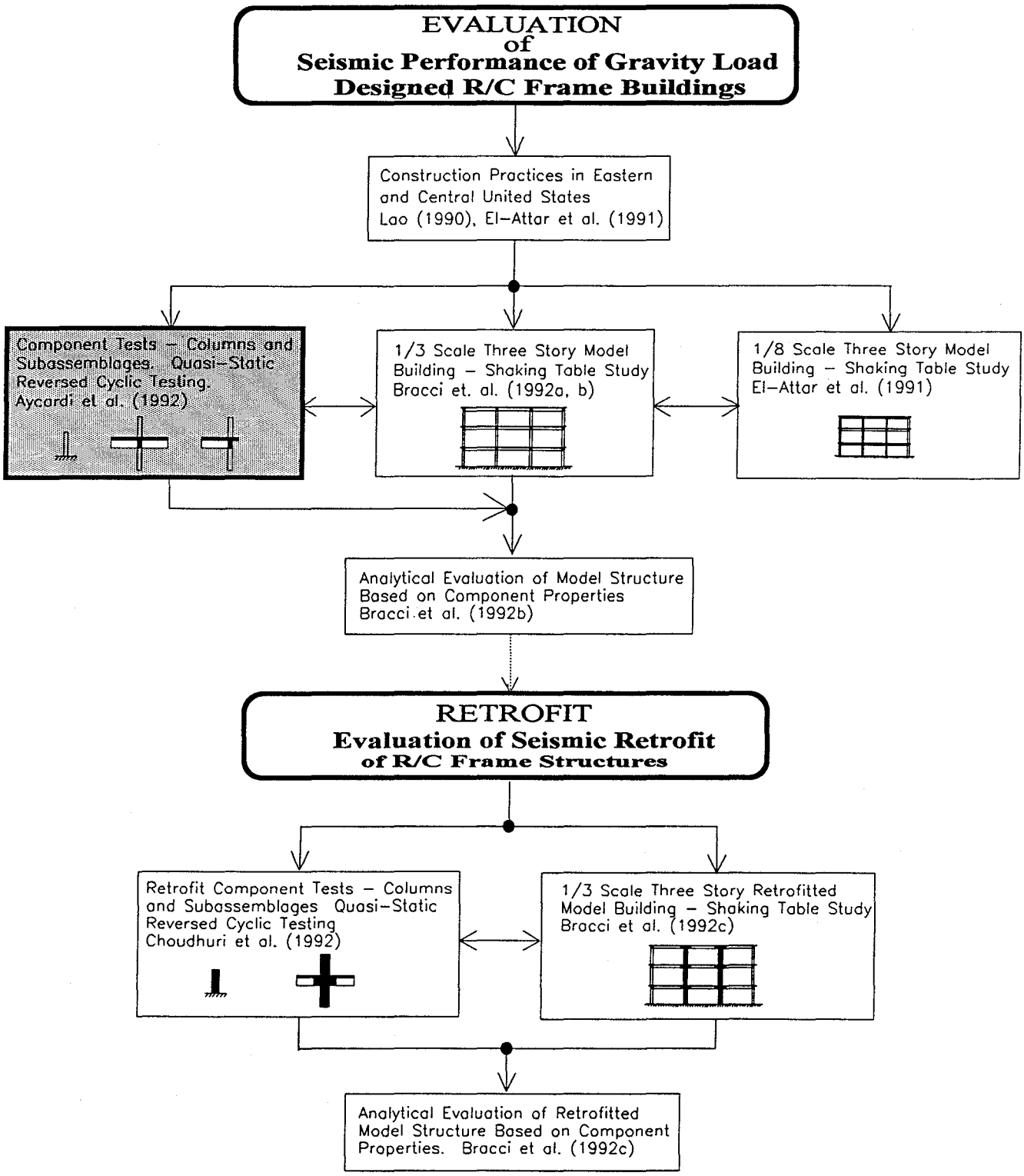

Fig. 1.1 Research Context - Seismic Performance of Gravity Load Designed Reinforced Concrete Buildings

1.2 Overall Objectives of Research Program

The objectives of the overall research program are summarized below along with the corresponding NCEER publications from Table 1.1:

1. Investigate the performance and principal deficiencies of typical LRC frame buildings during earthquakes through shaking table testing of a one-third scale model under minor, moderate, and severe earthquakes. (*Seismic Resistance of R/C Frame Structures Designed only for Gravity Loads: Parts I and III*, by J.M. Bracci, A.M. Reinhorn, and J.B. Mander)

2. Identify the potential collapse mechanisms for typical LRC frame buildings. (*Seismic Resistance of R/C Frame Structures Designed only for Gravity Loads: Part III*, by J.M. Bracci, A.M. Reinhorn, and J.B. Mander)

3. Determine the behavior and material properties of individual members and subassemblages of the structure. (*Seismic Resistance of R/C Frame Structures Designed only for Gravity Loads: Part II*, by L.E. Aycardi, J.B. Mander, and A.M. Reinhorn)

4. Determine the contribution of components in the overall response of the structure near collapse. (*Seismic Resistance of R/C Frame Structures Designed only for Gravity Loads: Parts II and III*, by J.M. Bracci, L.E. Aycardi, A.M. Reinhorn, and J.B. Mander)

5. Compare the measured response of the model building with that predicted by analytical models developed from engineering approximations or from component tests using a non-linear time history dynamic analysis. (*Seismic Resistance of R/C Frame Structures Designed only for Gravity Loads: Part III*, by J.M. Bracci, A.M. Reinhorn, and J.B. Mander)

6. Investigate appropriate local and global retrofit techniques for improving the seismic performance of LRC buildings. (*Evaluation of Seismic Retrofit of R/C Frame Structures: Part II*, by J.M. Bracci, A.M. Reinhorn, and J.B. Mander)

7. Investigate the seismic performance of the retroffited model building and compare the measured response with the response of the original (unretroffited) model for the same earthquakes. (*Evaluation of Seismic Retrofit of R/C Frame Structures: Part II*, by J.M. Bracci, A.M. Reinhorn, and J.B. Mander)

8. Determine the behavior and material properties of the retroffited members and subassemblages of the structure. (*Evaluation of Seismic Retrofit of R/C Frame Structures: Part I*, by D. Choudhuri, J.B. Mander, and A.M. Reinhorn)

9. Determine the contribution of retroffited and unretroffited components in the overall response of the structure near collapse. (*Evaluation of Seismic Retrofit of R/C Frame Structures: Part I*, by D. Choudhuri, J.B. Mander, and A.M. Reinhorn)

10. Compare the measured response of the retroffited model building with that predicted by analytical models developed from engineering approximations or from component tests using a non-linear time history dynamic analysis. (*Evaluation of Seismic Retrofit of R/C Frame Structures: Part II*, by J.M. Bracci, A.M. Reinhorn, and J.B. Mander)

1.3 Background

Seismic design for reinforced concrete structures relies on energy absorption and dissipation by inelastic deformations. Therefore, it is considered important to detail the structure for ductility in order to avoid brittle failure of structural members. A good design should not only give the minimum design strength but also take into consideration the behavior of the structure at deformations beyond the elastic region. The intrinsic lateral strength a structure possesses, based on gravity load design alone, may be sufficient to resist low to moderate earthquakes. However, the performance may not be satisfactory if the structure has been inappropriately detailed for the ductility demand. This report presents an experimental investigation on the behavior of column components and beam-column subassemblages of a one-third scale model of a prototype designed for gravity loads according to ACI 318 non-seismic detailing. Particular emphasis is paid to behavior in the post-elastic range and the adequacy of such performance in a seismic environment.

Table 1.1 NCEER Publications Summarizing Current Study

Evaluation Report Series

Seismic Resistance of R/C Frame Structures Designed only for Gravity Loads

Part I: Design and Properties of a One-third Scale Model Structure
(by J.M. Bracci, A.M. Reinhorn, and J.B. Mander), NCEER-92-0027

(i)	Identification of deficiencies of current engineering practice.
(ii)	Scale modeling.
(iii)	Experimental identification of structural characteristics.
(iv)	Ground motion for structural evaluation and experimental program.
Note:	This report serves as bare material for evaluation of analytical tools.

Part II: Experimental Performance of Subassemblages
(by L.E. Aycardi, J.B. Mander, and A.M. Reinhorn), NCEER-92-0028

(i)	Identify behavior and deficiencies of various components in structures.
(ii)	Identify member characteristics for developing analytical models to predict the seismic response of the one-third scale model structure.
Note:	This report serves as evaluation of structural characteristics to be incorporated in the evaluation of the entire structural system.

Part III: Experimental Performance and Analytical Study of Structural Model
(by J.M. Bracci, A.M. Reinhorn, and J.B. Mander), NCEER-92-0029

(i)	Investigate the performance and the principal deficiencies of typical gravity load designed frame buildings during earthquakes through shaking table testing of a one-third scale model under minor, moderate and severe earthquakes.
(ii)	Identify the potential collapse mechanisms for such typical frame buildings.
(iii)	Compare the measured response of the model building with that predicted by analytical models developed from (1) engineering approximations, (2) component tests, and (3) an experimental fit using a non-linear time history dynamic analysis.
Note:	This report emphasizes the structural behavior, collapse margins via damage, and efficiency of predictions using component properties evaluated from tests.

Retrofit Report Series

Evaluation of Seismic Retrofit of R/C Frame Structures

Part I: Experimental Performance of Retrofitted Subassemblages
(by D. Choudhuri, J.B. Mander, and A. M. Reinhorn), NCEER-92-0030

(i)	Presentation of retrofit techniques.
(ii)	Identify constructability and behavior of retrofitted components
(iii)	Identify retrofitted member characteristics for developing analytical models to predict seismic response of the retrofitted model building.

Part II: Experimental Performance and Analytical Study of Retrofitted Structural Model
(by J.M. Bracci, A.M. Reinhorn, and J.B. Mander), NCEER-92-0031

(i)	An analytical seismic evaluation of retrofitted gravity load designed frame buildings using various local and global retrofit techniques.
(ii)	Shaking table testing of one of the proposed retrofit techniques on the one-third scale model under minor, moderate and severe earthquakes.
(iii)	Verify a change in the formation of the potential collapse mechanism under ultimate load from an undesirable column-sidesway mechanism to a more desirable beam-sidesway mechanism.
(iv)	Compare the measured response of the retrofitted model building with that predicted by analytical models developed from engineering approximations and component tests using non-linear time-history dynamic analysis.

The remainder of Section 1 presents a description of the prototype and the one-third scale model buildings. The properties of the materials used in the construction of the model, components and subassemblages are described. Section 2 presents the testing of four column specimens under quasi static cyclic lateral loads. The specimens were taken as model replicas from the first story (ground floor) of the prototype structure. Testing of two beam-column subassemblages under cyclic lateral forces is given in Section 3. The subassemblages were selected as model duplicates from one interior and one exterior beam-column joint of the prototype building. In Section 4, a comparison between the analytical modeling and the experimental results of the four columns is presented. A computer program developed by Mander (1984) was used to model the behavior of the column specimens. Finally, the conclusions are presented in Section 5.

1.4 The Prototype and the Model

The prototype was a three story moment resisting reinforced concrete frame building with typical office loads, considered to be representative of a type of structure designed primarily for gravity loads (1.4D+1.7L). The structural form of the prototype was selected such that the one-third scale model could be built and tested on the SUNY at Buffalo shaking table as part of a companion study. Details of the design of the prototype are presented in Part I of the evaluation report series (Bracci et.al. 1992a). The dimensions and layout of the prototype are shown in Fig. 1.2.

The specified material strengths used for the design of the prototype were Grade 40 steel (f_y =40 ksi) and ordinary Portland cement concrete (f'_c =3.5 ksi). Although, Grade 60 steel is commonly used nowadays in construction, Grade 40 was adopted due to its historical use in older buildings. Furthermore, all materials used for the construction of the model building were chosen to be representative of those currently used in the United States for concrete structures. The prototype was designed for a slab load including self weight and imposed dead load from partitions, etc, of D=110 psf and L=50 psf.

The one-third scale model building represented the interior transverse frames 1 and 2 of the prototype as shown in Fig. 1.2. The geometry of the model building is presented in Fig. 1.3.

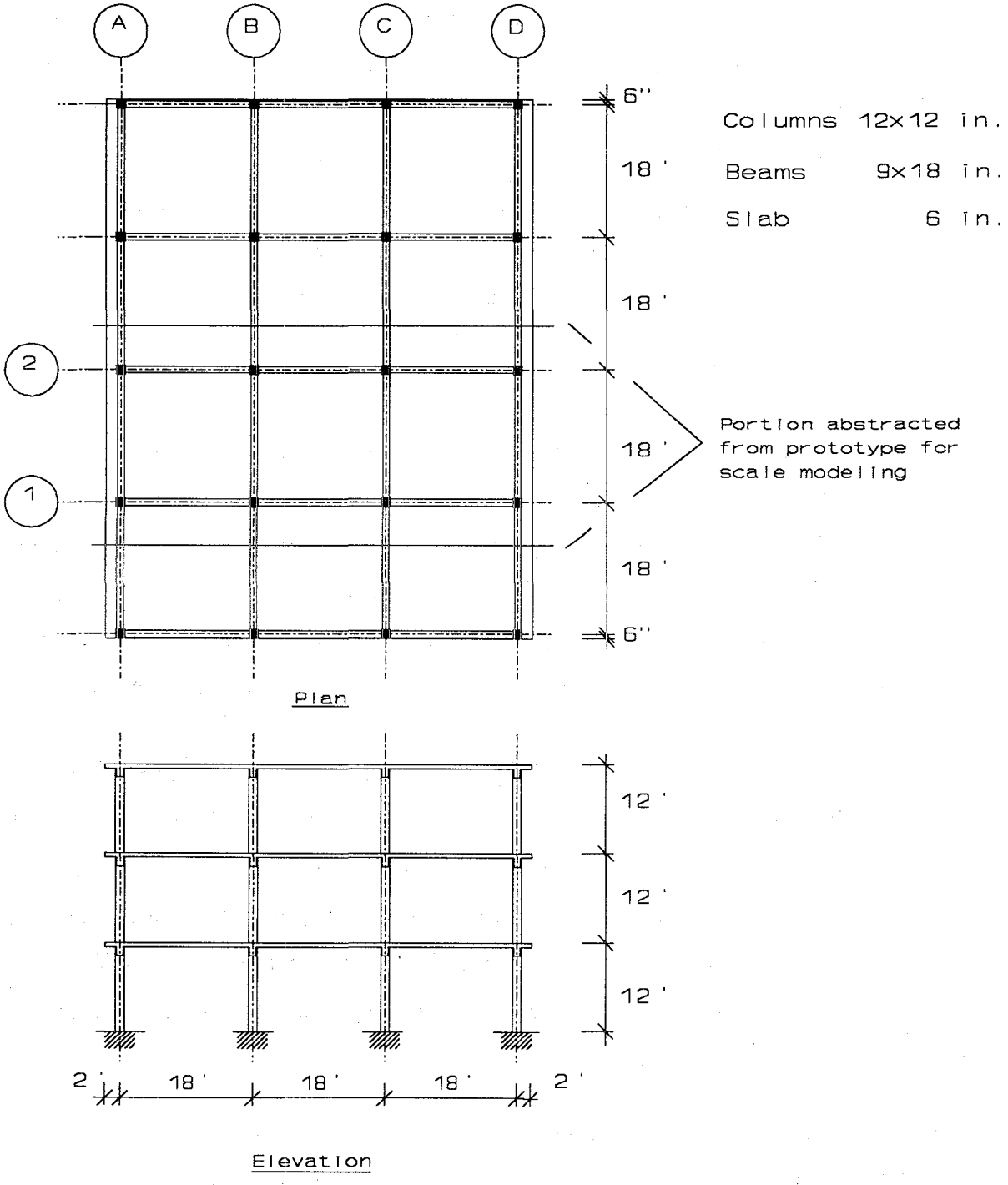

Fig. 1.2 Prototype Dimensions and Layout

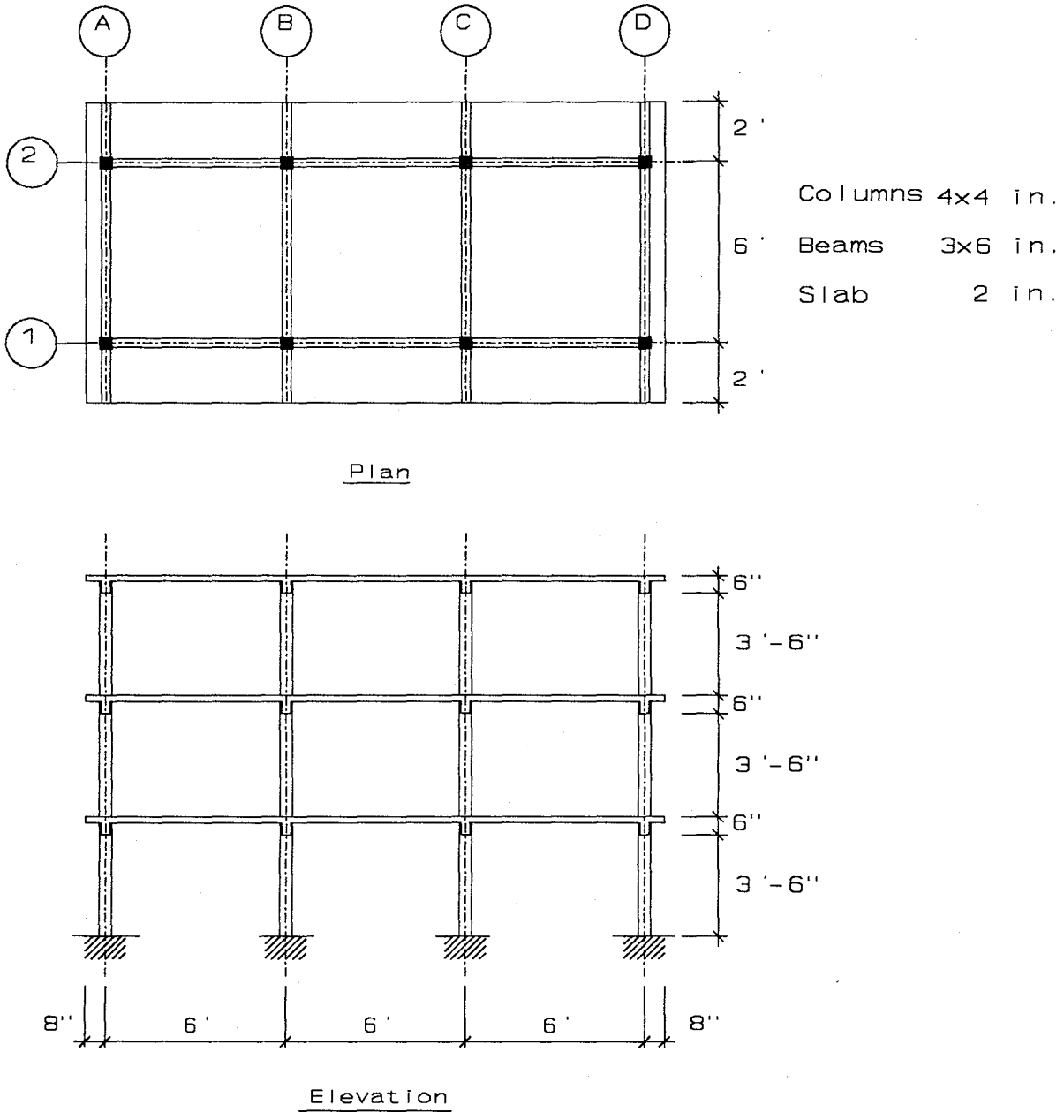

Fig. 1.3 Model Dimensions and Layout

1.5 Column and Beam-Column Subassemblage Specimens

The current design philosophy requires a ductile failure mechanism form when the structure's lateral strength capacity has been attained. Three possible failure scenarios may be considered for structural frames as shown in Fig. 1.4:

a. Column Sidesway mechanism.
b. Beam Sidesway mechanism.
c. Hybrid mechanism.

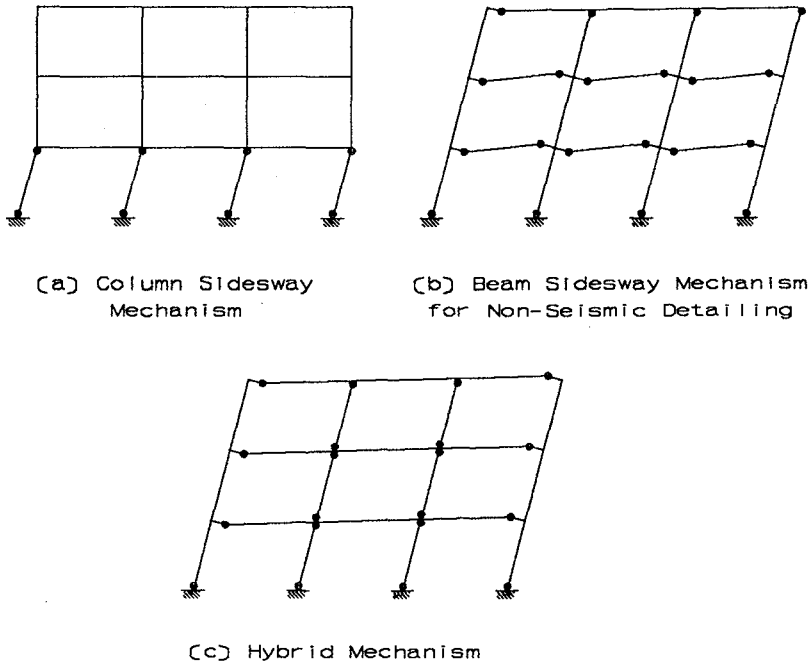

Fig. 1.4 Frame Failure Mechanisms

The column sidesway or soft story mechanism, which is common for strong beam-weak column systems, led to the choice of testing four column specimens from the first story. The beam sidesway mechanism, which is typical of strong column-weak beam structures, and the hybrid mechanism, which can occur in systems with strong exterior column-weak beam and weak interior column-strong beam, showed the need to test two different beam-column joint subassemblages at the first floor level. Results of the experiments should show whether mechanism (a), (b), or (c) is likely to occur.

The column specimens were built in two groups of two columns each. The first group (Specimens 1 and 3) represented the lower half and the second group (Specimens 2 and 4) the upper half of the first story columns of the model building. Identification of different specimens is made in Fig. 1.5.

The beam-column subassemblages were intended to represent one interior and one exterior joint connection of the first story of the model building as shown in Fig. 1.5.

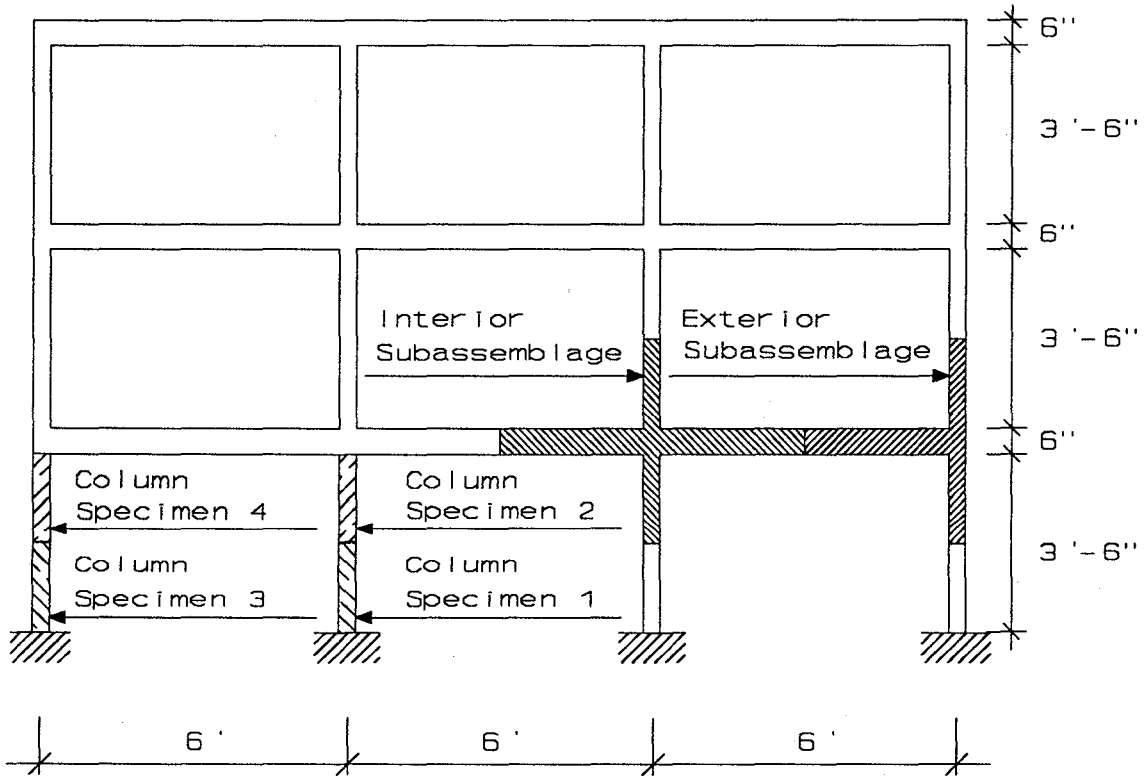

Fig. 1.5 Identification of Column Specimens and Beam-Column Subassemblages

1.5.1 Materials

All the specimens were built simultaneously with the one-third scale model building using the same constituent materials for the column and the beam-column subassemblage specimens and the building.

The concrete was specified to have a target strength of 3.5 ksi, a coarse aggregate type #1 crushed stone, and a slump of 4". The concrete was mixed in place except the slab and beam concrete which was provided by a local ready-mix supplier. In all cases the mix proportions by weight were

Water	:	Cement	:	Aggregate (fine + coarse)
0.47	:	1	:	6.83 (3.19 + 3.64)

A water reducer (1160 ml/yd^3) and an air entraining agent (86 ml/yd^3) were also added to the mix. For every pour, approximately 21 cylinders 8 x 4 in. diameter were cast to determine the compression strength (f_c') at 28 days as well as strength gain and stress-strain curves. Results of cylinder tests are presented in Fig. 1.6.

The steel used to reinforce the specimens can be divided in two groups:

1. Annealed steel: deformed rebars designated D4 (d_b=0.225 in, A_b=0.04 in^2) and D5 (d_b=0.252 in, A_b=0.05 in^2) which were annealed for a total of three hours at 1140°F to give yield strengths of f_y =68 and 38 ksi, respectively.

2. Regular steel: #2 round and #3 deformed rebars (f_y =40 ksi), plain round #11 gage wire (f_y =56 ksi), and galvanized wire #12 gage (f_y =58 ksi).

Results of coupon tests of the wires, D4 and D5 rebars are presented in Fig. 1.7.
Details about heat treatment (annealing) of the steel can be found in Part I (Bracci et.al. 1992a).

Concrete Pour	f'_{co} (ksi)	ε_{co}	E_c (ksi)	ε_{spall}
Lower Column 1st. Story	3.40	0.0023	2920	0.015
Upper Column 1st. Story	4.35	0.0023	3900	0.020
Beams Slab	5.00	0.0021	3900	0.009
Lower Column 2nd. Story	4.35	0.0026	3900	0.014

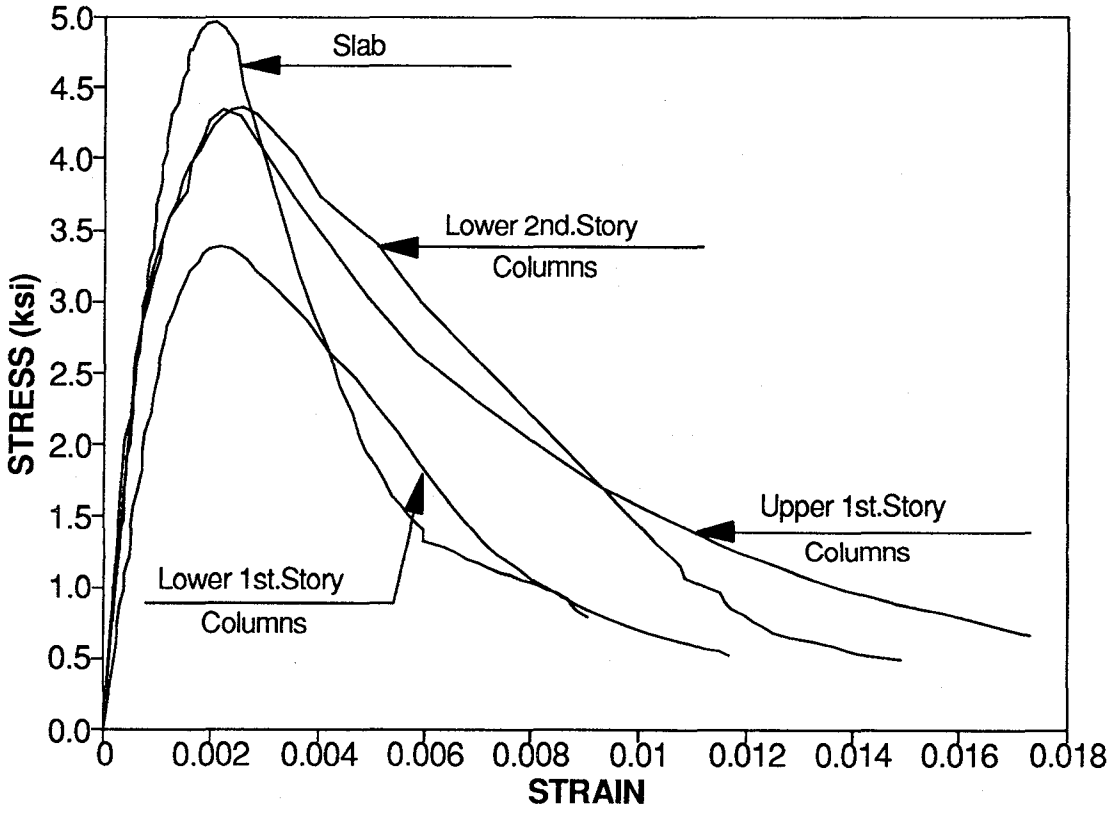

Fig. 1.6 Concrete Properties

Steel Type	f_y (ksi)	E_s (ksi)	ε_{sh}	E_{sh} (ksi)	f_{su} (ksi)	ε_{su}	ε_{sf}
D4	65	31050	0.026	750	73	0.107	0.15
D5	38	31050	0.027	950	54	0.142	-
#11 Gage	56	29800	0.014	450	70	0.140	-
#12 Gage	58	29900	-	-	64	0.081	0.13

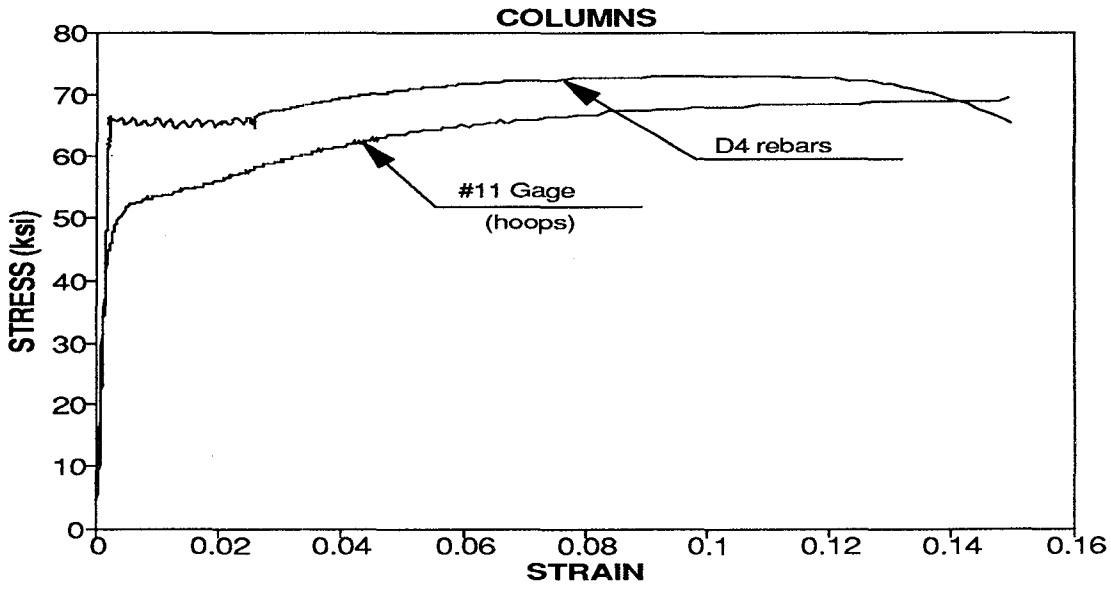

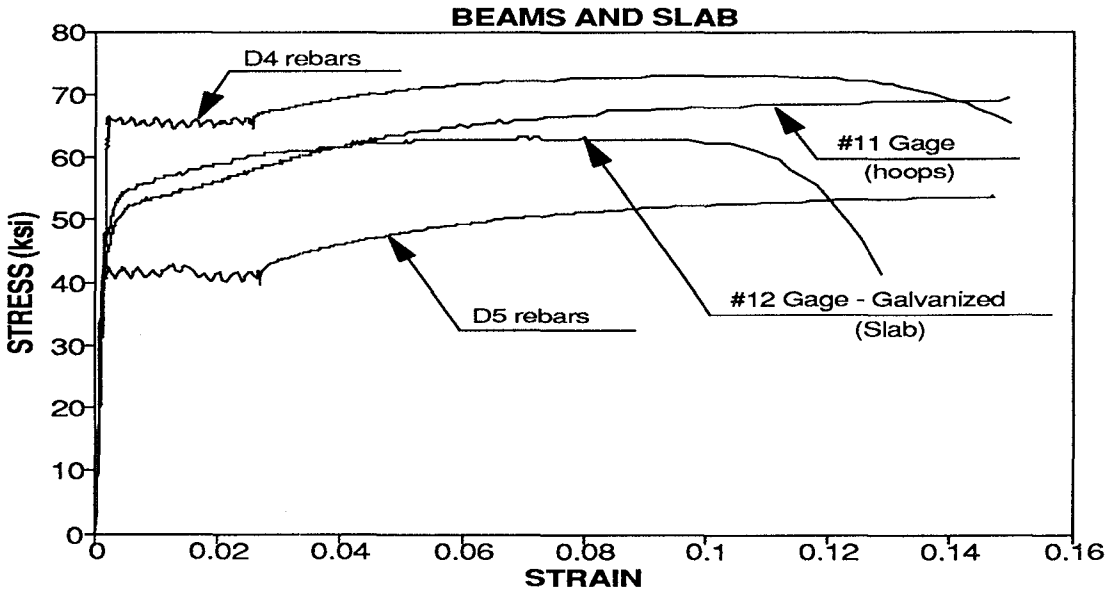

Fig. 1.7 Reinforcement Steel Properties

SECTION 2

EXPERIMENTAL BEHAVIOR OF NON-SEISMICALLY DESIGNED COLUMNS

2.1 Introduction

In this section, an experimental study of gravity load designed columns subjected to reversed cyclic lateral forces is presented. The design, construction, instrumentation, and testing of four square column specimens are described. The specimens were taken as components of the three story model building columns and constructed at the same time with the same constituent materials as described in Section 1. Details of the design of the model building are presented in Part I of the evaluation report series (Bracci et.al. 1992a).

Each column specimen was 28 in. tall, and had a 4 in. square cross section, containing 4 longitudinal bars. All column specimens were loaded 21 in. above the base, representing the approximate point of contraflexure for an expected soft story mechanism. Specimens 1 and 2 were subjected to a constant level of axial load representing the gravity load in the lower story. Specimens 3 and 4 were subjected to an axial load which varied throughout testing representing the fluctuating level of axial force due to lateral load reversals in an exterior column of a frame. All the specimens were subjected to cyclic inelastic lateral displacements of increasing amplitude which were representative of severe seismic loading.

2.2 Design and Construction of the Test Specimens

2.2.1 Reinforcement

Four 0.225 in. diameter deformed rebars (designated D4 with area A_b=0.04 in^2) were used to longitudinally reinforce each column specimen giving a volumetric ratio of 0.01. The results of coupon tests are given in Section 1.3. Specimens 1 and 3 had 6 in. lap splices at the base level, while specimens 2 and 4 had the longitudinal steel bars entering 6 in. into the base as shown in Fig. 2.2. The upper part of the column specimen was reinforced with an extra four longitudinal D4 rebars as well as additional hoops in order to prevent local failure due to the concentration of stresses from the application of the loads.

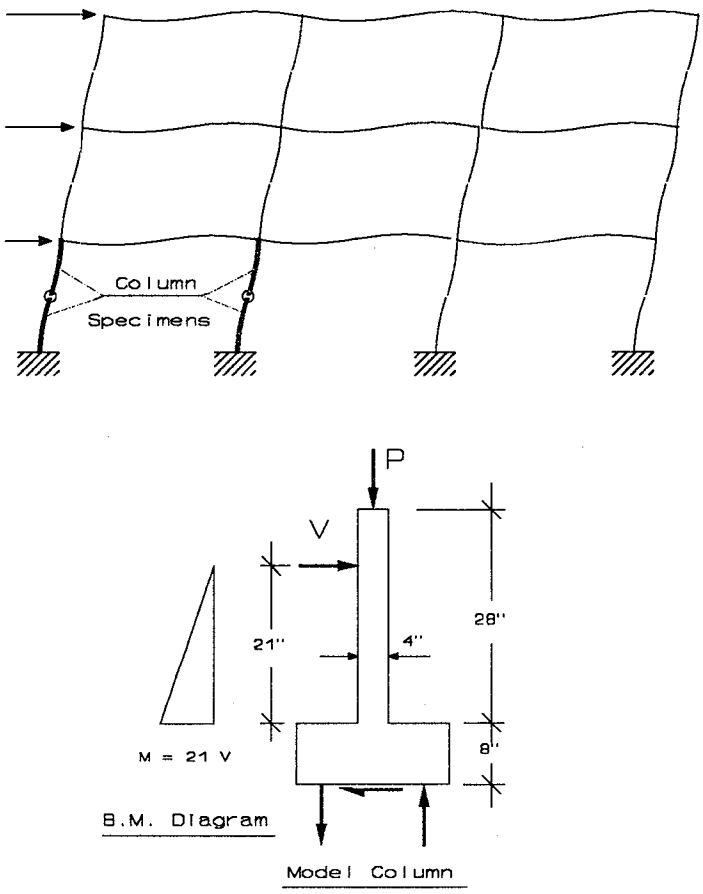

Fig. 2.1 Specimen Modeling

The steel used for transverse reinforcement was 0.12 in. diameter smooth round wire (#11 gage). The results of coupon tests are presented in Section 1.3. Details of the transverse reinforcement spacing are shown in Fig. 2.2.

2.2.2 Column Base

The base of each specimen consisted of a rectangular reinforced concrete prism 9 x 20 x 8 in., as shown in Fig. 2.3. The column base was designed to provide anchorage and stability for the specimen. Four vertical 1 in. diameter pipes provided the space for 5/8 in. diameter threaded rods that connected the base to the test rig. The base reinforcement consisted of one closed hoop and two #3 deformed rebars at the top and bottom, connected by seven closed and five open vertical hoops made from #2 smooth round bar.

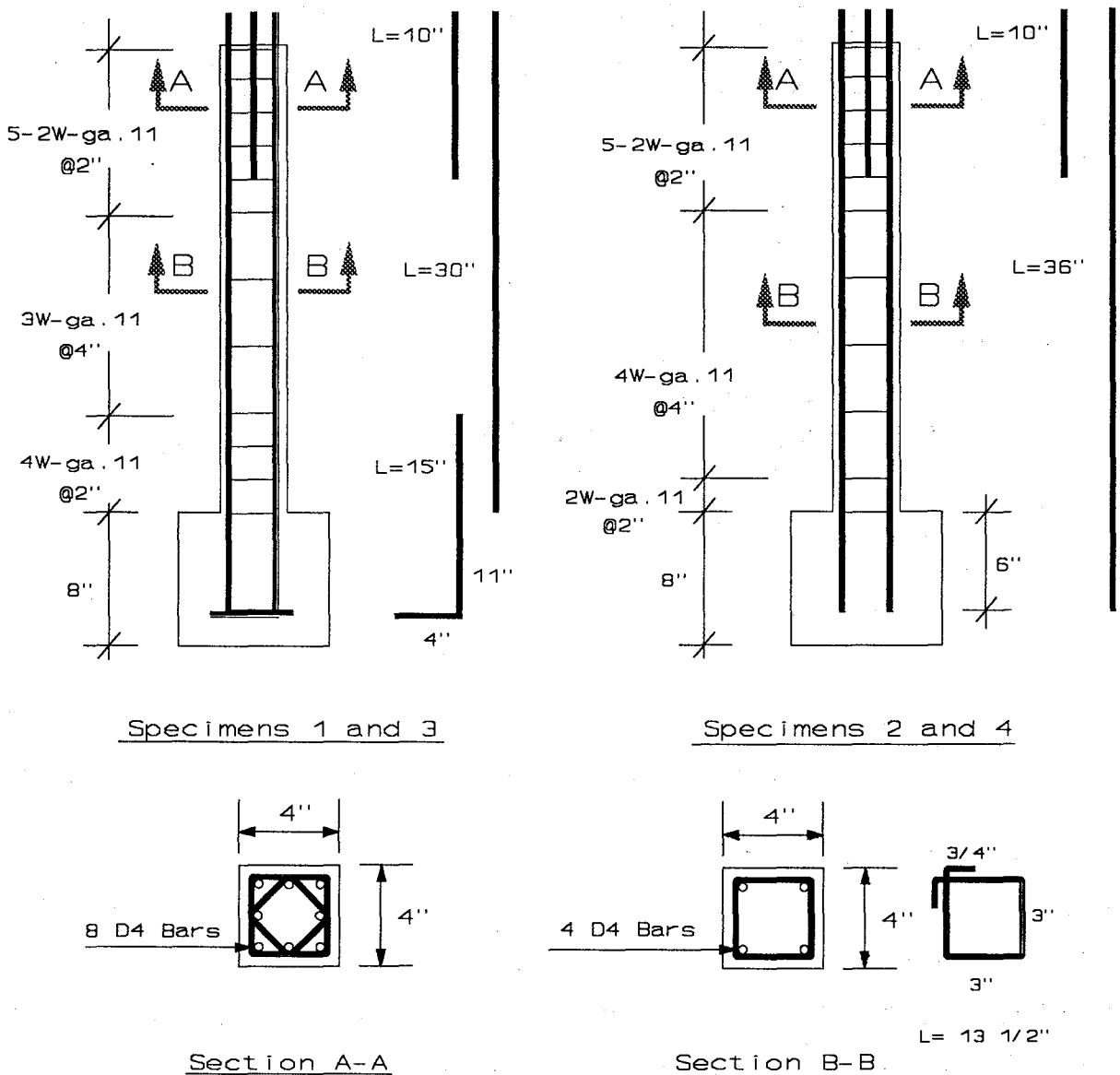

Fig. 2.2 Reinforcement of Column Specimens

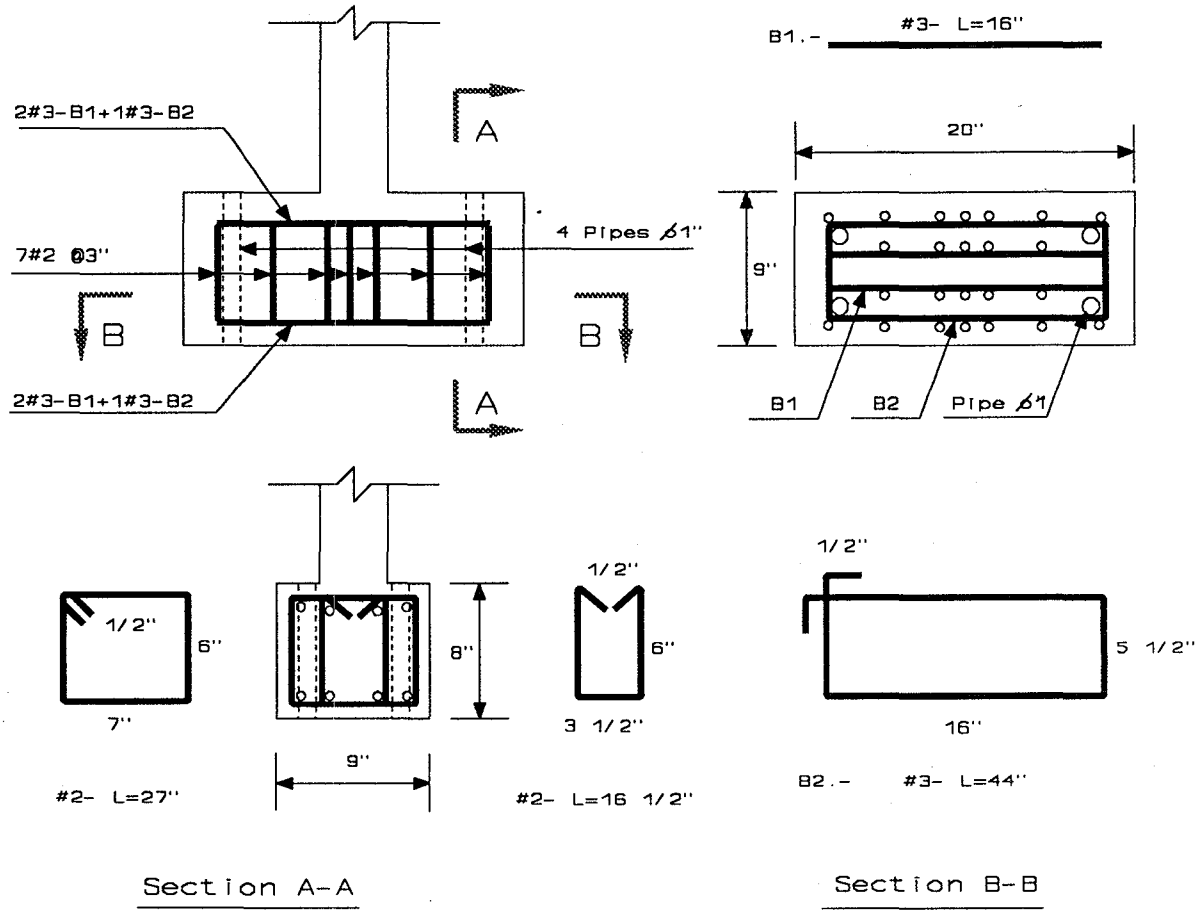

Fig. 2.3 Reinforcement of the Base

2.2.3 Construction of the Column Specimens

Bases

Forms for the bases were assembled from plywood and 2x10 in. wood. The base steel cages were tied and placed in the forms. The four vertical 1 in. diameter pipes were placed and tack welded to the cages to ensure the vertical column bars (or starter bars) were precisely located. The pipes were secured by plugs into the base of the formwork as well as cleats across the top of the forms. The vertical column bars were passed through a piece of pre-bored wood which was secured to the forms.

Concrete was placed in one lift in the bases and mechanically vibrated. Test cylinders 8 x 4 in. diameter were also cast. The concrete was kept moist during curing with the forms being removed after two days.

Columns

Firstly, the transverse hoops were fixed to the vertical bars by tie wire. Next, the cages were placed in forms constructed from plywood and 2x4 in. wood. Four 5/16 in. diameter threaded rods were passed through pre-bored holes near the base of each column. These rods were used for mounting potentiometers for curvature measurements.

Concrete was placed in the formwork and mechanically vibrated. Test cylinders 8 x 4 in. diameter were also cast. After one day of curing, the formwork was removed and the concrete moist cured.

2.3 Design and Construction of the Test Rig

The general set up of the test rig is shown in Fig. 2.4. An existing L shaped reaction frame made from two pieces of W 14x145 was utilized for these series of experiments. The frame was modified by attaching a 27 x 41 x 2 in. steel plate to the horizontal beam to provide enough room to locate the specimen sufficiently far from the vertical frame member to accommodate the horizontal 5.5 Kip hydraulic actuator. The plate was connected by four 1 in. diameter bolts to the horizontal beam. Four threaded holes were made in the plate for the 5/8 in. diameter threaded rods which connected the base of the specimen to the test rig.

MTS servo-hydraulic actuators of ± 5.5 and a ± 22 Kip capacity were used to apply the horizontal and the vertical loads, respectively. Hence, bending moment, shear force and axial load were applied to the member, the critical section being located just above the base.

The piston of the vertical 22 Kip actuator was passed through a pre-bored hole in an 8 x 16 x 1½ in. steel plate, with the body of the actuator bolted to that plate. Two 3/4 in. diameter vertical tiedown bars were connected to the plate and to the test rig hence providing the necessary prestress reaction to apply the axial load to the column. Details of the seating of the vertical actuator on the column are illustrated in Fig. 2.5. Details of the connection of the vertical tiedown bars are shown in Fig. 2.6(a).

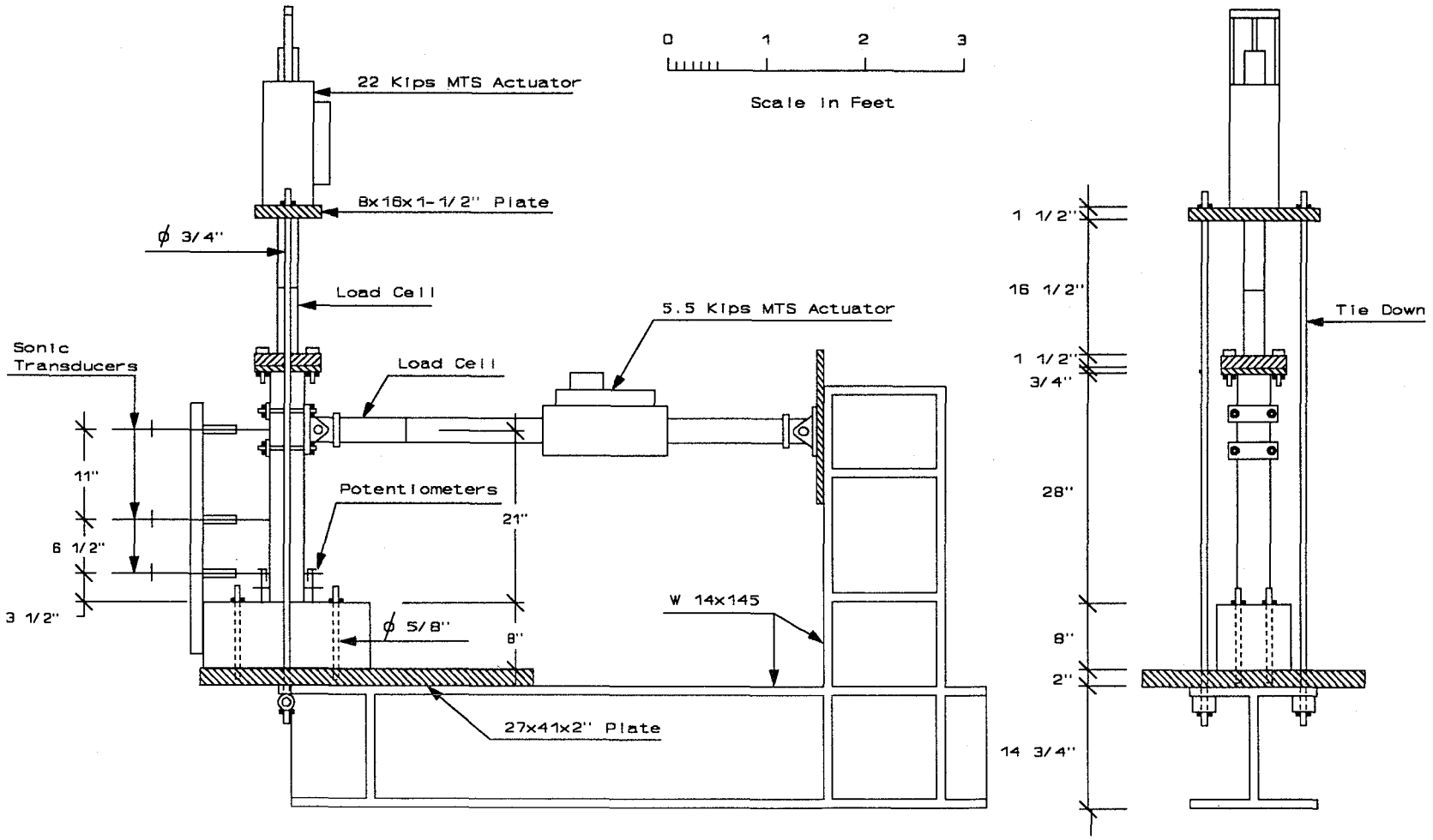

Fig. 2.4 Set up of Test Rig and Column Specimen

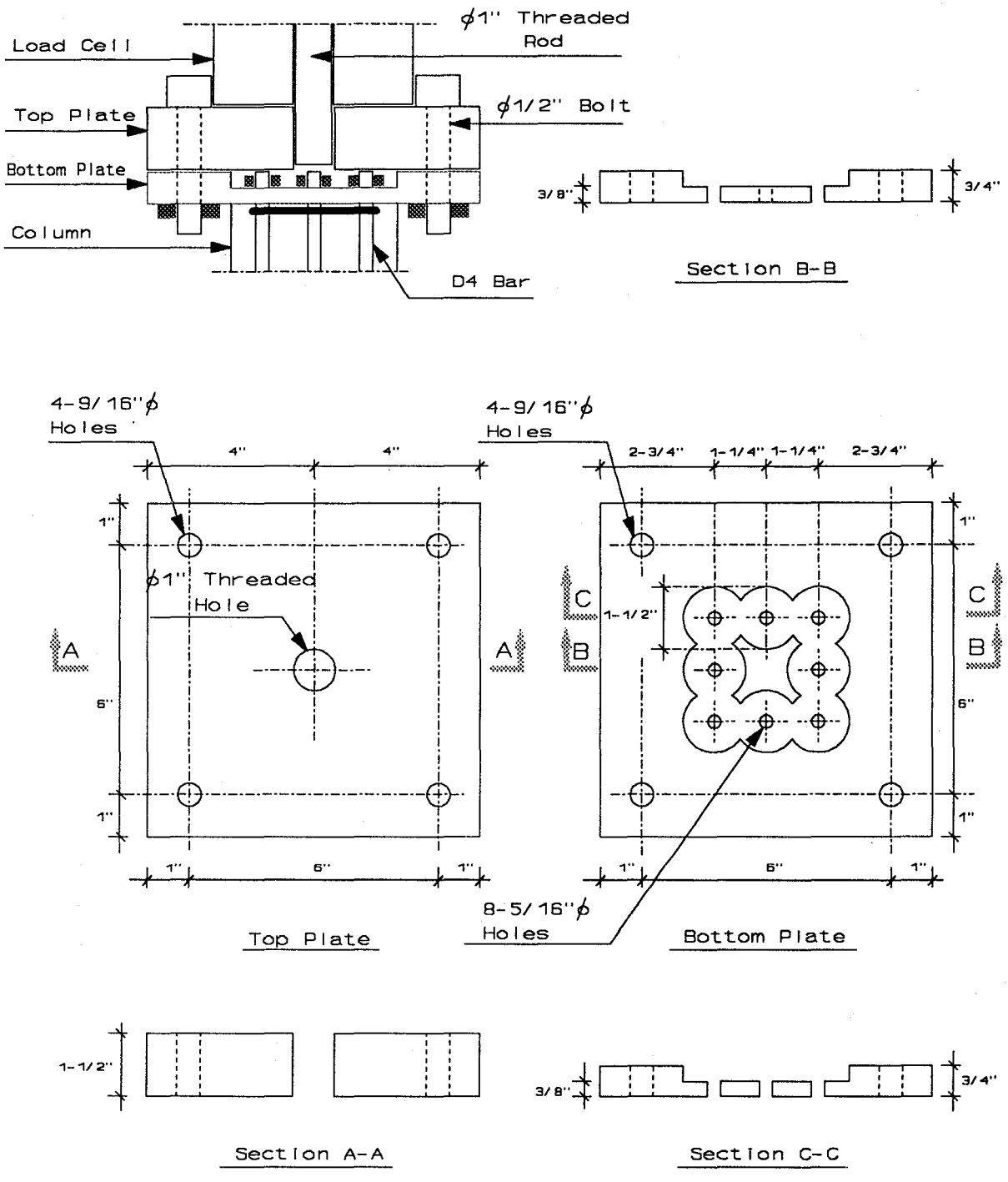

Fig. 2.5 Connection Vertical Actuator and Column

The horizontal 5.5 Kip actuator was connected to the vertical member of the reaction frame via a 1 in. thick steel plate. Four 3/4 in. diameter threaded bolts connected the actuator hinge to the plate and four 1 in. diameter bolts joined the plate and the vertical frame member. At the opposite end, the actuator hinge was connected to the column by four ½ in. threaded rods and a pair of 2 x 6 x ½ in. steel plates. Details of the connection are shown in Fig. 2.6(b).

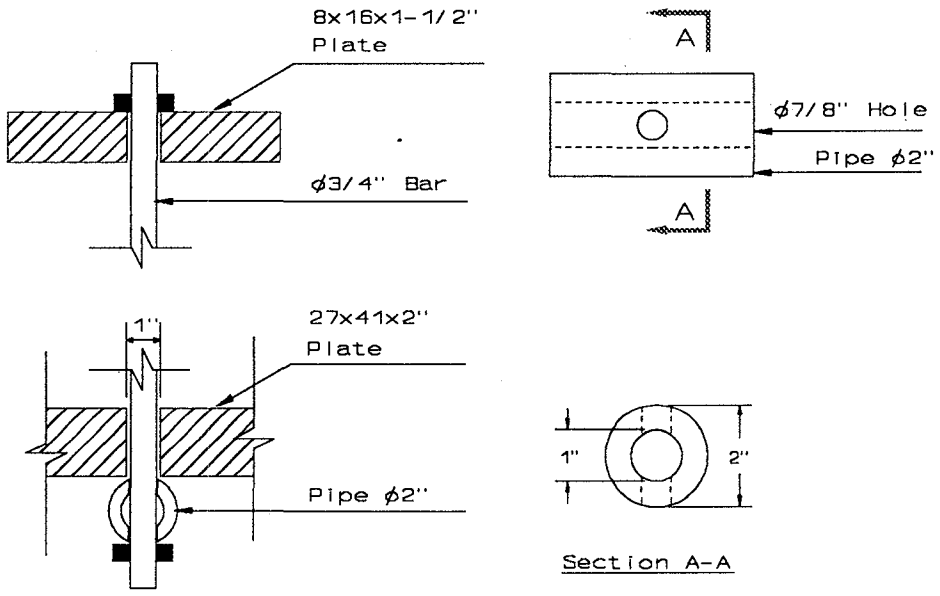

(a) Connection Vertical 3/4" bar and Test Rig

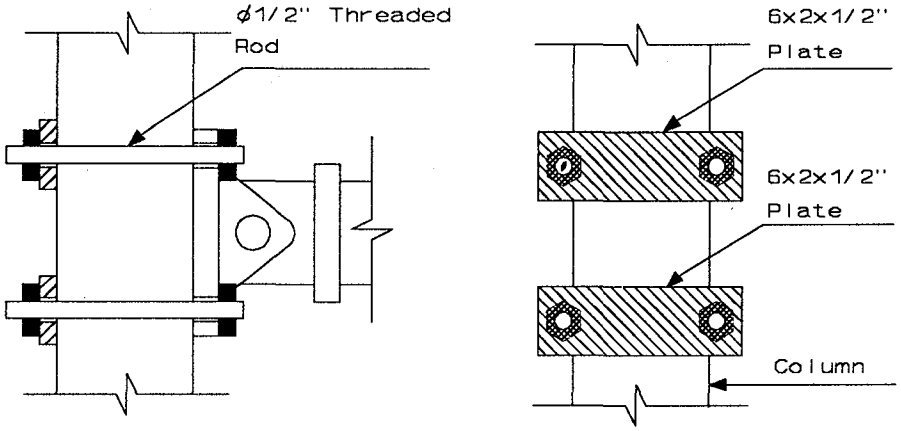

(b) Connection Horizontal Actuator and Column

Fig. 2.6 Details Connections

2.4 Instrumentation

2.4.1 Loads

The lateral and vertical loads applied to the specimen were measured by the load cells shown in Fig. 2.4. Before testing the load cells were calibrated using a Tinius Olsen Testing Machine to an accuracy of ± 0.01 Kip.

2.4.2 Lateral Displacements

The lateral displacements of the column were measured using sonic transducers located at three different heights: at the level of application of the horizontal load and 3½ and 11 in. from the base of the column. Each sonic transducer was attached to a piece of Unistrut that was fixed to the side of the base of the specimen such that the relative displacement of the column with respect to its base was measured. Two holes for 3/8 in. diameter anchors were drilled in the side of the base of all the specimens in order to attach the Unistrut. Finally, a mechanical dial gage was used to monitor movement of the base with respect to the test rig.

2.4.3 Column Curvatures

Two pairs of linear potentiometers located at opposite column faces were used to enable the column curvatures to be measured. Fig. 2.7 shows the potentiometers attached to aluminum plates which were in turn connected to 5/16 in. diameter threaded rods which passed through the column. These potentiometers allowed the average curvatures to be calculated over two sequential gage lengths of 1.75 in. in the plastic hinge region. All the potentiometers were calibrated with a digital volt meter to give a displacement accuracy of ±0.0001 in.

2.4.4 Data Acquisition

At selected times during the test, the output voltages of all the instruments were recorded using a Optim Megadac 5533A Data Acquisition System. From these records, force-displacement (drift) and moment-curvature relations could be calculated. During the test, the lateral load measured by the load cell and the lateral displacement measured by the sonic transducer at that level were recorded on a Type 7090A analogue Hewlett-Packard X-Y Plotter.

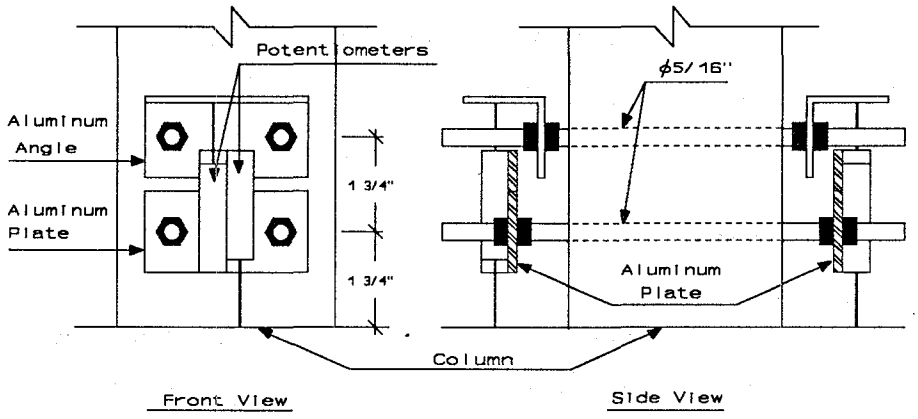

Fig. 2.7 Details of Potentiometers

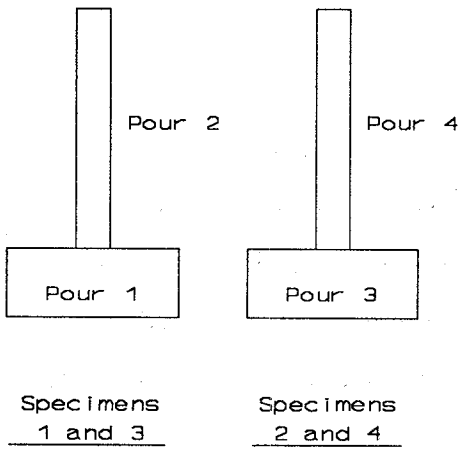

POUR	CONCRETE STRENGTH AT 28 DAYS (ksi)	CONCRETE STRENGTH AT TESTING (ksi)
1	3.50	4.15
2	3.40	3.40
3	5.50	5.50
4	4.35	4.35

Fig. 2.8 Concrete Pouring Sequence

2.5 Material Properties of the Test Specimens

The concrete pouring sequence together with the measured concrete cylinder strengths at 28 days and at testing are shown in Fig. 2.8.

The complete collection of material properties is presented in Section 1.5.1.

2.6 Testing Procedure

2.6.1 Specimen Preparation

After the installation of the specimen in the test rig, the instrumentation was mounted and calibration of the data recording devices was carried out. A safety frame made from Unistrut was installed in order to hold the vertical actuator in case of an unexpected failure of the system. Each specimen was painted with a white lime solution in order to improve the identification of the cracks during testing. The position of the rebars was drawn on the sides of the specimens with a black pencil.

2.6.2 Specimen Testing

Fig. 2.9 shows the displacement function used for the test program. This consisted of two complete displacement controlled cycles at each drift level of ±0.25%, ±0.50%, ±1%, ±2%, ±3%, ±4%, and ±5%, unless premature failure of the specimen governed. The signal for the horizontal actuator was a sine wave with a frequency of 0.01 Hz and the control was made using the measured displacement coming from the sonic transducer at the level of the applied load.
At the end of every two cycles the zero displacement was held, cracks were marked, photographs taken and the displacement amplitude adjusted for the next two cycles. Readings from all the instruments were recorded continuously by the Megadac Data System using a sampling rate of 1 Hz. In addition, VHS video tape was used to provide a visual record.

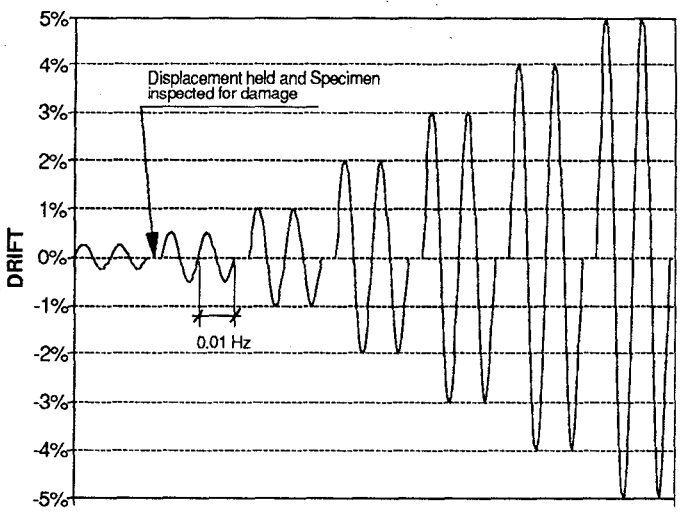

Fig. 2.9 Test Program

2.7 Experimental Results and Observations

This section presents general observations made during testing of the four column specimens. Photographs of the specimens taken during testing are presented in Figs. 2.10-2.13. Note that the horizontal and vertical lines represent the position of the reinforcement. The irregular lines show the flexure-shear cracks noticeable in the concrete cover. Specific observations for each specimen are presented as follows.

Specimen 1 - Lower Interior Column with lap splice

This specimen was provided with a 6 in. lap splice emerging from the base into the column and was tested with a constant axial load of 21.2 Kip equal to $P=0.39\ f_c' A_g$. The high level of axial load applied to the specimen was planned to represent the actual load on an interior column in the first story (ground floor) of the one-third scale model building.

Flexural cracks were first observed at the bottom of the specimen at the end of the ±1% drift cycles. Further cracking developed as the lateral displacement levels were increased. At ±3% drift the concrete cover started spalling at the bottom of the specimen and also above the lap splice region. At the end of the ±4% drift cycles, buckling of the longitudinal bars had commenced. Following the completion of the first peak of the first cycle of ±5% drift, the column failed due to complete loss of the cover concrete above the splice region and the consequent buckling of the longitudinal bars. Crushing of the concrete within the core was also observed. Hoop fracture was not observed, however one hoop lost its corner hook and opened out. Progressive damage to the column is shown in Fig. 2.10.

Specimen 2 - Upper Interior Column

This specimen, which had continuous rebars into the base, was tested at the same constant 21.2 Kip axial load as in Specimen 1 resulting in $P=0.30\ f_c' A_g$.

Flexural cracks at the bottom of the specimen were first observed at the end of the ±1% drift cycles. Further cracking developed as lateral displacement levels increased. During the ±3% drift cycles, the concrete cover started spalling at the bottom of the specimen between 2 and 6 in. from the base. At the end of the ±4% drift cycles, buckling of the longitudinal bars commenced.

Before starting the ±5% drift cycles, the potentiometers and the bottom sonic transducer were removed to prevent destruction while in the final stage of testing. During a third cycle of ±5% drift, the column failed due to buckling of the longitudinal bars and crushing of the core concrete. Progressive damage to the column is shown in Fig. 2.11.

Specimen 3 - Lower Exterior Column with lap splice

This specimen was provided with the same 6 in. lap splice at the bottom as Specimen 1. The axial load P, applied by the vertical actuator, was given by the following proportional loading relationship

$$P = 6.95 + 2\,V \quad (Kips) \tag{2.1}$$

where V = the lateral load provided by the horizontal actuator.

Note that the axial load would decrease or increase when the sign of the lateral load was respectively negative or positive. This was intended to represent a lateral force from the left and the right for the exterior column, respectively, as shown in Fig. 2.1. The coefficient 2, in Eq.(2.1), was adopted based on elastic and inelastic structural analysis of the entire model building frame.

Flexural cracks were first observed at the bottom of the specimen at the end of the ±1% drift cycles. These first cracks were horizontal at the level of the hoops (2,4, and 6 in. from the base). Further cracking developed as lateral displacement levels increased. During the ±3% drift cycles, the concrete cover started spalling at the bottom of the specimen especially under positive loading when the axial load was also increasing. In addition, a crack just at the connection of the column and the base was evident. At the end of the ±4% drift cycles, the testing procedure changed because there was very little damage. The potentiometers and the bottom sonic transducer were removed. The cycling frequency was increased to 0.1 Hz and the drift level was kept at ±4%. After 10 cycles without significant increase in damage, the drift level was raised to ±5%. After 85 cycles and about 60% strength degradation, the test was concluded. The last part of the test was characterized by a large crack between the column and the base, spalling of the concrete cover sides up to 2 in. from the base, and spalling of the concrete cover of the corners up to 6 in. from the base. The loss of bond in the lap splice zone reduced the strength such that the

concrete within the column core did not experience any more damage but merely rocked about the base. Progressive damage to the column is shown in Fig. 2.12.

Specimen 4 - Upper Exterior Column

This specimen was provided with rebars continuous into the base. For both the vertical and lateral loads, the same loading sequences were used as for Specimen 3.

Flexural cracks at the bottom of the specimen were first observed at the end of the ±1% drift cycles. These first horizontal (flexural) cracks were 4 and 6 in. from the base. The upper ones correspond with the position of the hoop as shown in Fig. 2.13(a). Further cracking developed as lateral displacement levels increased. During the ±3% drift cycles, the concrete cover started spalling on both outer faces at the bottom of the specimen. After completion of the ±5% cycles, spalling had progressed 2 in. up the column. At this stage, the test program changed. The potentiometers and the bottom sonic transducer were removed. The cycling rate was set in 1 Hz and the drift level was kept at ±5%. After 14 cycles, two bars from the same side fractured due to low cycle fatigue. Fig. 2.13 shows photographs of the progression of damage to the column during testing to failure.

2.8 Hysteretic Performance

Hysteresis curves for all four column specimens are presented in Figs. 2.15 to 2.18. For each column specimen there is one lateral load-drift graph and one lateral load-rotation graph. The rotation was evaluated using the measurements from all of the potentiometers and represents the plastic rotation over the bottom 3.5" of each column. The nominal lateral load capacity of the specimen, which is based on the usual ACI nominal strength calculations (with $\phi = 1$), is plotted as a dashed line superimposed on the measured lateral load-drift and lateral load-rotation curves.

For Specimens 1 and 3 (columns with lap splice) only the net steel area at the base of the column has been considered in the calculation of the nominal capacity. The relationship of the axial load history of the tested specimens with respect to the axial load-moment interaction diagram is shown in Fig. 2.14.

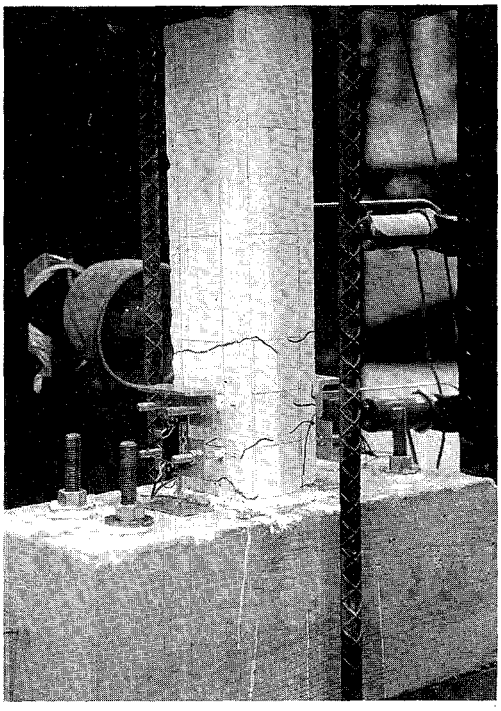

a.) End of 2% cycles

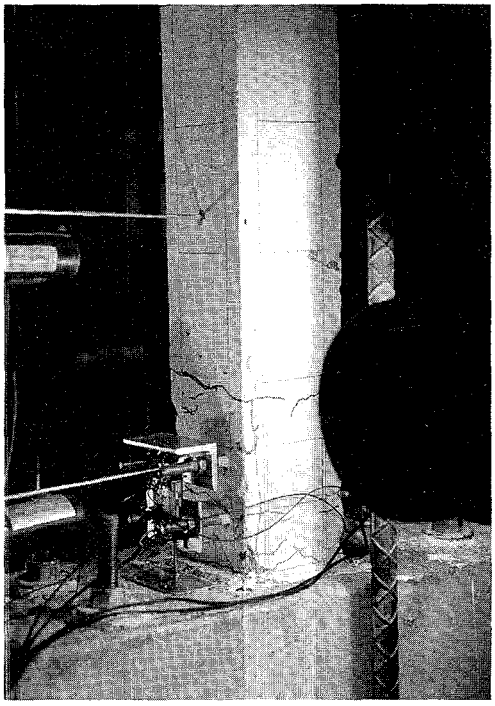

b.) End of 3% cycles

c.) End of testing

d.) End of testing

Fig. 2.10 Progressive Damage Lower Interior Column with lap splice

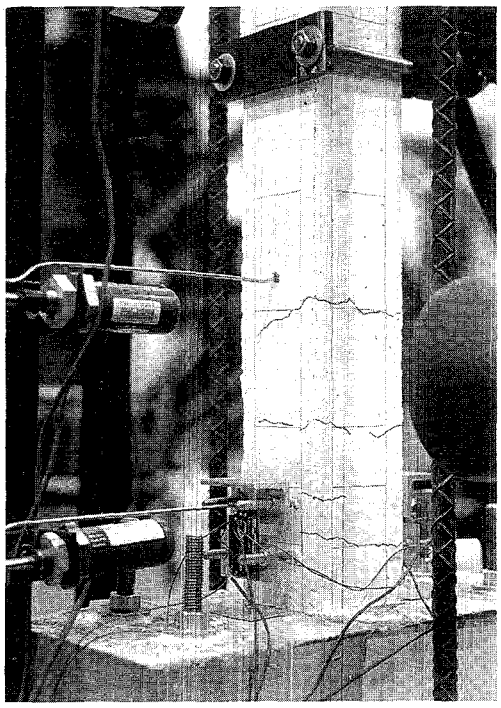

a.) End of 2% cycles

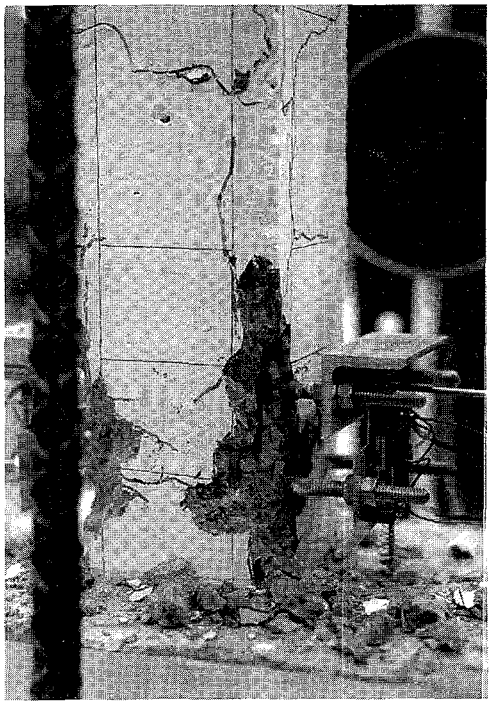

b.) End of 4% cycles

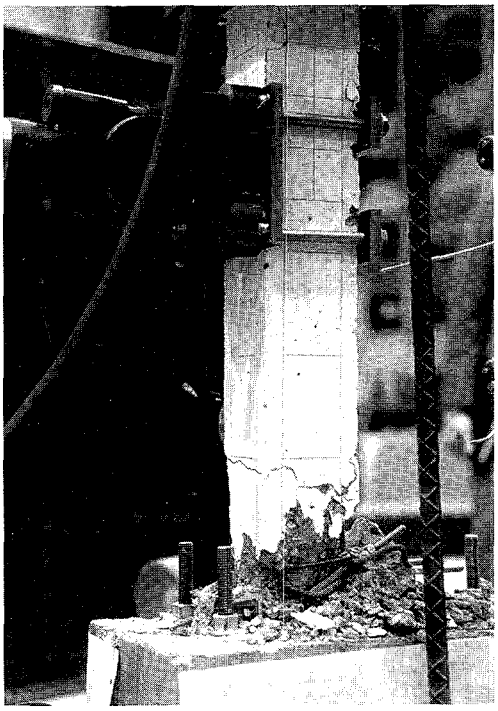

c.) End of testing

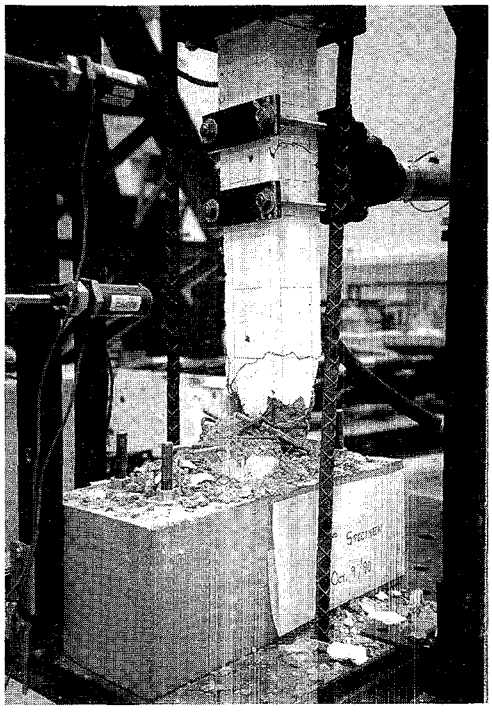

d.) End of testing

Fig. 2.11 Progressive Damage Upper Interior Column

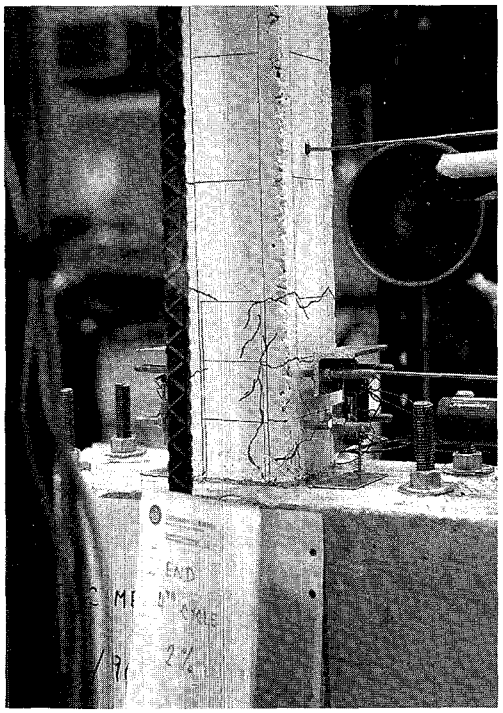

a.) End of 2% cycles

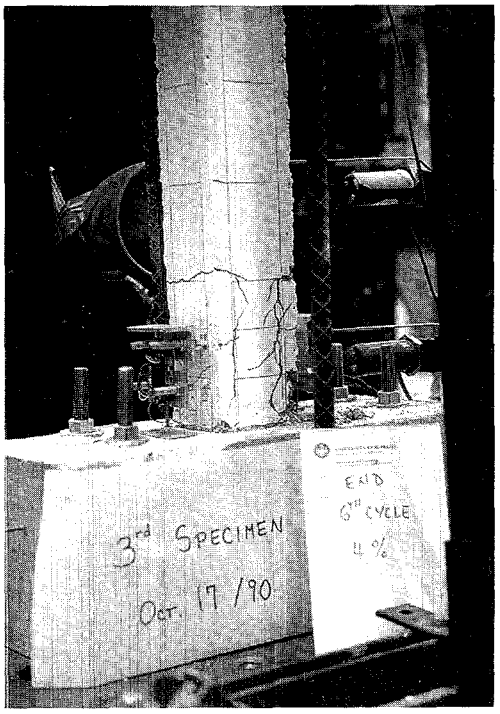

b.) End of 4% cycles

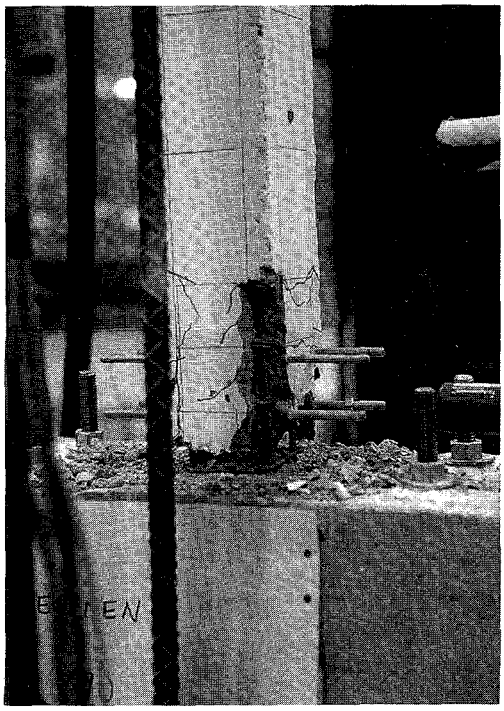

c.) End of testing

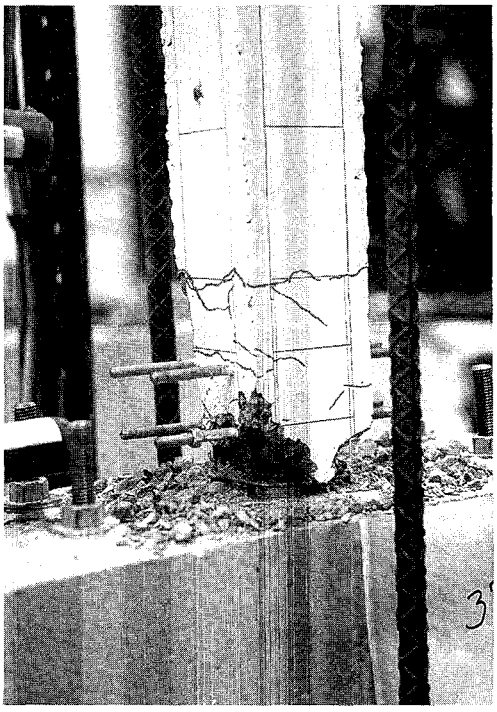

d.) End of testing

Fig. 2.12 Progressive Damage Lower Exterior Column with lap splice

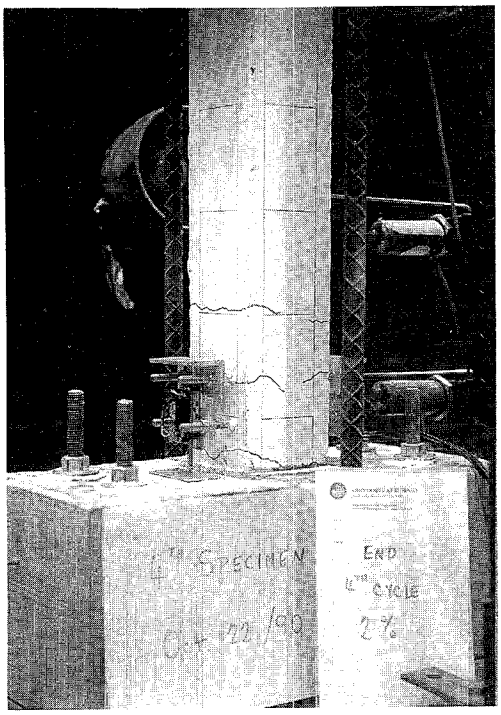

a.) End of 2% cycles

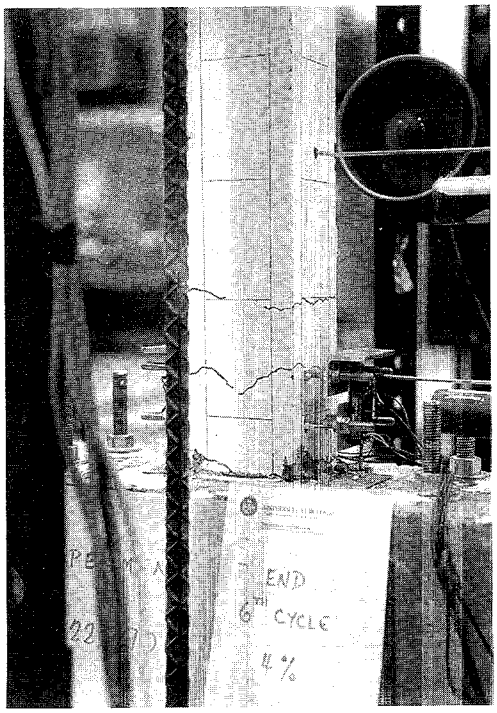

b.) End of 4% cycles

c.) End of testing

Fig. 2.13 Progressive Damage Upper Exterior Column

The hysteresis loops for the Upper Interior and Exterior columns (Specimens 2 and 4) show very good energy dissipating characteristics and stability. For both the lower columns which had the lap splice (Specimens 1 and 3), narrower hysteresis loops were observed. Clearly, the presence of lap splice in the lower columns inhibited some energy dissipation. However, it is evident that the lap was of sufficient length to initially attain the nominal strength capacity.

The columns behaved almost elastically for the ±0.25% and ± 0.50% drift levels. As the drift levels increased, it is evident that some stiffness degradation of the unloading curves occurred. Significant degradation of strength was evident with successive cycling while little degradation of stiffness was apparent on the second complete cycle at a given constant drift amplitude. Little sign of loss in strength was shown prior to column failure for the lightly loaded exterior columns, Specimens 3 and 4. For Specimen 1, there was a 38% loss in strength between the peak capacity at 3% drift to the final cycle at 4% drift, and for Specimen 2 there was a 28% loss in strength between the peak capacity at 3% drift to the final cycle at 5% drift. The additional strength loss in Specimen 1 appears due to the presence of the lap splice.

In general, the lateral load-drift and lateral load-rotation graphs for each column show that most of the inelastic displacement took place in the potential plastic hinge zone (3.5" at the bottom of the column). In the case of Specimens 1 and 2 (Interior Columns), the difference between the load-drift and load-rotation graphs is due to displacement that occurred outside the hinge zone, and in fact the columns ended up failing at a section between 5 to 6 inches from the base. In contrast, for Specimens 3 and 4 (Exterior Columns) the load-drift and load-rotation graphs are almost identical, which again is in good agreement with the damage observed occurring right at the base of the column.

The load-drift graph for Specimens 1 and 3 (Columns with lap splice) illustrates some pinching of the hysteresis loops. However, the shape of the loops is mainly attributed to compressive axial load causing the closure of open cracks and also to loss of bond in the lap splice. The low level of axial load for Specimen 3 led to very wide open cracks at large drifts and considerable bond slip with pinching of the hysteresis loops becoming more evident.

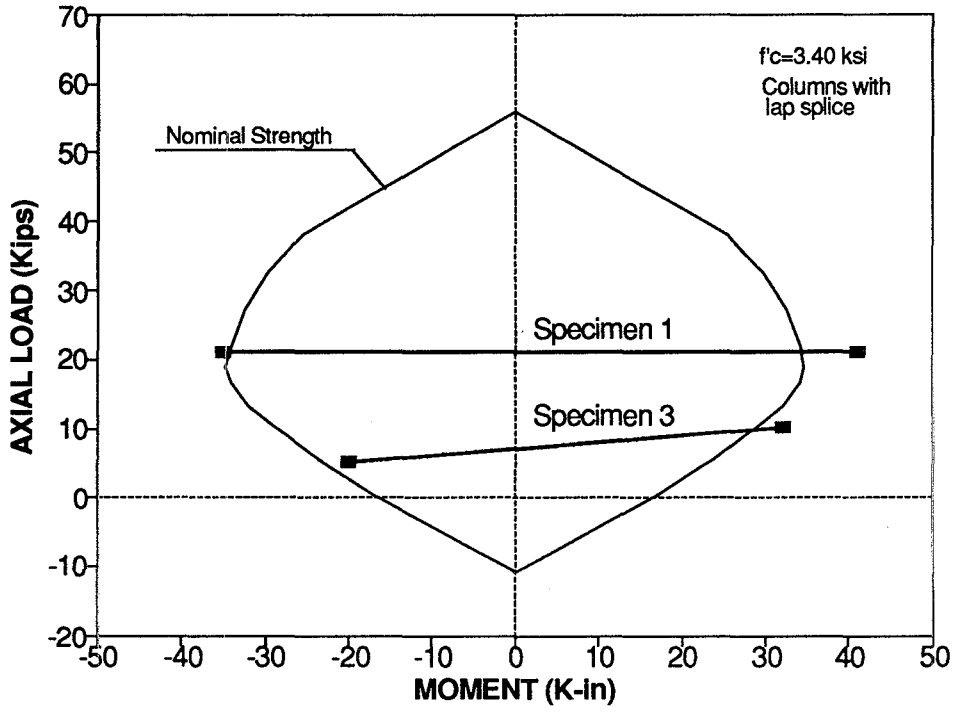

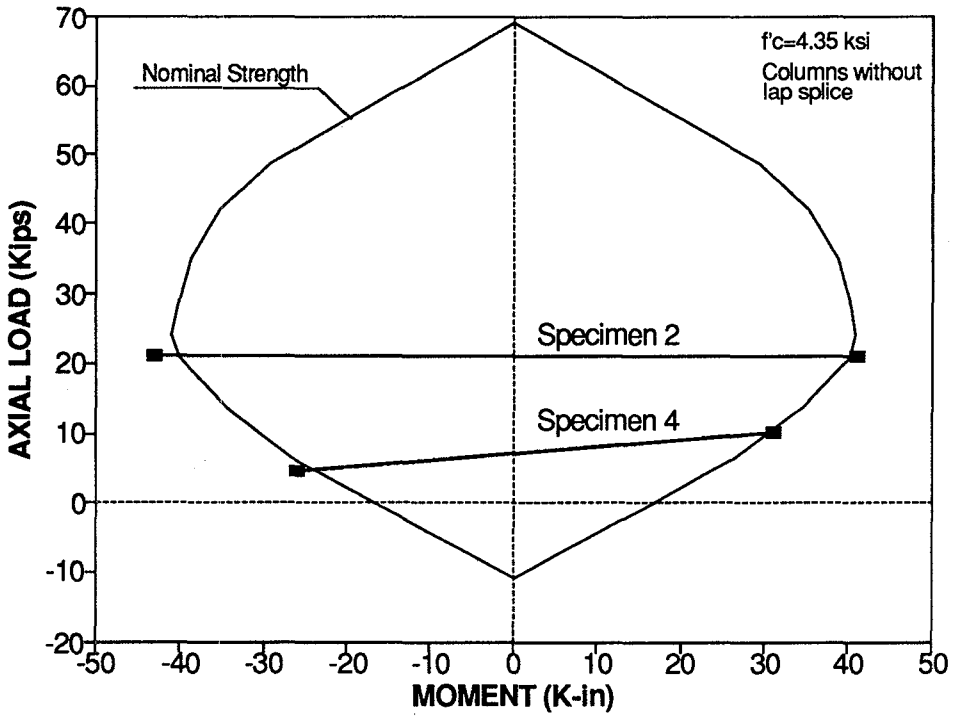

Fig. 2.14 Interaction Diagrams and Axial Load History for all Specimens

Finally, an experimental equivalent plastic hinge length can be calculated from the plastic displacement, Δ_p , by taking the first moment of area of an idealized rectangular distribution of plastic curvature about the top of the column

$$\Delta_p=(\phi_u-\phi_y)\ L_p\ (L-0.5\ L_p) \tag{2.2}$$

where $(\phi_u-\phi_y)$ is the plastic curvature measured beyond the yield curvature over the 1.75 in. lower gage length, L is the distance from the critical section to the point of contraflexure, and L_p is the equivalent plastic hinge length. Rearranging Eq.(2.2) gives the equivalent plastic hinge length in non-dimensional form as follows:

$$\frac{L_p}{h}=\frac{L}{h}\left(1-\sqrt{1-\frac{2}{L}\frac{(D_u-D_y)}{(\phi_u-\phi_y)}}\right) \tag{2.3}$$

where (D_u-D_y) is the plastic drift measured beyond the yield drift over the 1.75 in. lower gage length, and h is the depth of the column. For each specimen, Table 2.1 lists the experimental equivalent plastic hinge lengths for drifts of 2,3,4, and 5%.

Table 2.1 Experimental Equivalent Plastic Hinge Length

Specimen		1	2	3	4
D_y (%)		0.65	0.78	0.85	0.84
ϕ_y (rad/in)		0.0010	0.0010	0.0030	0.0020
D_u=2%	ϕ_u	0.0043	0.0043	0.0081	0.0081
	L_p/h	**1.15**	**1.02**	**0.60**	**0.50**
D_u=3%	ϕ_u	0.0070	0.0081	0.0132	0.0138
	L_p/h	**1.09**	**0.85**	**0.56**	**0.48**
D_u=4%	ϕ_u	0.0086	0.0127	0.0181	0.0195
	L_p/h	**1.25**	**0.74**	**0.55**	**0.47**
D_u=5%	ϕ_u	---	---	---	0.0251
	L_p/h	---	---	---	**0.47**

In general, the equivalent plastic hinge length appears to remain relatively constant with increasing drift amplitude. However, the equivalent plastic hinge length increases with increasing axial load. There is also a slight increase if a lap splice is present. Columns with high level of axial load (Specimens 1 and 2) have a range of L_p from 0.74 to 1.25 h, and columns with low level of axial load (Specimens 3 and 4) have a range of L_p from 0.47 to 0.60 h.

2.9 Section Curvatures and Strains

Lateral load-curvature hysteresis curves are shown in Figs. 2.19 to 2.22. For each column specimen, two graphs are presented in which the average curvature was measured over the two sequential 1.75 in. gage lengths from the column base.

The larger curvature response in the lower gage length for the Exterior columns indicates that most of the damage as well as the plastic deformation occurred in the critical moment region (right at the base of the column), while quite similar curvature response for both gage lengths for the Interior columns indicates more evenly distributed damage and plastic deformation over the potential plastic hinge region.

In addition to the lateral load-curvature graphs, for each gage length, two strain profile graphs evaluated at the first cycle of each successive drift peak are presented in Figs. 2.23 to 2.30. Again, the strain profiles show concentration of deformation in the first gage length for the Exterior columns and evenly distributed deformations for both gage lengths for the Interior columns.

According to the observations presented in Section 2.7, the concrete cover started spalling at ±3% drift level for all the columns. Table 2.2 presents the compression strain values for the lower gage length for each column specimen at ±3% drift level.

The apparent spalling strain for the Lower columns varied from 0.007 to 0.011 and for the Upper columns varied from 0.007 to 0.016. These values are in reasonable agreement with the strains observed at the end of the uniaxial stress-strain tests presented in Fig. 1.6.

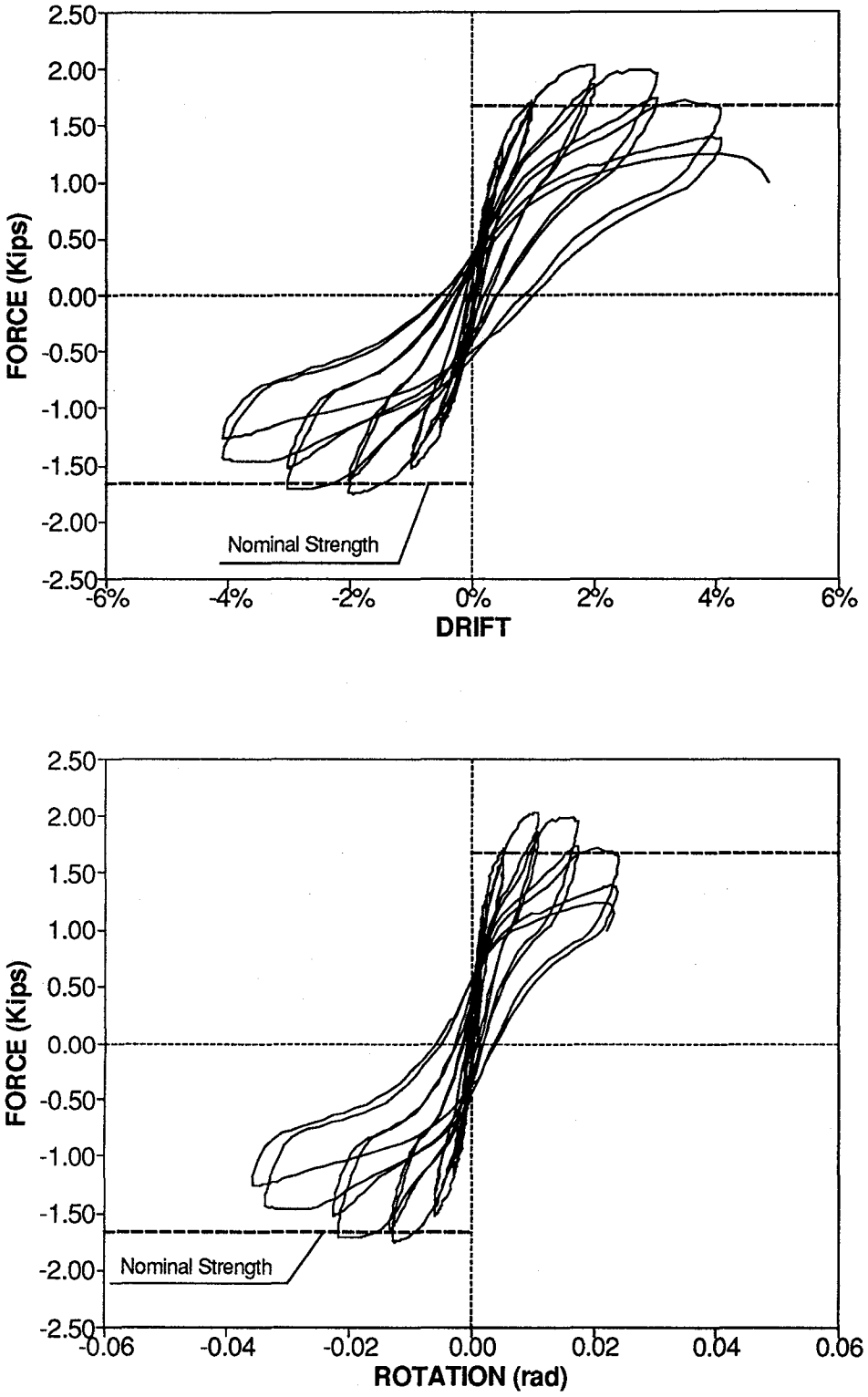

Fig. 2.15 Experimental Lateral Load-Drift and Lateral Load-Rotation graphs for Specimen 1 (Lower Interior Column with lap splice)

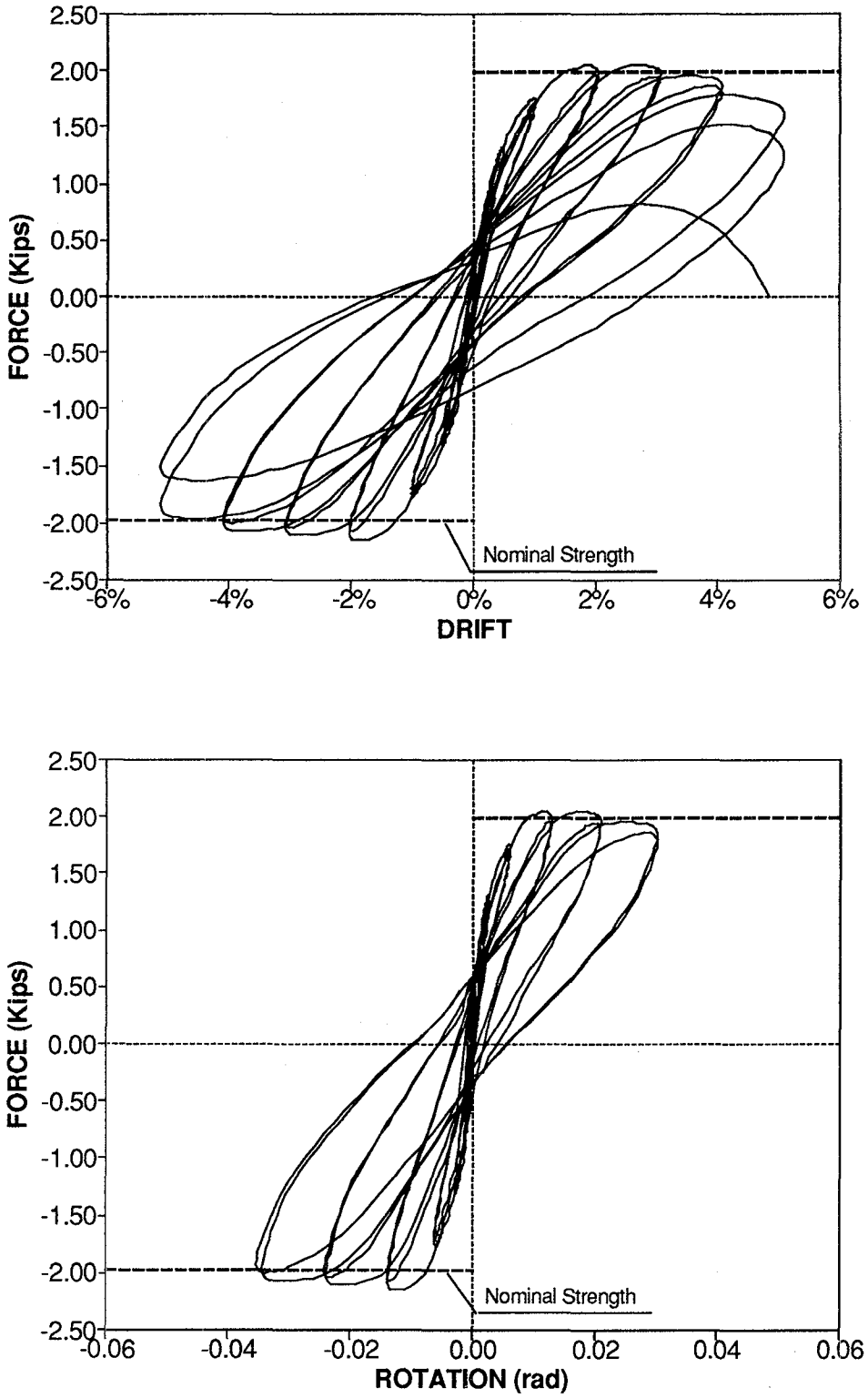

Fig. 2.16 Experimental Lateral Load-Drift and Lateral Load-Rotation graphs for Specimen 2 (Upper Interior Column)

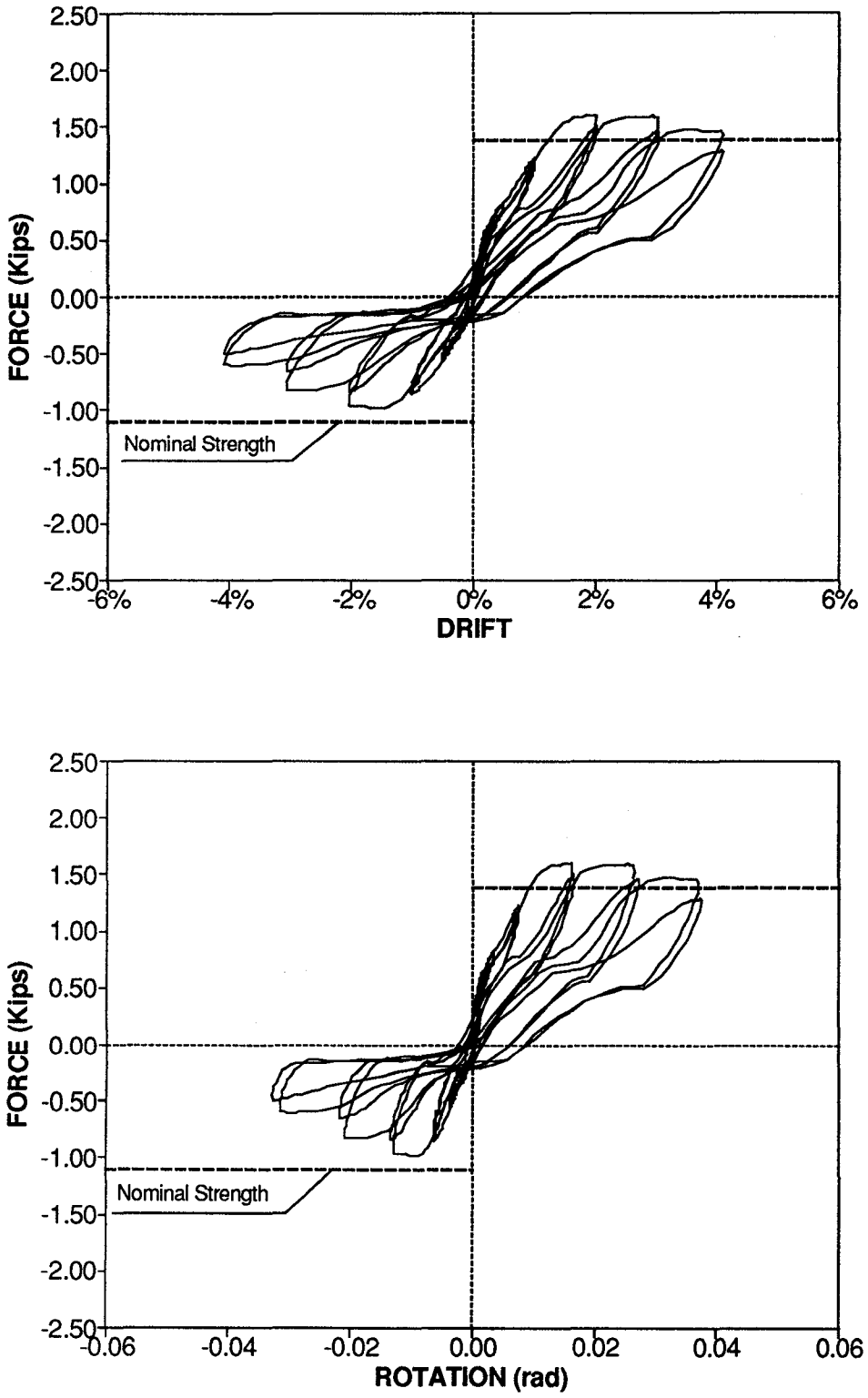

Fig. 2.17 Experimental Lateral Load-Drift and Lateral Load-Rotation graphs for Specimen 3 (Lower Exterior Column with lap splice)

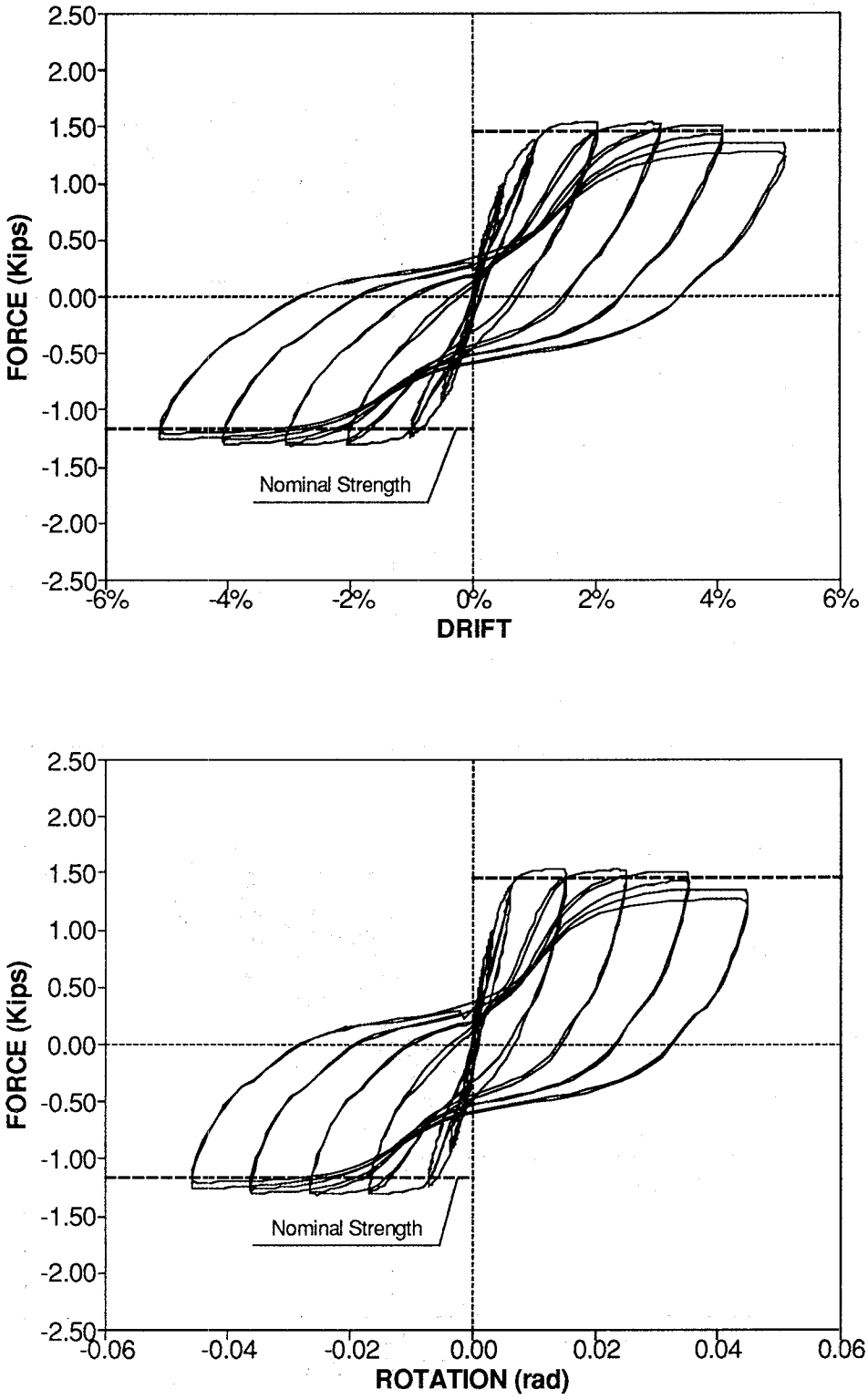

Fig. 2.18 Experimental Lateral Load-Drift and Lateral Load-Rotation graphs for Specimen 4 (Upper Exterior Column)

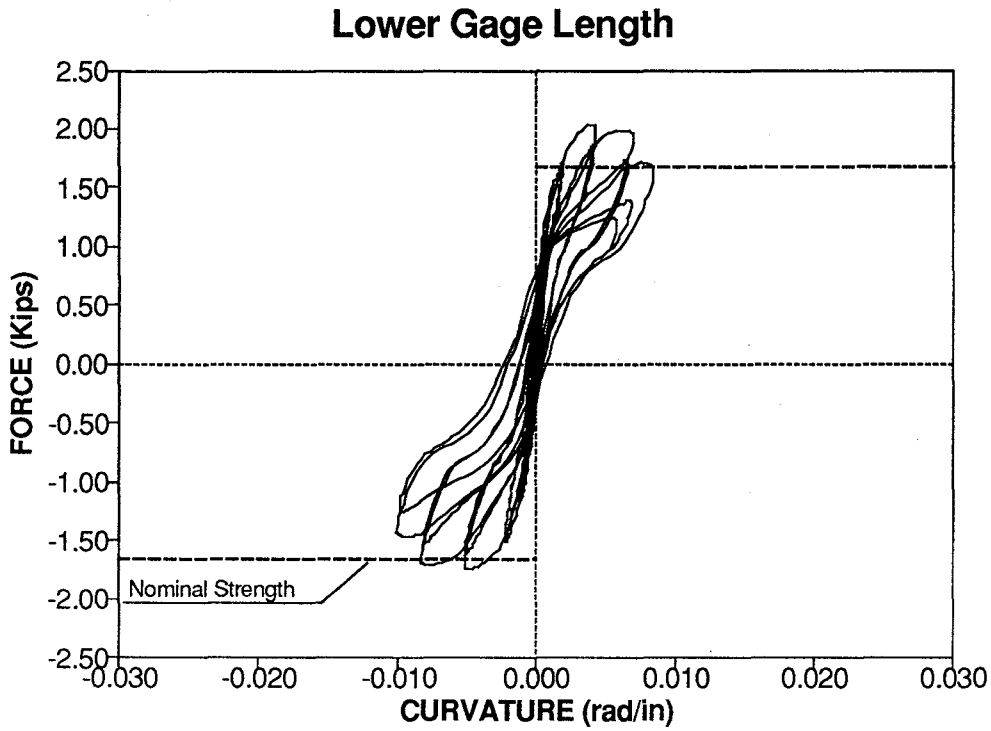

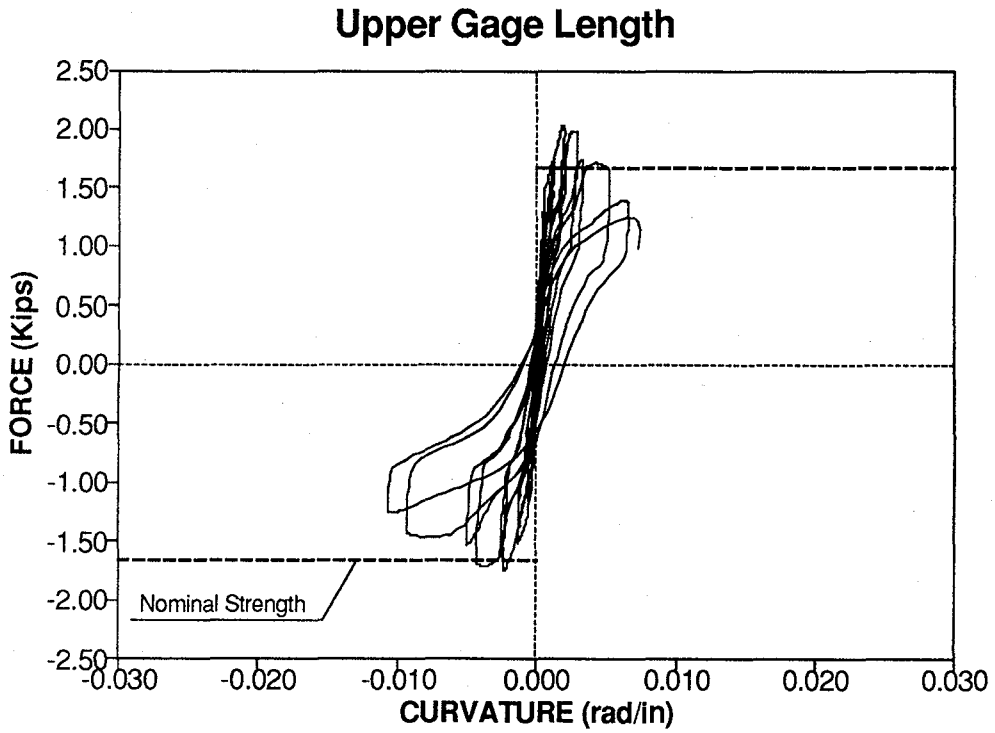

Fig. 2.19 Experimental Lateral Load-Curvature graphs for Specimen 1 (Lower Interior Column with lap splice)

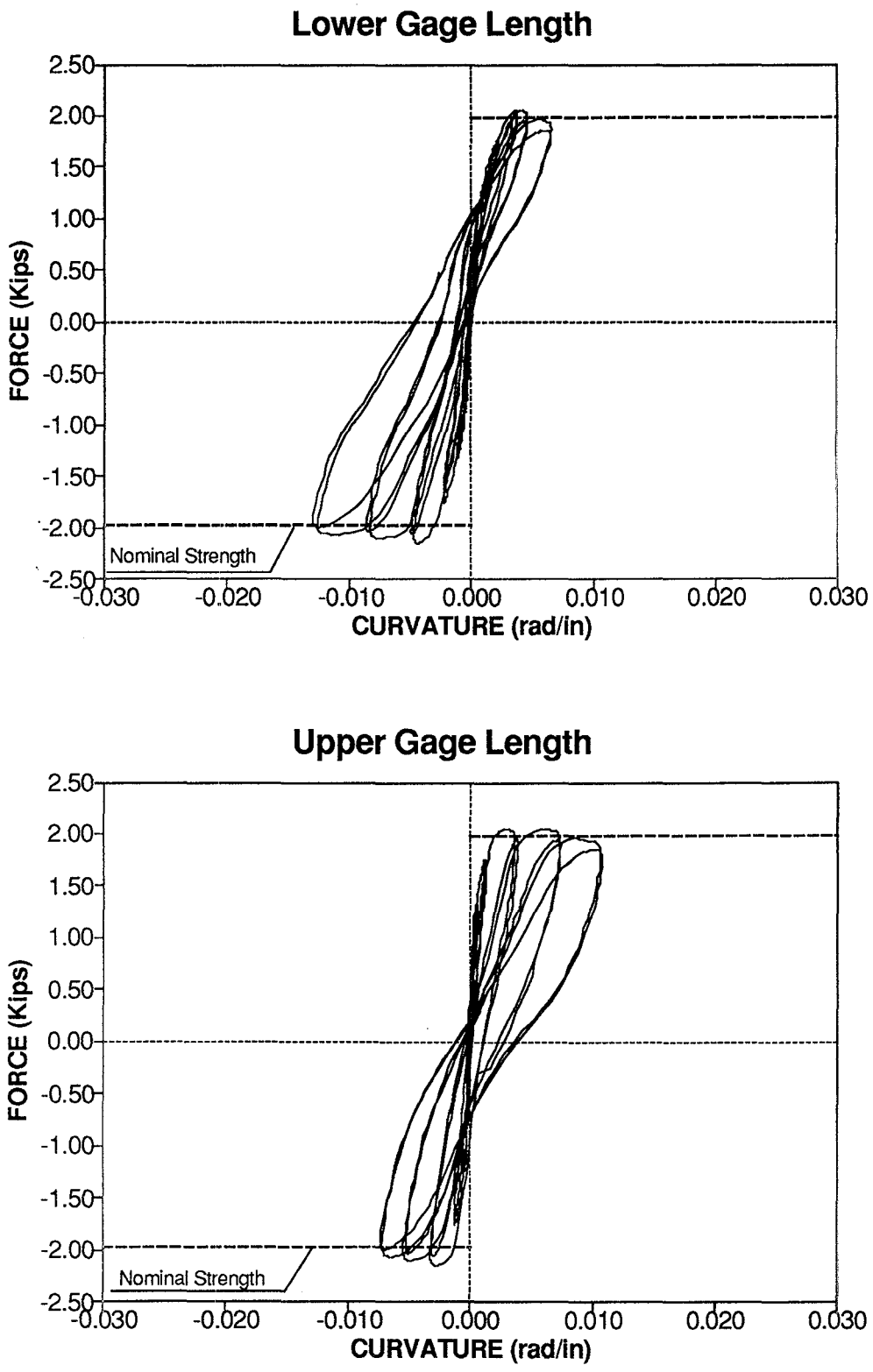

Fig. 2.20 Experimental Lateral Load-Curvature graphs for Specimen 2 (Upper Interior Column)

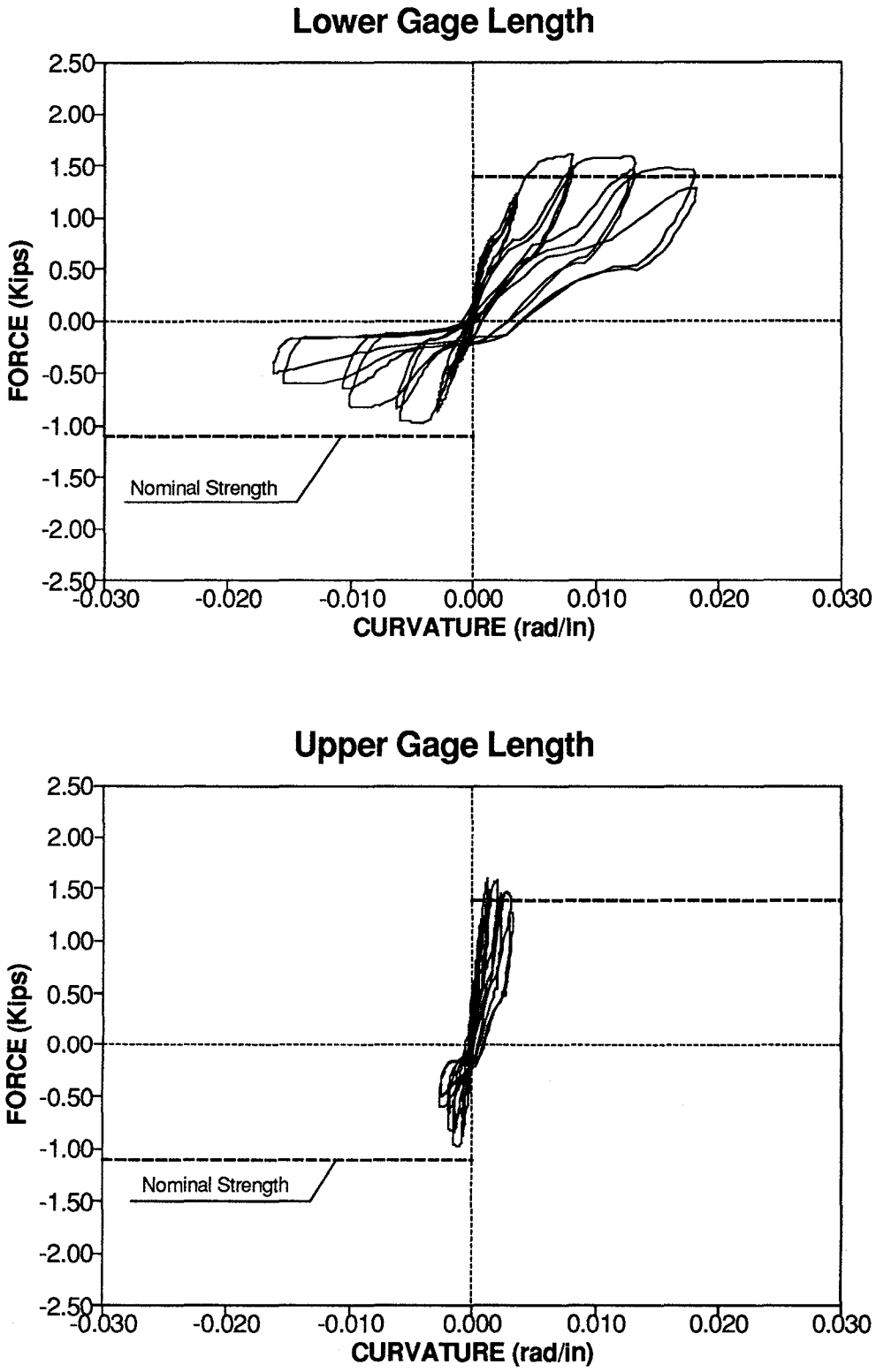

Fig. 2.21 Experimental Lateral Load-Curvature graphs for Specimen 3 (Lower Exterior Column with lap splice)

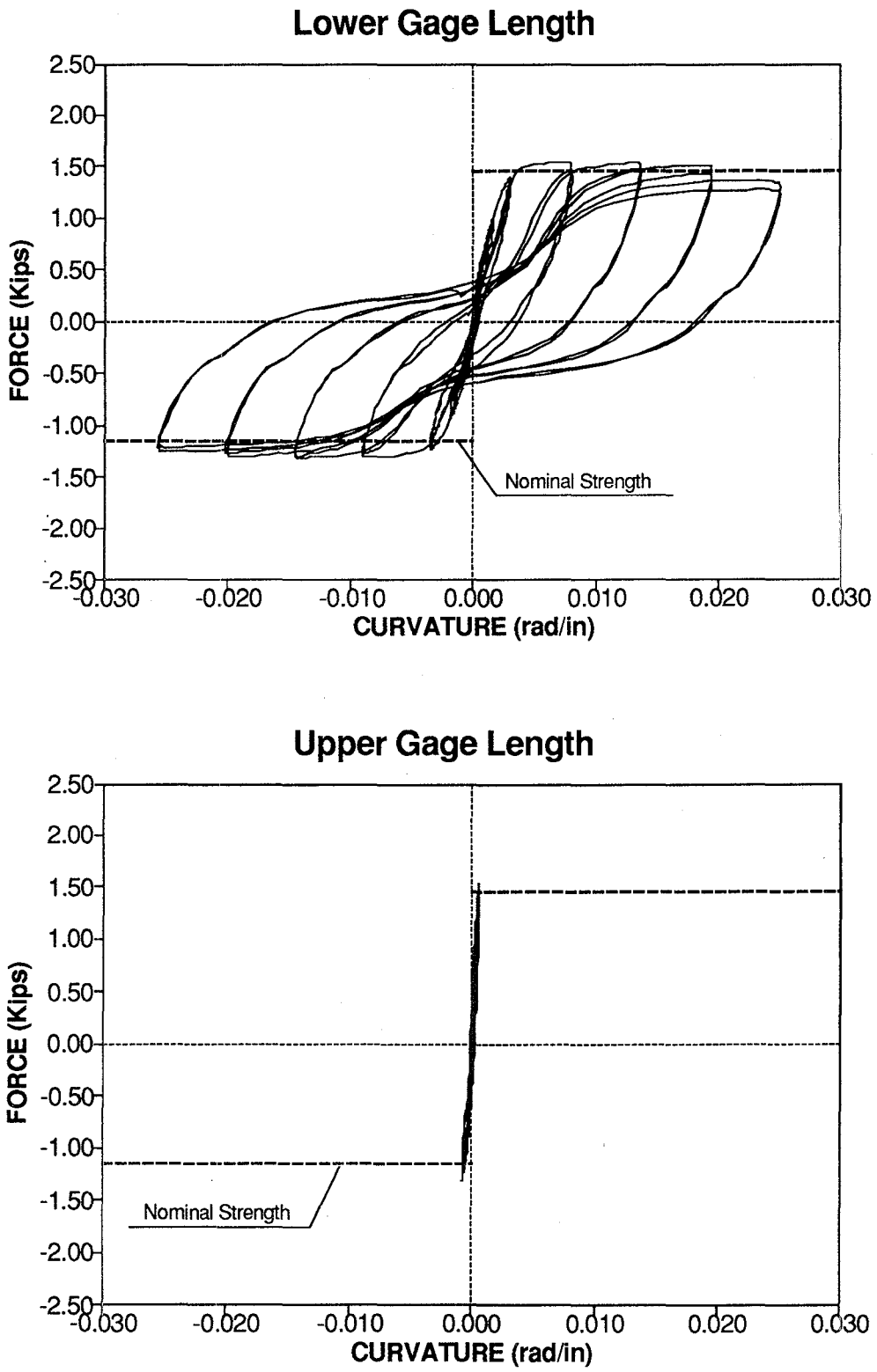

Fig. 2.22 Experimental Lateral Load-Curvature graphs for Specimen 4 (Upper Exterior Column)

Table 2.2 Experimental Apparent Spalling Strain

Loading	Specimen 1 Lower Int. Col.	Specimen 2 Upper Int. Col.	Specimen 3 Lower Ext. Col.	Specimen 4 Upper Ext. Col.
Forward	0.007	0.008	0.013	0.010
Reverse	0.011	0.016	0.010	0.007

As already mentioned in Section 2.7, Specimens 1 and 2 failed due to buckling of the longitudinal bars. Specimen 1 failed above the lap splice and Specimen 2 failed about 3 inches from the base, where in both cases s/d_b=17.8, which is considerably greater than the anti-buckling requirement of s/d_b=8 recommended by ACI 318. For both Specimens, the strain profiles show steel compression strains of about 0.015, for the last cycles, which combined with the high level of axial load (21.2 Kip), loss of the concrete cover and some concrete crushing within the core caused the type of failure previously described.

Finally, Specimens 3 and 4 failed due to low cycle fatigue of the vertical reinforcement. Table 2.3 presents strain amplitudes ε_a for the longitudinal bars for each Specimen where

$$\varepsilon_a = 1/2\ (\varepsilon_{max} - \varepsilon_{min}) \tag{2.4}$$

in which ε_{max} = maximum tensile strain, and ε_{min} = maximum compression strain (negative sign).

Table 2.3 Experimental Steel Strain Amplitudes

Strain	Specimen 1 Lower Int. Col.	Specimen 2 Upper Int. Col.	Specimen 3 Lower Ext. Col.	Specimen 4 Upper Ext. Col.
ε_a	0.013	0.014	0.022	0.033

These high values of strain amplitude for Specimens 3 and 4 help explain why a low cycle fatigue failure was observed.

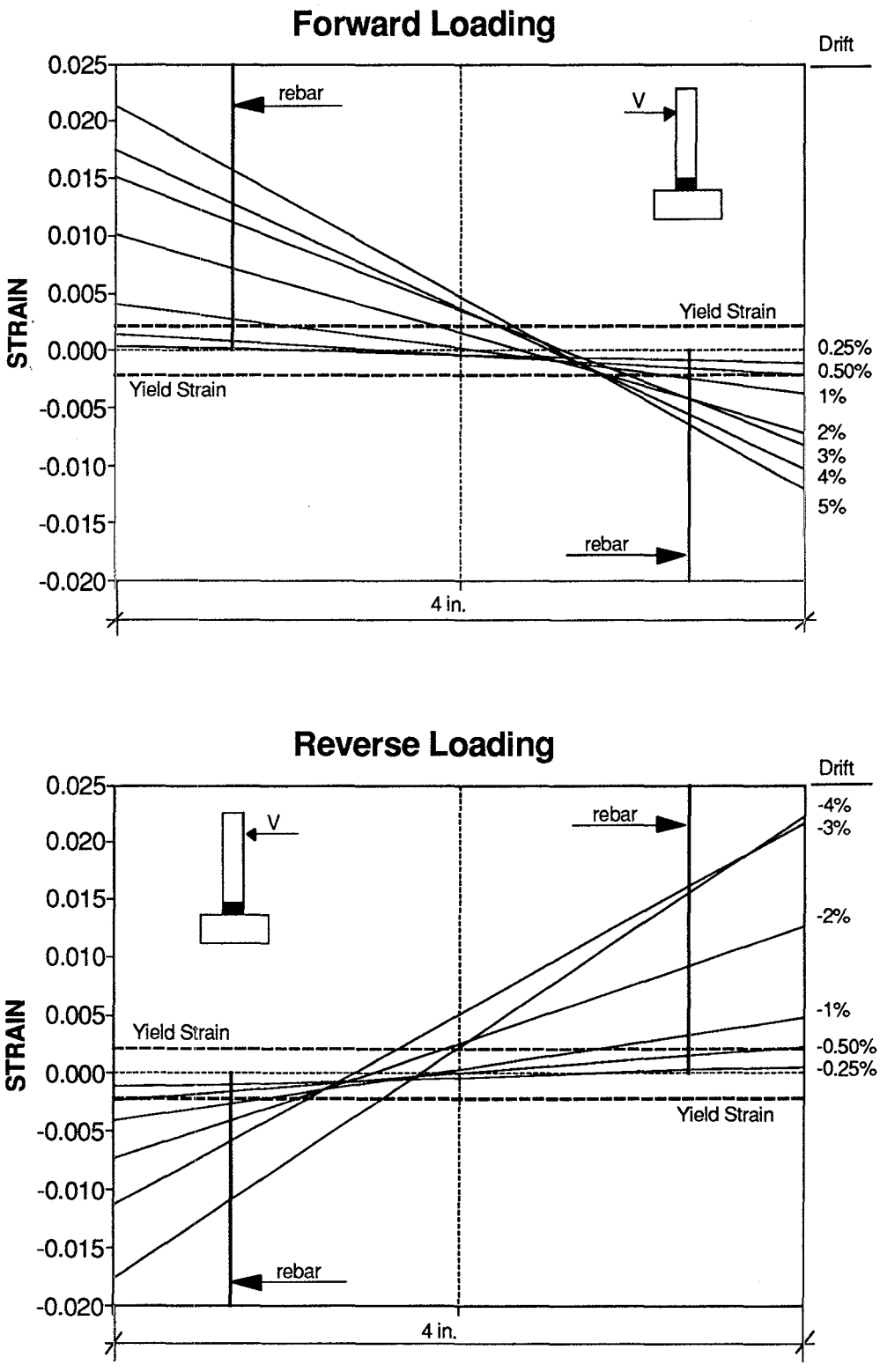

Fig. 2.23 Strain Profiles Lower Gage Length for Specimen 1 (Lower Interior Column with lap splice)

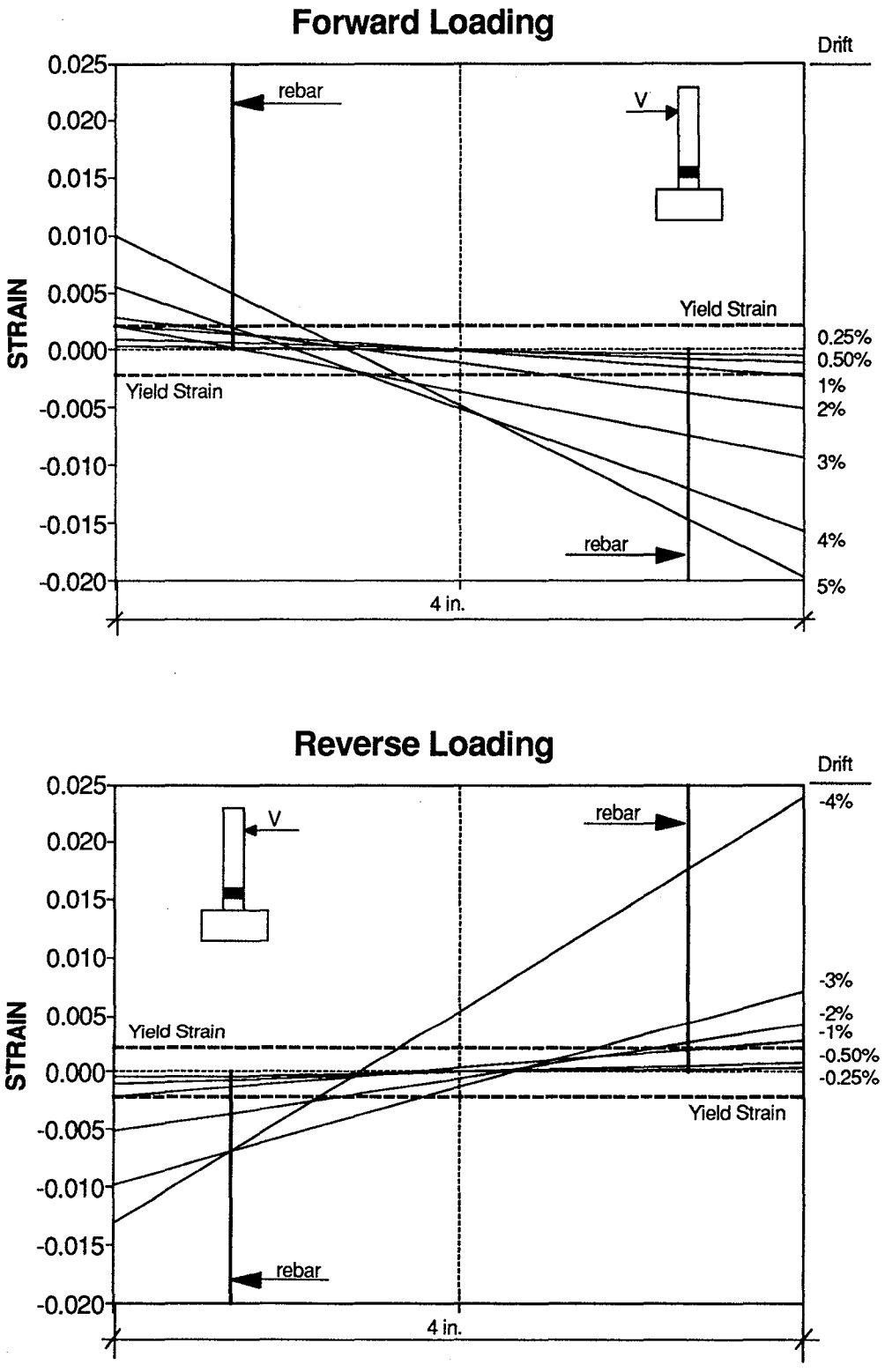

Fig. 2.24 Strain Profiles Upper Gage Length for Specimen 1 (Lower Interior Column with lap splice)

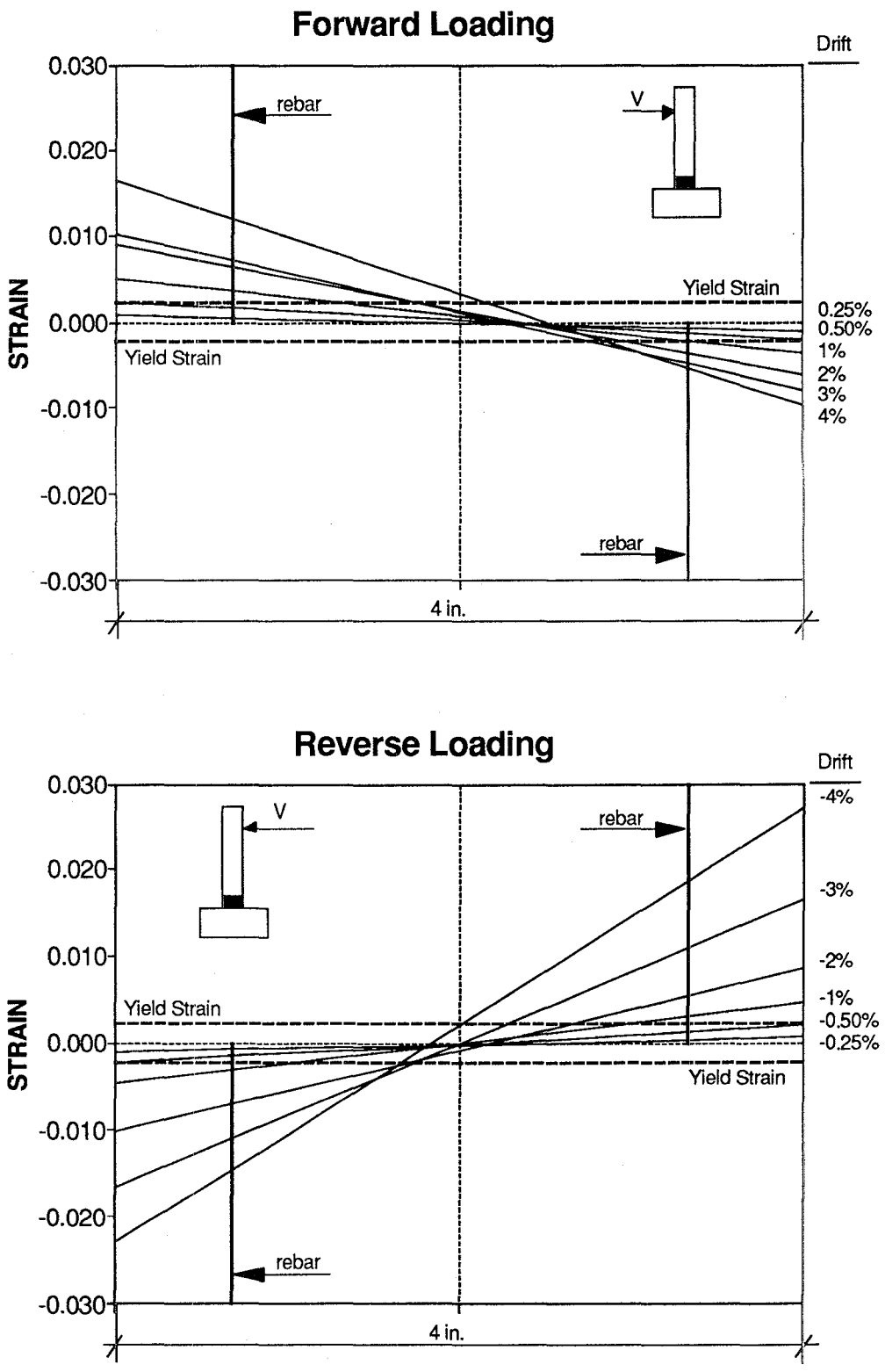

Fig. 2.25 Strain Profiles Lower Gage Length for Specimen 2 (Upper Interior Column)

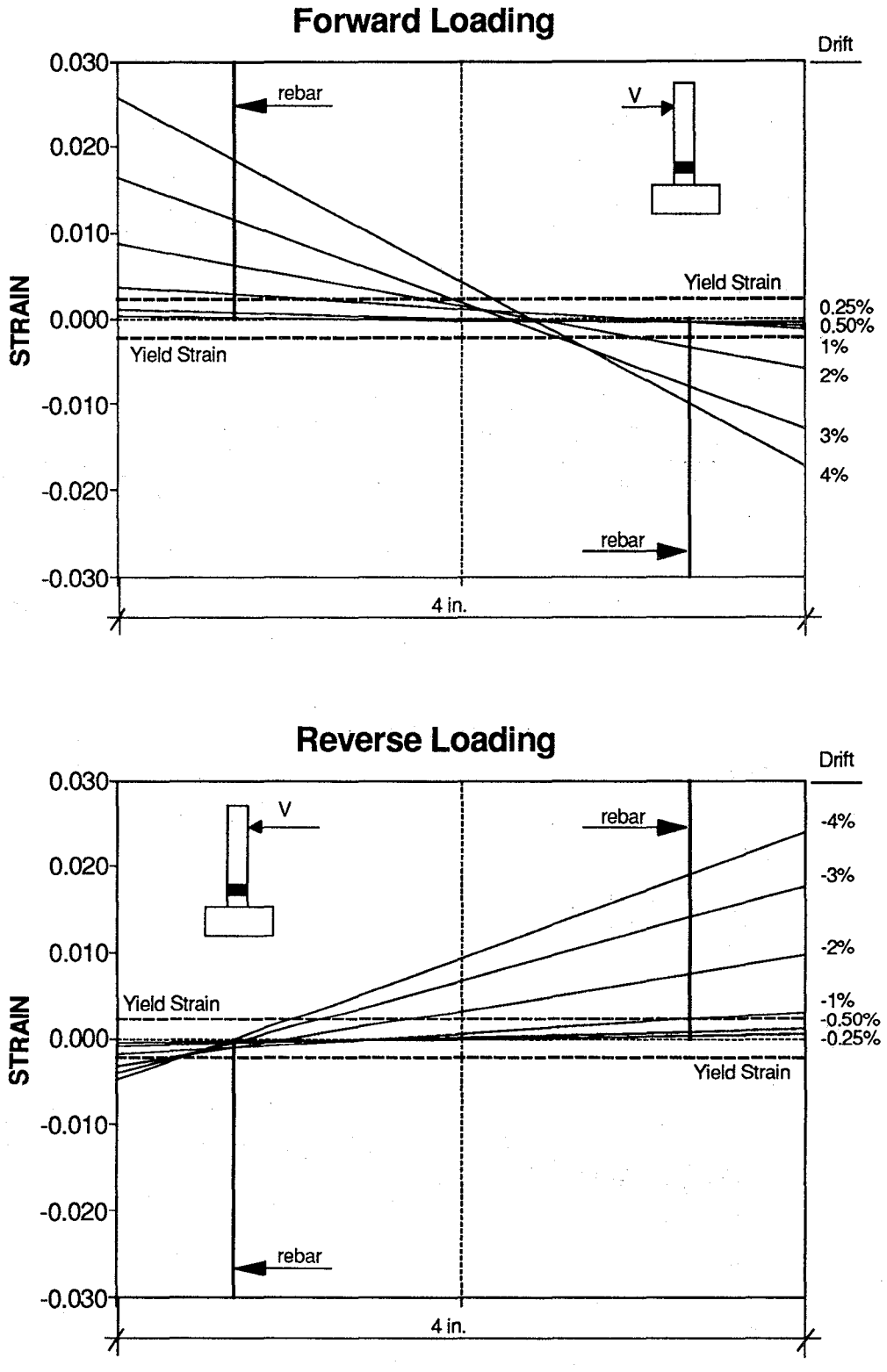

Fig. 2.26 Strain Profiles Upper Gage Length for Specimen 2 (Upper Interior Column)

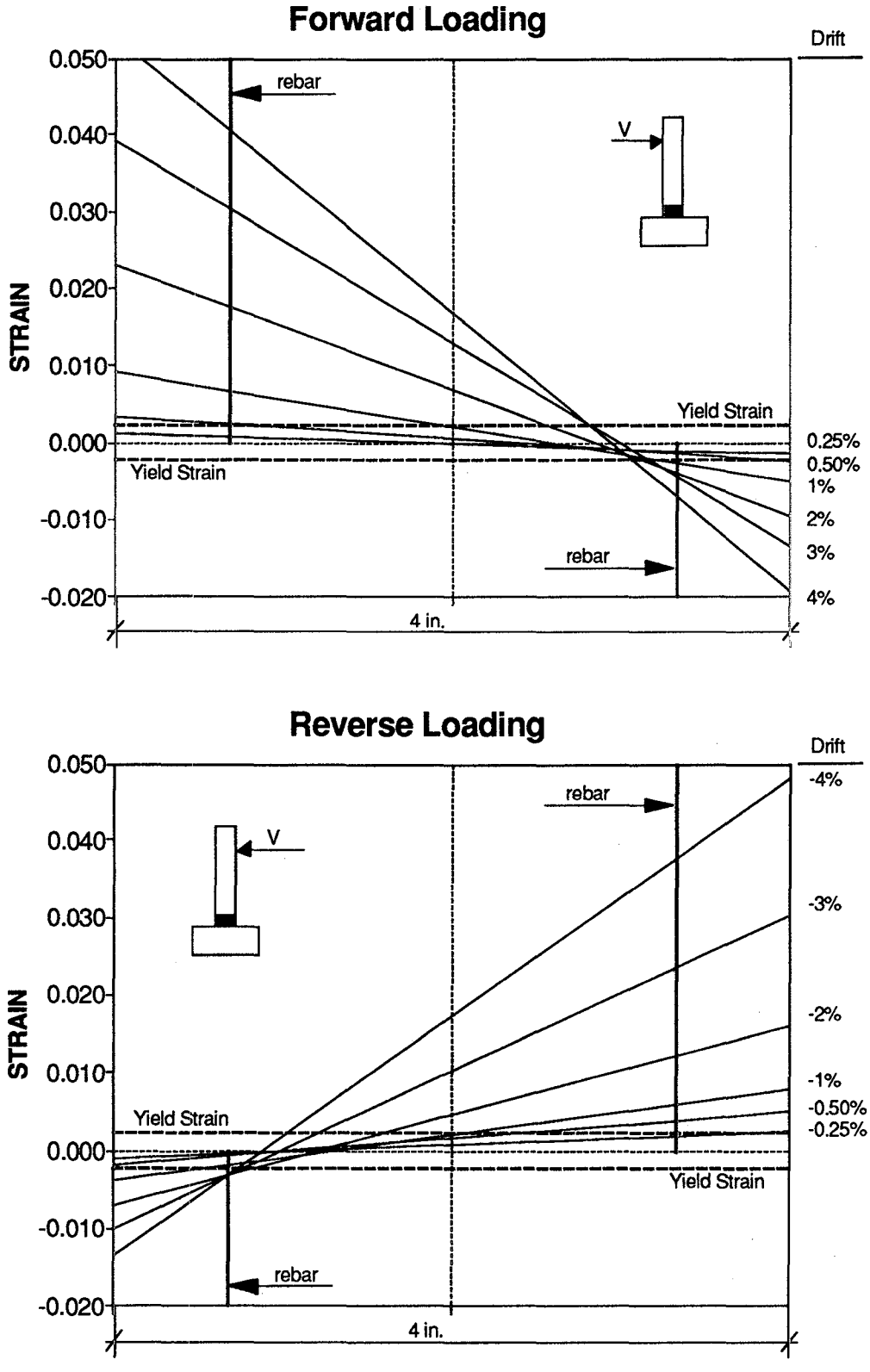

Fig. 2.27 Strain Profiles Lower Gage Length for Specimen 3 (Lower Exterior Column with lap splice)

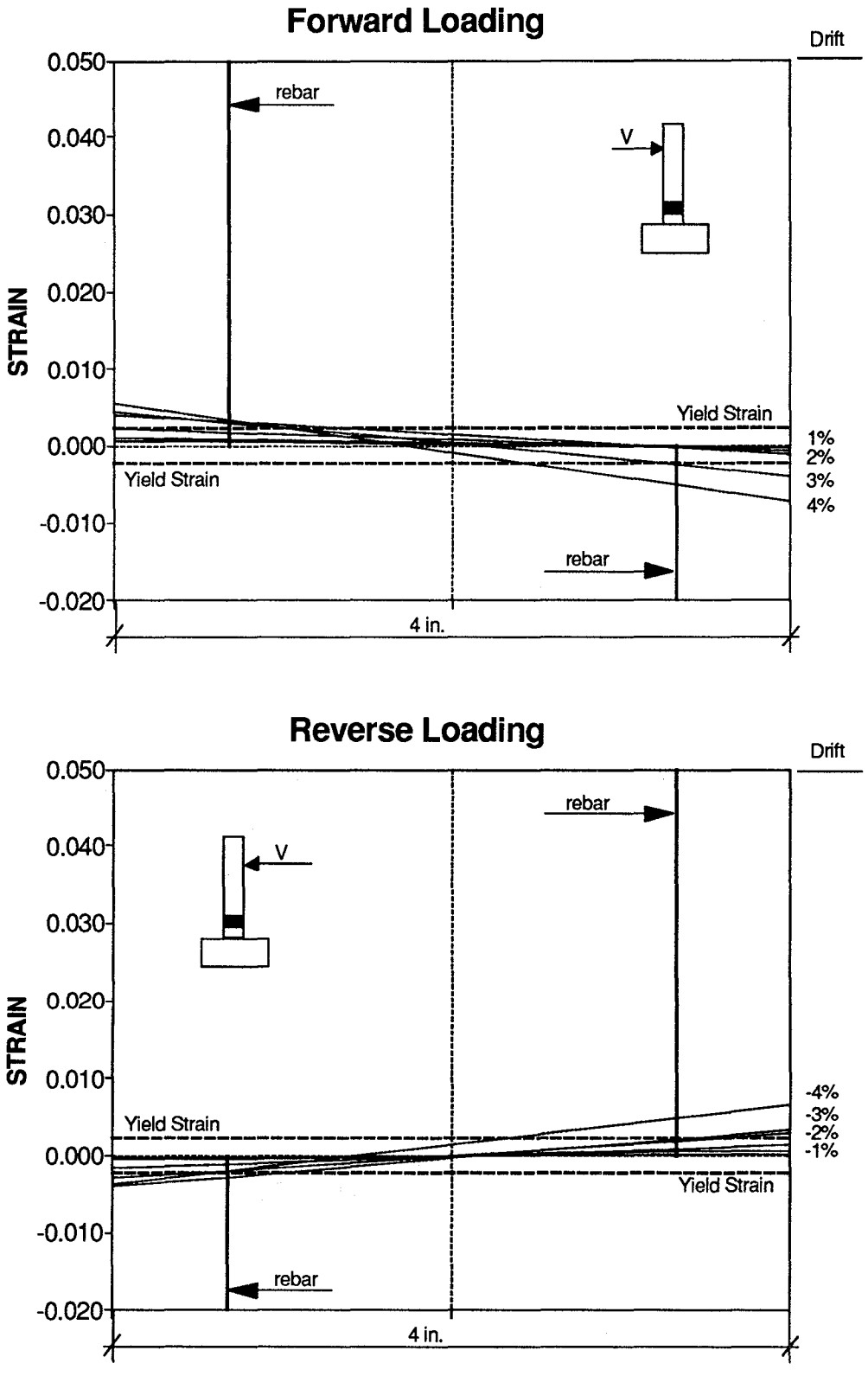

Fig. 2.28 Strain Profiles Upper Gage Length for Specimen 3 (Lower Exterior Column with lap splice)

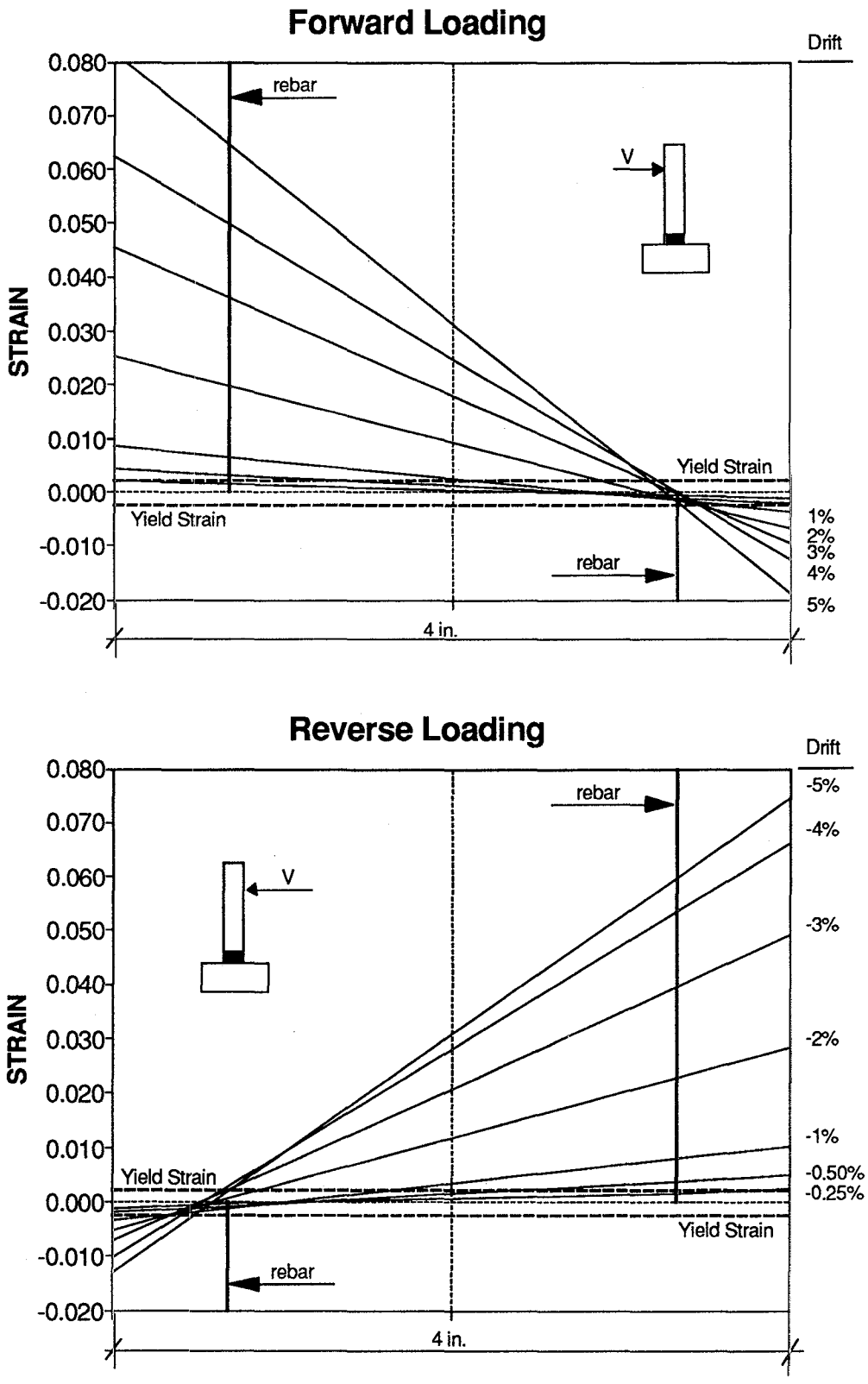

Fig. 2.29 Strain Profiles Lower Gage Length for Specimen 4 (Upper Exterior Column)

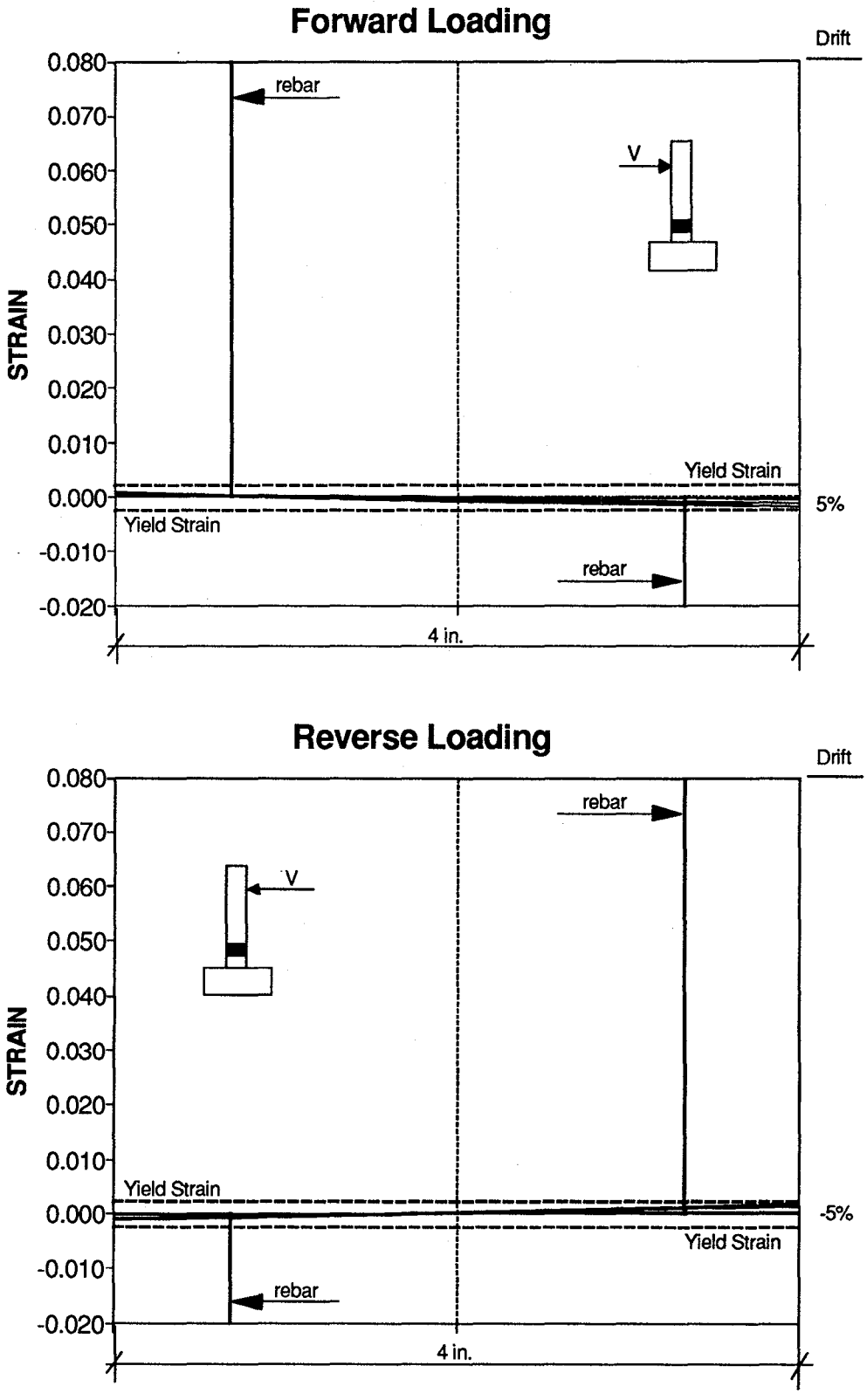

Fig. 2.30 Strain Profiles Upper Gage Length for Specimen 4 (Upper Exterior Column)

2.10 Conclusions

From the results of the four column specimens tests, the following conclusions can be drawn:

1. As might be expected, columns without lap splices showed better energy dissipation characteristics than columns with lap splices.

2. In all cases, the nominal lateral strength was exceeded except for the reverse loading of Specimen 3. For Specimens 1 and 3 (columns with lap splice) the flexural capacity exceeded the nominal strength by up to 25% and up to 10% for Specimens 2 and 4 (columns without lap splice). For all Specimens, maximum strength was observed between 2 and 3% drift which was followed by the onset of spalling of the cover concrete.

3. A higher level of axial load caused more strength degradation and the presence of lap splices accelerated the degradation even more. In addition, Specimen 3 (column with lap splice) showed increasing degradation as axial load decreased.

4. Column failure was flexurally dominated, either resulting from concrete crushing and subsequent buckling of the longitudinal bars (Specimens 1 and 2), or from low cycle fatigue of the longitudinal reinforcement (Specimens 3 and 4).

SECTION 3

EXPERIMENTAL BEHAVIOR OF NON-SEISMICALLY DESIGNED BEAM-COLUMN SUBASSEMBLAGES

3.1 Introduction

In this section, an experimental study of gravity load designed beam-column subassemblages subjected to lateral forces is presented. Design, construction, instrumentation, and testing of an exterior and interior beam-column connection are described. The subassemblage specimens were cast as companions at the same time the one-third scale model building was being constructed. Details of the design of the model building are presented in Part I of this series of evaluation method reports (Bracci et.al. 1992a). It is important to note that the subassemblages included the floor slab and the transverse beams. The slabs were loaded with additional kentleges intended to represent the same situation as the joint connection and components in the complete model building structure. The interior specimen was subjected to a constant level of axial load. To represent the fluctuation in axial forces in the perimeter columns of a building under lateral load, the exterior specimen testing started at a specific axial load equal to the tributary gravity load and then this load was varied by algebraically adding a quantity proportional to the horizontal force. The specimens were subjected to increasing amplitudes of reversed cyclic lateral displacements comparable to seismic loading until failure occurred.

3.2 Design and Construction of the Subassemblage Specimens

3.2.1 Units Size

The dimensions of the specimens were determined based on the interstory height and the typical spans of the building, and assuming that the points of contraflexure were to occur at the mid height and mid span as shown in Fig. 3.1. However, the upper column of both specimens was made sufficiently high (28 in.) to have room to connect the horizontal and vertical actuators. Detailed geometry of both specimens is shown in Fig. 3.2.

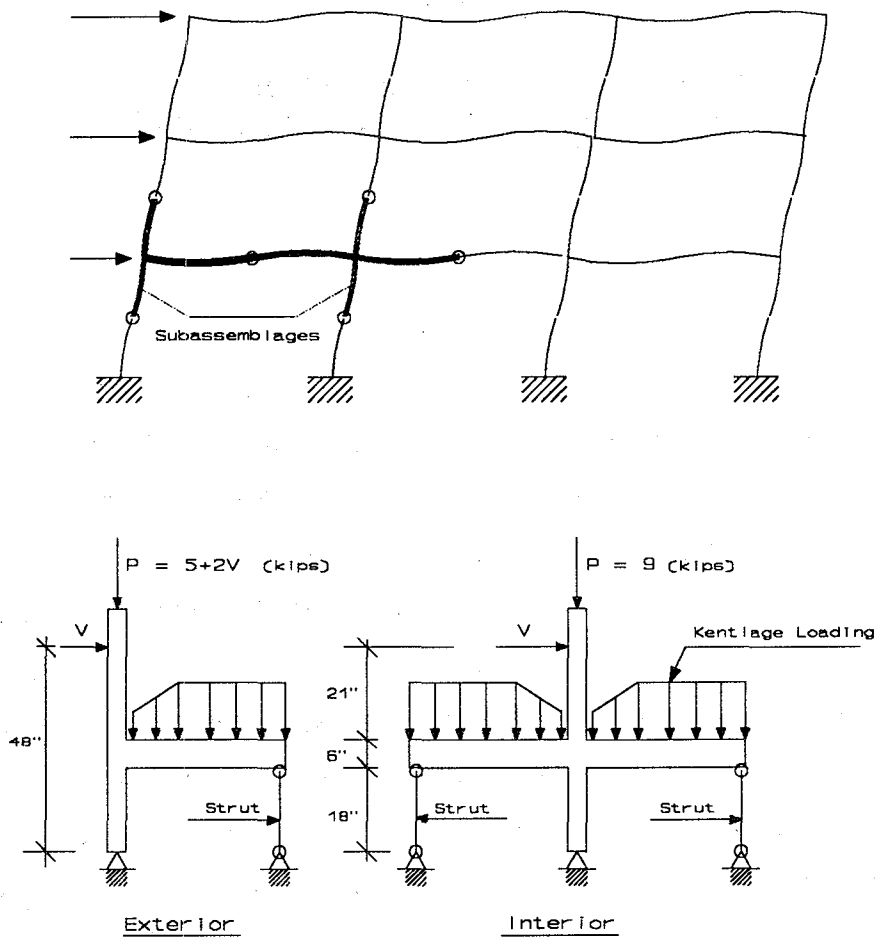

Fig. 3.1 Subassemblage Modeling

3.2.2 Specimen Reinforcement

Four 0.225 in. diameter deformed rebars (D4) were used to longitudinally reinforce the upper and lower columns, giving a volumetric ratio of 0.01. The upper column had a 6 in. lap splice at the floor slab level and was reinforced with some extra steel in the upper part. This reinforcement was to prevent local failure due to the concentration of stresses from the application of the loads from both actuators. Details of the columns' reinforcement are shown in Fig. 3.3.

The transverse beam for both specimens and the longitudinal beam for the interior specimen were reinforced using three 0.225 in. diameter deformed rebars (D4) at the top and two at the bottom. The top reinforcement was continuous across the joint while the bottom bars were extended just to the middle of the column. Details of the reinforcement are shown in Figs. 3.4 and 3.5.

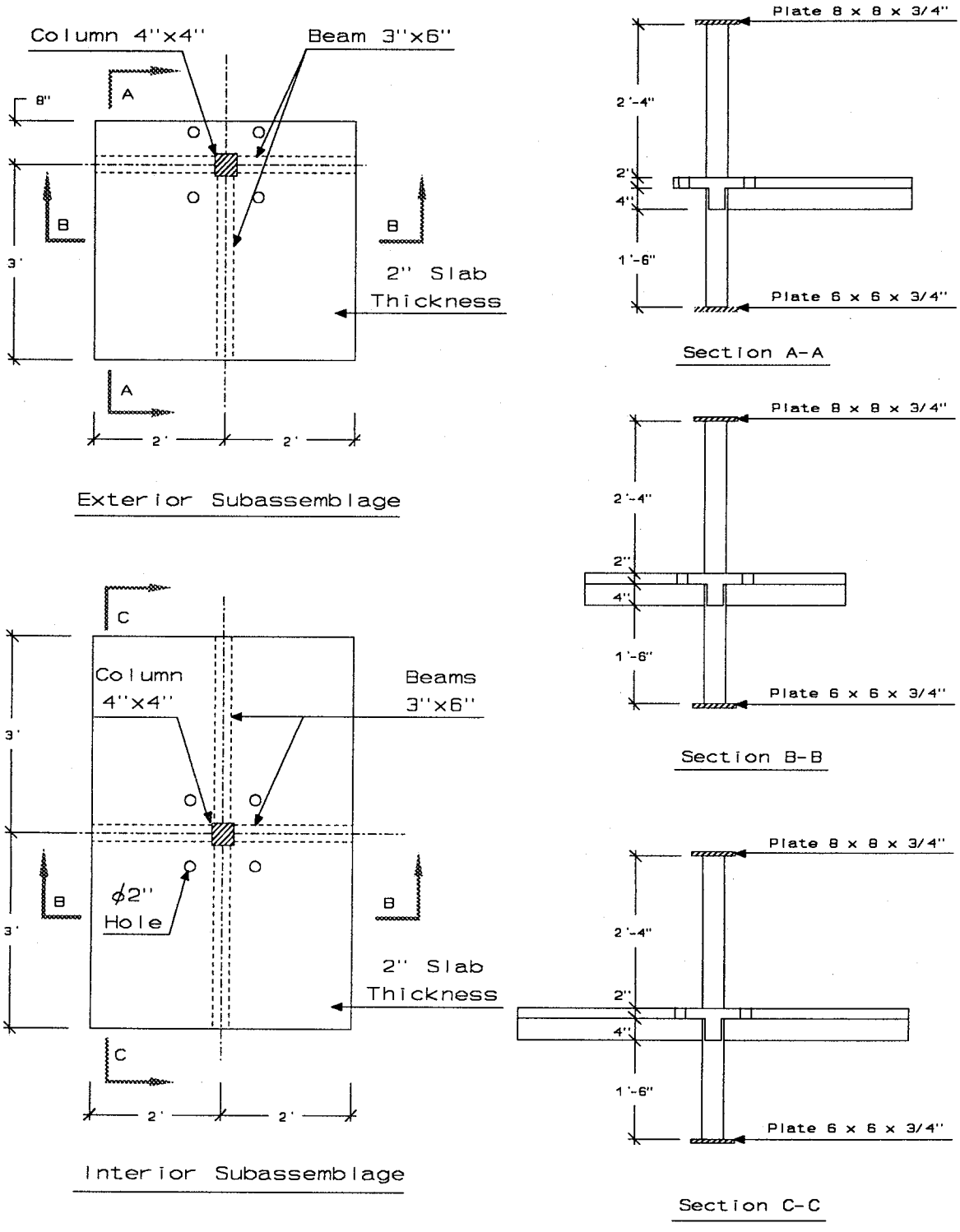

Fig. 3.2 Subassemblages Geometry

The longitudinal beam for the exterior specimen was reinforced as follows: two 0.252 in. diameter deformed rebars (designated D5 with area A_b=0.05 in^2) at the top and two 0.225 in. diameter deformed rebars (D4) at the bottom. The top bars were extended to the far face of the joint and anchored with a 2 in. hook at 90 degrees while the bottom bars were just extended to the middle of the column. Details of the reinforcement are shown in Fig. 3.6.

The steel used for transverse reinforcement was 0.12 in. diameter smooth round wire (#11 gage). Spacing of the hoops for the columns was 4 in. except for the lap splice zone and the upper part of the top column where the hoops were 2 in. apart. It is important to note that two horizontal hoops were placed inside the joint of the exterior specimen while the interior specimen had no joint core steel at all. Details of the reinforcement are shown in Fig. 3.3. Spacing of the hoops for the beams was 2.67 in.. Closed hoops were used where three top longitudinal bars appeared and open "U" hoops in the remaining sections of the beams. Details of the reinforcement are shown in Figs. 3.4 to 3.6.

The slabs were reinforced with an upper and lower layer of 2 x 2 in. galvanized welded wire mesh of 0.10 in. diameter (#12 gage). The mesh was cut and placed to the dimensions shown in Fig. 3.7. The top layer of slab steel was passed continuously over the longitudinal beam steel, while the bottom steel was butted up against the beam stirrups.

Four 2 in. diameter pipes were precisely located to provide room for the vertical bars that give the reaction to apply the vertical load to the column.

3.2.3 Construction of the Beam-Column Subassemblage Specimens

The specimens were built simultaneously with the model building as well as with the group of columns representing the upper half of the first story. Each specimen was built in three stages. The construction procedure valid for both specimens is described as follows:

Lower Column

Firstly, the transverse hoops were fixed to the vertical bars by tie wire. Next the cages were placed in the forms constructed from plywood, 2x4, and 2x10 in. wood. The formwork for the lower column, the beams and the slab was built as a unit.

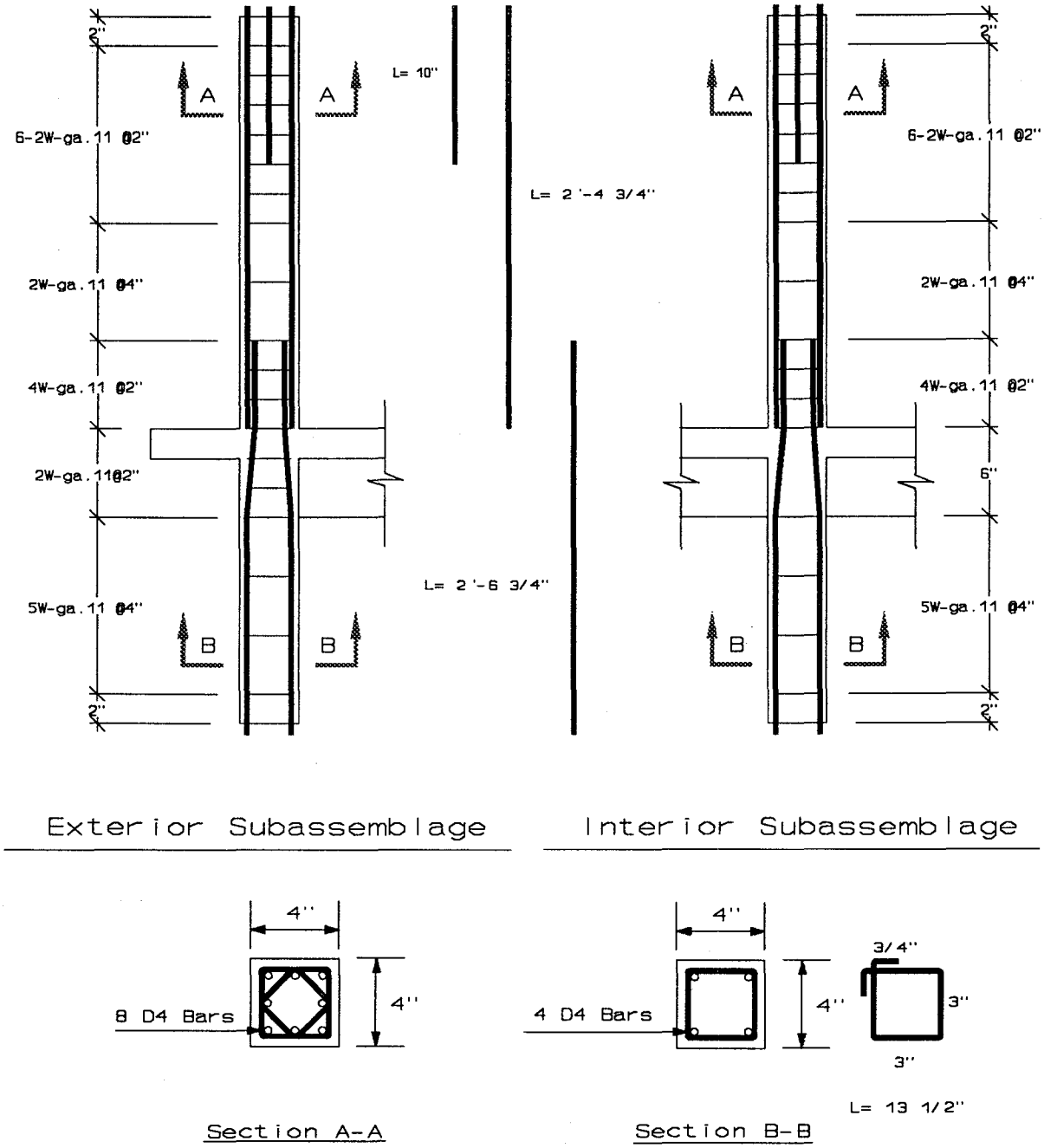

Fig. 3.3 Reinforcement Details of the Columns

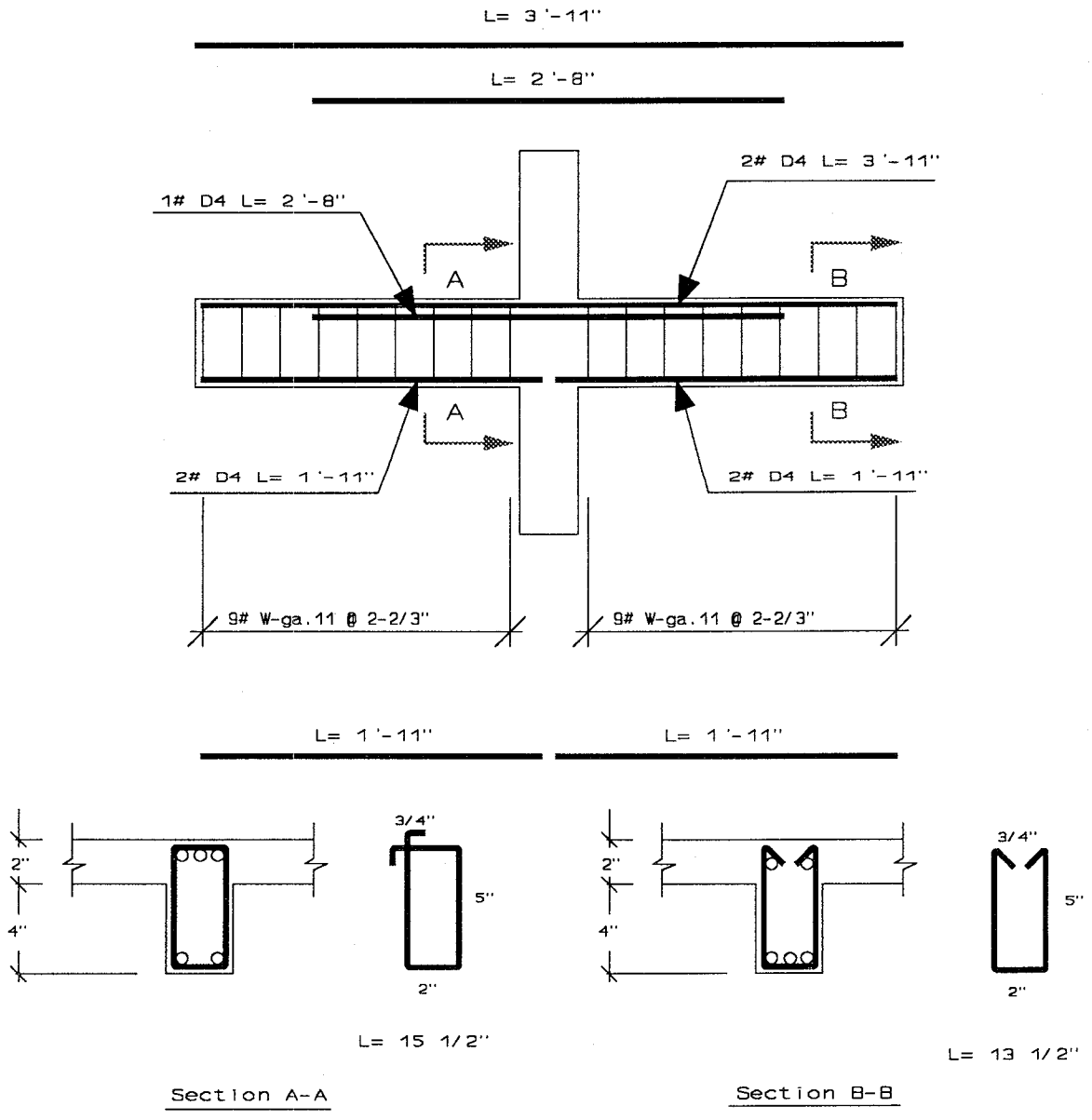

Fig. 3.4 Transverse Beam for both Subassemblages

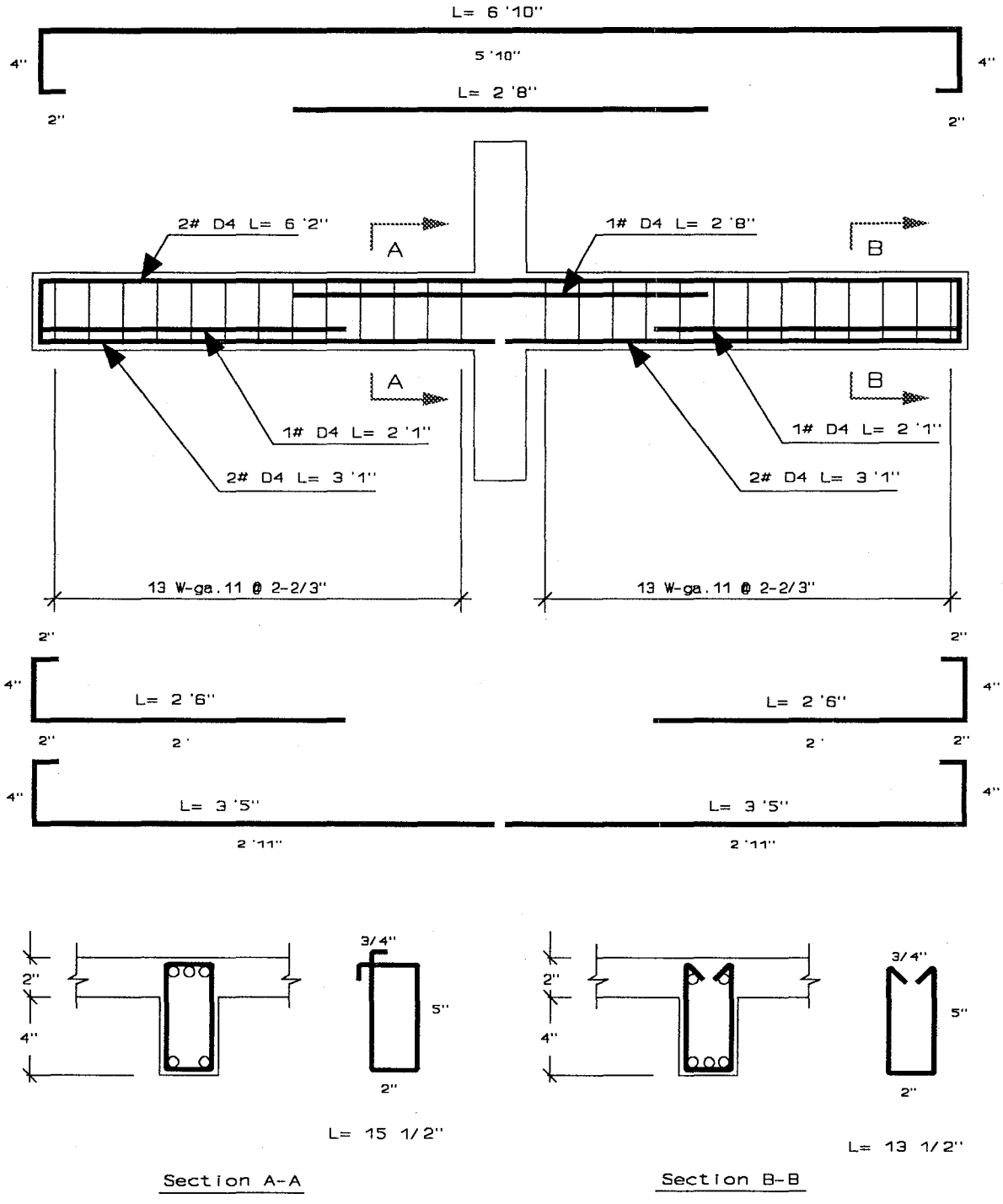

Fig. 3.5 Longitudinal Beam for Interior Subassemblage

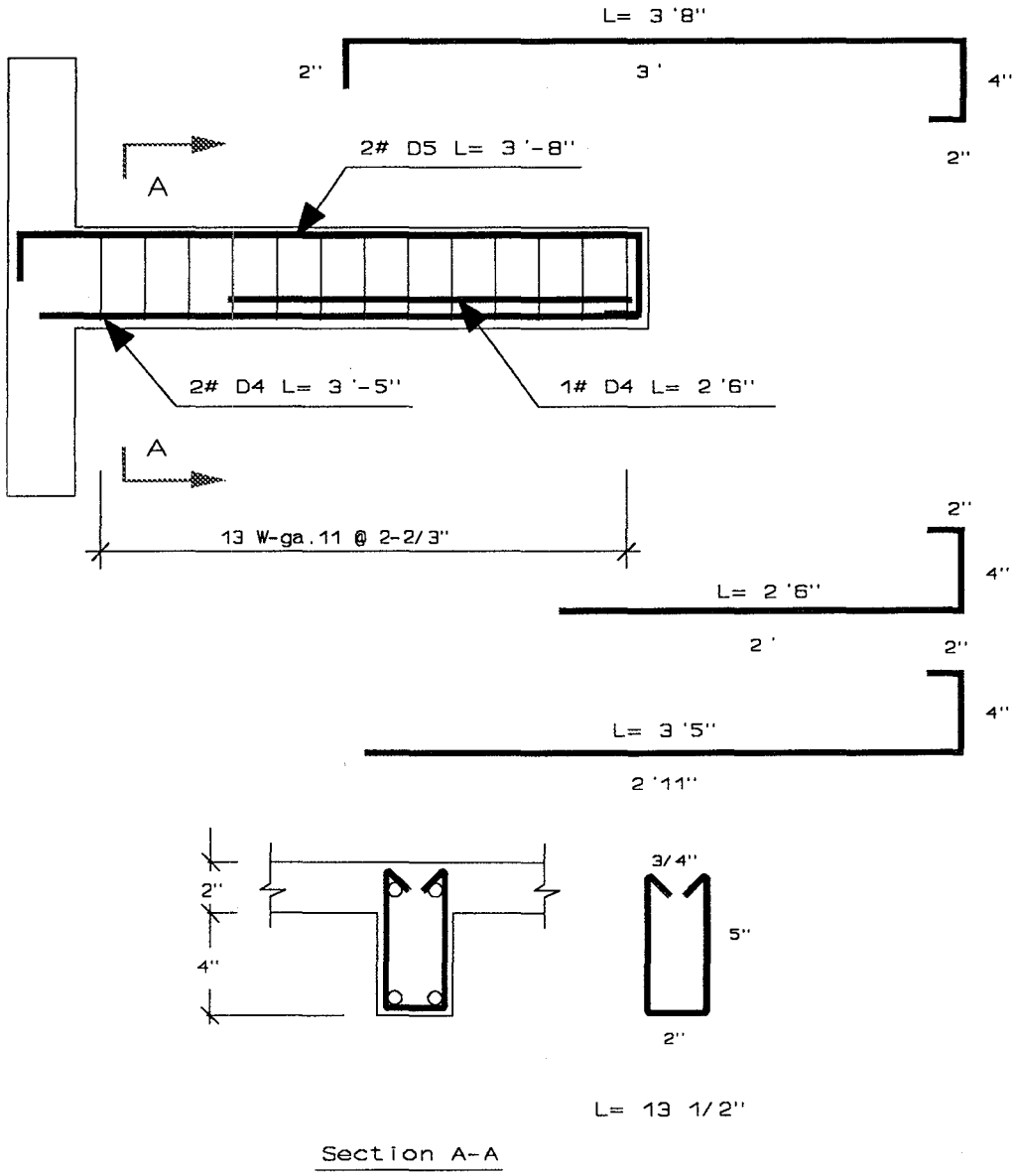

Section A-A

Fig. 3.6 Longitudinal Beam for Exterior Subassemblage

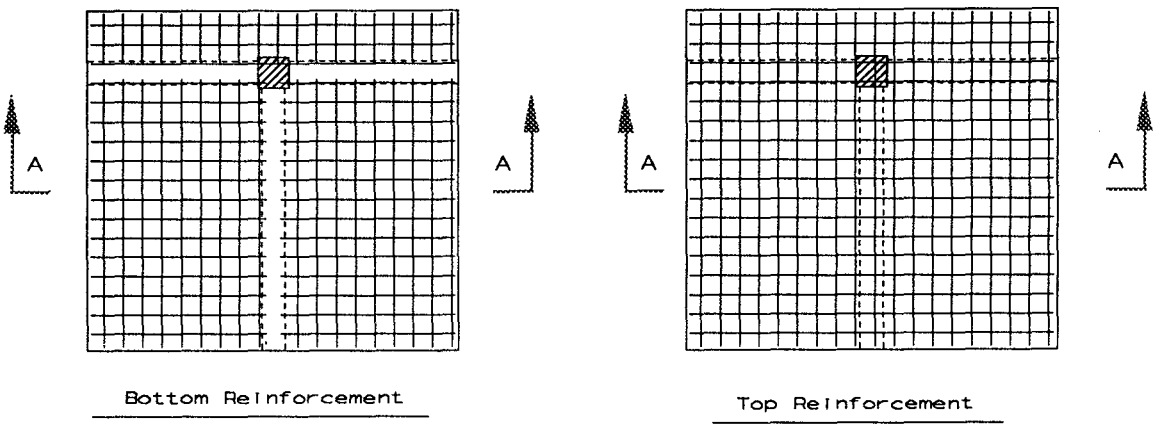

Exterior Subassemblage

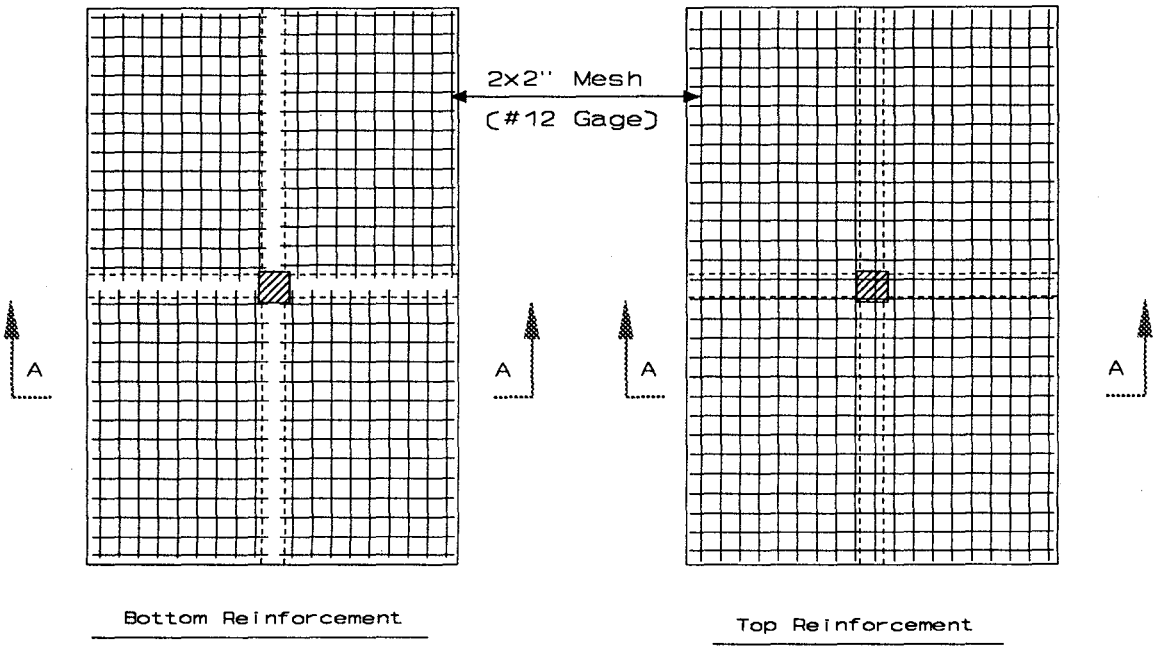

Interior Subassemblage

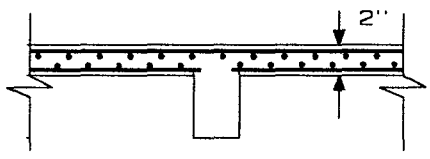

Section A-A

Fig. 3.7 Slab Reinforcement

After the formwork was assembled, a 6 in. x 6 in. x 3/4 in. steel plate was fixed to the bottom of the formwork of the lower column. This plate was necessary to secure the longitudinal bars of the column and later on to attach the specimen to the test rig. Four 5/16 in. diameter threaded rods were passed through pre-bored holes near the joint. These rods were used for mounting potentiometers for curvature measurements.

The concrete was placed in the formwork and mechanically vibrated. Test cylinders 8 x 4 in. diameter were also cast.

Slab and Beams

The transverse hoops were fixed to the horizontal bars by tie wire. The steel cages for both beams were set in place. Six wood plugs were screwed to the formwork of the slab at each end of the longitudinal beams. These plugs were removed after casting and provide the holes for the connection of the pin-ended struts shown in Fig. 3.8. Four 2 in. diameter wood plugs were placed and screwed to the plywood form of the slab, and the four 2 in. diameter pipes were placed. The slab reinforcing mesh was placed. Where the 2 in. diameter pipes intercepted the mesh bars, these were cut and tack welded to the pipes to provide continuity.

Four 5/16 in. diameter threaded rods were placed in two pairs on each longitudinal beam, and passed through pre-bored holes near the joint and in pieces of 2x4 that did not allow the rods to move during pouring of the concrete. These rods were used for fixing potentiometers for curvature measurements.

Concrete was placed in one lift in the formwork and mechanically vibrated. Test cylinders 8 x 4 in. diameter were also cast.

Upper Column

Firstly, the transverse hoops were fixed to the vertical bars by tie wire. Next, the steel cage was placed in the same formwork built from construction plywood used for the individual columns described in Section 2. The formwork was set in place and stiffened by pieces of 2x4 connected to the sides of the slab formwork. Then, the four 5/16 in. diameter threaded rods, used for mounting potentiometers for curvature measurements, were passed through the pre-bored holes near the base of the column.

The concrete was placed in the formwork and mechanically vibrated. Test cylinders 8 x 4 in. diameter were also cast.

After one day of curing, the formwork of the upper column was removed and the concrete moist cured. The remainder of the formwork was removed about two weeks before testing.

3.3 Modification of the Test Rig

The general set up of the test rig is shown in Fig. 3.8.

The L shaped reaction frame used for the test of the single columns described in Section 2 was modified for the subassemblage experiments. The modification consisted of attaching two W 8x10 and one W 6x20 to the back of the vertical column, hence providing sufficient room to locate the specimen and to accommodate the horizontal actuator. The W 8x10 were connected by four 1 in. diameter bolts to the vertical column and the W 6x20 was connected by four ½ in. diameter bolts to each W 8x10.

Additionally, an 8½ x 18 x 2 in. steel plate was fixed close to the vertical column. This plate was used to fix the pin-ended strut support for the longitudinal beam of the interior specimen.

As for the column specimens described in Section 2, the same ± 5.5 and ± 22 Kip capacity MTS servo-hydraulic loading actuators were used to apply the horizontal and vertical load respectively.

The piston of the vertical actuator was passed through a pre-bored hole of an 8 x 16 x 1½ in. steel plate, and the body of the actuator was bolted to that plate. Two 3/4 in. diameter vertical bars were connected to the plate and to 6 x 16 x 1 in. steel plates. Then four ½ in. diameter bars were connected between the pairs of 6 x 16 x 1 in. and another two 3/4 in. diameter bars were connected to the bottom plates and to the test rig hence providing the necessary reaction to apply the axial load to the column. Details of the seating of the vertical actuator on the column are illustrated in Fig. 2.6. Detail of the connection of the vertical bars are presented in Fig. 3.10.

Load cells were connected in series with both actuators. The horizontal actuator was connected to the W 6x20 by four 3/4 in. diameter threaded bolts. At the opposite end, the actuator hinge was connected to the column by four ½ in. threaded rods and a pair of 2 x 6 x ½ in. steel plates.

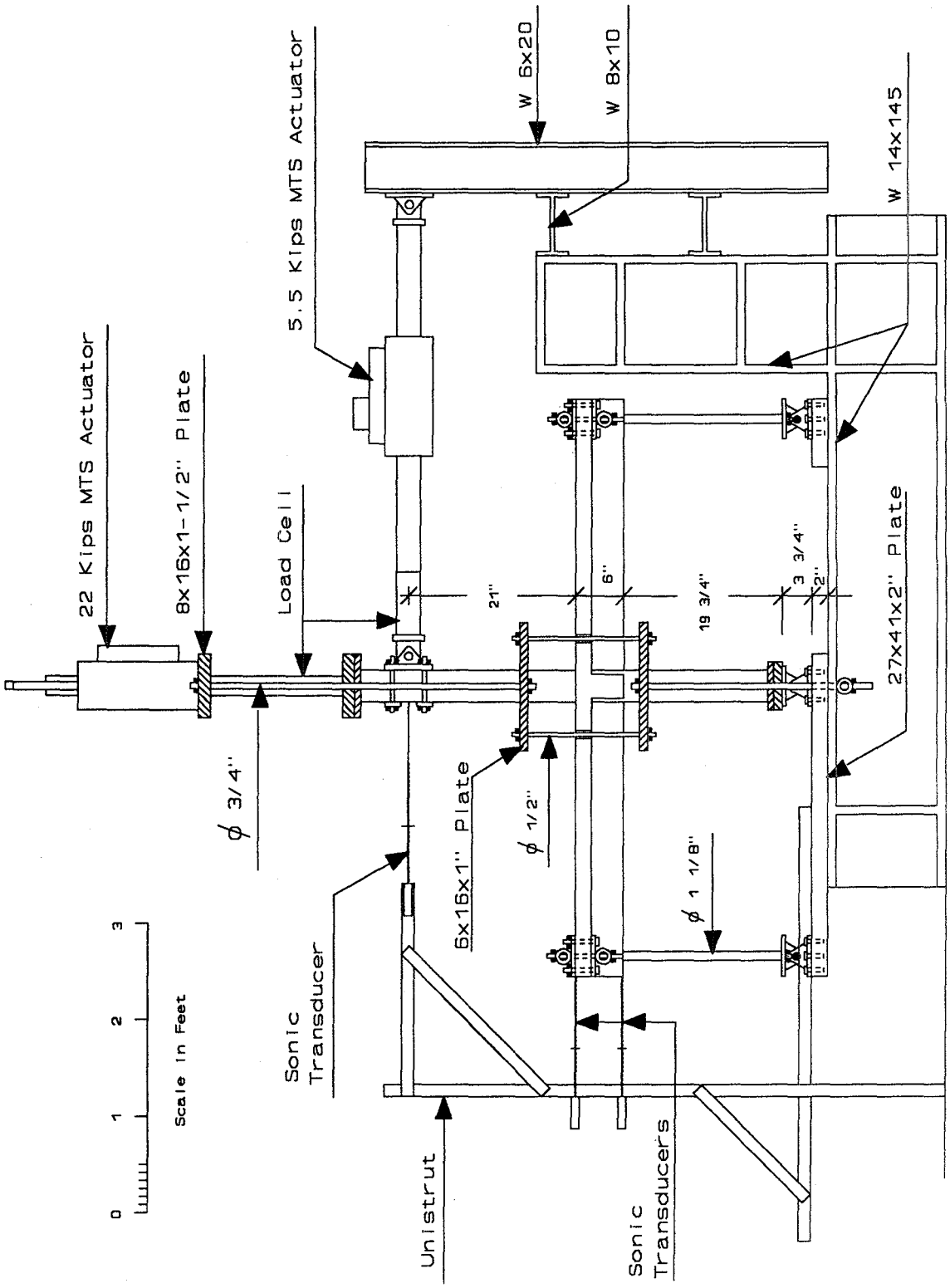

Fig. 3.8 Set up of Test Rig and Subassemblage

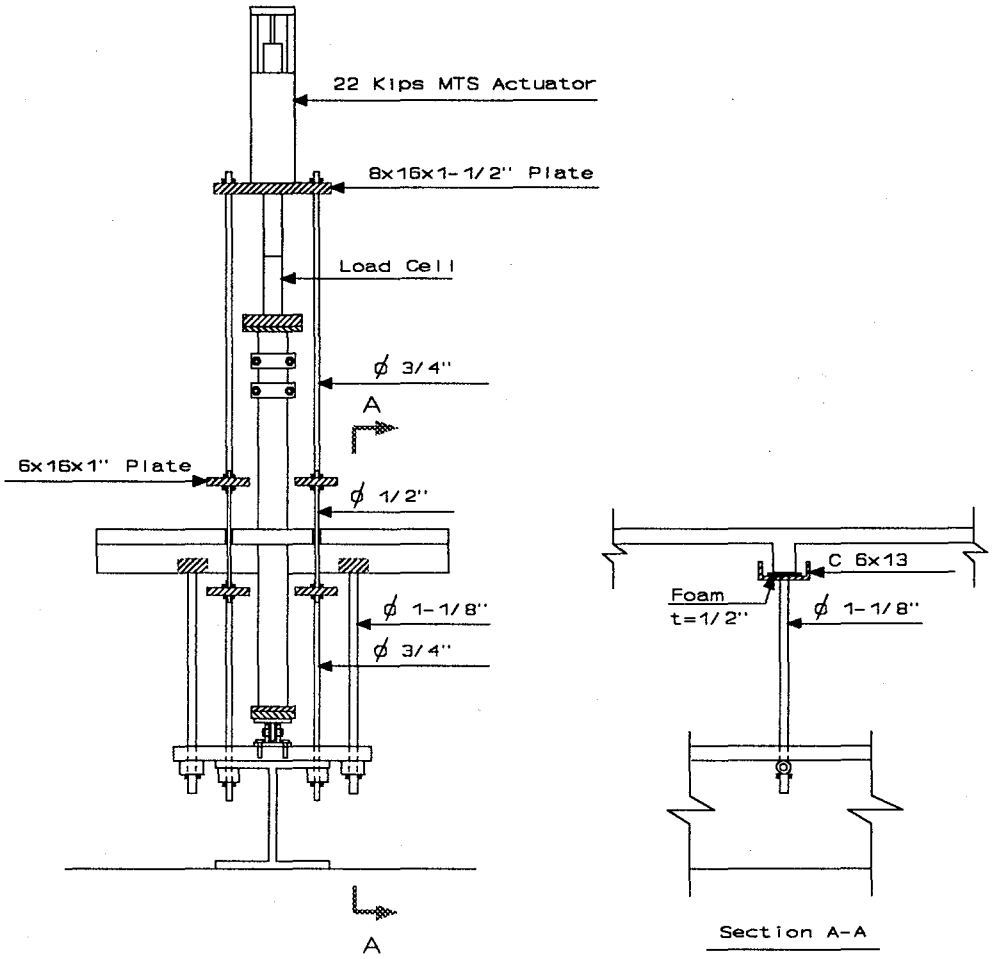

Fig. 3.9 Transverse Section of Test Rig and Subassemblage

3.4 Instrumentation

The lateral and vertical loads applied to the specimen were measured by the load cells shown in Fig. 3.8. Before testing, the load cells were calibrated using a Tinius Olsen Testing machine to an accuracy of ± 0.01 Kip.

Lateral displacements of the specimen were measured using sonic transducers located at three different heights: at the level of application of the horizontal load, and at the top and bottom of the longitudinal beam. In order to measure column displacements relative to the base, all the transducers were attached to a reference frame constructed from Unistrut that was fixed to the 27 x 41 x 2 in. horizontal steel base plate.

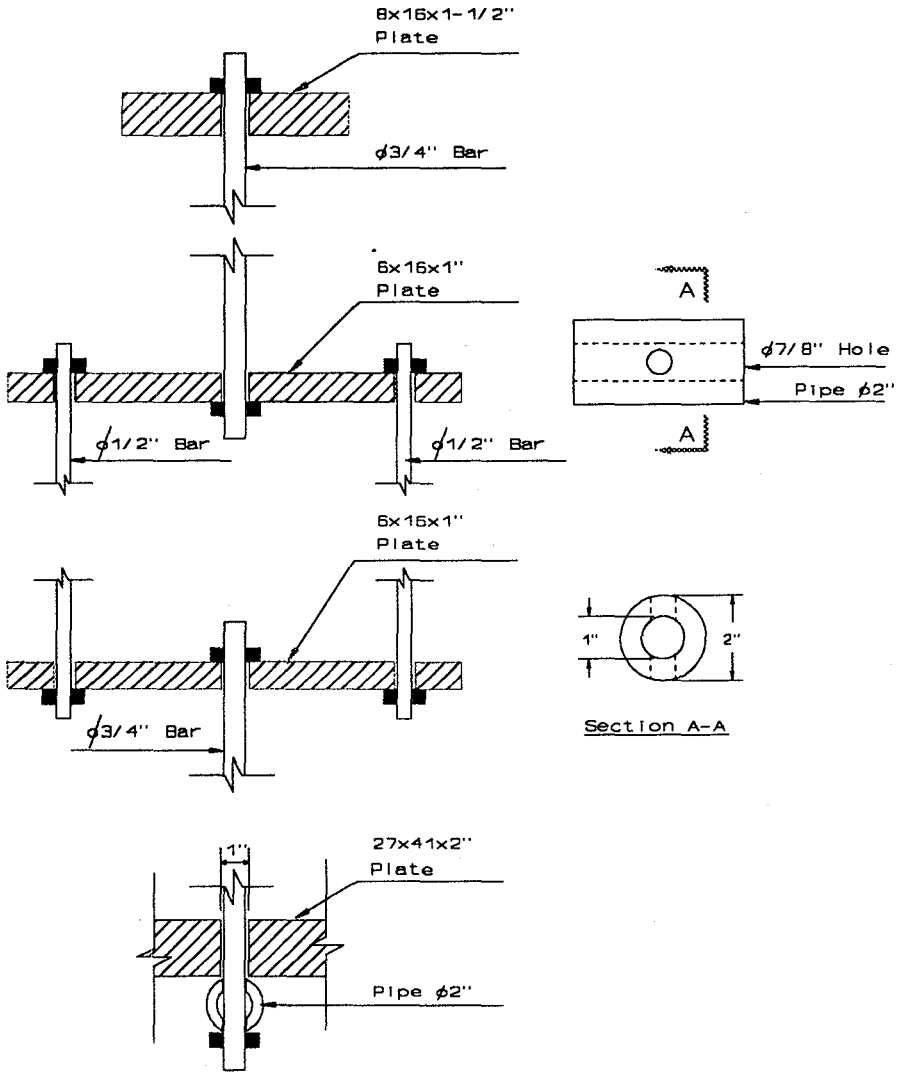

Fig. 3.10 Detail Connection Vertical 3/4" diameter bars and Test Rig

Two pairs of linear potentiometers were attached to each side of the columns and longitudinal beams to enable the curvatures to be measured. Fig. 3.11 shows the potentiometers attached to aluminum plates which were in turn connected to the 5/16 in. diameter threaded rods which were previously installed in the columns and beams. These potentiometers allowed the average curvatures to be calculated over two sequential gage lengths of 1.75 in. in each of the potential plastic hinge regions. All the potentiometers were calibrated with a digital volt meter to give a displacement record with an accuracy of ±0.0001 in.

During testing, output voltages of all the instruments were recorded using an Optim Megadac 5533A Data Acquisition System at a 1 Hz frequency. From these records, force-drift and moment-curvature relations could be calculated.

During the test, the lateral load measured by the load cell and the lateral displacement measured by the sonic transducer at that level were recorded on a Type 7090A analogue Hewlett-Packard X-Y Plotter.

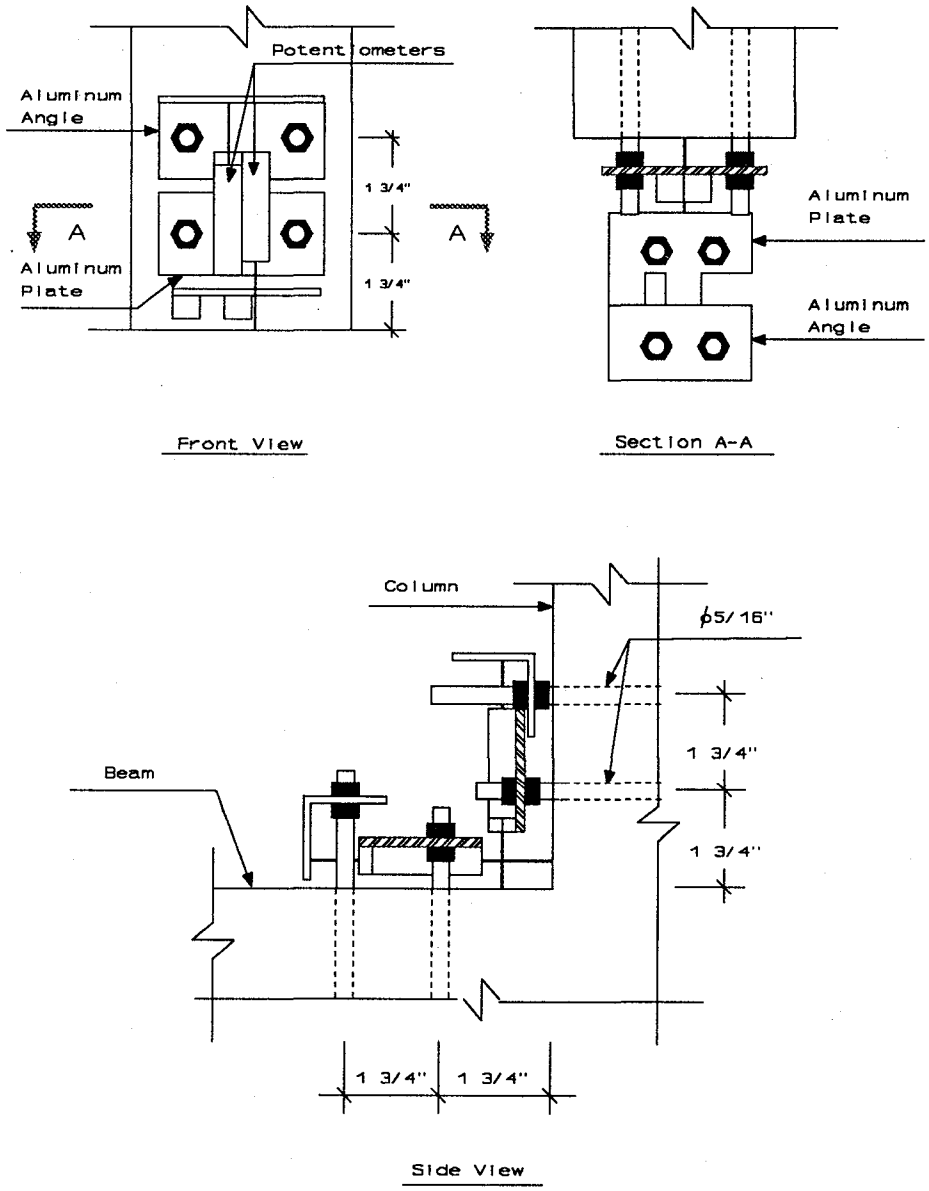

Fig. 3.11 Details Potentiometers

3.5 Material Properties of the Subassemblage Specimens

The concrete pouring sequence together with the measured concrete cylinder strengths at 28 days and at testing are shown in Fig.3.12. Details about material properties of the specimens are presented in Section 1.5.1. Note that specimens 2 and 4 were constructed at the same time as the lower columns for the subassemblages.

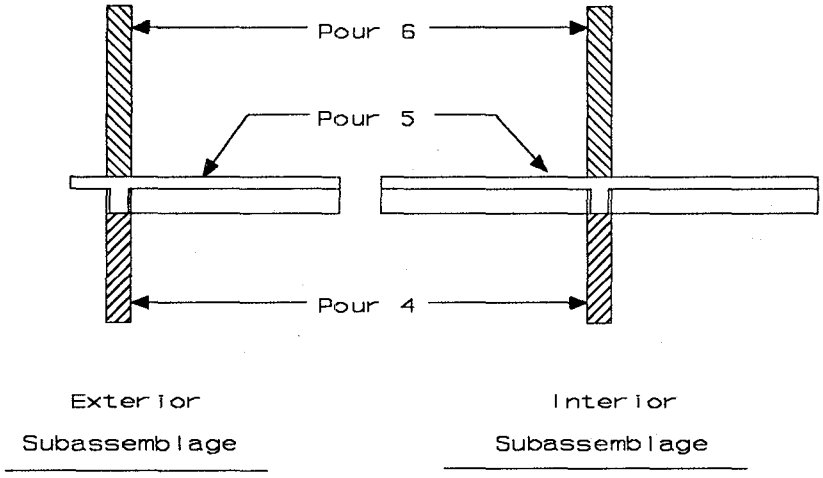

POUR	CONCRETE STRENGTH AT 28 DAYS (ksi)	CONCRETE STRENGTH AT TESTING (ksi)
4	4.35	4.35
5	5.00	5.00
6	4.35	4.35

Fig. 3.12 Concrete Pouring Sequence

3.6 Testing Procedure

3.6.1 Specimen Preparation

After the installation of the specimen in the test rig, the instrumentation was mounted and calibration of the data recording devices completed. A safety frame made of two W 8x31 columns and Unistrut was installed in order to hold the vertical actuator in case of an unexpected failure of the system. Both specimens were painted with a white lime solution in order to facilitate the identification of cracks during testing. The position of the rebars was drawn on the sides of columns and beams with a black pencil.

Finally, lead bricks weighing 26 lb. each were precisely placed on the slab in order to represent the loading on the prototype beams and bottom columns. The 2 x 4 x 8 in. lead bricks were placed in two stages described as follows:

1. While the rigid vertical links at the end of the longitudinal beams were kept lose, enough lead bricks were added to produce the gravity load moments in the beams. The required value of the moment was determined by an elastic analysis of a longitudinal frame of the model building.

2. The rigid vertical links were fixed and the additional lead bricks necessary to complete the vertical load were set in place. Diagrams showing the position of the lead bricks are presented in Fig. 3.13.

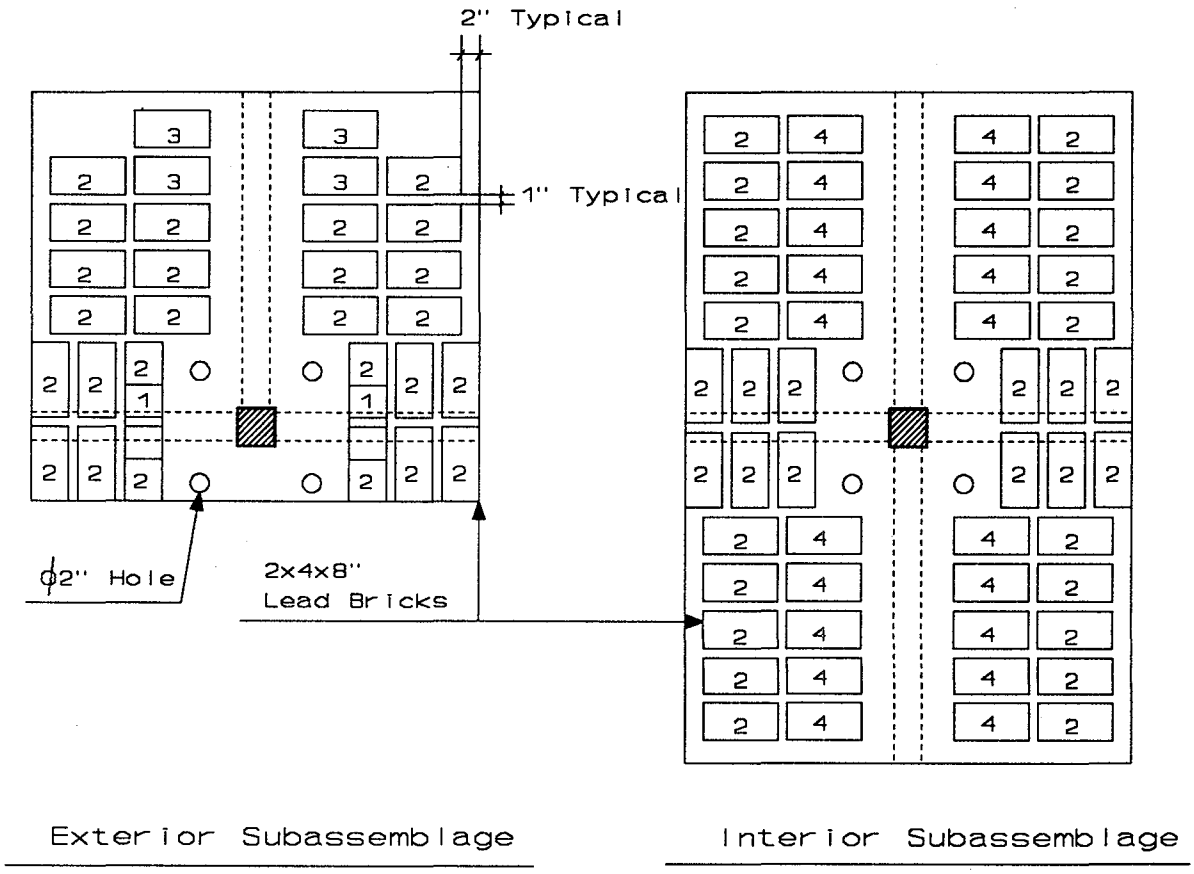

Fig. 3.13 Position of Lead Bricks

3.6.2 Specimen Testing

The initial phase of testing each specimen consisted of two complete displacement controlled cycles at each drift level of ±0.25%, ±0.50%, ±1%, ±2%, ±3%, and ±4%. The second phase of testing was either continued at 4% drift, or the test geometry was reconfigured, as explained in the following sections. The displacement function used for the initial phase is presented in Fig. 3.14. The signal for the horizontal actuator was a sine wave with frequency of 0.02 Hz for the three drift levels below 2% and 0.01 Hz for all other cycles. The control was made using the measured displacement coming from the sonic transducer at the level of the applied load.

At the end of each two cycle set the displacement was held, cracks were marked, photographs taken, and the displacement amplitude adjusted for the next two cycles. Readings from all the instruments were recorded continuously by the Megadac Data System using a sampling at the rate of 100 samples per cycle of loading. In addition, VHS video tape was used to provide a visual record.

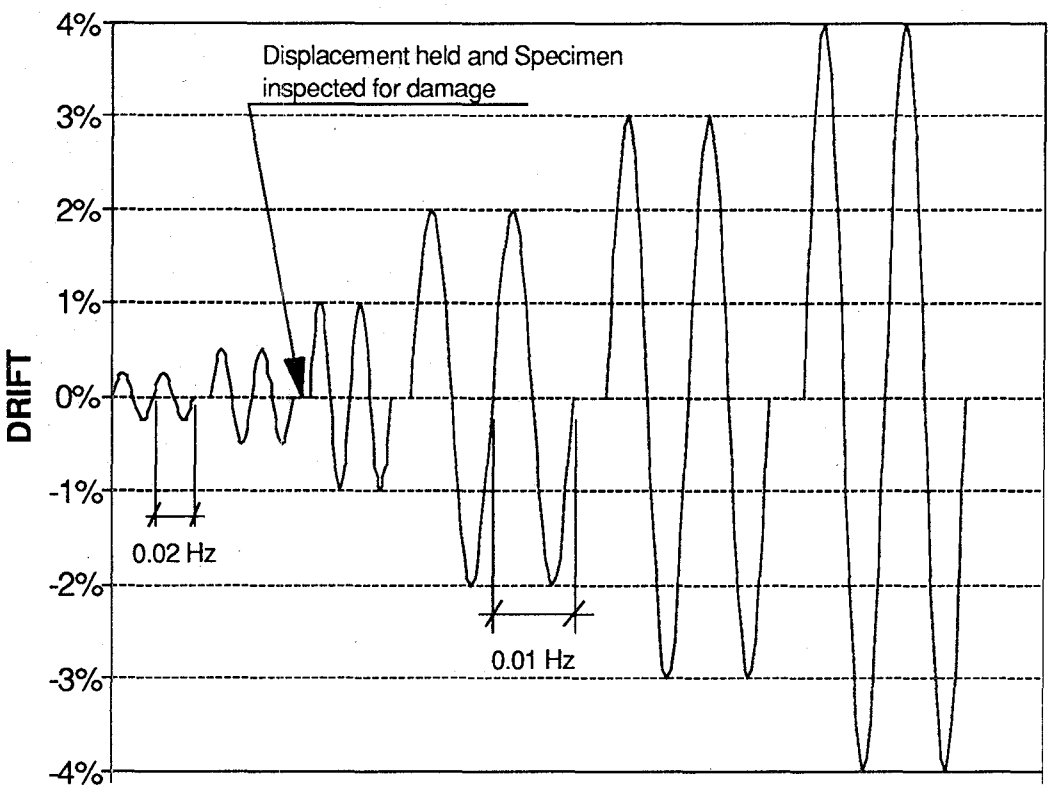

Fig. 3.14 Test Program

3.7 Experimental Results for Exterior Subassemblage

Visual Observations

This section presents general observations made during the test of the subassemblage. Photographs taken during testing are shown in Fig. 3.15.

The vertical load P, applied by the vertical actuator was given by the following proportional loading relationship

$$P = 5 + 2V \quad (Kips) \tag{3.1}$$

where V = the lateral load provided by the horizontal actuator.

This was intended to represent the fluctuation of the vertical load in an exterior column of a frame as previously discussed for Specimens 3 and 4 in Section 2.

After the lead bricks were placed, flexural cracks were observed in the exterior face of the column and in the top face of the longitudinal beam. Testing was carried out to the drift levels mentioned in Section 3.6.2. At the end of the ±1% drift cycles, flexural cracks were observed at mid height of the upper column, column-beam interfaces and transverse beam-slab interface. After completion of the ±3% drift cycles, the concrete cover started spalling at the corners of the top and bottom columns. The crack at the transverse beam-slab interface increased and ran all across the slab. After two more cycles at 3% drift, more spalling was observed. During the ±4% drift cycles, pull-out of the bottom bars of the longitudinal beam was evident. Large cracks at the beam-column and beam-slab interfaces opened and closed as the lateral load was cycled back and forth. Crushing of the concrete increased especially in the bottom column-beam interface. The longitudinal reinforcement of the column was exposed at the bottom column-beam interface, and damage to the joint was evident. The testing program continued with 40 cycles at ±4% drift without significant degradation. At this stage, the potentiometers and lead bricks were removed, the cycling rate was set in 0.5 Hz and the drift level in ±5%. After 220 cycles, only some additional spalling was observed. The axial load was then increased to a constant value of 22 Kip and after 4 cycles the subassemblage failed due to crushing of the joint core concrete. Fig. 3.15 shows progressive damage to the subassemblage.

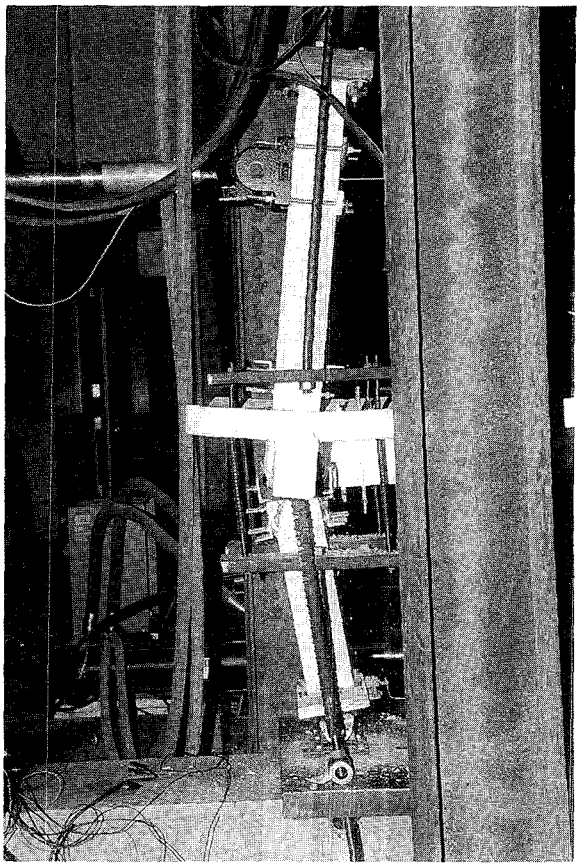

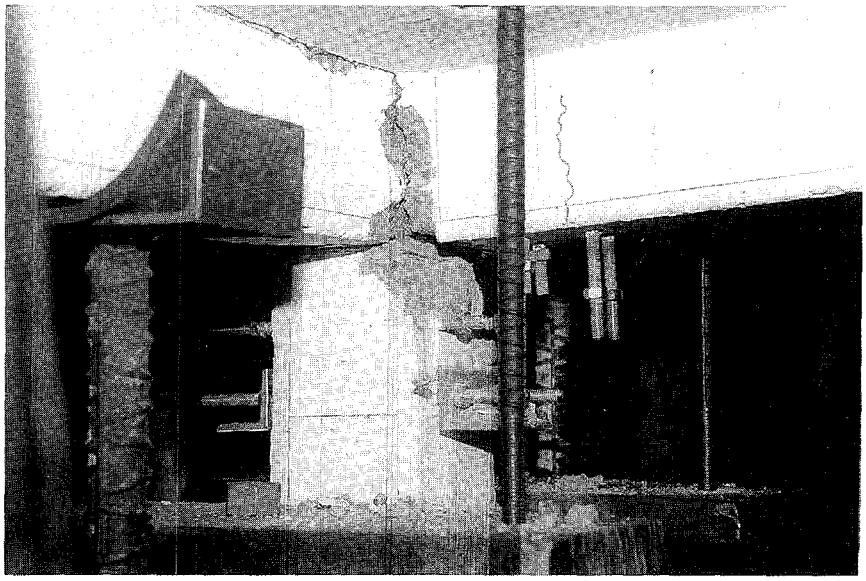

Fig. 3.15 Progressive Damage Exterior Subassemblage

Hysteretic Performance

Load-drift and load-rotation hysteresis curves of the three potential plastic hinge zones are presented in Figs. 3.17 and 3.18. Drift is defined as the relative displacement measured by the upper sonic transducer with respect to the base. Rotations were calculated for each member using the measurements from the potentiometers. This represents the plastic rotation over the end 3.5 in. in each member adjacent to the joint.

The nominal capacity of the specimen is plotted as a dashed line superimposed on the load-drift and load-rotation curves. For each case, there is an illustration besides the graph showing the type of failure mechanism considered in order to define the nominal capacity curve. Once the failure mechanism was chosen, an expression of the lateral force, as a function of the individual nominal capacities of the members and the geometry of the subassemblage, was derived from equilibrium.

In all cases, the nominal capacity of each member (column or beam) was evaluated based on the usual ACI strength calculations. For the top column of the subassemblage (column with lap splice), only the net steel area at the base of the column has been considered. Also, the distance from the edge of the column to the center of the vertical bars was taken as 1 in. instead of 0.67 in. (for the bottom column), since the vertical reinforcement coming from the bottom column was slightly bent inside the joint and repositioned in order to be able to get the lap splice with the reinforcement of the top column. For the nominal capacity of the beams, three cases were considered for positive moment capacity: bottom bars fully bonded, partially bonded, and unbonded. For the case of fully bonded, the total area of bottom steel was considered, whereas for the unbonded case no bottom steel at all was taken into account. Finally, for the case of partially bonded, the area of bottom reinforcement was multiplied by 0.50, since this factor is the ratio of the embedment length to the development length of the bars. For negative moment capacity of the beam, two cases were contemplated: full participation of the top slab reinforcement, and no participation at all. In all, positive and negative moment capacity cases, a T-section beam was considered.

Narrow hysteresis loops were observed. Clearly the short anchorage of the beam's bottom reinforcement and the subsequent pull-out of the bars caused about 55% difference in maximum

strength between forward and reverse loading. Forward loading resulted in little strength degradation after pull-out of the bottom steel occurred. However, under reverse loading, significant strength degradation with successive cycling was apparent due to continued crushing of the concrete at the bottom of the beam.

Some pinching of the hysteresis loops was observed. However, this was mainly due to loss of bond in the lap splice of the top column and in the beam's bottom reinforcement.

The lateral load-drift graph shows that for positive loading, the nominal capacity given by partial bonding of the beam's bottom steel was exceeded but as expected the nominal capacity for full bond was not attained. For reverse loading, it is evident that just part of the top slab reinforcement contributed to the actual strength since the maximum strength laid between the two extremes curves (full and no participation of slab steel).

The load-rotation graphs show that the nominal capacity of the columns was exceeded for reverse loading, whereas for positive loading the demand was about 50% of the nominal capacity. This was due to the pull out of the beam's bottom steel which relieved the demand on the columns.

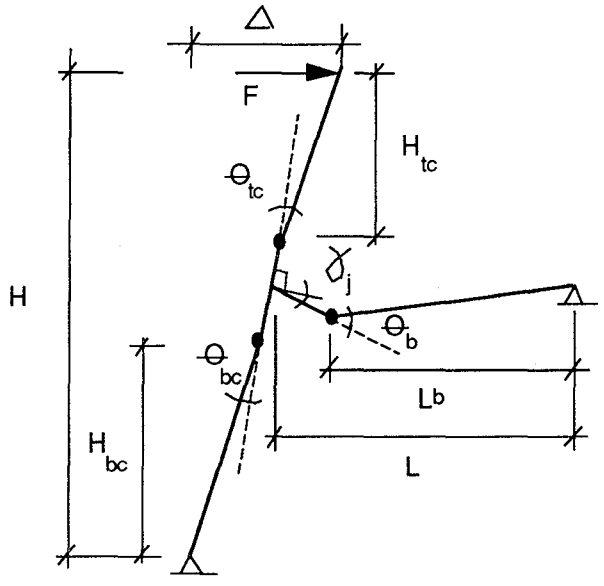

Fig. 3.16 Idealized Plastic Deformed Geometry

Fig. 3.16 shows the idealized plastic deformed geometry of the subassemblage. The total applied drift can be calculated from geometry, as follows:

$$D_u=\frac{\Delta}{H}=\theta_e+\theta_b\frac{L_b}{L}+\theta_{tc}\frac{H_{tc}}{H}+\theta_{bc}\frac{H_{bc}}{H}+\gamma_j \tag{3.2}$$

in which

$D_u=\frac{\Delta}{H}$ = *total applied drift*

θ_e = *elastic component of drift for the total subassemblage*

$\theta_b,\theta_{tc},\theta_{bc}$ = *plastic rotations of the beam, top and bottom columns, respectively.*

L,H = *length of the beam and height of the subassemblage*

L_b,H_{tc},H_{bc} = *distance from the plastic hinge to the end of the member (beam, top and bottom columns, respectively)*

γ_j = *apparent joint core plastic shear displacement*

The elastic drift and the plastic rotations were evaluated for the first peak at each drift level, and Fig. 3.19 presents the drift contribution of each member versus the total drift for each drift amplitude. By rearranging Eq. (3.2) as follows, joint shear distortion can be inferred as the difference between the total applied drift, and the component sums of the plastic and elastic displacements:

$$\gamma_j= D_u-\left[\theta_e+\theta_b\frac{L_b}{L}+\theta_{tc}\frac{H_{tc}}{H}+\theta_{bc}\frac{H_{bc}}{H}\right] \tag{3.3}$$

The drift contribution graph shows no evidence of joint shear distortion to the overall displacement for reverse loading, whereas there is notable contribution for the case of forward loading at 3 and 4% drift amplitudes. This is in good agreement with the spalling of the concrete cover observed at the exterior face of the joint, as mentioned in the visual observations. Forward loading presents a large beam drift contribution from the early stages, whereas reverse loading shows even contribution from columns and beam. This difference is due to the beam's weakness under forward loading caused by pull-out of the bottom reinforcement resulting in large inelastic beam rotations.

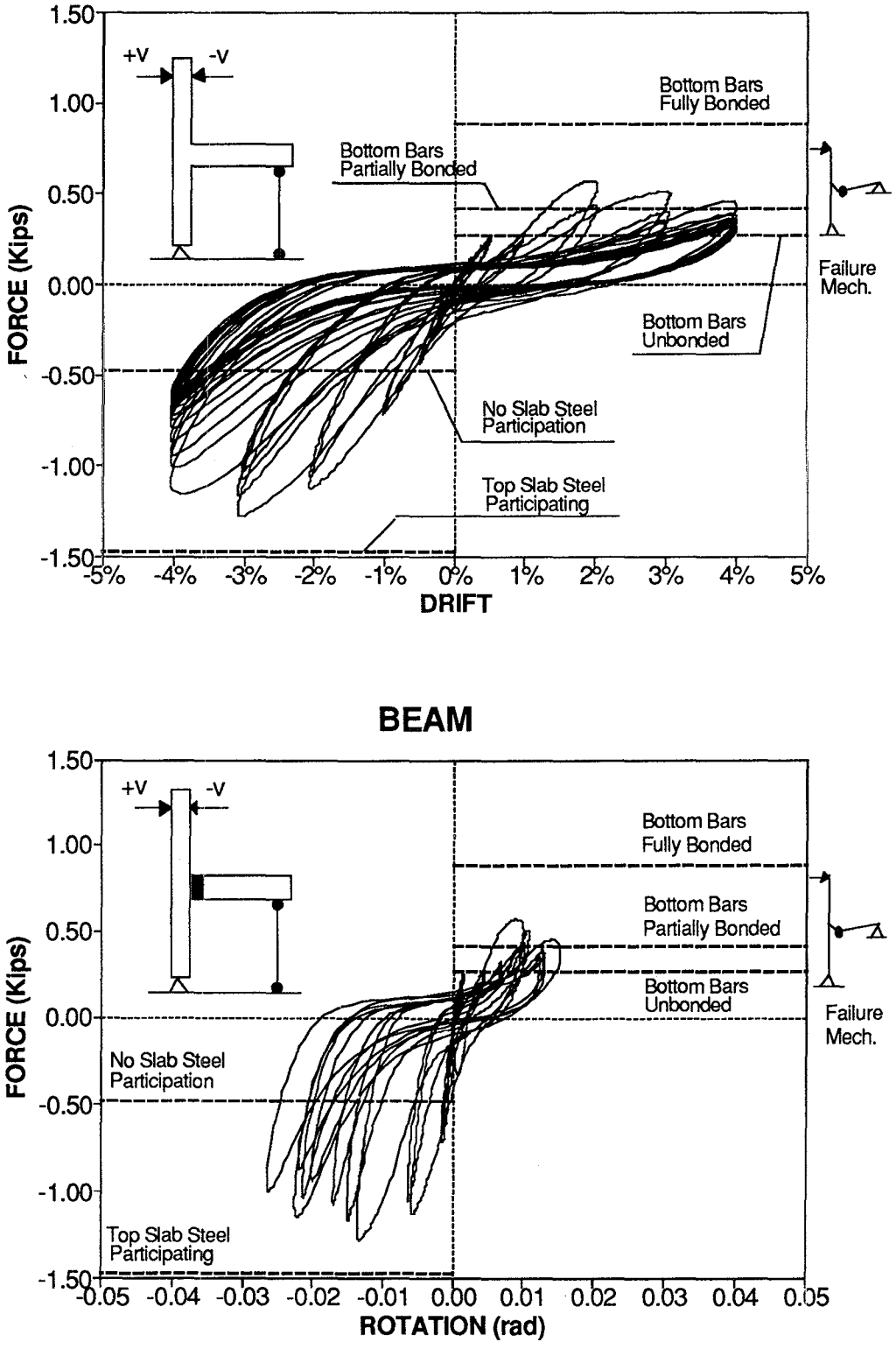

Fig. 3.17 Experimental Lateral Load-Drift and Lateral Load-Beam Rotation graphs for Exterior Subassemblage

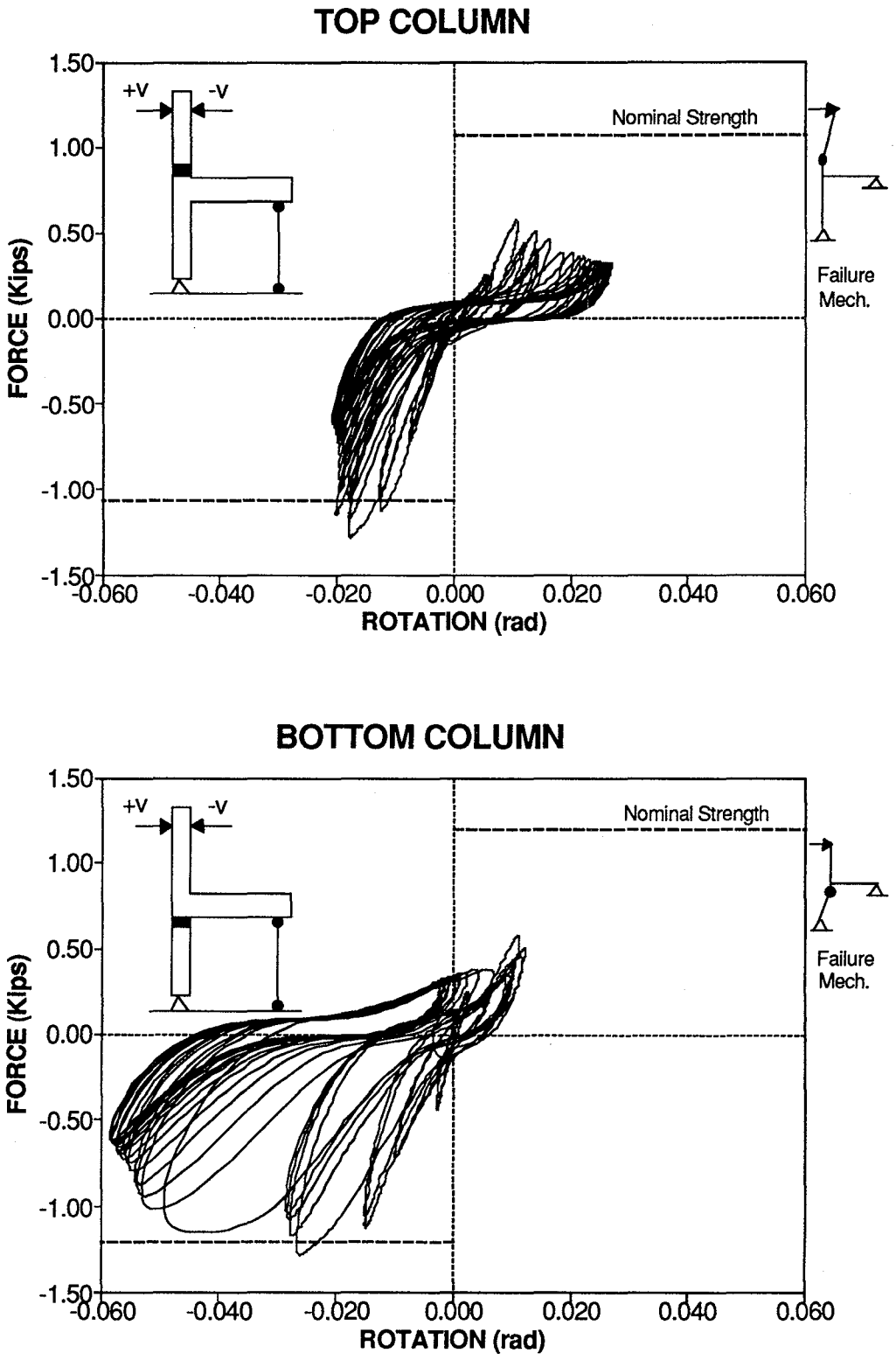

Fig. 3.18 Experimental Lateral Load-Rotation graphs Top and Bottom Columns for Exterior Subassemblage

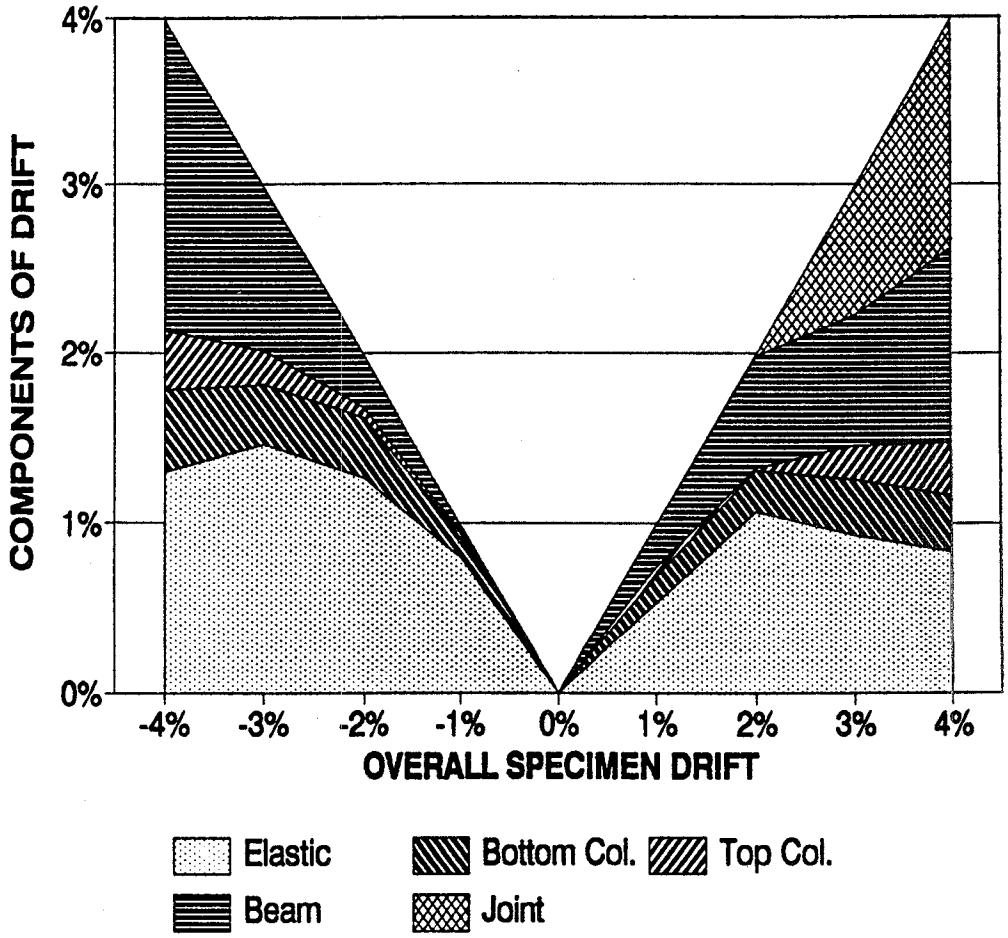

Fig. 3.19 Drift Contributions from each member
Exterior Subassemblage

Section Curvatures

Lateral load-curvature hysteresis curves are presented in Figs. 3.20 to 3.22. For each member (columns and beams), two graphs are shown in which the curvature was evaluated over the two sequential 1.75 in. gage lengths. Herein the first gage length refers to the 1.75 in. gage length adjacent to the joint.

The load-curvature graphs (Figs. 3.20 to 3.22) show that most of the damage and the plastic deformation took place at the critical sections being right at the joint's faces.

Section Strains

In addition to the lateral load-curvature graphs, for each gage length, strain profile graphs calculated at the first cycle of each successive drift peak are presented in Figs. 3.23 to 3.25. Based on the observation of the lateral load-curvature graphs, strain profiles which were going to show almost no deformation were omitted.

The strain profiles also show concentration of the plastic deformation and the damage at the first gage length of the members.

As mentioned in the visual observations, the concrete cover started spalling at ±3% drift level for the columns and beam. Table 3.1 lists the compression strain values for the first gage length for the different members.

Table 3.1 Experimental Apparent Spalling Strain
Exterior Subassemblage

Loading	Top Column	Bottom Column	Long. Beam
Forward	0.017	---	0.005
Reverse	0.010	0.013	0.027

In general, the experimental apparent spalling strain values are in good agreement with respect to the spalling strains observed at the end of the cylinder tests presented in Fig. 1.6.

3.8 Experimental Results for Interior Subassemblage

Visual Observations

In this section, general comments collected during testing of the subassemblage are presented. Photographs taken during testing are shown in Figs. 3.26 and 3.27.

The axial load was kept constant at 9 Kip throughout the test. Testing was carried out in three stages.

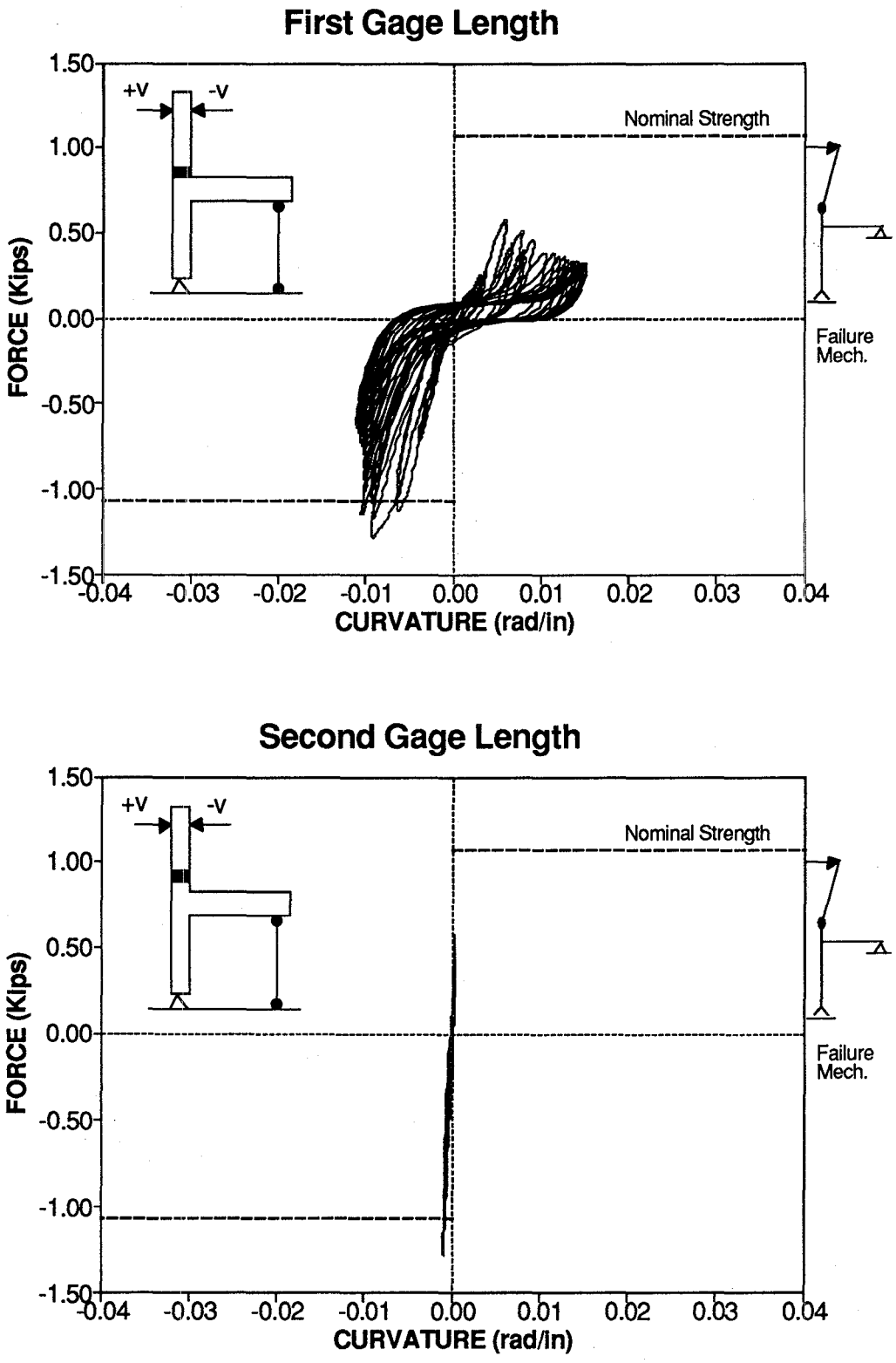

Fig. 3.20 Experimental Lateral Load-Curvature graphs
Top Column - Exterior Subassemblage

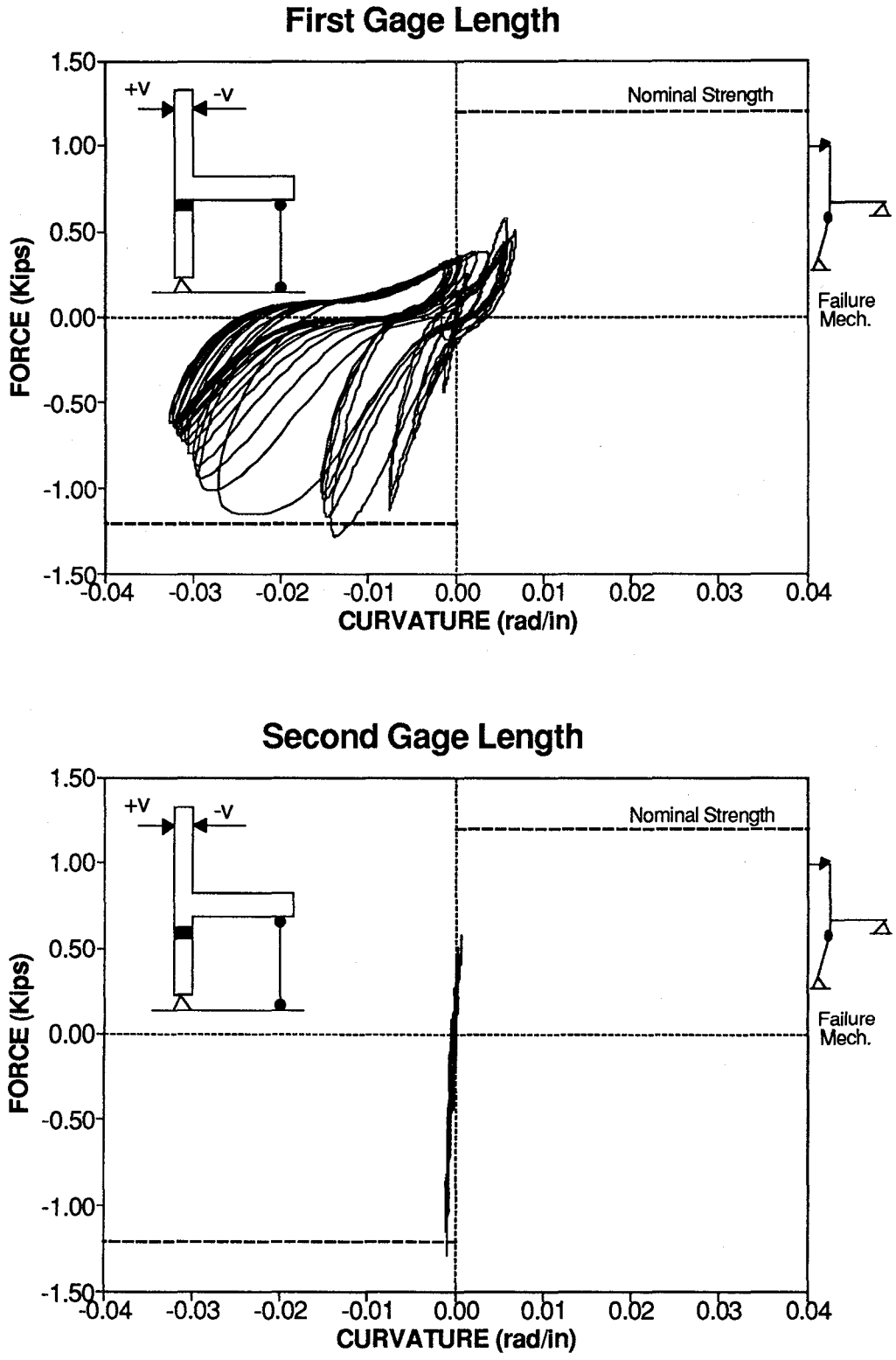

Fig. 3.21 Experimental Lateral Load-Curvature graphs
Bottom Column - Exterior Subassemblage

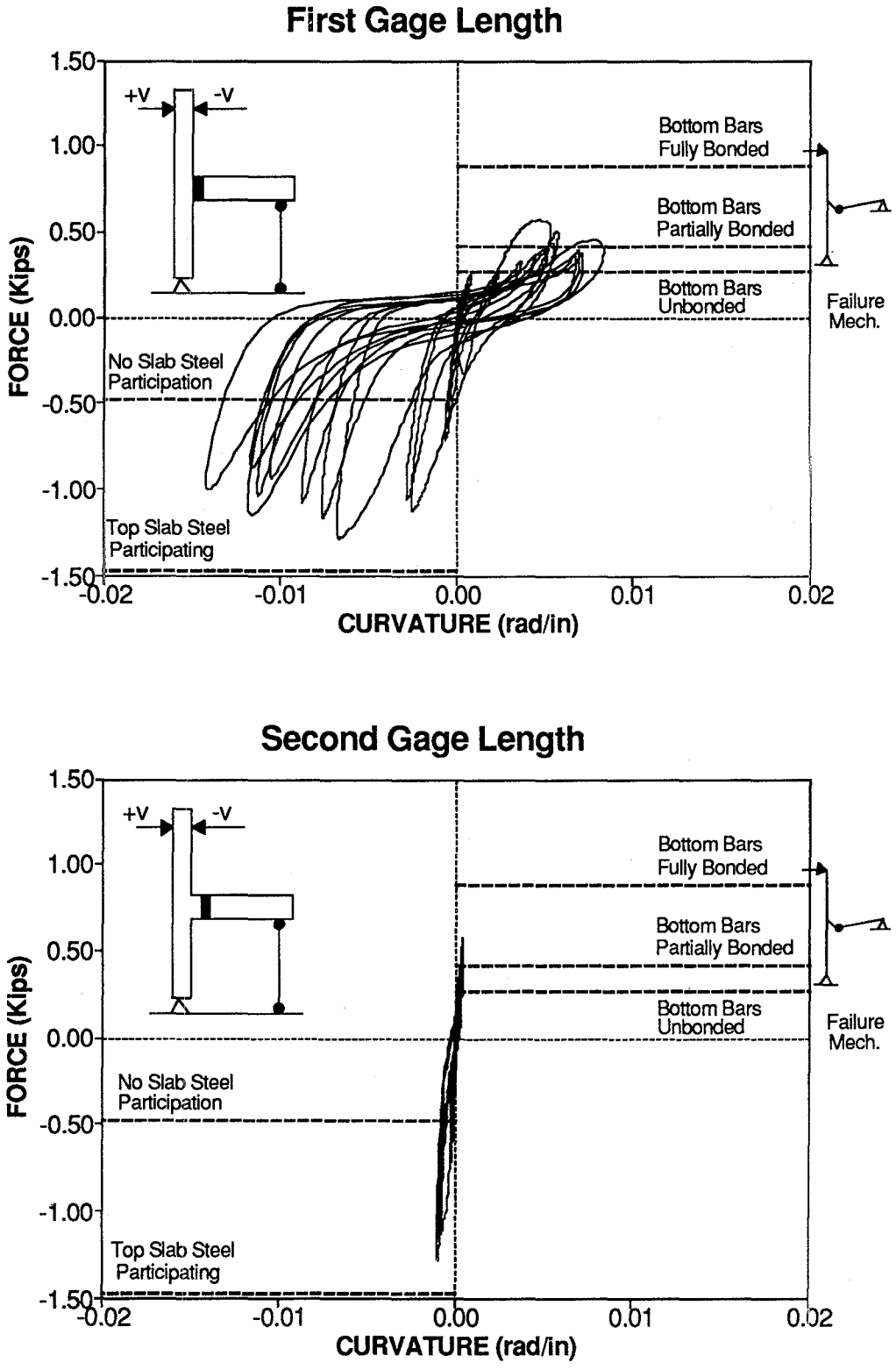

Fig. 3.22 Experimental Lateral Load-Curvature graphs
Longitudinal Beam - Exterior Subassemblage

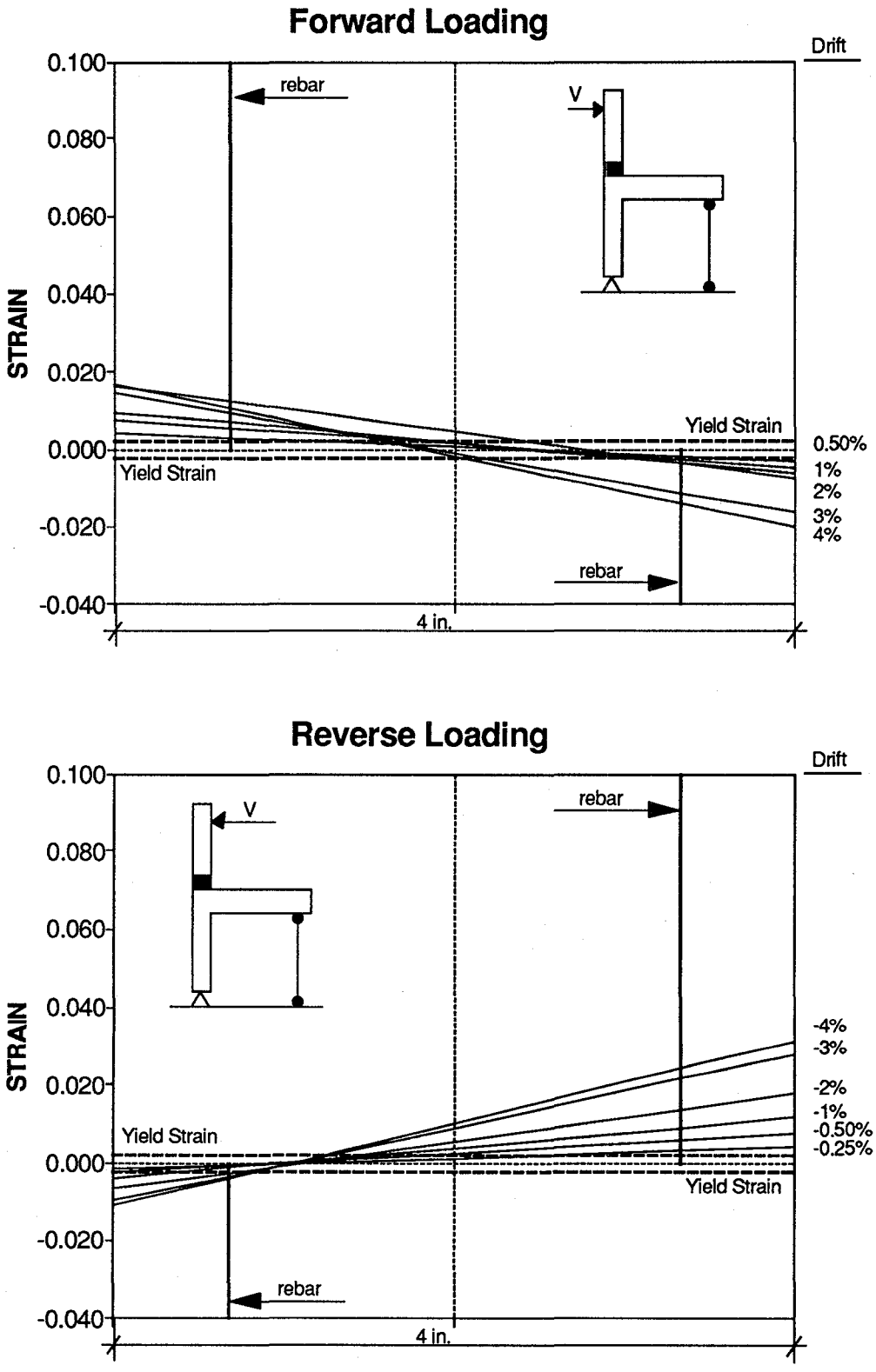

Fig. 3.23 Strain Profiles First Gage Length
Top Column - Exterior Subassemblage

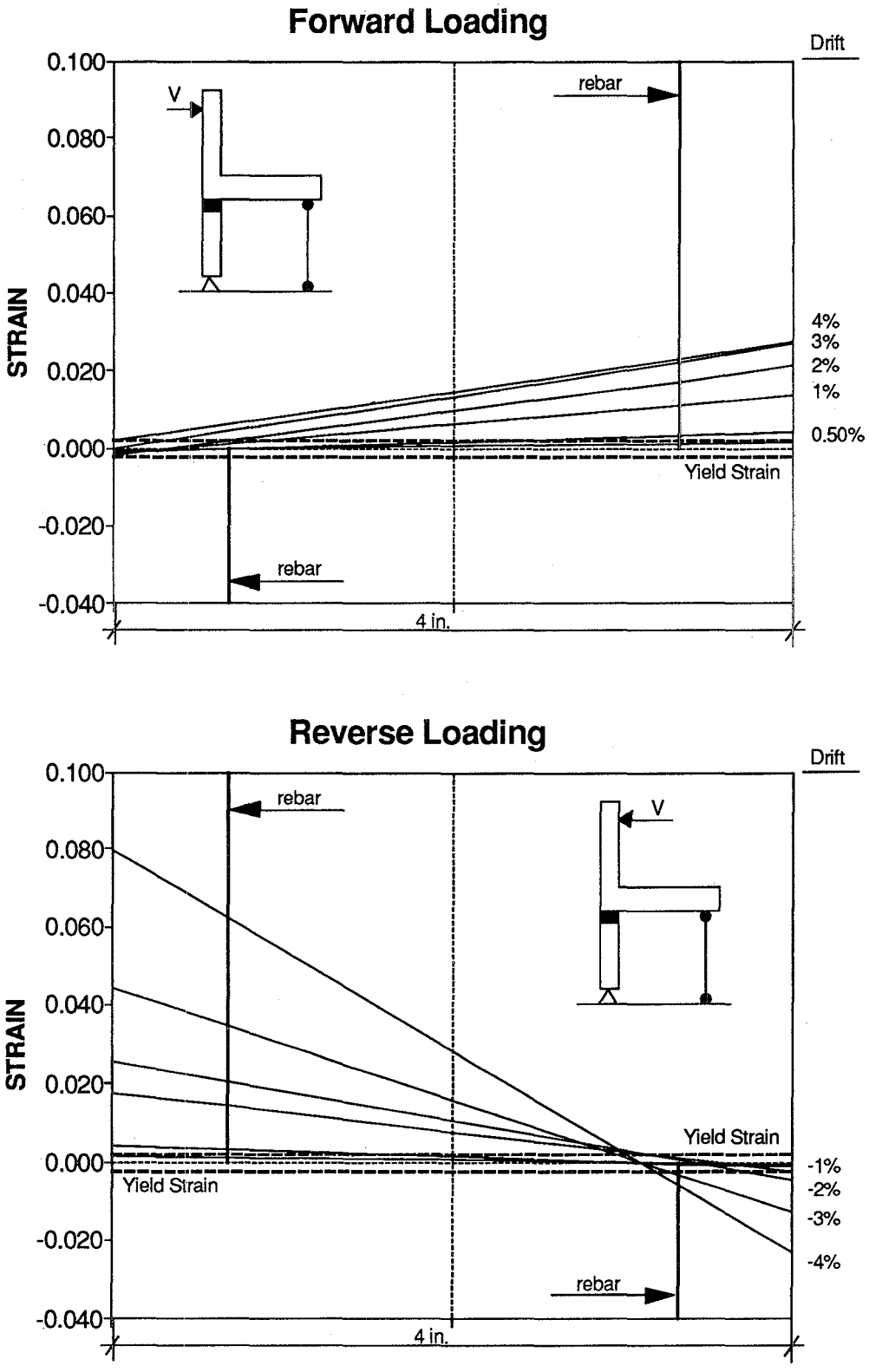

Fig. 3.24 Strain Profiles First Gage Length
Bottom Column - Exterior Subassemblage

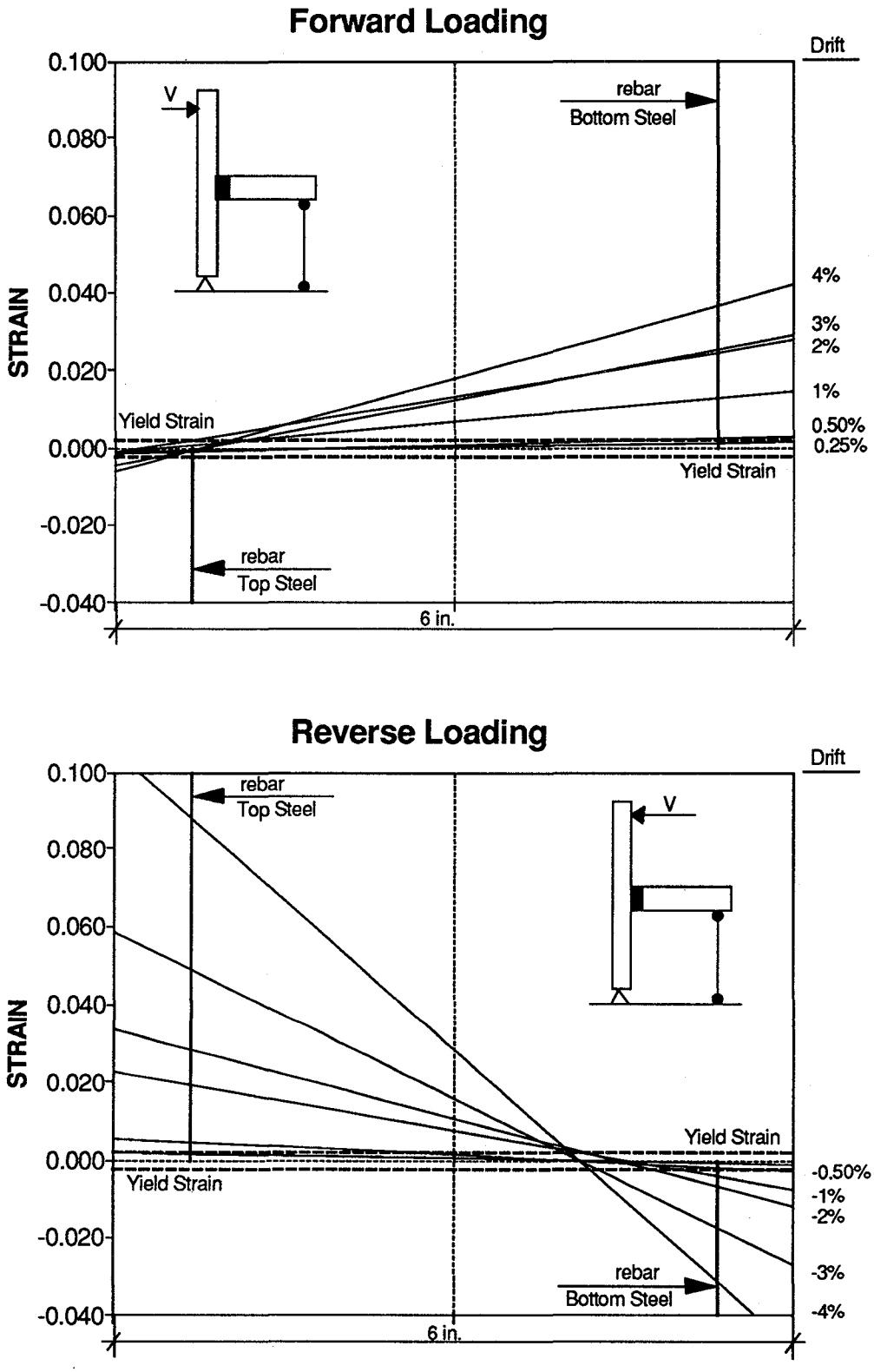

Fig. 3.25 Strain Profiles First Gage Length
Longitudinal Beam - Exterior Subassemblage

STAGE 1: Testing was carried out to the drift levels mentioned in Section 3.6.2. At the end of the ±2% drift cycles, some cracks were observed only in the upper column. After completion of the ±3% drift cycles, flexural cracks increased and some spalling was observed. It was evident that after both ±4% drift cycles were complete, the damage was principally concentrated in the upper column lap splice region. Little damage, apart from some superficial cracking, was apparent in the beams and lower column.

STAGE 2: The horizontal actuator was moved down to apply the load 10 in. from the top of the slab. This was to simulate the downward movement of the point of contraflexure in the second story due to early formation of a column hinge. This second stage followed a different test sequence: two complete cycles at each drift level of ±1%, ±2%, and ±4%. Upon completion of this test sequence, spalling and flexural cracks in the upper and lower columns were observed and buckling of the longitudinal bars of the lower column had commenced. No further damage was apparent in the beams. It was thus evident that a weak column-strong beam failure mechanism had occurred. This, coupled with the previously described exterior subassemblage results, would strongly indicate that a hybrid type of structural failure mechanism, as shown in Fig. 1.4, would occur in a complete structural frame.

STAGE 3: Since no information about the strength of the beams was obtained, the testing procedure was again changed. The vertical actuator was fixed using two MC 6x18 beams which were connected to the W 8x31 columns of the safety frame and to the steel plate to which the actuator body was bolted. Also, the lower column was disconnected and the hinge was removed. In that manner, the subassemblage was free to move when the vertical load was applied. The monotonic test was executed by pushing down and then pulling up the upper column with the vertical actuator at a rate of 0.005 in/sec. While pushing down, a large crack at the beam-column interface was developed and pull out of the bottom rebars was evident. Finally, while pulling up, flexural cracks and spalling of the cover at the lower face of the beam were observed. Most of the top slab steel layer fractured across a yield line during this stage. Figs. 3.26 and 3.27 show progressive damage to the subassemblage.

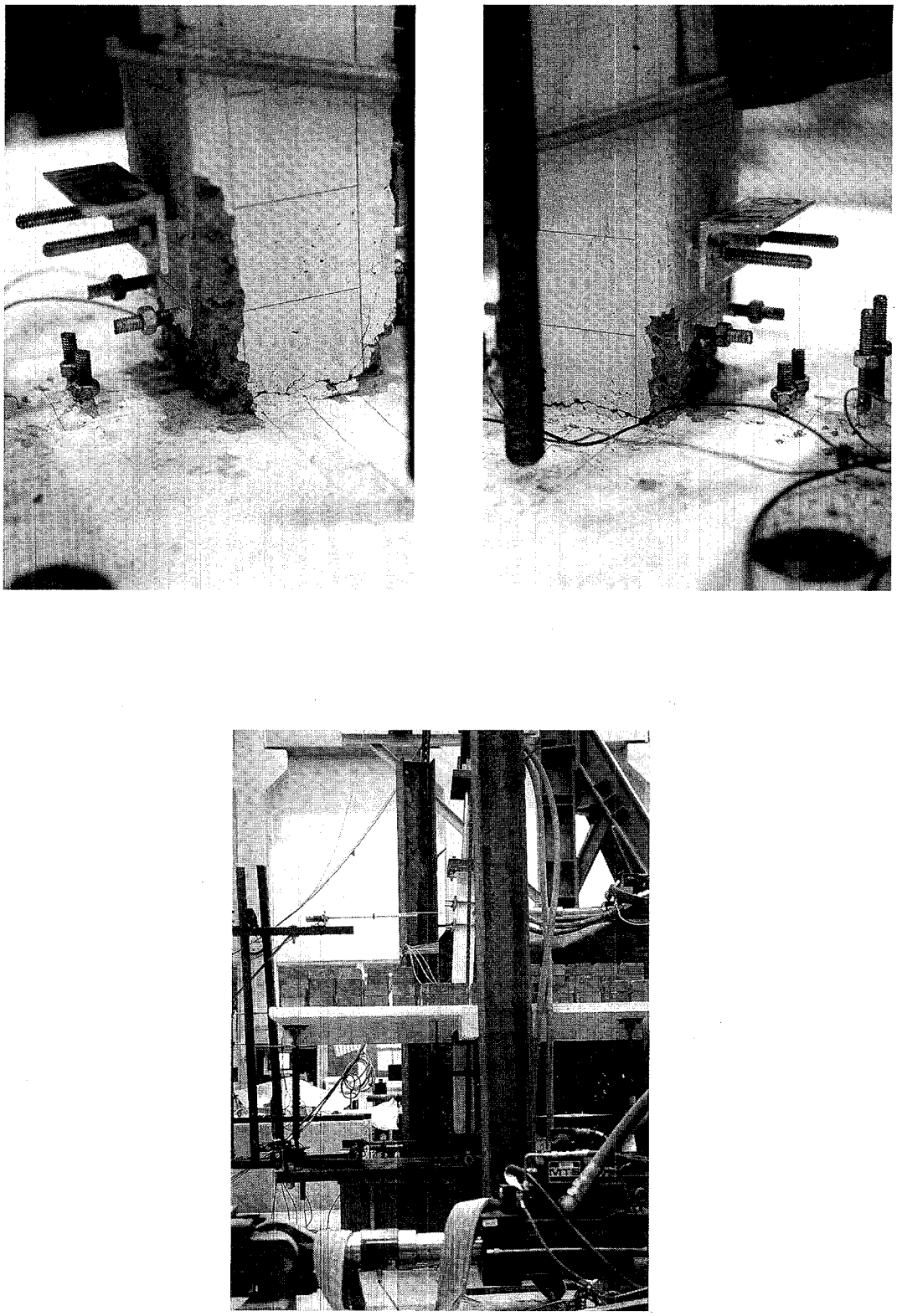

Fig. 3.26 Progressive Damage Interior Subassemblage - STAGE 1

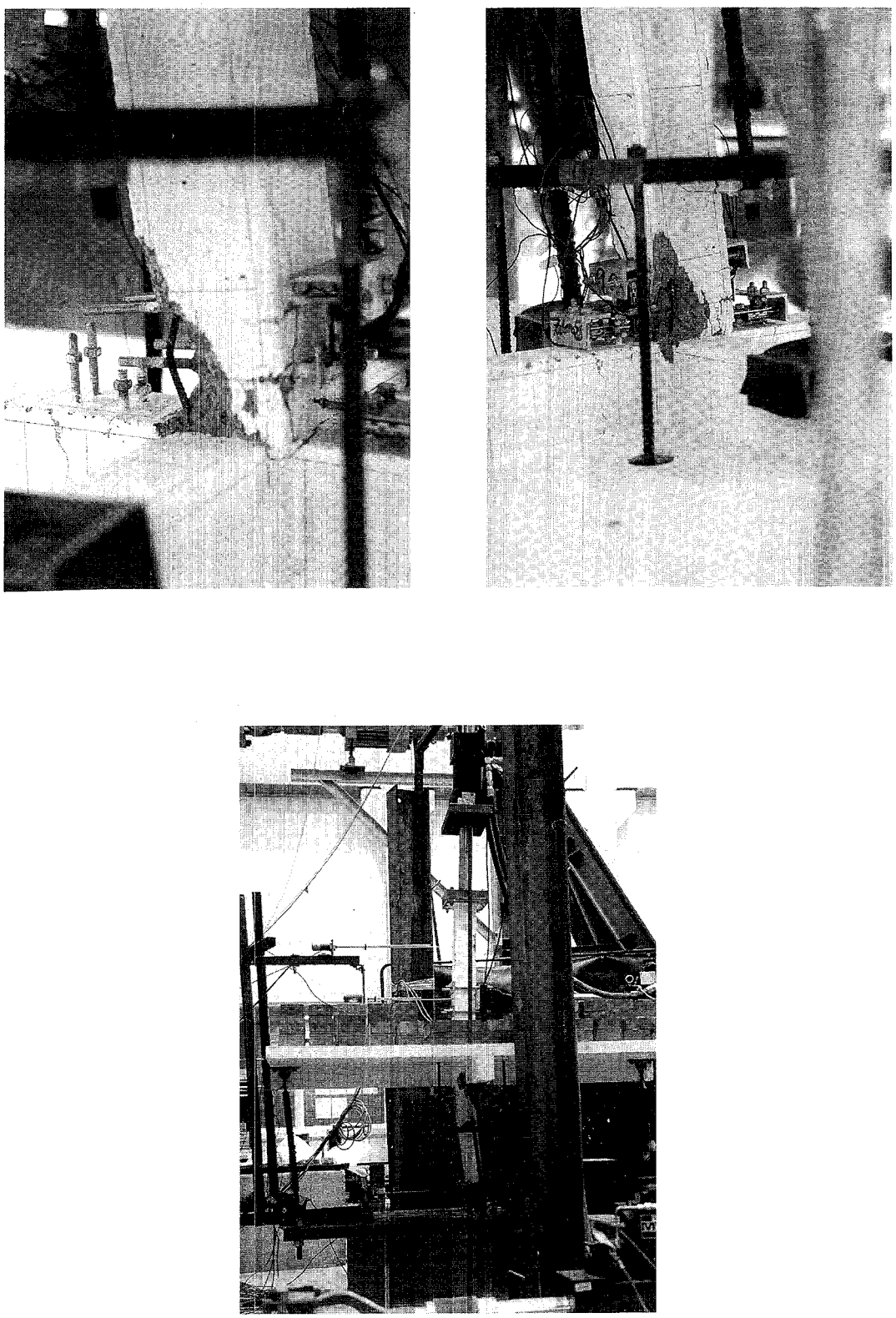

Fig. 3.27 Progressive Damage Interior Subassemblage - STAGE 2

Hysteretic Performance

Fig. 3.29 presents two lateral load-drift graphs corresponding to stages 1 and 2 previously described in the visual observations. Additionally, Figs. 3.30 to 3.32 present lateral load-rotation graphs for each of the plastic hinge rotations. The rotation was evaluated for columns and beams using the measurements from all the potentiometers for each member and again represents the plastic rotation over the 3.5 in. gage length contiguous to the joint. As for the exterior subassemblage, nominal load capacity curves are plotted as dashed lines superimposed on the hysteresis graphs. Once more, drawn besides each graph, there are diagrams of the various failure mechanisms considered in the calculation of the nominal capacity. The same general considerations regarding the evaluation of the individual nominal capacities for the members explained for the exterior subassemblage are valid for the interior.

Fig. 3.28 presents the idealized plastic deformed geometry of the subassemblage. It is evident from Fig. 3.36 that the beams did not reach their yield capacity and as a result there is negligible plastic rotation in the beams. For that case, Eq. (3.2) can be rewritten as follows

$$D_u=\frac{\Delta}{H}=\theta_e+\theta_{bc}\frac{H_{bc}}{H}+\theta_{tc}\frac{H_{tc}}{H}+\gamma_j \tag{3.4}$$

in which

$D_u=\frac{\Delta}{H}$ = *total applied drift*

θ_e = *elastic component of drift for the total subassemblage*

θ_{bc},θ_{tc} = *plastic rotations of the top and bottom columns, respectively*

H = *height of the subassemblage*

H_{tc},H_{bc} = *distance from the plastic hinge to the end of the columns*

γ_j = *apparent joint core plastic shear displacement*

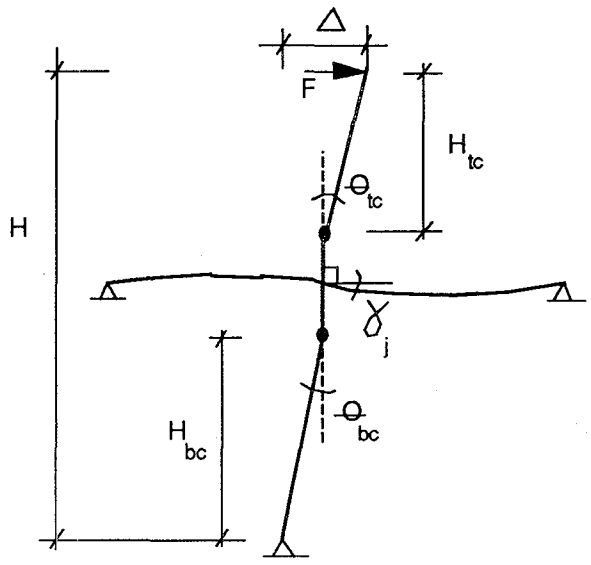

Fig. 3.28 Idealized Plastic Deformed Geometry

The elastic drift and the plastic rotations were evaluated for the first peak at each different drift amplitude, and two drift contribution graphs for stages 1 and 2 were constructed and are presented in Fig. 3.33. By rearranging Eq. (3.4) as follows, joint shear distortion can be inferred as the difference between the total applied drift and the component sums of the plastic and elastic displacements:

$$\gamma_j = D_u - \left[\theta_e + \theta_{tc}\frac{H_{tc}}{H} + \theta_{bc}\frac{H_{bc}}{H}\right] \tag{3.5}$$

STAGE 1: Wide hysteresis loops were observed. Little sign of strength degradation was shown with successive cycling as well as on the second cycle at the same drift amplitude. The load-drift graph shows that the nominal capacity of the top column was exceeded but the nominal capacity given by the beams was far to be reached. The load-rotation graphs show hysteretic and plastic behavior of the top column, whereas the bottom column and the beams behaved almost elastically.

Fig. 3.33 shows that the top column had the predominant plastic component of drift with only a little contribution from the bottom column. It is also evident that there was an appreciable contribution to the total displacement from the joint shear distortion.

STAGE 2: Again, wide hysteresis loops were observed. The load-drift graph shows that the maximum strength exceeded the nominal capacity given by the bottom column, whereas the nominal capacity given by the strength of the beams was far to be attained. The load-rotation graph for the top column, in contrast to the graph of stage 1, shows narrower hysteresis loops. Furthermore, the nominal capacity was not reached, basically due to the previous damage suffered in stage 1. For the bottom column, the nominal capacity was exceeded and some plastic behavior observed, especially for positive loading.

Once more, the drift contribution graph shows large contribution from the top column but there is an increase in the contribution from the bottom column.

Section Curvatures

Figs. 3.34 to 3.38 present lateral load-curvature hysteresis curves. Similar to the results presented in Section 3.7, for each member (columns and beams), two graphs were built in which the curvature was estimated over the two sequential 1.75 in. gage lengths. Again, the first gage length refers to the 1.75 in. gage length adjacent to the joint.

STAGE 1: the load-curvature graphs (Figs. 3.34 to 3.36) indicate that all the damage as well as the plastic deformation occurred at the first gage length of the top column.

STAGE 2: only load-curvature graphs (Figs. 3.37 and 3.38) for the columns (top and bottom) are presented since in comparison to the beam's lateral load-curvature graphs of stage 1 insignificant change was found. For stage 2, the plastic deformation and the damage are distributed over the first gage length of both columns. The specimen failed and the beams practically did not show damage at all.

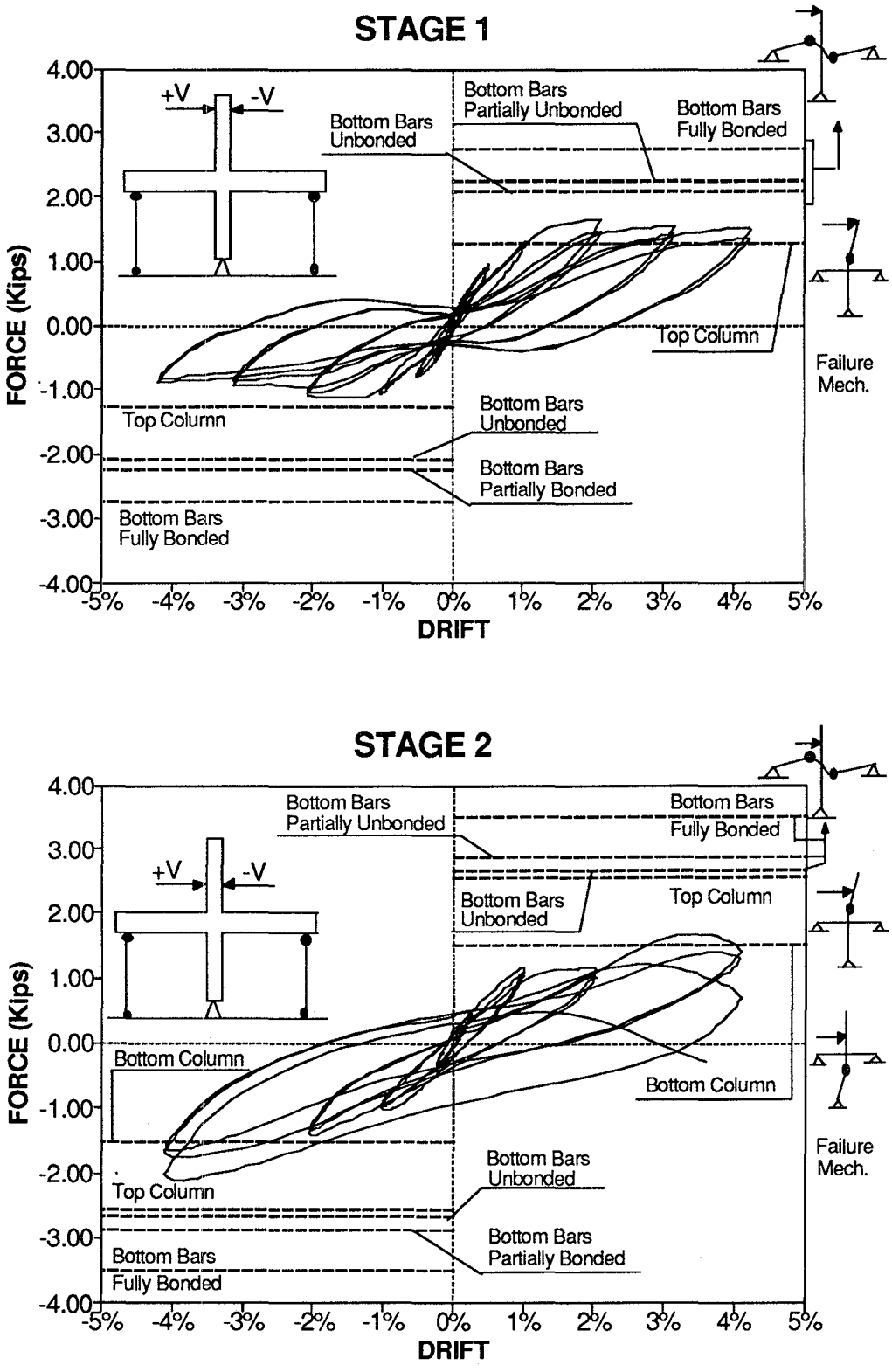

Fig. 3.29 Experimental Lateral Load-Drift graphs for Interior Subassemblage

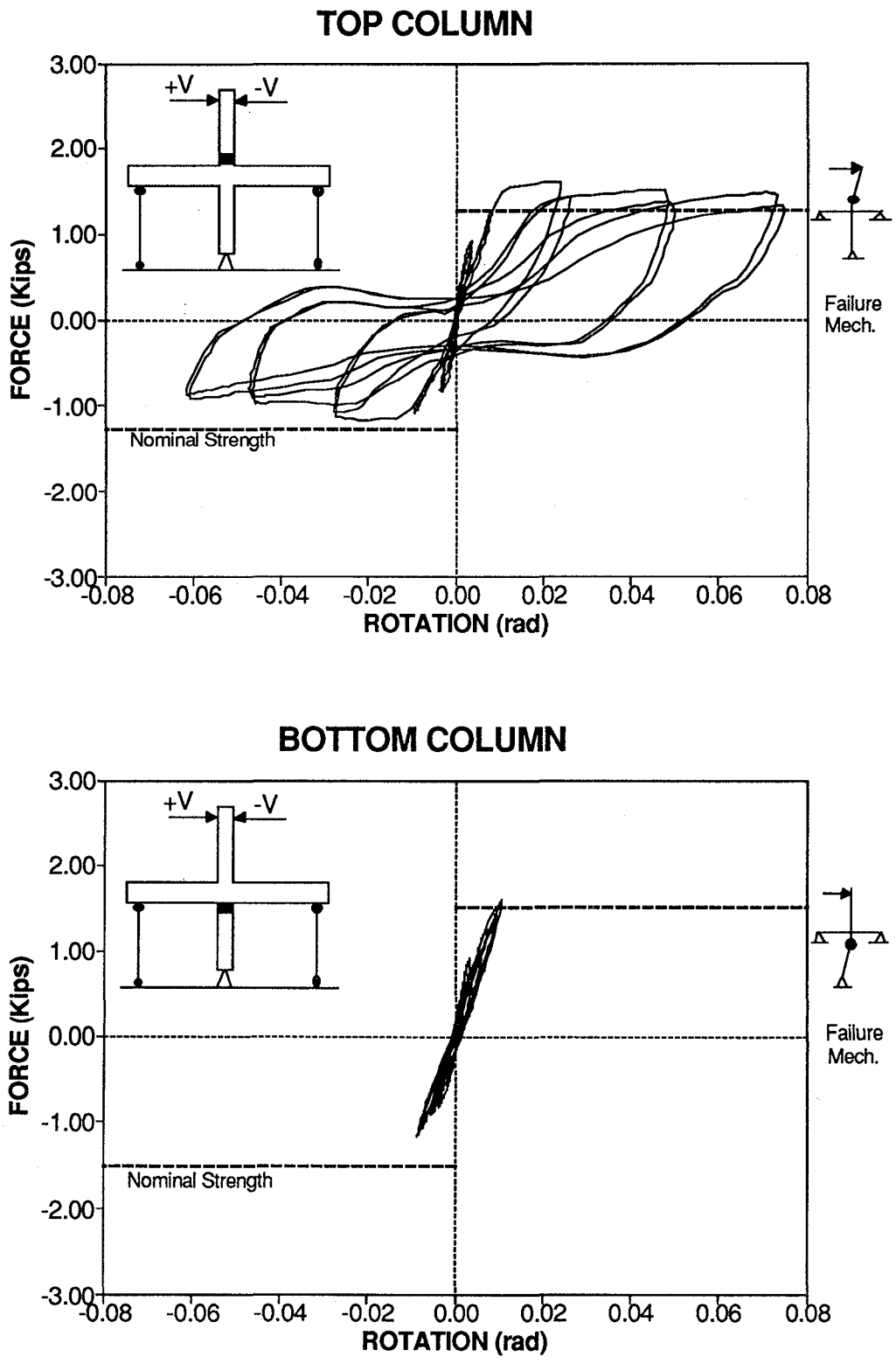

Fig. 3.30 Experimental Lateral Load-Rotation graphs
Top and Bottom Columns - STAGE 1 - Interior Subassemblage

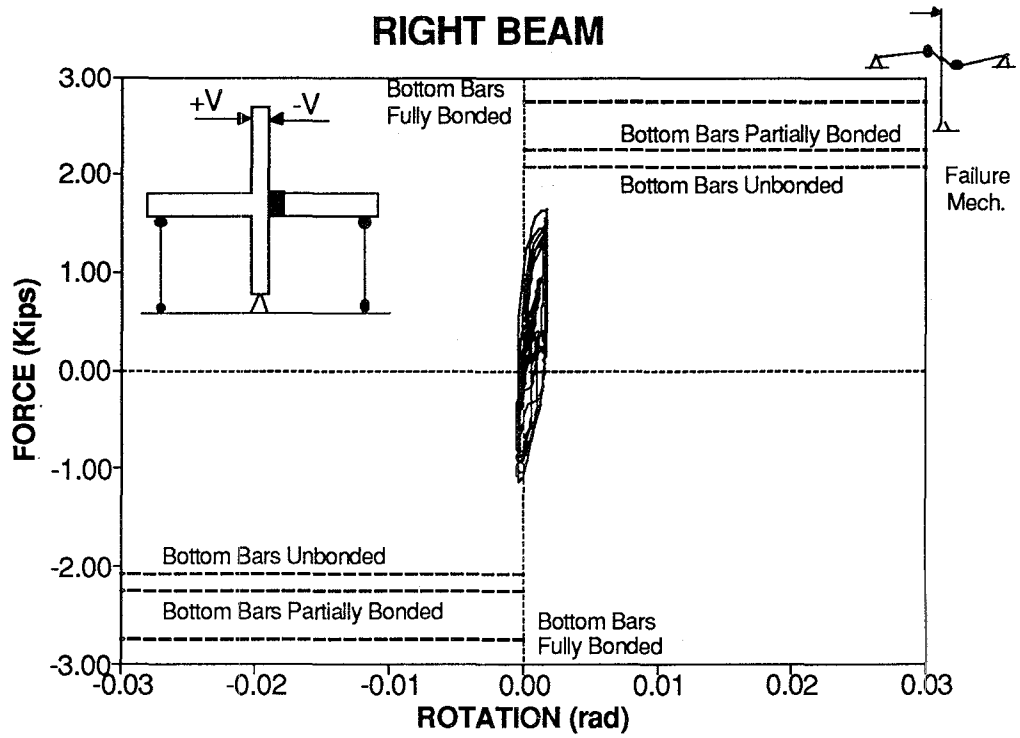

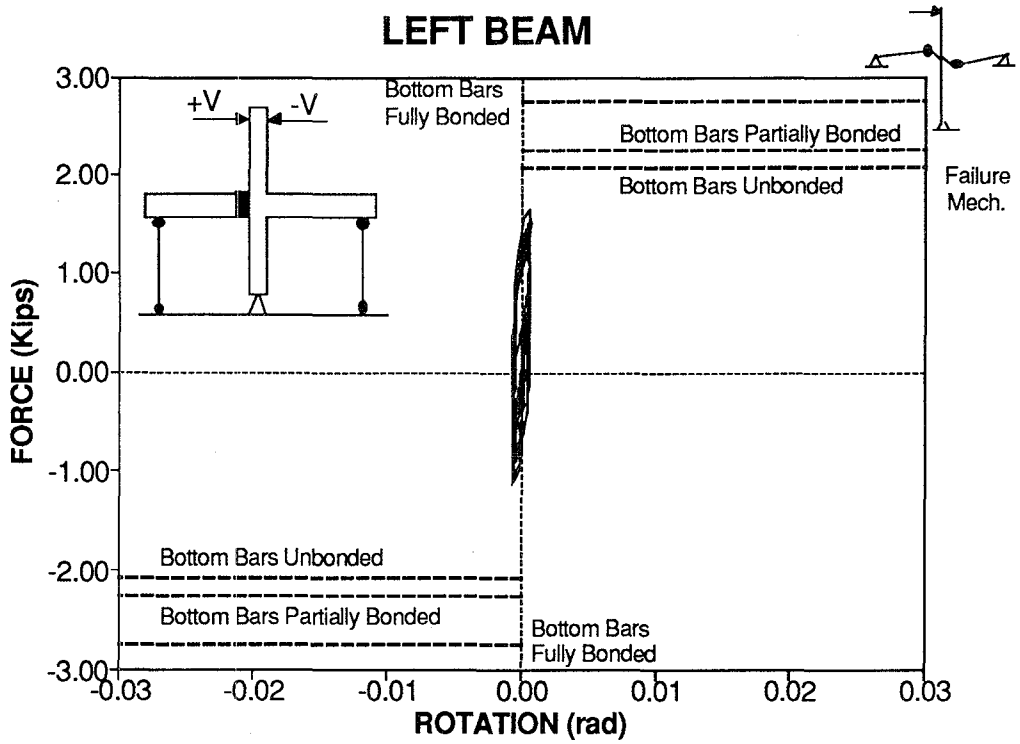

Fig. 3.31 Experimental Lateral Load-Rotation graphs
Longitudinal Beams - STAGE 1 - Interior Subassemblage

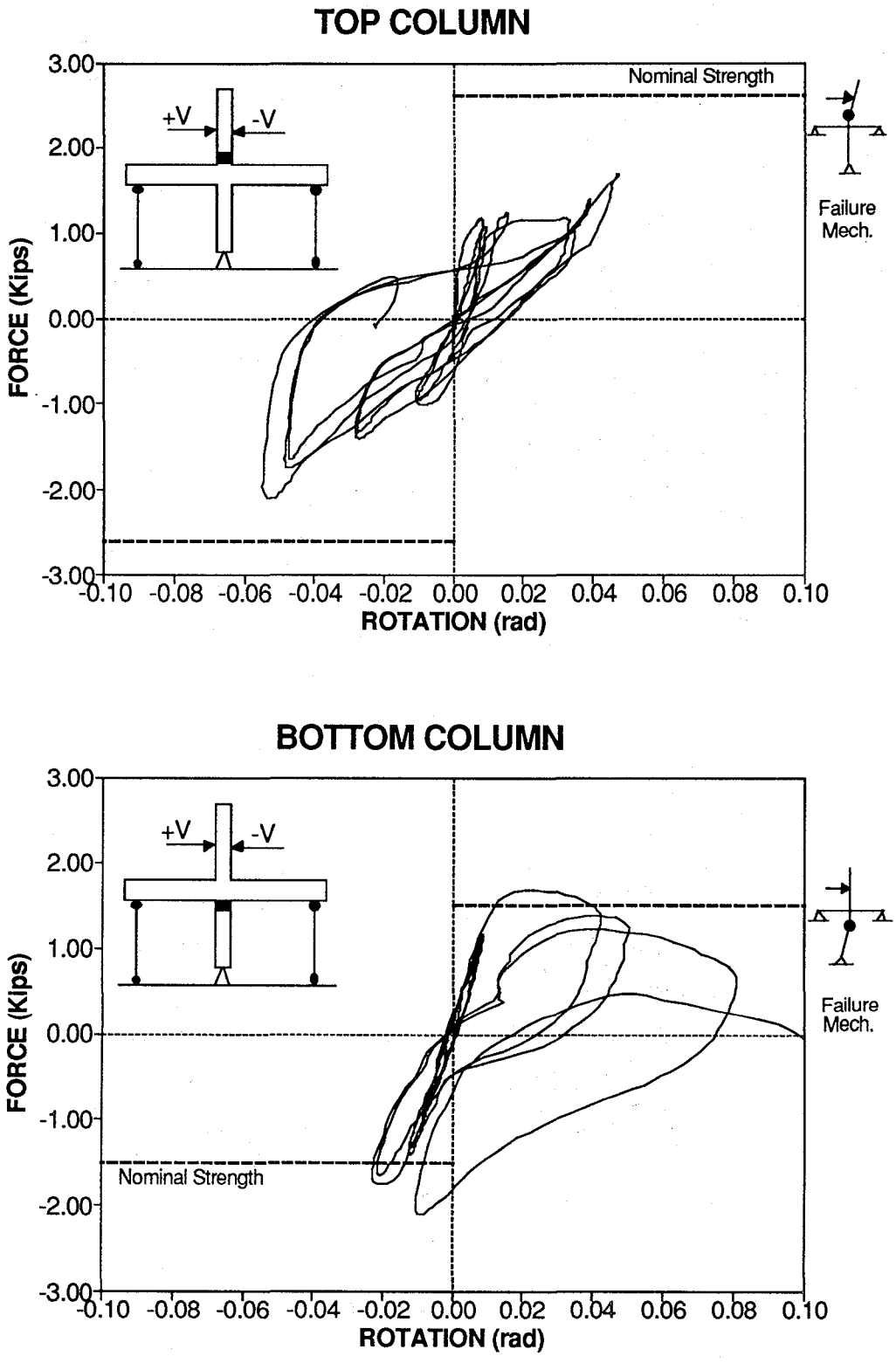

Fig. 3.32 Experimental Lateral Load-Rotation graphs
Top and Bottom Columns - STAGE 2 - Interior Subassemblage

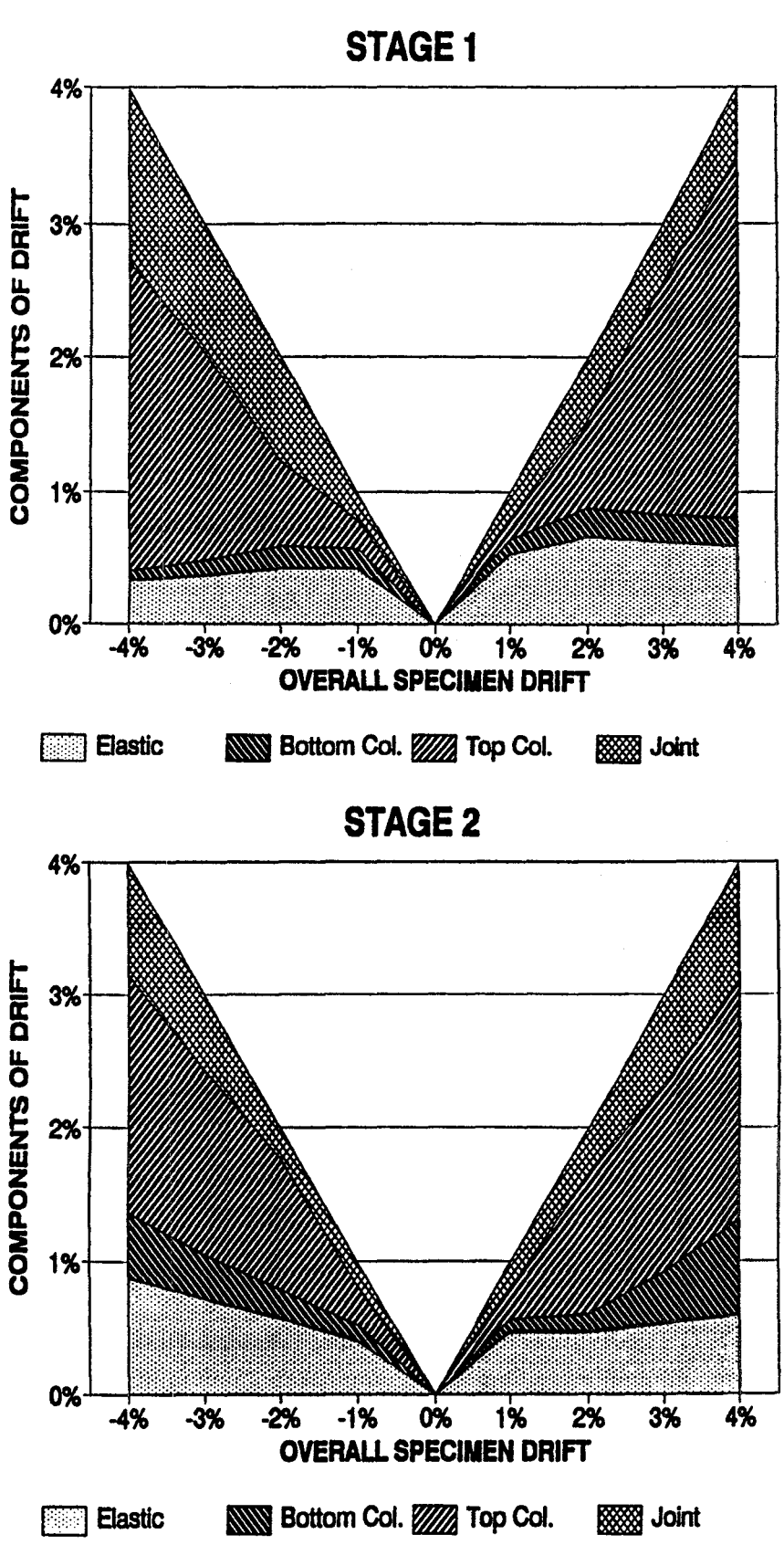

Fig. 3.33 Drift Contributions from each member Interior Subassemblage

STAGE 3: as previously discussed in the visual observations, the experiment continued with a monotonic test of the beams. The moment-curvature graph for the first gage length of one of the beams is presented in Fig. 3.39. A 90% difference between the two maximum peaks is due to the lack of continuity of the beams' bottom reinforcement and the subsequent pull-out of the bars.

Section Strains

For each gage length, strain profile graphs calculated at the first cycle of each successive drift peak are also presented in Figs. 3.40 to 3.42. Once more, based on the examination of the lateral load-curvature graphs, strain profiles were selected to show only the relevant ones.

The strain profiles show concentration of the plastic deformation and the damage at the first gage length of the top column for the first stage, and at the first gage length of both columns for stage 2.

As mentioned in the visual observations, the concrete cover started spalling at ±3% drift level for the top column at stage 1, and at 4% drift cycles of stage 2 for the bottom column. Table 3.2 lists the compression strain values for the first gage length for both cases.

Table 3.2 Experimental Apparent Spalling Strain Interior Subassemblage

Loading	Top Column Stage 1	Bottom Col. Stage 2
Forward	0.015	0.008
Reverse	0.030	0.008

The apparent spalling strain for the top column varied from 0.015 to 0.030, which is in good agreement with respect to the strains observed at the end of the cylinder compression tests presented in Fig. 1.6. However, for the bottom column, the experimental apparent strain value of 0.008 appears to be low compare with the value of 0.020 observed in Fig. 1.6.

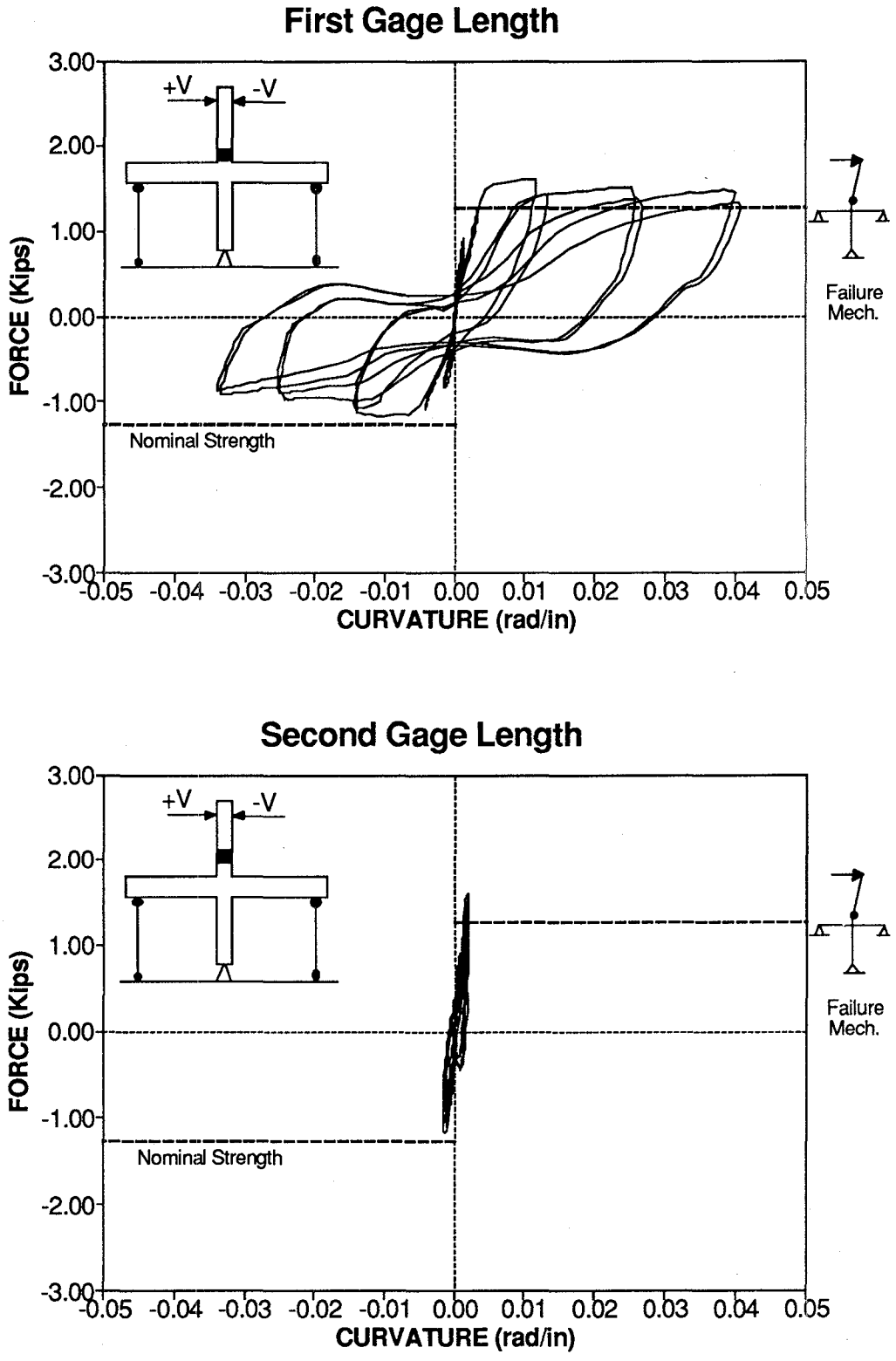

Fig. 3.34 Experimental Lateral Load-Curvature graphs
Top Column - STAGE 1 - Interior Subassemblage

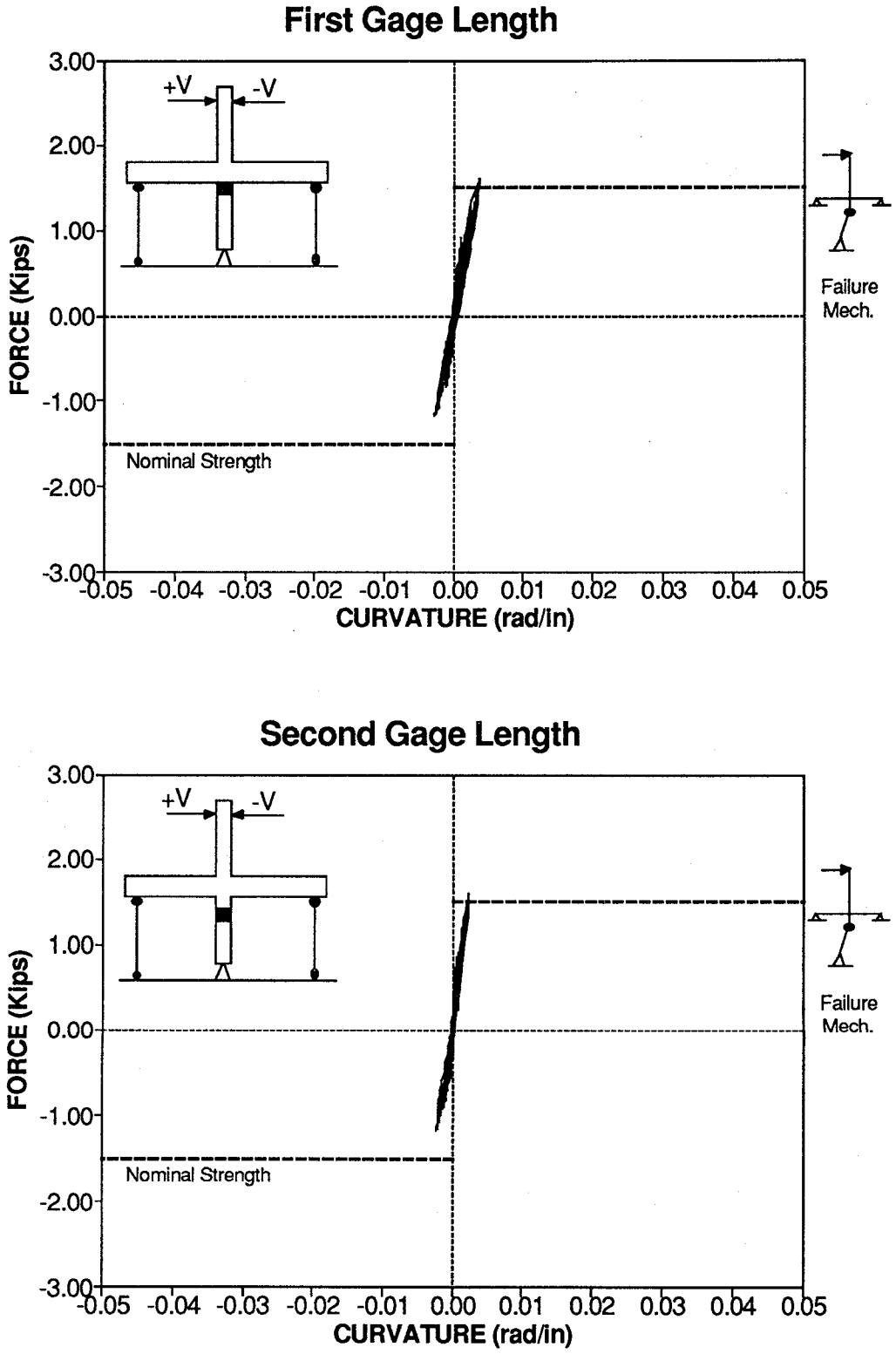

Fig. 3.35 Experimental Lateral Load-Curvature graphs
Bottom Column - STAGE 1 - Interior Subassemblage

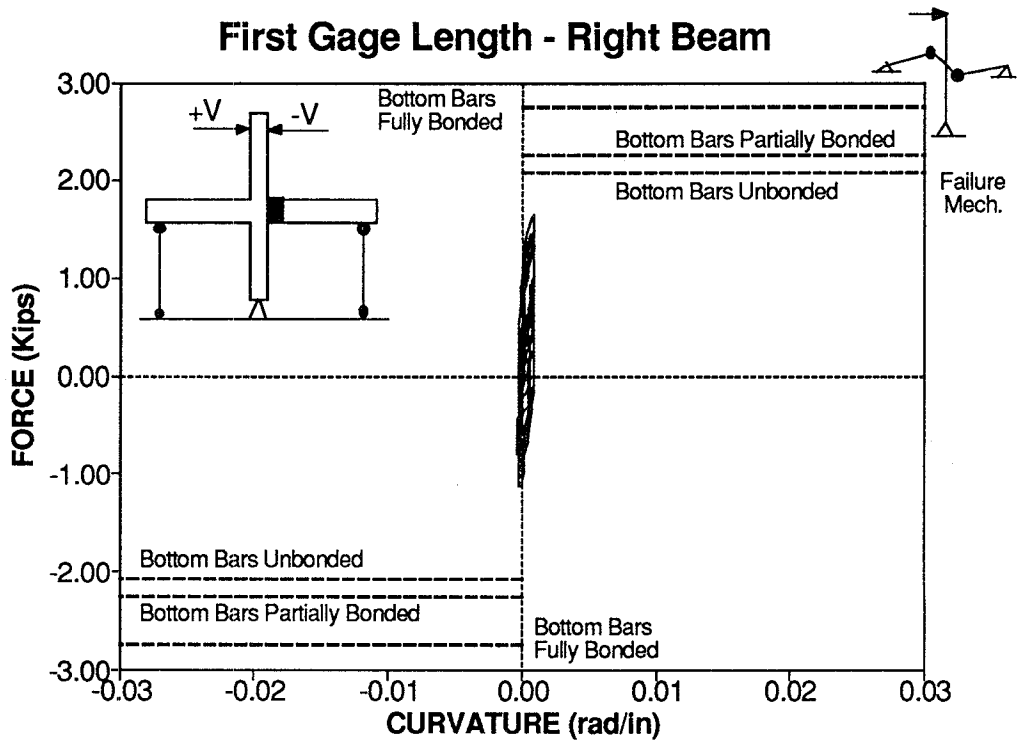

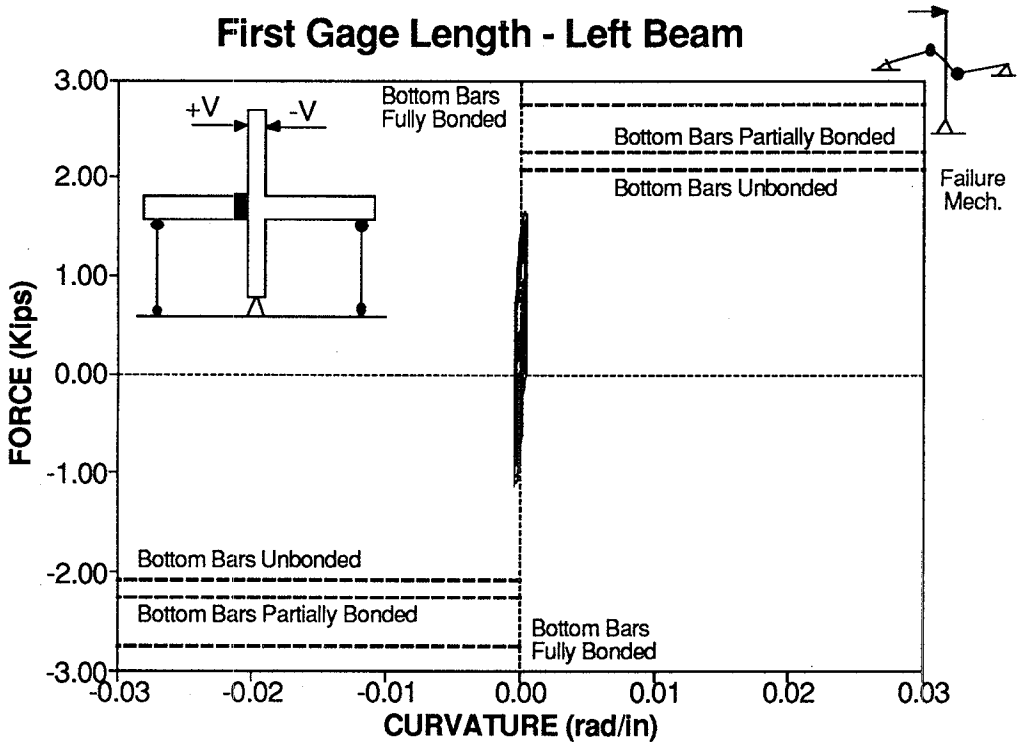

Fig. 3.36 Experimental Lateral Load-Curvature graphs
Longitudinal Beams - STAGE 1 - Interior Subassemblage

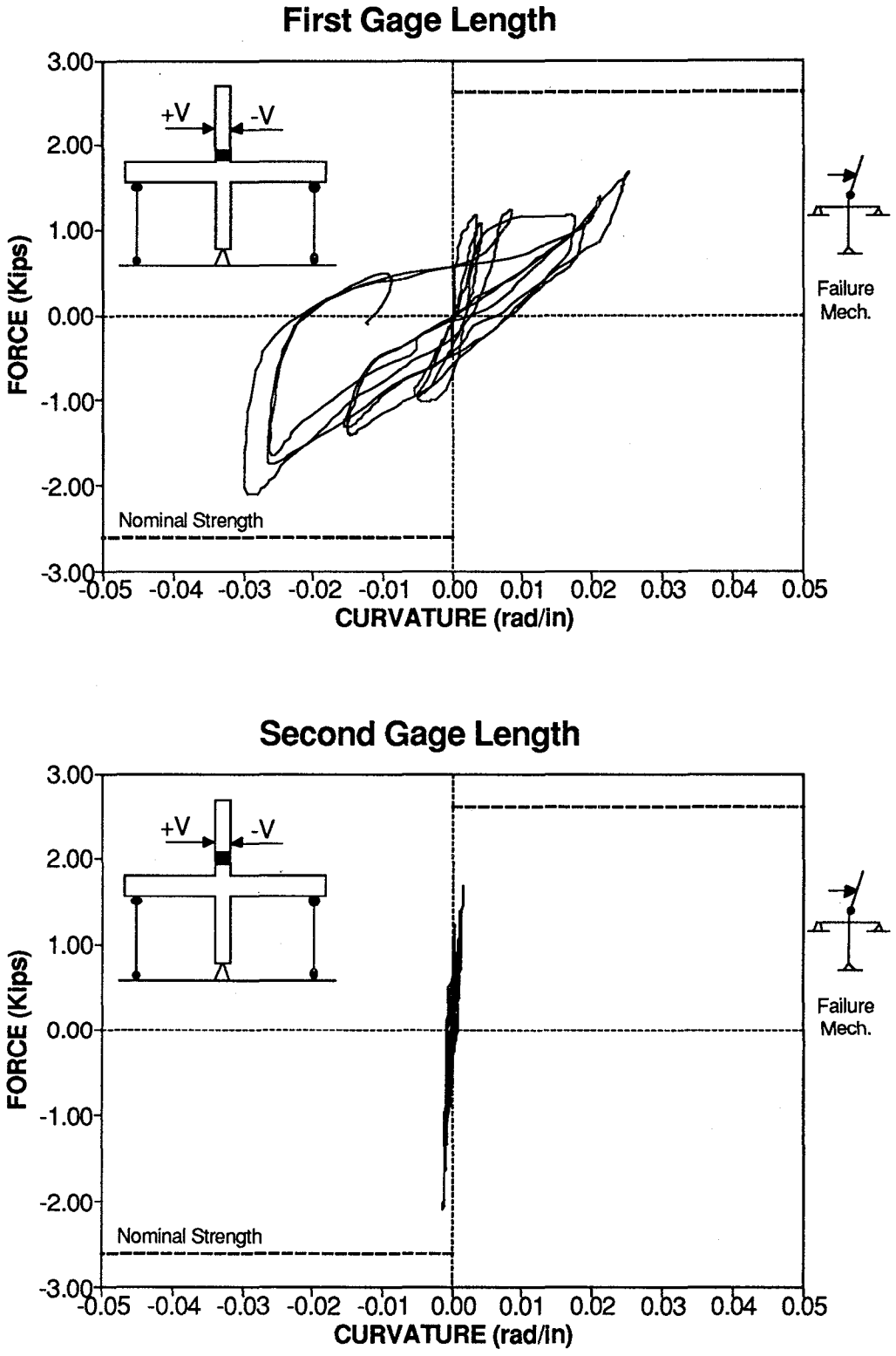

Fig. 3.37 Experimental Lateral Load-Curvature graphs
Top Column - STAGE 2 - Interior Subassemblage

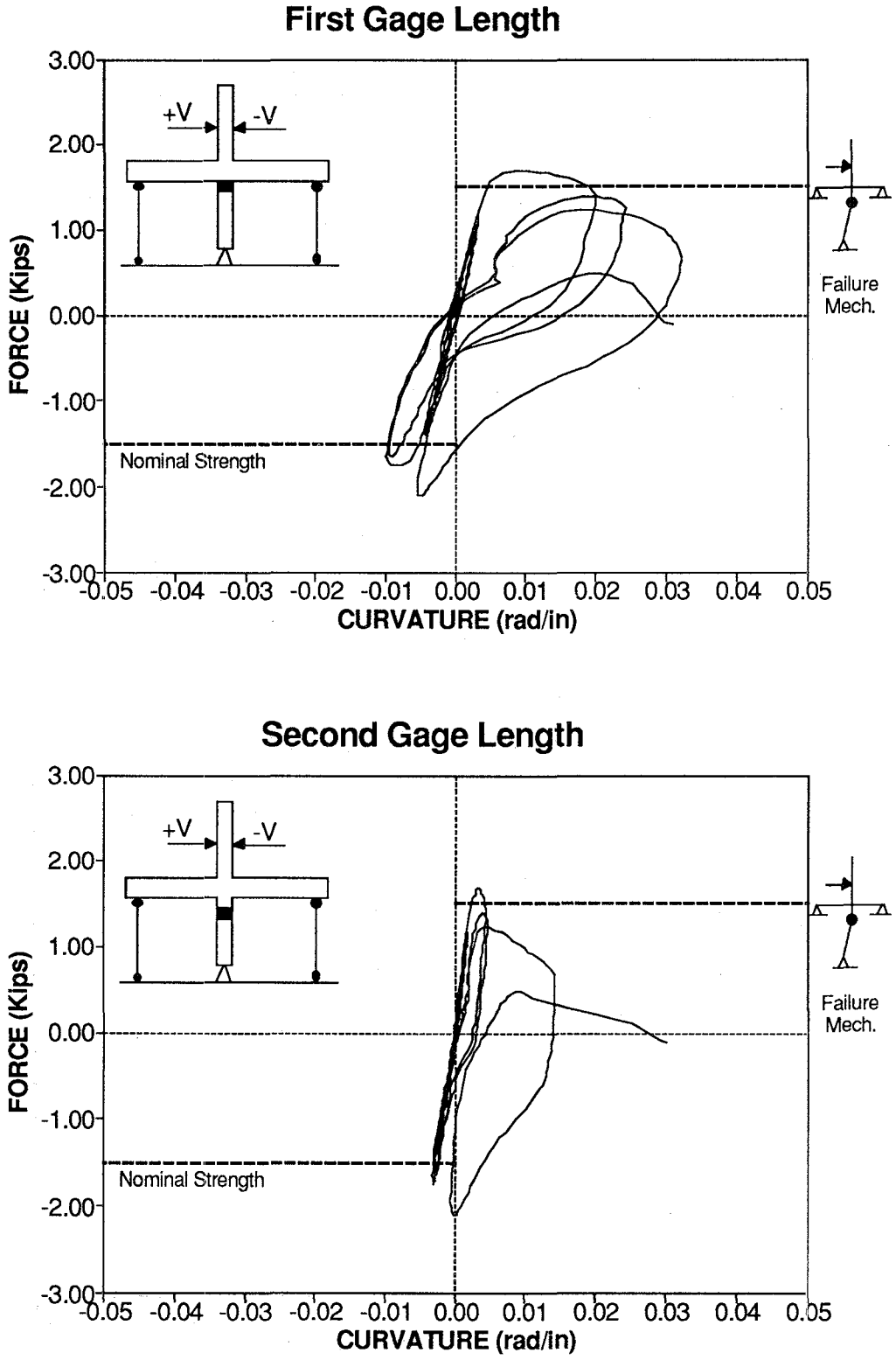

Fig. 3.38 Experimental Lateral Load-Curvature graphs
Bottom Column - STAGE 2 - Interior Subassemblage

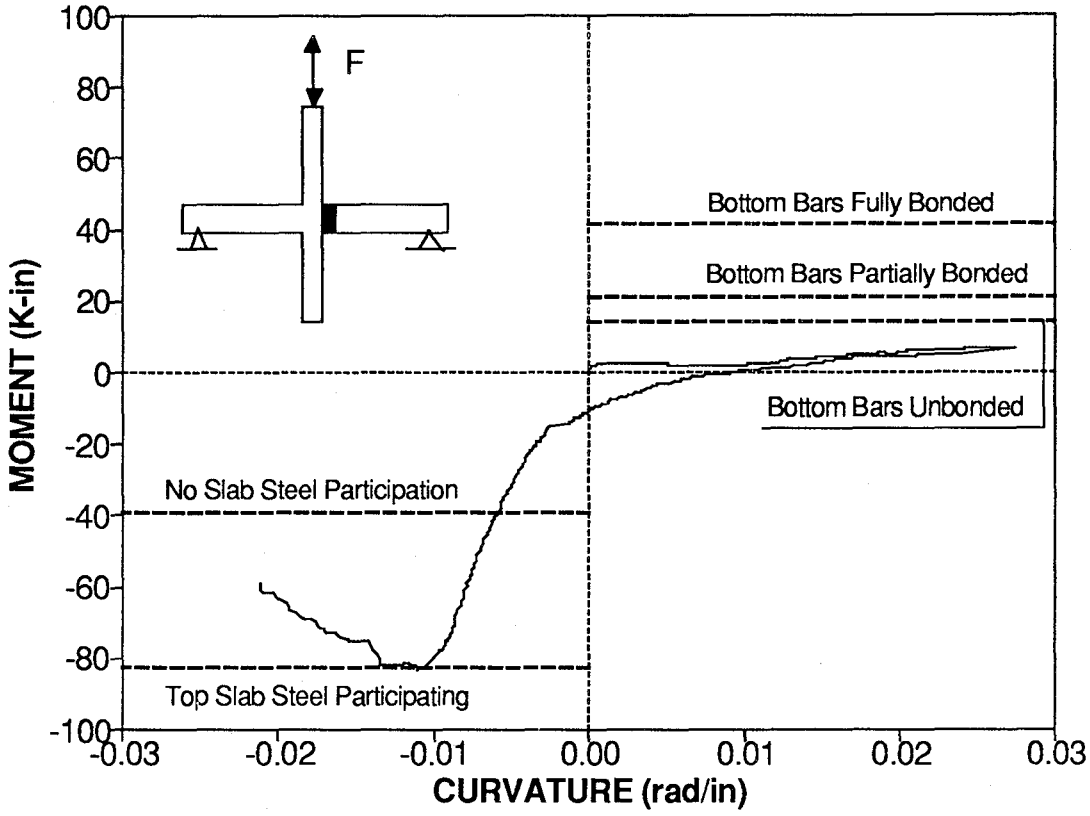

Fig. 3.39 Experimental Moment-Curvature graph First Gage Length Longitudinal Beam - STAGE 3 - Interior Subassemblage

According to the observations in Section 3.8, the vertical reinforcing steel of the bottom column of the Interior Subassemblage started buckling after the completion of stage 2. The observed buckling was detected at the first gage length where $s/d_b=17.8$ which, as already discussed for Specimens 1 and 2 in Section 2.9, is substantially greater than the recommended by the anti-buckling $s/d_b=8$ in ACI 318. The strain profiles show steel compression strains of about 0.005 which are small. However, the presence of high axial load (12.8 Kip), loss of cover concrete, some crushing of the core concrete, and the previously mentioned $s/d_b=17.8$ caused buckling of the longitudinal reinforcement.

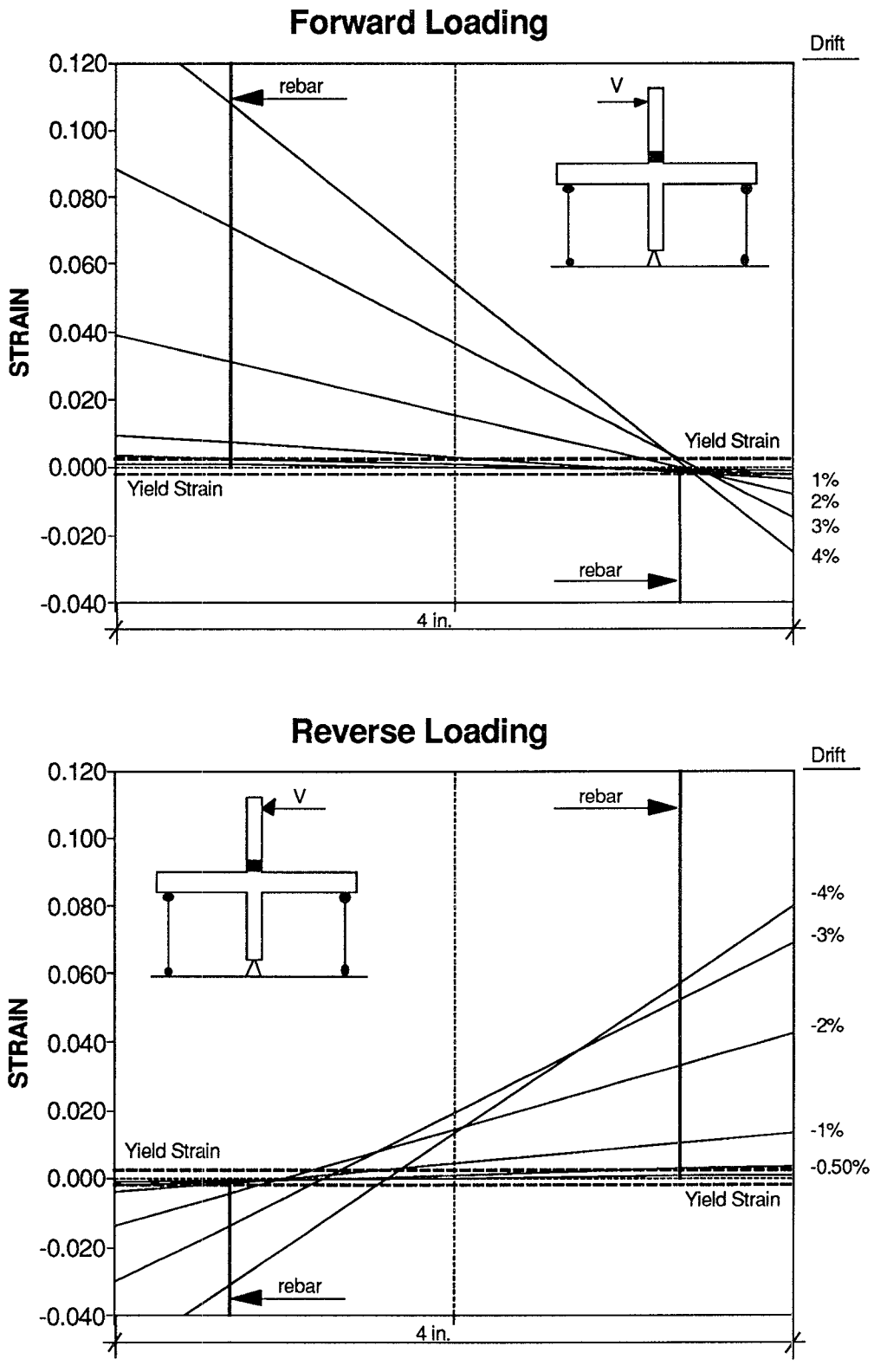

Fig. 3.40 Strain Profiles First Gage Length
Top Column - STAGE 1 - Interior Subassemblage

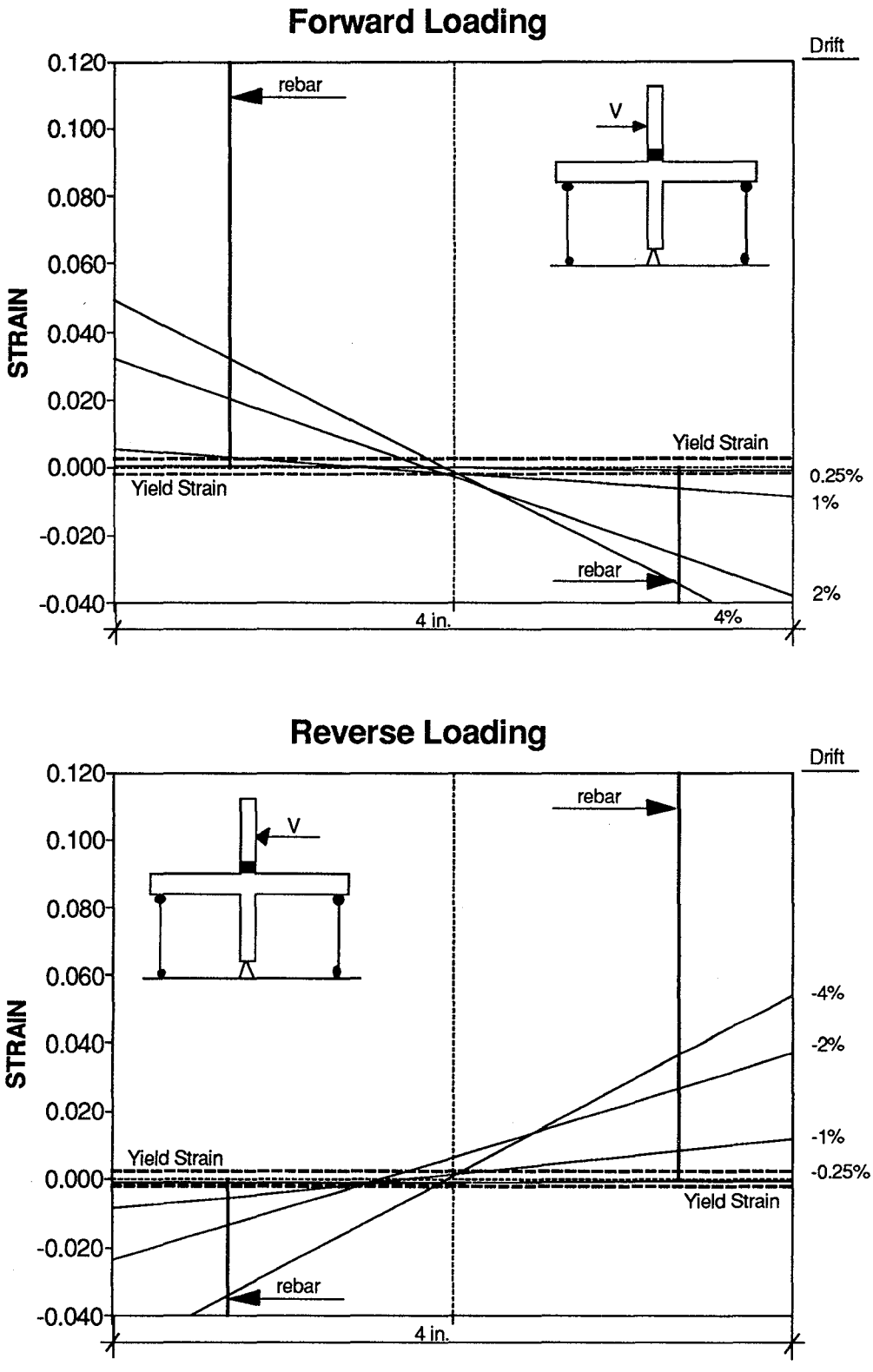

Fig. 3.41 Strain Profiles First Gage Length
Top Column - STAGE 2 - Interior Subassemblage

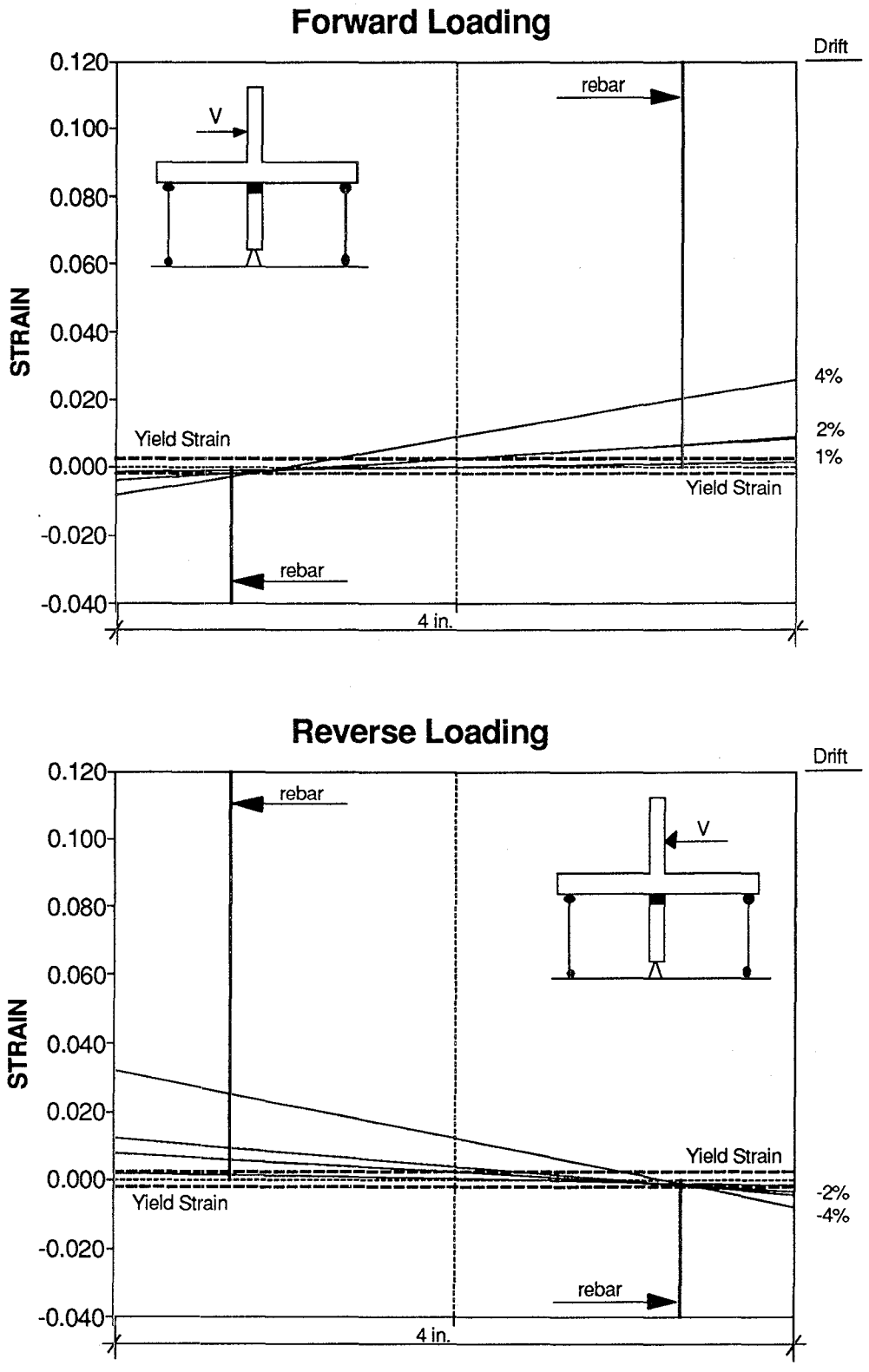

Fig. 3.42 Strain Profiles First Gage Length
Bottom Column - STAGE 2 - Interior Subassemblage

3.9 Conclusions

From the results of the experiments of the two subassemblages, the following conclusions are given:

1. The Exterior Subassemblage showed progressive damage starting in the beam (pull-out of the bottom bars) and later continuing in the columns. There is clear evidence of a weak beam-strong column failure mechanism. In contrast, the Interior Subassemblage exhibited progressive damage only in the columns with little discernable damage to the beams. Clearly this presents a weak column-strong beam failure mechanism. As previously mentioned, these results would strongly suggest that a hybrid type of failure mechanism would occur in a complete frame.

2. Little joint damage was detected for both subassemblages. Some visual damage to the joint of the Exterior Subassemblage was apparent due to spalling of the concrete at the beam-bottom column interface. Damage in the joint of the Interior Subassemblage was not visually observed. However, the analysis showed that there was some inelastic joint shear distortion which amounted to about 25% percent of the plastic displacement at large drifts.

3. It is apparent that the positive reinforcement framing into the joint zone debonds at a strength approximately equal to 0.50 Kip. The resulting pull-out of the bars relieves the moment demand on the beams and columns minimizing joint shear distortion and column hinging for the exterior subassemblage.

4. Maximum strength was observed to occur between 2 to 3% of drift, in both cases.

SECTION 4

ANALYTICAL STUDY OF NON-SEISMICALLY DESIGNED COLUMNS

4.1 Introduction

This section presents the analytical prediction of the experimental results of the column tests presented in Section 2. The specimens were taken as replicas of the first story columns of the one-third scale model building (Fig. 1.5). Details of the design, testing program, and experimental results are included in Section 2.

4.2 Analytical Modeling

A computer program developed by Mander (1984) was used to predict the hysteretic performance of the column specimens. The program was developed to obtain the force-displacement and moment-curvature response of reinforced concrete columns under combined axial load and dynamic cyclic flexure.

4.2.1 Stress-Strain Relations

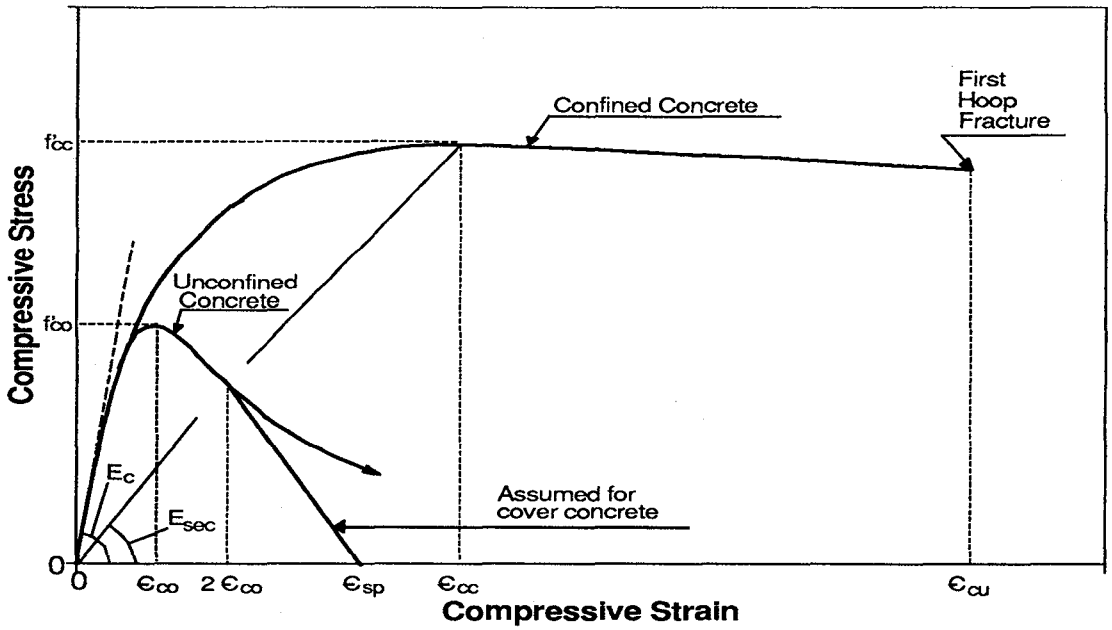

Fig. 4.1 Concrete Compressive Stress-Strain model proposed by Mander et.al. (1988a)

Monotonic Loading

Fig. 4.1 presents the idealization of the stress-strain relation for confined and unconfined concrete proposed and verified by Mander et.al. (1988a,b). This model is based on an equation by Popovics (1973). For a slow strain rate and monotonic loading, the compressive stress f_c is given by

$$f_c = \frac{f'_{cc}\, x\, r}{r-1+x^r} \tag{4.1}$$

where

$$x = \varepsilon_c / \varepsilon_{cc} \tag{4.2}$$

$$\varepsilon_{cc} = \varepsilon_{co}\left[\, 1+ 5\,(K - 1)\,\right] \tag{4.3}$$

$$K = f'_{cc} / f'_{co} \tag{4.4}$$

$$r = \frac{E_c}{E_c - E_{sec}} \tag{4.5}$$

$$E_{sec} = f'_{cc} / \varepsilon_{cc} \tag{4.6}$$

in which f'_{cc} = compressive strength of confined concrete, ε_c = compressive concrete strain, f'_{co} = compressive strength of unconfined concrete, ε_{co} = compressive concrete strain corresponding to f'_{co}, and E_c = tangent modulus of elasticity of the concrete.

To define the cover concrete stress-strain behavior, the falling branch where $\varepsilon_c > 2\,\varepsilon_{co}$ is represented by a straight line which attains zero stress at ε_{sp} (spalling strain). The ultimate compression strain for confined concrete is limited by eventual fracture of the hoops. The prediction of the strain corresponding to first hoop fracture can be estimated by energy considerations. The passive lateral confining produced by the transverse reinforcement results in an increase of the axial compression strength and a very ductile stress behavior. The strength enhancement ratio ($K = f'_{cc} / f'_{co}$), which is the most important parameter for design, is based on a 5-parameter multi-axial failure criterion developed by Willam and Warkne (1975). For the

columns considered in this study, equi-biaxial (triaxial) confinement of the concrete core results from the presence of transverse hoop reinforcement. The ultimate concrete strength is given by

$$K = \frac{f'_{cc}}{f'_{co}} = 2.254 \sqrt{1 + 7.94 \frac{f'_l}{f'_{co}}} - 2 \frac{f'_l}{f'_{co}} - 1.254 \tag{4.7}$$

where f'_l = effective lateral confining pressure given by

$$f'_l = \frac{1}{2} k_e \rho_s f_{yh} \tag{4.8}$$

in which f_{yh} = yield stress of the hoop reinforcement, k_e = a confinement effectiveness coefficient defined below, and ρ_s = volumetric ratio of the transverse reinforcement given by

$$\rho_s = \frac{2 A_{sh}}{s d_c} \tag{4.9}$$

where A_{sh} = total area of transverse reinforcement measured parallel to the principal bending axis, s = center-to-center spacing of the hoopsets, and d_c = width of the core measured from the centerline of the perimeter hoop. The confinement effectiveness coefficient for a square column is given by

$$k_e = \left(1 - \frac{n}{6}\left(\frac{w'}{d_c}\right)^2\right) \frac{(1 - 0.5\, s'/d_c)^2}{(1 - \rho_{cc})} \tag{4.10}$$

in which , n = number of longitudinal bars in the column, w' = clear spacing between longitudinal bars, s' = clear spacing between transverse hoops, and $\rho_{cc} = A_{st} / d_c^2$ = volumetric ratio of the longitudinal reinforcement with respect to the confined core.

Cyclic Loading

The monotonic loading stress-strain curve for confined concrete presented in Fig. 4.1 is used as an envelope to the cyclic loading response. Unloading and reloading curves are developed following paths which are described by modified forms of Equations 4.1 to 4.6. Finally, the model allows for a dynamic response by modifying the concrete parameters (f'_{cc}, ε_{cc}, and E_c) by magnification factors which are a function of the strain ε_c and the stress f'_{co}.

4.2.2 Moment-Curvature Analysis

The moment-curvature analysis is based on the following general assumptions:

1. Plane sections remain plane due to bending.
2. The cover concrete has zero strength after the spalling strain ε_{spall} is exceeded.
3. The concrete is assumed to crack once the tensile strength has been exceeded.
4. Shear deformation due to sliding shear and diagonal cracking is ignored.
5. No effects of creep and shrinkage have been considered.
6. Bond slip between the longitudinal bars and the concrete core has been ignored.
7. The longitudinal reinforcing steel is prevented to buckle by the transverse hoops.

The conventions and idealization employed in the analysis are presented in Fig. 4.2.

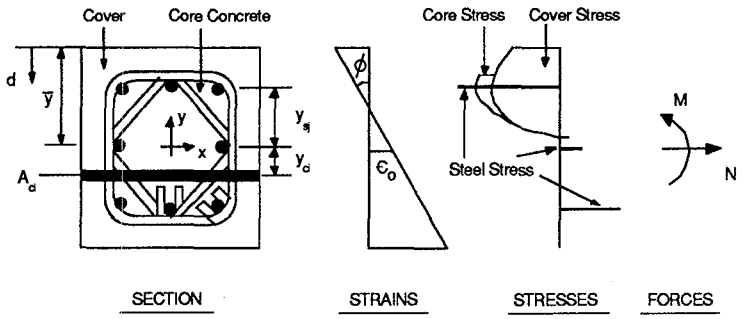

Fig. 4.2 Conventions for Section Analysis

For the analysis, the section is divided into a number of discrete laminae with the long sides parallel to the neutral axis of bending. Similarly the longitudinal steel is divided into a number of levels. As shown in Fig. 4.2, the strain distribution for the cross section can be expressed as follows

$$\varepsilon(y) = \varepsilon_o + \phi\, y \tag{4.11}$$

in which ε_o = strain at the centroidal axis, ϕ = section curvature, and y = distance from the reference axis.

The axial load, N, and the bending moment, M, can be determined from Eqs. 4.12 and 4.13 once the stresses for concrete and steel have been determined for each laminae and level.

$$N = \sum_{i=1}^{nc} f_{ci} A_{ci} + \sum_{j=1}^{ns} f_{sj} A_{sj} \tag{4.12}$$

$$M = \sum_{i=1}^{nc} f_{ci} A_{ci} y_{ci} + \sum_{j=1}^{ns} f_{sj} A_{sj} y_{sj} \tag{4.13}$$

in which nc = number of concrete elements, ns = number of steel levels, f_{ci} and f_{sj} = stresses in the ith concrete lamina or in the jth steel level, and finally, y_{ci} and y_{sj} = distance from the centroidal axis to the center of the ith concrete lamina or the jth steel level.

The stresses for both the confined and unconfined concrete are determined from the relations presented in the previous section. The centerline of the transverse hoops is considered as the borderline between confined and unconfined concrete.

Usually, the moment-curvature relationships are determined for a preestablished axial load, $\mathbf{P_e}$, therefore force and strain compatibility is required and Eqs. 4.11 and 4.12 must be solved simultaneously. In this study an incremental approach has been adopted. Incremental forces (ΔM, ΔP)are related to incremental deformations ($\Delta\phi$, $\Delta\varepsilon_o$)by the instantaneous section stiffness according to the following equation

$$\begin{pmatrix} \Delta M \\ \Delta P \end{pmatrix} = \begin{bmatrix} EI & EZ \\ EZ & EA \end{bmatrix} \begin{pmatrix} \Delta\phi \\ \Delta\varepsilon_o \end{pmatrix} \tag{4.14}$$

The section stiffness coefficients are obtained by numerically integrating across the section as follows

$$EA = \sum_{i=1}^{nc} E_{ci} A_{ci} + \sum_{j=1}^{ns} E_{sj} A_{sj} \tag{4.15}$$

$$EZ = \sum_{i=1}^{nc} E_{ci} A_{ci} y_{ci} + \sum_{j=1}^{ns} E_{sj} A_{sj} y_{sj} \tag{4.16}$$

in which EA = effective axial stiffness, and EZ = first moment of area.

The effective flexural stiffness, EI, is now defined as

$$EI = \sum_{i=1}^{nc} E_{ci} A_{ci} y_{ci}^2 + \sum_{j=1}^{ns} E_{sj} A_{sj} y_{sj}^2 - EA\ e_y^2 \tag{4.17}$$

where the eccentricity from the neutral axis of the incremental section stiffness, e_y, is given by

$$e_y = \frac{EZ}{EA} \tag{4.18}$$

Finally, Eq. 4.14 can be rewritten as

$$\Delta P = EZ\ \Delta\phi + EA\ \Delta\varepsilon_o \tag{4.19}$$

where the out of balance force ΔP is

$$\Delta P = N - P_e \tag{4.20}$$

in which the axial load, N, is calculated using Eqs. 4.14 and 4.15.

4.2.3 Force-Deformation Analysis

It is very important to realize that the curvature calculated by the computer model was evaluated at the critical section being located just above the base, while the experimental curvature presented is an average curvature measured over the 1.75 in. lower gage length. This method of determining the curvature includes the effect of yield penetration into the base. Fig. 4.3 presents the assumed distribution of plastic curvature considered in the analysis. A parabolic distribution of plastic curvature is assumed when the bending moment and corresponding curvature surpass the first yield moment and curvature.

The plastic curvature ϕ_p at the critical section is given by the following expression

$$\phi_p = \left(\phi - \phi_y' \frac{M}{M_y} \right) \tag{4.21}$$

in which ϕ = current curvature in thge analysis, ϕ_y' = first yield curvature, M = current moment in the analysis, and M_y = yield moment.

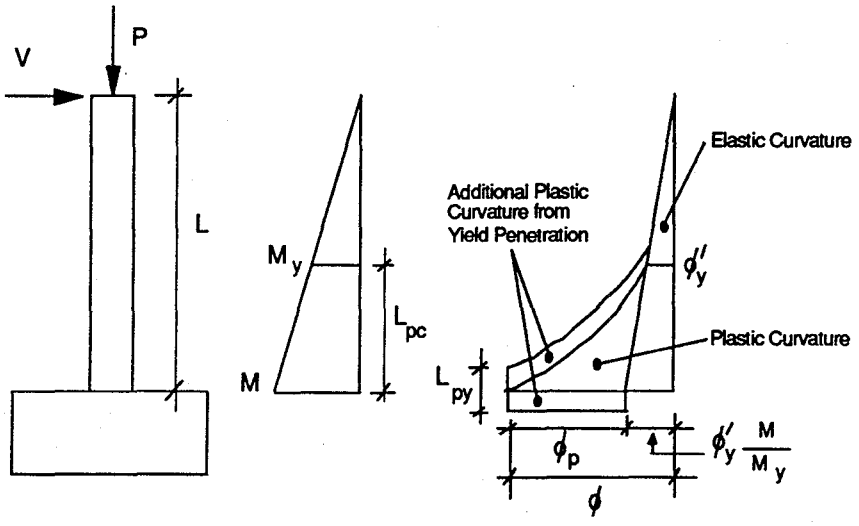

Fig. 4.3 Assumed Distribution of Plastic Curvature

As shown in Fig. 4.3, some additional plastic curvature comes from yield penetration in both the region of plastic curvature and the end base region of the column. Assuming that the shape of the plastic curvature can be approximated by a second order parabola, the plastic displacement Δ_p can be obtained as follows

$$\Delta_p = \phi_p \left(\frac{L_{pc}}{3} + L_{py} \right) \left(L - \frac{L_{pc}}{4} \right) \tag{4.22}$$

where the length of the plastic curvature distribution L_{pc} is given by

$$\frac{L_{pc}}{L} = 1 - \left| \frac{M_y}{M_{max}} \right| \tag{4.23}$$

in which L = length of the column, M_{max} = maximum bending moment, and L_{py} = length of yield penetration.

Shear deformations are incorporated into the analysis by assigning the column member cracked and uncracked stiffness. Cracked shear stiffness analysis is based on the equivalent truss approach described in Park and Paulay (1975).

4.3 Results of Cyclic Force-Deformation Analysis

A comparison between the predicted hysteresis curves using the computer program and the experimental results is presented. Figs. 4.4 to 4.11 present experimental and analytical lateral load-drift and lateral load-curvature hysteresis curves for all four column specimens. The nominal lateral load capacity of the specimen is plotted as a dashed line superimposed on the experimental and analytical curves.

The nominal capacity is based on the usual ACI strength calculations using the ACI stress block and assuming the reinforcing steel behaves elasto-plastically. Measured material properties were used and no undercapacity factor has been included (i.e. $\phi = 1$). For Specimens 1 and 3 (columns with lap splice) only the net steel area at the base of the column has been considered.

For the computer analysis, input data presented in Tables 4.1 to 4.3 was obtained as follows. Experimental values of the stress and strain parameters for the longitudinal and transverse steel presented in Fig. 1.8 were used for tension, while the compressive values were estimated from the recommendations made by Mander et.al. (1984). Results of cylinder tests presented in Table 4.2 were used to characterize the unconfined concrete. Table 4.3 presents the parameters of the confined core concrete which were determined from Eqs. 4.3 and 4.7.

Table 4.1 Steel Properties

Longitudinal Bars (D4)	f_y (ksi)	E_s (ksi)	ε_{sh}	E_{sh} (ksi)	f_{su} (ksi)	ε_{su}
Tension	65	31050	0.026	750	73	0.107
Compression	65	32290	0.014	1035	70	0.066

Table 4.2 Unconfined Concrete Properties

Concrete Pour	f'_{co} (ksi)	ε_{co}	E_c (ksi)	ε_{spall}
Lower Columns	3.40	0.0023	2920	0.015
Upper Columns	4.35	0.0023	3900	0.020

Table 4.3 Confined Concrete Properties

Concrete Pour	f'_{cc} (ksi)	ε_{cc}	E_c (ksi)	ε_{cu}
Lower Columns	4.50	0.0057	2920	0.050
Upper Columns	5.00	0.0042	3900	0.050

The hysteresis graphs show that the strength and degradation of the columns were generally predicted quite well. In each case the analytical maximum lateral load was within ±8% of the experimentally observed maximum lateral load. For Specimens 4 and 2, the columns without lap splice, the shape of the hysteresis loops including degradation of strength due to cyclic loading was also estimated well. The variation of axial load during testing of Specimen 4 caused different maximum strength values for forward and reverse loading. This aspect was well predicted by the model.

As expected, in the case of Specimens 1 and 3, the columns with a lap splice, there are some discrepancies in the shape of the hysteresis loops. These discrepancies are principally due to the influence of the lap splice which is an aspect that has been ignored in the present study. However, such an analysis clearly shows the effects of the lap zone on the overall response. It is important to point out that for the specimen with the high axial load (Specimen 1, P=0.39 $f'_c A_g$) the discrepancy in the shape of the hysteresis loops is less significant. It appears that in this case the lap splice was principally behaving as a compression splice with little slippage.

Even though the difference in maximum strength values for forward and reverse loading for Specimen 3 was captured by the model, it is noticeable that the strength degradation for reverse loading was not so well predicted, once again due to the lack of consideration of bond deterioration within the lap splice zone combined with the low level of axial load which tended to cause the lap splice to behave primarily as a tension splice. Furthermore, the low level of axial load for Specimen 3 (P=0.13 $f'_c A_g$) led to pinching of the experimental hysteresis loops which was not predicted well in the analytical curves. Clearly, this difference is due to the bond slippage within the tension splice zone.

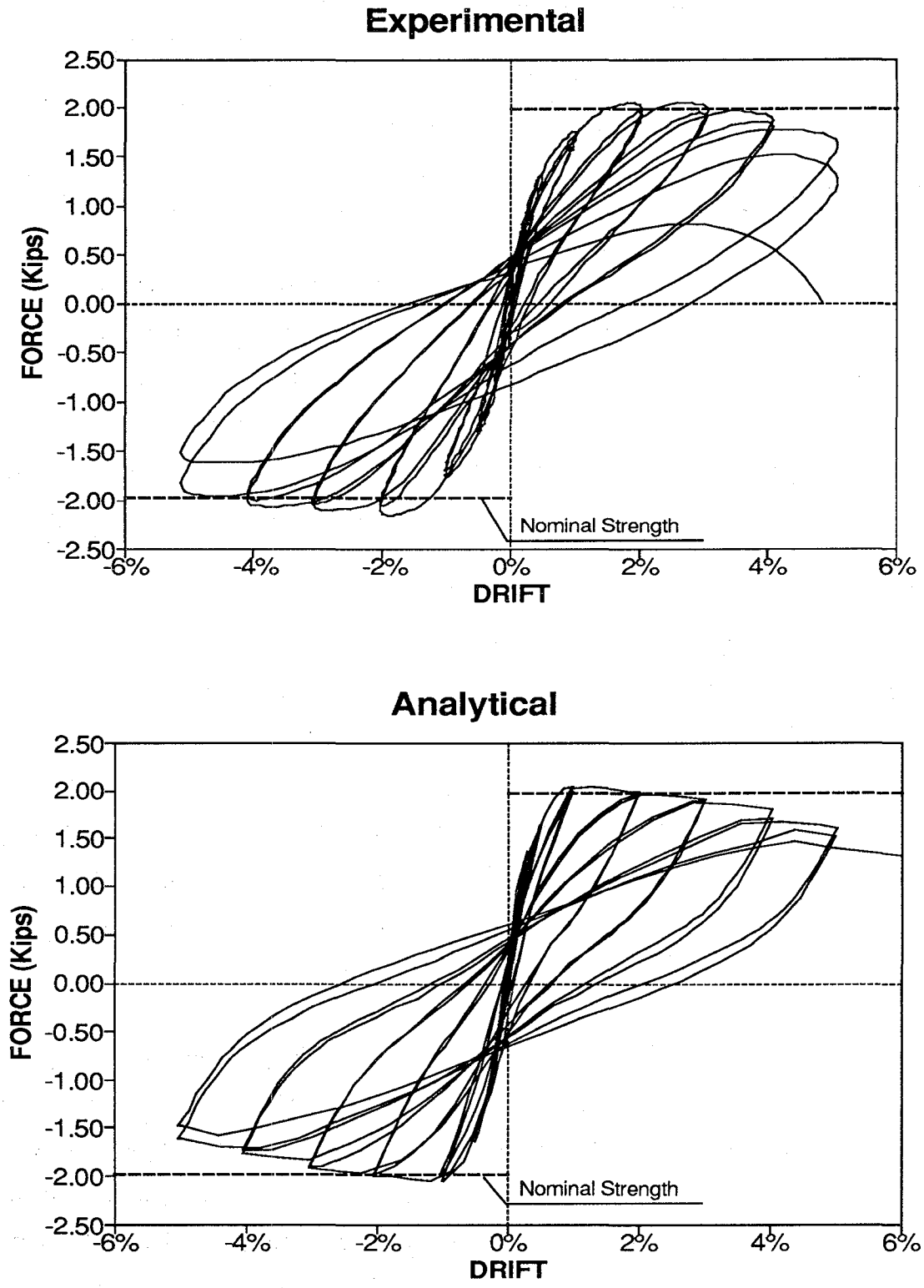

Fig. 4.4 Experimental and Analytical Lateral Load-Drift Response for Upper Interior Column (Specimen 2)

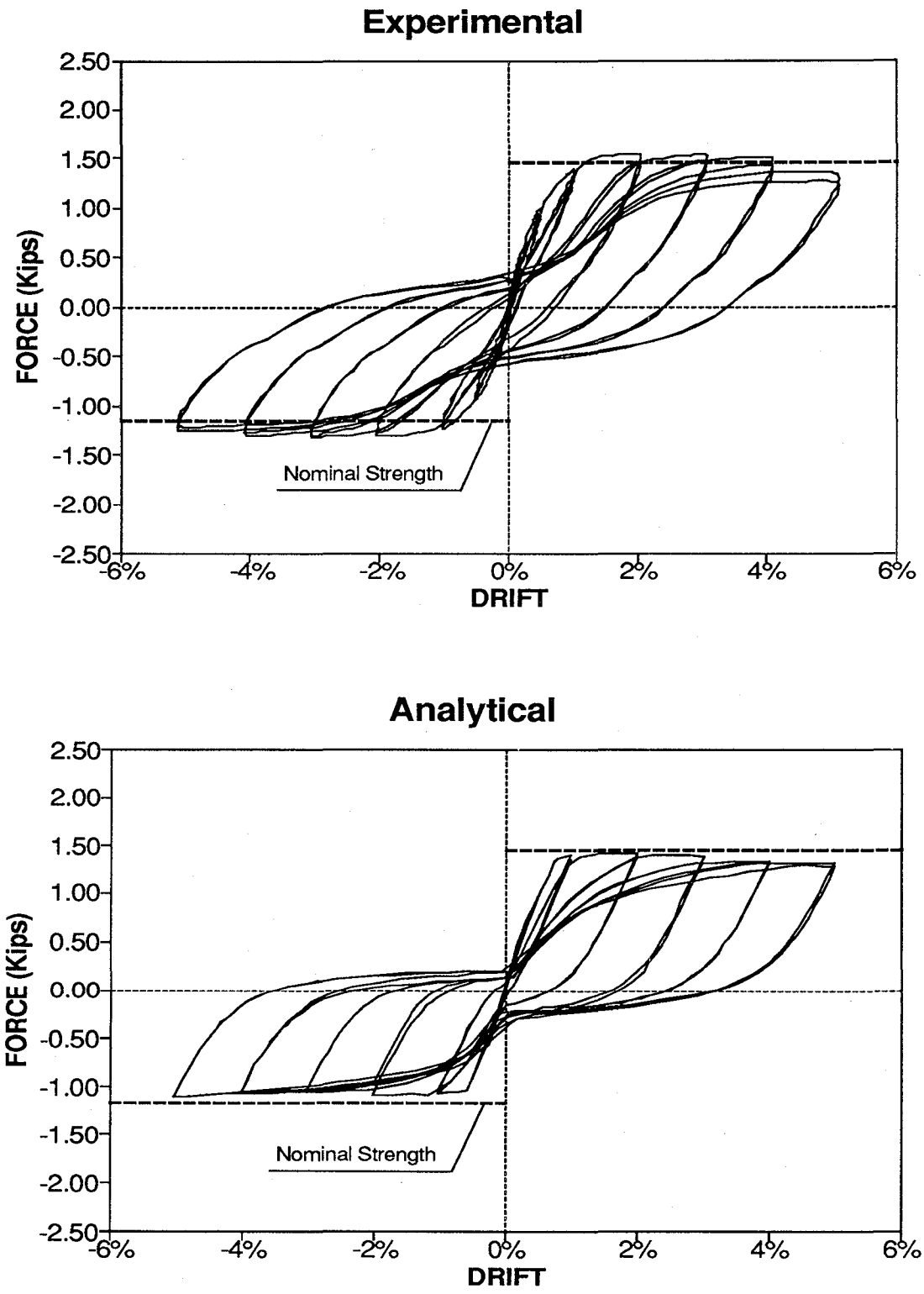

Fig. 4.5 Experimental and Analytical Lateral Load-Drift Response for Upper Exterior Column (Specimen 4)

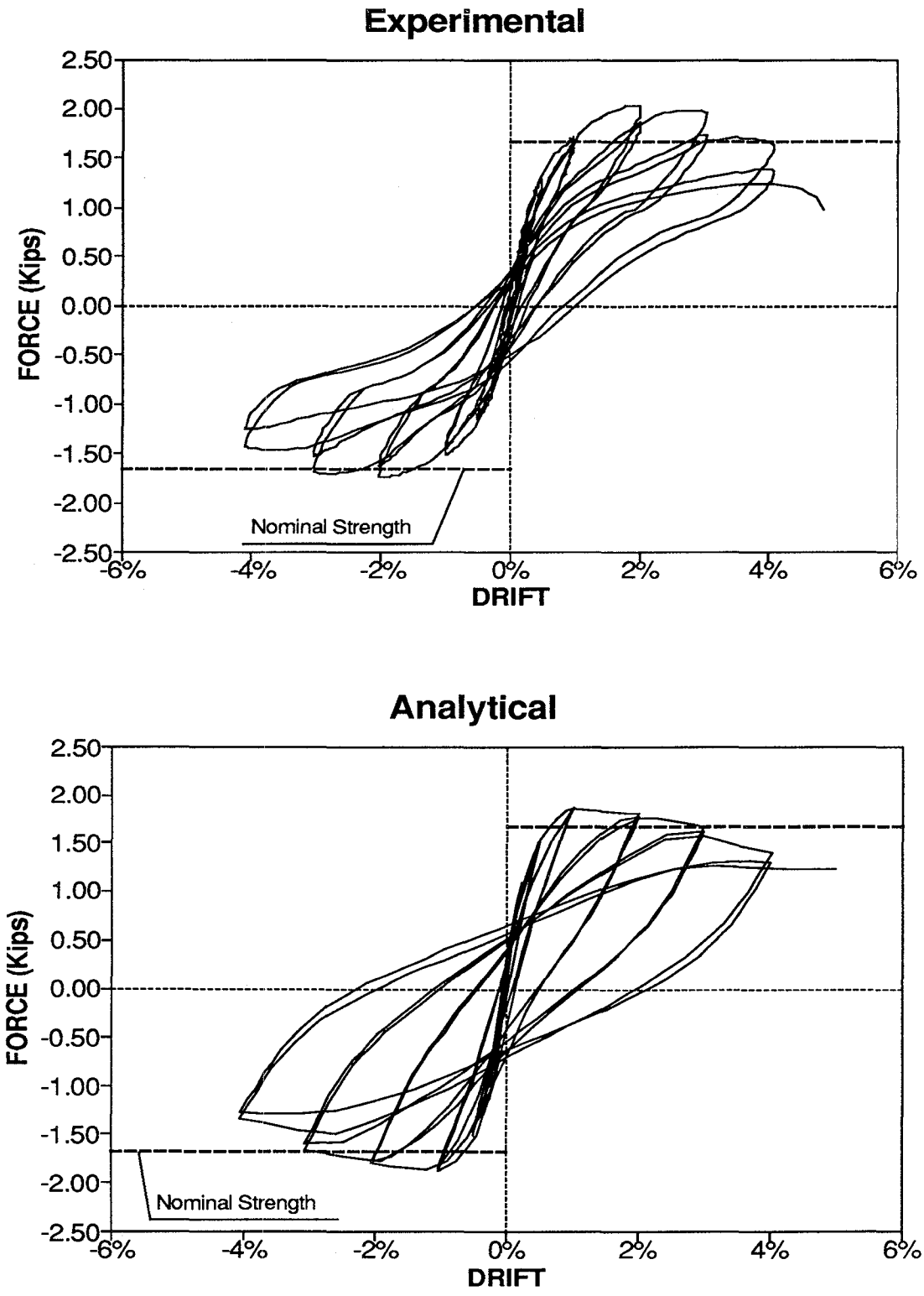

Fig. 4.6 Experimental and Analytical Lateral Load-Drift Response for Lower Interior Column with lap splice (Specimen 1)

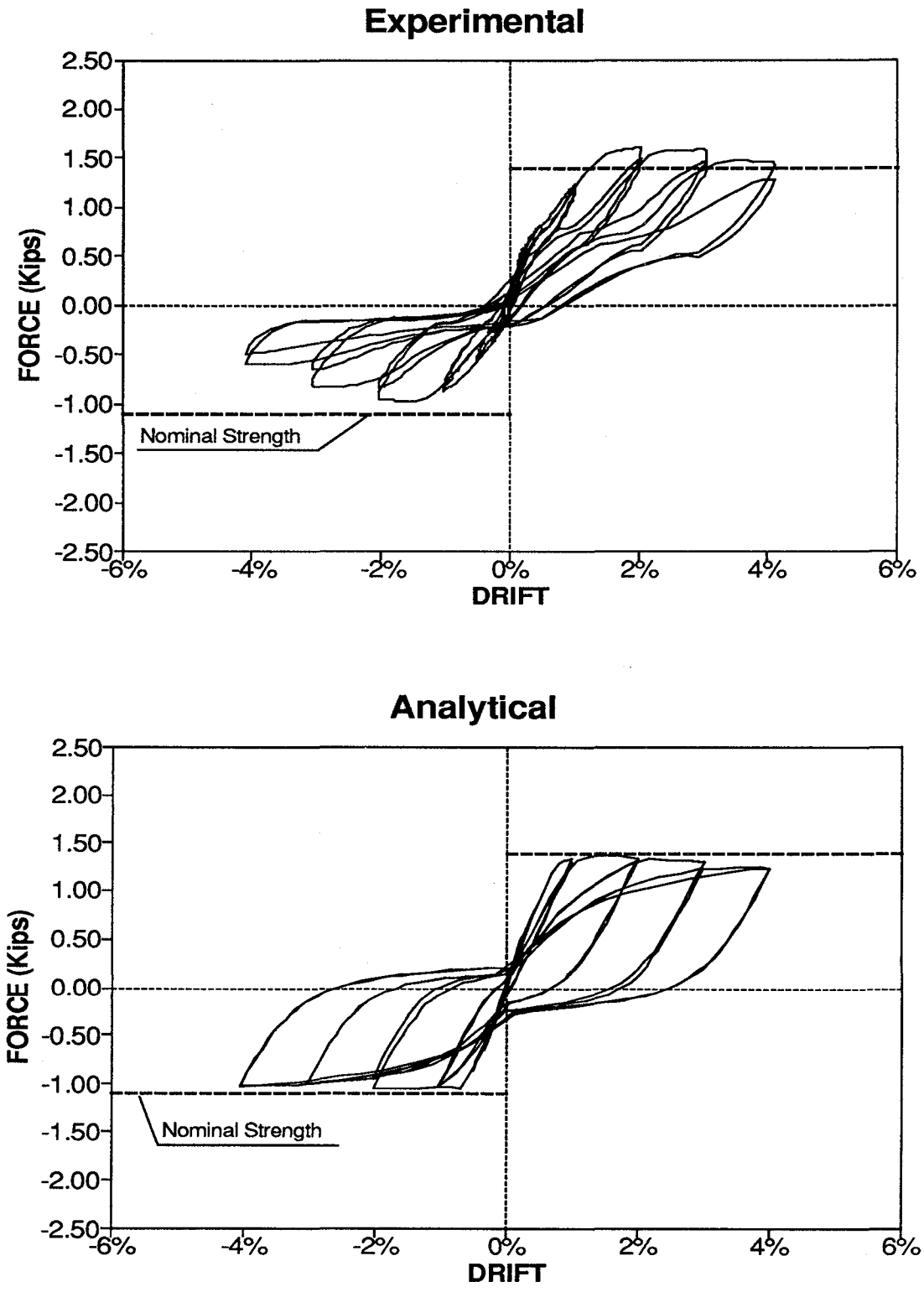

Fig. 4.7 Experimental and Analytical Lateral Load-Drift Response for Lower Exterior Column with lap splice (Specimen 3)

It is evident that the closure of cracks appears to occur abruptly in the analytical curves when compared to the experimental behavior. The analytical model considers that cracked concrete does not carry compressive stress before the cracks fully close. In reality, shear displacements offset the cracks surfaces causing high peaks to come into contact more gradually, and therefore some compressive stress is gradually transferred across the cracks. A more gentle stress-strain reloading branch reflecting this phenomenon would improve the results.

The lateral load-curvature graphs presented in Figs. 4.8 to 4.11 show reasonable agreement. It should be recalled that the experimental curvatures are an average measured over a 1.75" gage length at the end of the column. The experimental curvatures are therefore under-estimations of the critical curvature measured at the end of the column proper.

It is worth noting that the length of yield penetration L_{py} is the only undefined control parameter for the complete determination of the plastic displacement. Based on calibrating different experimental studies, Mander et.al. (1984) suggested that L_{py} could be approximated in terms of the longitudinal bar diameter d_b such that

$$L_{py} = 32\sqrt{d_b} \quad (mm) \quad = \quad 6.35\sqrt{d_b} \quad (in) \tag{4.24}$$

This was based on near full size column specimen tests where the axial load was varied up to $0.60\, f_c' A_g$. The values of L_{py} obtained in the present analytical study are presented in Table 4.4.

Table 4.4 Analytical Length of Yield Penetration

Specimen	1	2	3	4	$32\sqrt{d_b}$
L_{py} (in)	4.75	4.75	2.00	2.00	3.00

The value given by Eq. (4.24) seems to be low for Specimens 1 and 2 (Columns with high axial load and high for Specimens 3 and 4 (Columns lightly loaded). As all other variables were the same there appears to be a strong influence from the axial load intensity on the value of L_{py}. However, the value given by Eq. (4.24) could be taken as an average reference, as the variation does not seriously affect the shape of the resulting hysteretic loops, but rather affects the ultimate curvature and hence maximum concrete and steel strains.

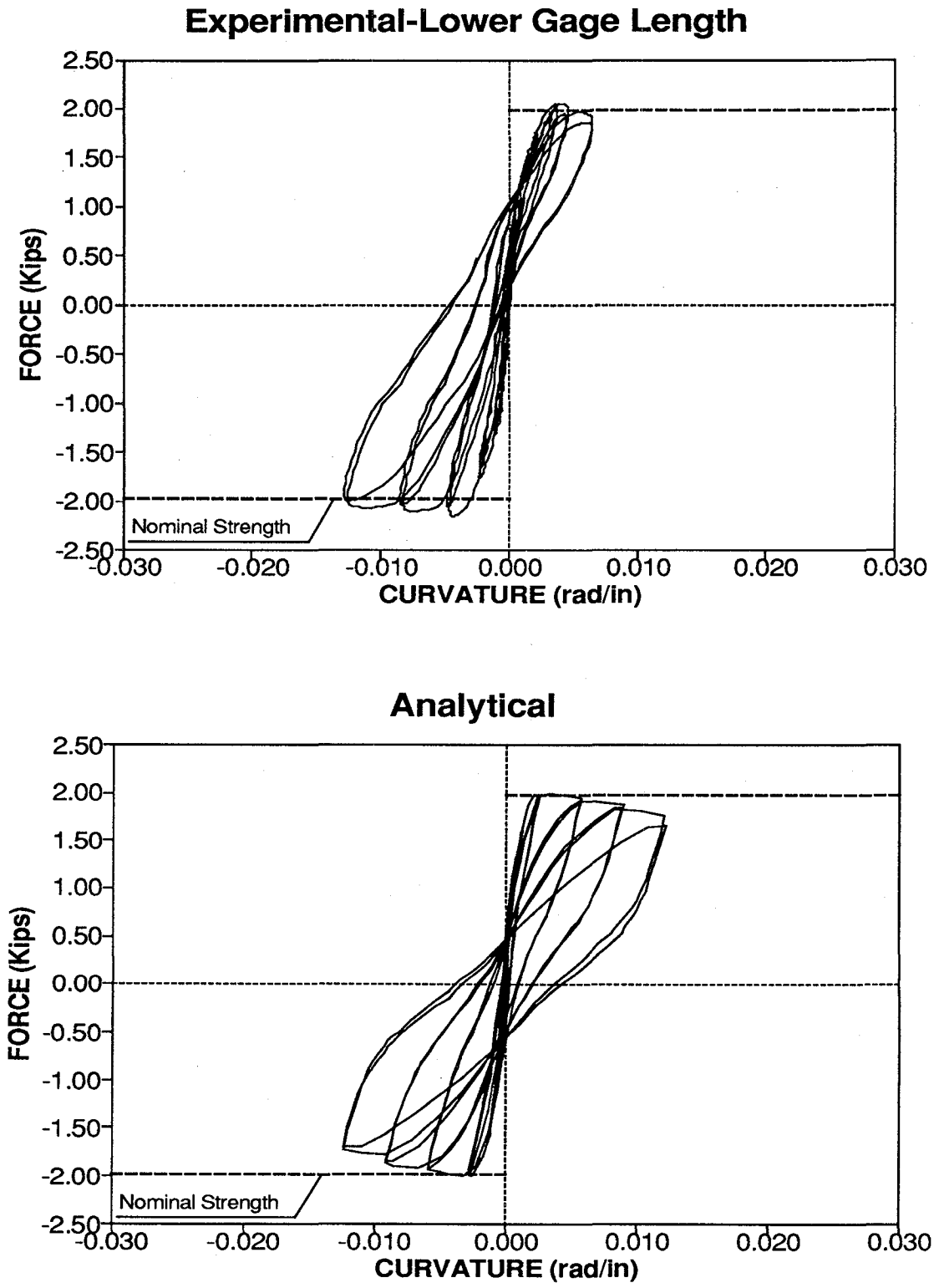

Fig. 4.8 Experimental and Analytical Lateral Load-Curvature Response for Upper Interior Column (Specimen 2)

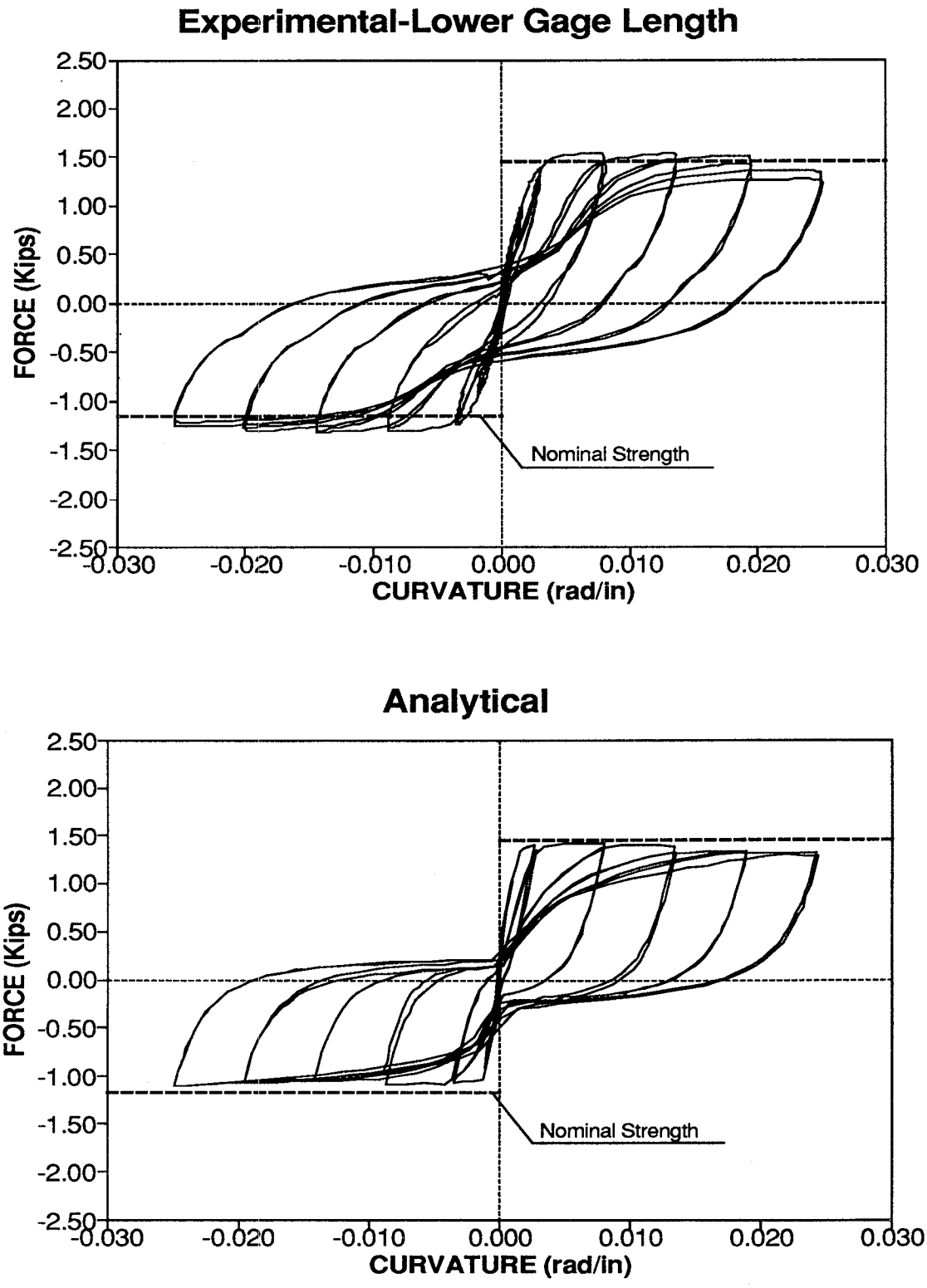

Fig. 4.9 Experimental and Analytical Lateral Load-Curvature Response for Upper Exterior Column (Specimen 4)

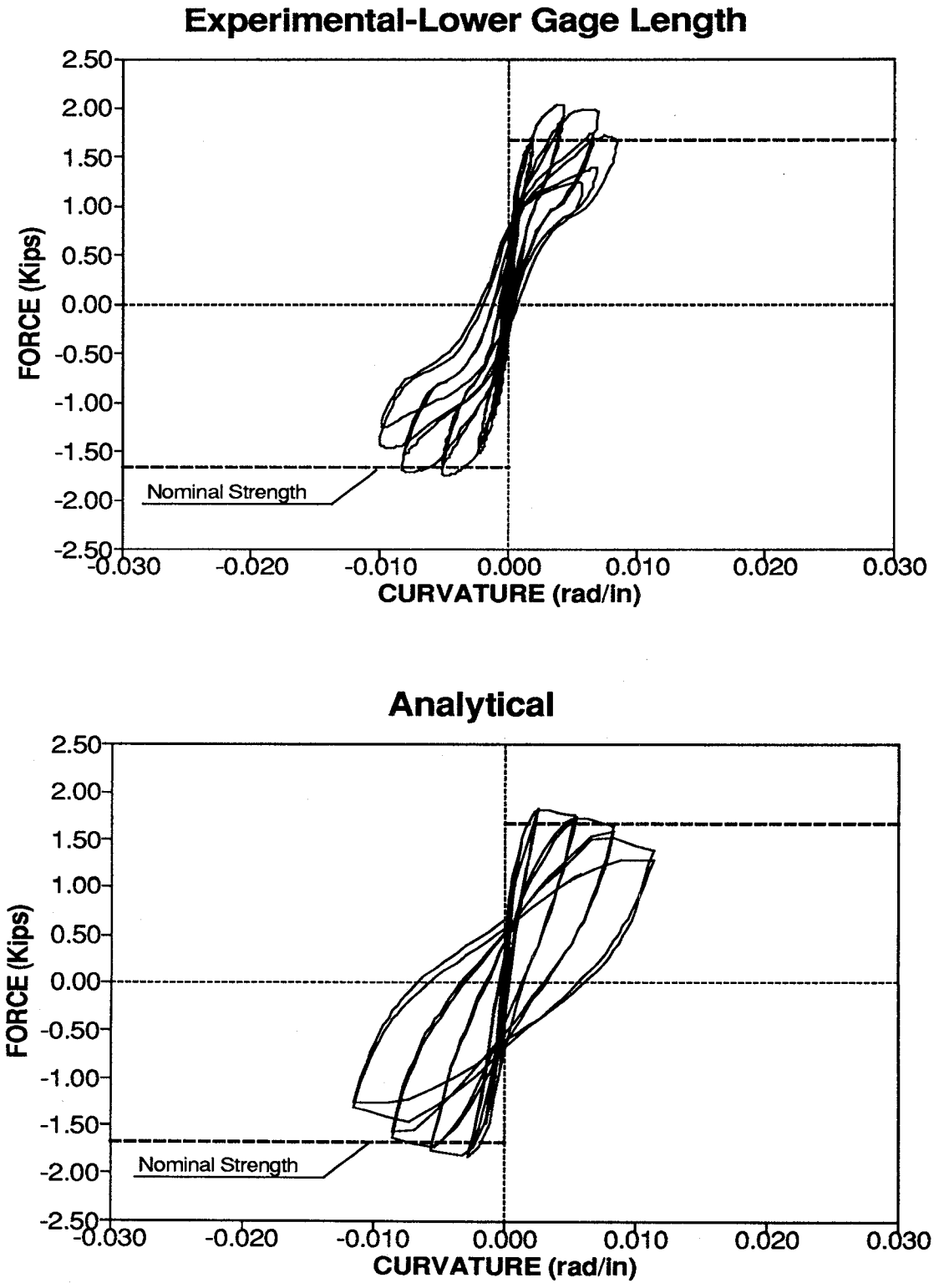

Fig. 4.10 Experimental and Analytical Lateral Load-Curvature Response for Lower Interior Column with lap splice (Specimen 1)

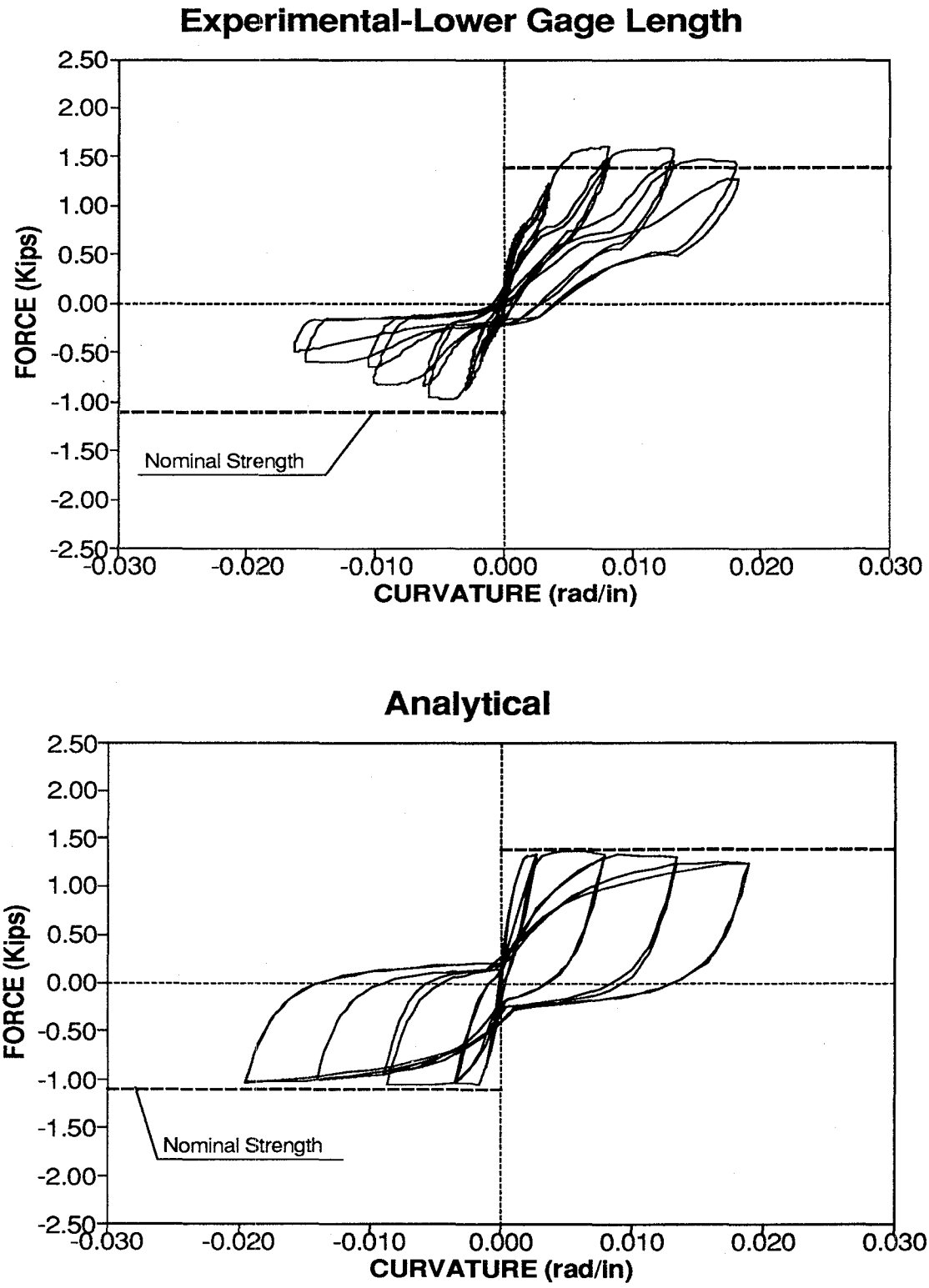

Fig. 4.11 Experimental and Analytical Lateral Load-Curvature Response for Lower Exterior Column with lap splice (Specimen 3)

4.4 Conclusions

1. Prediction of the maximum lateral load strength of the column specimens was achieved. The shape of the hysteresis loops was also well predicted in general. Therefore, the energy dissipated by the columns under cyclic loading was well estimated.

2. The major discrepancies occurred where lap splices were present. However, the disparity diminished for high level of axial load. It is suspected that in the case of high axial load, there might be some compression contribution from the upper lap splice bars as they are compressed against the base concrete. Special considerations for lap splices should be introduced in the analytical model, particularly for tension splices.

3. The analytical graphs for the lightly loaded exterior columns (Specimens 3 and 4) displayed some pinching. This is due to the fact that the model assumes that cracked concrete in the compression zone does not carry any compressive stress before the cracks entirely close. This pinching effect is more evident in Specimens 3 and 4 because the low level of axial load leads to very wide open cracks. A more gradual reloading branch which considers some compression transfer across the cracks should be implemented in the model.

4. The yield penetration length showed to be a determinant factor in the prediction of the plastic curvature. A recommended value of $L_{py} = 32\sqrt{d_b}$ $(mm) = 6.35\sqrt{d_b}$ (in) by Mander et.al. (1984) appears to be a reasonable average value. However, it is worth noting that the yield penetration length appears to be quite sensitive to the level of axial load.

SECTION 5

SUMMARY AND CONCLUSIONS

The results presented in this report were used to identify member characteristics which could be used for: (i) Plastic analysis of the model frame structure; and (ii) Development of specific hysteretic rules for non-linear time history analysis of the model frame structure. The comparison between the experimental performance of the one-third scale model building and the predicted behavior using the results from component tests is presented in Part III of the evaluation report series (Bracci et.al. 1992a).

It is well known and accepted that structural detailing such as lap splices in potential plastic hinge zones, lack of joint core reinforcement, minimal transverse reinforcement in columns for shear and confinement, particularly in plastic hinge zones, and discontinuous positive bottom beam flexural reinforcement in the beam-column joint could lead to an undesirable soft-story or column sidesway failure mechanism. However, the results of this experimental program showed that structural components with such detrimental details could reach their nominal strength capacities and sustain their gravity loads for large cyclic deformations. These results suggest, as presented in Part II of the retrofit report series (Bracci et.al. 1992c), that simple retrofit techniques for the interior columns will improve the hysteretic behavior of the model and most importantly prevent the undesirable column failure mechanism.

Tables 5.1 to 5.7 give a summary of important characteristics of the experimental results. The remainder of this section presents a summary of the conclusions given at the end of Sections 2 to 4, as well as some general recommendations.

Failure Modes:

Column failure was flexurally dominated. The hoop spacing in the columns appeared to be sufficient for shear demand. However, for high axial loads, the spacing was not appropriate to prevent buckling of the longitudinal reinforcement after spalling of the concrete cover occurred. This eventually led to column collapse. Had additional hoops been provided in the plastic hinge zone, the confining action would have prevented bar buckling and collapse.

For columns with a low level of axial load, large strain reversals in the longitudinal reinforcement led to a low cycle fatigue failure in that steel.

Test results of the subassemblages showed that a hybrid type of failure mechanism was more likely to occur for a complete structural frame. The exterior subassemblage showed a weak beam-strong column mechanism basically due to the inappropriate anchorage of the bottom steel of the beam. The interior subassemblage presented a weak column-strong beam mechanism which is totally undesirable.

Some joint damage was detected for exterior and interior joints. The exterior joint appeared to suffer damage at large drifts, whereas the interior joint showed progressive inelastic shear distortion from the early stages of the test. It appears that the limited joint reinforcement and the smaller shear demand, present in the exterior joint, helped in delaying the loss of integrity of that joint.

Even though the interior joint did not fail, appreciable inelastic joint shear distortion was detected. Therefore, some joint reinforcement should be necessary to inhibit inelastic joint core displacements even when the bottom bars are discontinuous.

For all column specimens and both subassemblages, maximum strength was observed between 2 and 3% drift amplitude which suggests that the drift limit of 1% set by the codes is unnecessarily conservative. If appropriate detailing of the structure were provided, this limit could be increased without hesitation.

Lap Splices:

Tests results of the four column specimens showed that columns without lap splices had better energy dissipation characteristics. Columns with a lap splice failed after a smaller severe number of cycles, displaying a smaller total energy dissipation. However, the lap splice appeared to be of sufficient length to enable the column to reach its nominal flexural strength capacity.

The columns with a lap splice have smaller hysteretic energy dissipation per cycle primarily due to the bond slip of the lap splice as reflected in pinched hysteretic curves.

Lap splices for the columns should be avoided at the slab level, if that location is a potential plastic hinge zone. However, a beam sidesway mechanism can be enforced if the column is made appreciably stronger than the beams. Furthermore, if an undercapacity factor of 0.5 is used for column design, then there is little chance of column hinging thus, for ease of construction, lap splices could be located at floor slab level in the upper stories of a frame as recommended by Paulay and Priestley (1992). In any case, laps should be avoided at the ground level.

Plastic Hinge Zone:

A lower bound for the equivalent plastic hinge length can be taken as 50% of the column width. This is appropriate if the level of axial load is relatively low. As the axial load increases, so does the equivalent plastic hinge length. Columns with a high level of axial load and a lap splice provide an upper bound for the equivalent plastic hinge length. Here the hinge length is approximately equal to the lap splice length.

Analytical Modeling:

A reasonable analytical prediction of the hysteretic behavior of the column specimens was accomplished. The maximum lateral strength as well as the main hysteretic characteristics (initial stiffness, energy dissipation, strength and stiffness degradation) were successfully predicted. As expected, some differences were found in the case of columns with lap splices. The most important aspect that should be introduced in the model is a gradual reloading branch considering that some compression stress is gradually transferred prior to complete closure of the tensile flexure cracks.

Table 5.1 Column Specimens Strength

Specimen		Strength		
		Nominal (Kips)	Achieved (ratio)[*1]	Degraded min. (ratio)[*1]
1. Lower Interior		1.67	1.22	0.83 (4%)[*3]
2. Upper Interior		1.98	1.03	0.76 (5%)[*3]
3. Lower Exterior	(F)[*2]	1.38	1.15	0.93 (4%)[*3]
	(R)[*2]	1.11	0.88	0.45 (4%)[*3]
4. Upper Exterior	(F)[*2]	1.46	1.05	0.87 (5%)[*3]
	(R)[*2]	1.16	1.14	1.04 (5%)[*3]

[*1] - Ratio with respect to the nominal strength.
[*2] - (F)= forward loading.
(R)= reverse loading.
[*3] - Level of drift at which the maximum degradation occurred.

Table 5.2 Exterior Subassemblage - Columns Strength

Member	Strength		
	Nominal (Kips)	Achieved	
		Forward[*1] (ratio)[*2]	Reverse[*1] (ratio)[*2]
Top Column	1.07	0.53	1.20
Bottom Column	1.20	0.48	1.07

[*1] - Loading direction.
[*2] - Ratio with respect to the nominal strength.

Table 5.3 Exterior Subassemblage - Longitudinal Beam Strength

Nominal (F)[*1]			Achieved (ratio)[*3]	Nominal (R)[*1]		Achieved (ratio)[*4]
Full B.[*2] (Kips)	Part. B.[*2] (ratio)[*3]	No B.[*2] (ratio)[*3]		No Slab (Kips)	Top Slab Steel Part. (ratio)[*4]	
0.88	0.47	0.31	0.65	0.48	3.06	2.67

[*1] - (F)= forward loading.
(R)= reverse loading.
[*2] - Refers to bottom bars fully bonded, partially bonded and unbonded (see Section 3.7).
[*3] - Ratio with respect to the nominal strength for bottom bars fully bonded.
[*4] - Ratio with respect to the nominal strength for no slab participation.

Table 5.4 Interior Subassemblage - Columns Strength

Member	Stage 1		Stage 2	
	Nominal (Kips)	Achieved (ratio)*1	Nominal (Kips)	Achieved (ratio)*1
Top Column	1.27	1.29	2.55	0.83
Bottom Column	1.51	1.09	1.51	1.40

*1 - Ratio with respect to the nominal strength.

Table 5.5 Interior Subassemblage - Longitudinal Beam Strength (Stages 1 and 2)

Stage 1				Stage 2			
Nominal			Achieved (rat.)*2	Nominal			Achieved (rat.)*2
Full B.*1 (Kips)	P.B.*1 (rat.)*2	No B.*1 (rat.)*2		Full B.*1 (Kips)	P. B.*1 (rat.)*2	No B.*1 (rat.)*2	
2.75	0.82	0.76	0.60	3.50	0.82	0.76	0.60

*1 - Refers to bottom bars fully bonded, partially bonded and unbonded (see Section 3.8).
*2 - Ratio with respect to the nominal strength for bottom bars fully bonded.

Table 5.6 Interior Subassemblage - Longitudinal Beam Strength (Stage 3)

Stage 3						
Positive Moment				Negative Moment		
Nominal			Achieved (ratio)*2	Nominal		Achieved (ratio)*3
Full B.*1 (K-in)	Part. B.*1 (ratio)*2	No B.*1 (ratio)*2		No Slab (K-in)	Top Slab Steel Part. (ratio)*3	
41.50	0.51	0.34	0.17	39.72	2.08	2.10

*1 - Refers to bottom bars fully bonded, partially bonded and unbonded (see Section 3.8).
*2 - Ratio with respect to the nominal strength for bottom bars fully bonded.
*3 - Ratio with respect to the nominal strength for no slab participation.

Table 5.7 Column Specimens - Stiffness

Specimen		Stiffness				
		Theor. Gross[*1] (EI_g)	Experiment. Observed[*2] (EI)	Experiment. Observed (ratio)[*3]	Experimental Post-Yielding[*4] (ratio)[*3]	Experimental Post-Yielding[*4] (ratio)[*5]
1. Lower Interior		70880	45231	0.64	0.025	0.038
2. Upper Interior		80200	52267	0.65	0.003	0.005
3. Lower Exterior	(F)[*6]	70880	32550	0.46	0.018	0.040
	(R)[*6]	70880	28462	0.40	-0.023	-0.058
4. Upper Exterior	(F)[*6]	80200	37137	0.46	0.006	0.013
	(R)[*6]	80200	37137	0.46	0.011	0.024

[*1] - The theoretical gross stiffness for the cantilever columns has been calculated using I_g = moment of inertia of gross concrete section neglecting the reinforcement, and $E = 57000\sqrt{f'_c}\ psi$.

[*2] - Observed experimental stiffness determined, from a secant slope, by $EI = \frac{P\,L^3}{3\,\Delta}$

where P is 75% of the nominal strength and Δ is the corresponding deflection.

[*3] - Ratio with respect to the theoretical gross stiffness.

[*4] - Experimental post-yielding stiffness measured from nominal ultimate strength at nominal yield to the strength at 3% drift.

[*5] - Ratio with respect to the elastic experimental stiffness.

[*6] - (F)= forward loading.
(R)= reverse loading.

SECTION 6

REFERENCES

1. *ACI Committee 318 (1989). "Building Code Requirements for Reinforced Concrete (ACI 318-89) and Commentary-ACI 318R-89", Detroit, Michigan.*

2. *Bracci, J.M., Reinhorn, A.M., and Mander, J.B. (1992a). "Seismic Resistance of Reinforced Concrete Frame Structures Designed only for Gravity Loads: Part I - Design and Properties of a One-Third Scale Model Structure.", Technical Report NCEER-92-0027.*

3. *Bracci, J.M., Reinhorn, A.M., and Mander, J.B. (1992b). "Seismic Resistance of Reinforced Concrete Frame Structures Designed only for Gravity Loads: Part III - Experimental Performance and Analytical Study of Structural Model.", Technical Report NCEER-92-0029.*

4. *Bracci, J.M., Reinhorn, A.M., and Mander, J.B. (1992c). "Evaluation of Seismic Retrofit of Reinforced Concrete Frame Structures: Part II - Experimental Performance and Analytical Study of Retrofitted Structural Model.", Technical Report NCEER-92-0031.*

5. *Choudhuri, D., Mander, J.B., and Reinhorn, A.M. (1992c). "Evaluation of Seismic Retrofit of Reinforced Concrete Frame Structures: Part I - Experimental Performance of Retrofitted Subassemblages.", Technical Report NCEER-92-0030.*

6. *El-Attar, A.G., White, R.N., and Gergely, P. (1991a). "Shaking Table Test of a 1/6 Scale Two-Story Lightly Reinforced Concrete Building", Technical Report NCEER-91-0017.*

7. *El-Attar, A.G., White, R.N., and Gergely, P. (1991b). "Shaking Table Test of a 1/8 Scale Two-Story Lightly Reinforced Concrete Building", Technical Report NCEER-91-0018.*

8. *Lao, L.F. (1990). "The Effect of Detailing on the Seismic Performance of Gravity Load Dominated Reinforced Concrete Frames", MS Thesis, State University of New York at Buffalo.*

9. *Mander, J.B., Priestley, M.J.N, and Park, R. (1984). "Seismic Design of Bridge Piers.", Research Report No. 84-2, University of Canterbury, Christchurch, New Zealand.*

10. *Mander, J.B., Priestley, M.J.N, and Park, R. (1988a). "Theoretical Stress-Strain Model for Confined Concrete.", J. Struct. Engrg., ASCE, 114(8), 1804-1826.*

11. *Mander, J.B., Priestley, M.J.N, and Park, R. (1988b). "Observed Stress-Strain Behavior of Confined Concrete.", J. Struct. Engrg., ASCE, 114(8), 1827-1849.*

12. *Park, R., and Paulay, T. (1975). "Reinforced Concrete Structures.", John Wiley & Sons, New York, N.Y.*

13. *Paulay, T., and Priestley, M.J.N. (1992). "Seismic Design of Reinforced Concrete and Masonry Buildings.", John Wiley & Sons, New York, N.Y.*

14. *Popovics, S., (1973) "A numerical approach to the complete stress-strain curves for concrete." Cement and Concr. Res., 3(5), 583-599.*

15. *Willam, K.J., and Warnke, E.P., (1975). "Constitutive Model for the Triaxial Behavior of Concrete." IABSE Proceedings, International Association for Bridge and Structural Engineering, Zurich, V.19.*

NATIONAL CENTER FOR EARTHQUAKE ENGINEERING RESEARCH
LIST OF TECHNICAL REPORTS

The National Center for Earthquake Engineering Research (NCEER) publishes technical reports on a variety of subjects related to earthquake engineering written by authors funded through NCEER. These reports are available from both NCEER's Publications Department and the National Technical Information Service (NTIS). Requests for reports should be directed to the Publications Department, National Center for Earthquake Engineering Research, State University of New York at Buffalo, Red Jacket Quadrangle, Buffalo, New York 14261. Reports can also be requested through NTIS, 5285 Port Royal Road, Springfield, Virginia 22161. NTIS accession numbers are shown in parenthesis, if available.

NCEER-87-0001 "First-Year Program in Research, Education and Technology Transfer," 3/5/87, (PB88-134275/AS).

NCEER-87-0002 "Experimental Evaluation of Instantaneous Optimal Algorithms for Structural Control," by R.C. Lin, T.T. Soong and A.M. Reinhorn, 4/20/87, (PB88-134341/AS).

NCEER-87-0003 "Experimentation Using the Earthquake Simulation Facilities at University at Buffalo," by A.M. Reinhorn and R.L. Ketter, to be published.

NCEER-87-0004 "The System Characteristics and Performance of a Shaking Table," by J.S. Hwang, K.C. Chang and G.C. Lee, 6/1/87, (PB88-134259/AS). This report is available only through NTIS (see address given above).

NCEER-87-0005 "A Finite Element Formulation for Nonlinear Viscoplastic Material Using a Q Model," by O. Gyebi and G. Dasgupta, 11/2/87, (PB88-213764/AS).

NCEER-87-0006 "Symbolic Manipulation Program (SMP) - Algebraic Codes for Two and Three Dimensional Finite Element Formulations," by X. Lee and G. Dasgupta, 11/9/87, (PB88-219522/AS).

NCEER-87-0007 "Instantaneous Optimal Control Laws for Tall Buildings Under Seismic Excitations," by J.N. Yang, A. Akbarpour and P. Ghaemmaghami, 6/10/87, (PB88-134333/AS).

NCEER-87-0008 "IDARC: Inelastic Damage Analysis of Reinforced Concrete Frame - Shear-Wall Structures," by Y.J. Park, A.M. Reinhorn and S.K. Kunnath, 7/20/87, (PB88-134325/AS).

NCEER-87-0009 "Liquefaction Potential for New York State: A Preliminary Report on Sites in Manhattan and Buffalo," by M. Budhu, V. Vijayakumar, R.F. Giese and L. Baumgras, 8/31/87, (PB88-163704/AS). This report is available only through NTIS (see address given above).

NCEER-87-0010 "Vertical and Torsional Vibration of Foundations in Inhomogeneous Media," by A.S. Veletsos and K.W. Dotson, 6/1/87, (PB88-134291/AS).

NCEER-87-0011 "Seismic Probabilistic Risk Assessment and Seismic Margins Studies for Nuclear Power Plants," by Howard H.M. Hwang, 6/15/87, (PB88-134267/AS).

NCEER-87-0012 "Parametric Studies of Frequency Response of Secondary Systems Under Ground-Acceleration Excitations," by Y. Yong and Y.K. Lin, 6/10/87, (PB88-134309/AS).

NCEER-87-0013 "Frequency Response of Secondary Systems Under Seismic Excitation," by J.A. HoLung, J. Cai and Y.K. Lin, 7/31/87, (PB88-134317/AS).

NCEER-87-0014 "Modelling Earthquake Ground Motions in Seismically Active Regions Using Parametric Time Series Methods," by G.W. Ellis and A.S. Cakmak, 8/25/87, (PB88-134283/AS).

NCEER-87-0015 "Detection and Assessment of Seismic Structural Damage," by E. DiPasquale and A.S. Cakmak, 8/25/87, (PB88-163712/AS).

NCEER-87-0016 "Pipeline Experiment at Parkfield, California," by J. Isenberg and E. Richardson, 9/15/87, (PB88-163720/AS). This report is available only through NTIS (see address given above).

NCEER-87-0017 "Digital Simulation of Seismic Ground Motion," by M. Shinozuka, G. Deodatis and T. Harada, 8/31/87, (PB88-155197/AS). This report is available only through NTIS (see address given above).

NCEER-87-0018 "Practical Considerations for Structural Control: System Uncertainty, System Time Delay and Truncation of Small Control Forces," J.N. Yang and A. Akbarpour, 8/10/87, (PB88-163738/AS).

NCEER-87-0019 "Modal Analysis of Nonclassically Damped Structural Systems Using Canonical Transformation," by J.N. Yang, S. Sarkani and F.X. Long, 9/27/87, (PB88-187851/AS).

NCEER-87-0020 "A Nonstationary Solution in Random Vibration Theory," by J.R. Red-Horse and P.D. Spanos, 11/3/87, (PB88-163746/AS).

NCEER-87-0021 "Horizontal Impedances for Radially Inhomogeneous Viscoelastic Soil Layers," by A.S. Veletsos and K.W. Dotson, 10/15/87, (PB88-150859/AS).

NCEER-87-0022 "Seismic Damage Assessment of Reinforced Concrete Members," by Y.S. Chung, C. Meyer and M. Shinozuka, 10/9/87, (PB88-150867/AS). This report is available only through NTIS (see address given above).

NCEER-87-0023 "Active Structural Control in Civil Engineering," by T.T. Soong, 11/11/87, (PB88-187778/AS).

NCEER-87-0024 "Vertical and Torsional Impedances for Radially Inhomogeneous Viscoelastic Soil Layers," by K.W. Dotson and A.S. Veletsos, 12/87, (PB88-187786/AS).

NCEER-87-0025 "Proceedings from the Symposium on Seismic Hazards, Ground Motions, Soil-Liquefaction and Engineering Practice in Eastern North America," October 20-22, 1987, edited by K.H. Jacob, 12/87, (PB88-188115/AS).

NCEER-87-0026 "Report on the Whittier-Narrows, California, Earthquake of October 1, 1987," by J. Pantelic and A. Reinhorn, 11/87, (PB88-187752/AS). This report is available only through NTIS (see address given above).

NCEER-87-0027 "Design of a Modular Program for Transient Nonlinear Analysis of Large 3-D Building Structures," by S. Srivastav and J.F. Abel, 12/30/87, (PB88-187950/AS).

NCEER-87-0028 "Second-Year Program in Research, Education and Technology Transfer," 3/8/88, (PB88-219480/AS).

NCEER-88-0001 "Workshop on Seismic Computer Analysis and Design of Buildings With Interactive Graphics," by W. McGuire, J.F. Abel and C.H. Conley, 1/18/88, (PB88-187760/AS).

NCEER-88-0002 "Optimal Control of Nonlinear Flexible Structures," by J.N. Yang, F.X. Long and D. Wong, 1/22/88, (PB88-213772/AS).

NCEER-88-0003 "Substructuring Techniques in the Time Domain for Primary-Secondary Structural Systems," by G.D. Manolis and G. Juhn, 2/10/88, (PB88-213780/AS).

NCEER-88-0004 "Iterative Seismic Analysis of Primary-Secondary Systems," by A. Singhal, L.D. Lutes and P.D. Spanos, 2/23/88, (PB88-213798/AS).

NCEER-88-0005 "Stochastic Finite Element Expansion for Random Media," by P.D. Spanos and R. Ghanem, 3/14/88, (PB88-213806/AS).

NCEER-88-0006 "Combining Structural Optimization and Structural Control," by F.Y. Cheng and C.P. Pantelides, 1/10/88, (PB88-213814/AS).

NCEER-88-0007 "Seismic Performance Assessment of Code-Designed Structures," by H.H-M. Hwang, J-W. Jaw and H-J. Shau, 3/20/88, (PB88-219423/AS).

NCEER-88-0008 "Reliability Analysis of Code-Designed Structures Under Natural Hazards," by H.H-M. Hwang, H. Ushiba and M. Shinozuka, 2/29/88, (PB88-229471/AS).

NCEER-88-0009 "Seismic Fragility Analysis of Shear Wall Structures," by J-W Jaw and H.H-M. Hwang, 4/30/88, (PB89-102867/AS).

NCEER-88-0010 "Base Isolation of a Multi-Story Building Under a Harmonic Ground Motion - A Comparison of Performances of Various Systems," by F-G Fan, G. Ahmadi and I.G. Tadjbakhsh, 5/18/88, (PB89-122238/AS).

NCEER-88-0011 "Seismic Floor Response Spectra for a Combined System by Green's Functions," by F.M. Lavelle, L.A. Bergman and P.D. Spanos, 5/1/88, (PB89-102875/AS).

NCEER-88-0012 "A New Solution Technique for Randomly Excited Hysteretic Structures," by G.Q. Cai and Y.K. Lin, 5/16/88, (PB89-102883/AS).

NCEER-88-0013 "A Study of Radiation Damping and Soil-Structure Interaction Effects in the Centrifuge," by K. Weissman, supervised by J.H. Prevost, 5/24/88, (PB89-144703/AS).

NCEER-88-0014 "Parameter Identification and Implementation of a Kinematic Plasticity Model for Frictional Soils," by J.H. Prevost and D.V. Griffiths, to be published.

NCEER-88-0015 "Two- and Three- Dimensional Dynamic Finite Element Analyses of the Long Valley Dam," by D.V. Griffiths and J.H. Prevost, 6/17/88, (PB89-144711/AS).

NCEER-88-0016 "Damage Assessment of Reinforced Concrete Structures in Eastern United States," by A.M. Reinhorn, M.J. Seidel, S.K. Kunnath and Y.J. Park, 6/15/88, (PB89-122220/AS).

NCEER-88-0017 "Dynamic Compliance of Vertically Loaded Strip Foundations in Multilayered Viscoelastic Soils," by S. Ahmad and A.S.M. Israil, 6/17/88, (PB89-102891/AS).

NCEER-88-0018 "An Experimental Study of Seismic Structural Response With Added Viscoelastic Dampers," by R.C. Lin, Z. Liang, T.T. Soong and R.H. Zhang, 6/30/88, (PB89-122212/AS). This report is available only through NTIS (see address given above).

NCEER-88-0019 "Experimental Investigation of Primary - Secondary System Interaction," by G.D. Manolis, G. Juhn and A.M. Reinhorn, 5/27/88, (PB89-122204/AS).

NCEER-88-0020 "A Response Spectrum Approach For Analysis of Nonclassically Damped Structures," by J.N. Yang, S. Sarkani and F.X. Long, 4/22/88, (PB89-102909/AS).

NCEER-88-0021 "Seismic Interaction of Structures and Soils: Stochastic Approach," by A.S. Veletsos and A.M. Prasad, 7/21/88, (PB89-122196/AS).

NCEER-88-0022 "Identification of the Serviceability Limit State and Detection of Seismic Structural Damage," by E. DiPasquale and A.S. Cakmak, 6/15/88, (PB89-122188/AS). This report is available only through NTIS (see address given above).

NCEER-88-0023 "Multi-Hazard Risk Analysis: Case of a Simple Offshore Structure," by B.K. Bhartia and E.H. Vanmarcke, 7/21/88, (PB89-145213/AS).

NCEER-88-0024 "Automated Seismic Design of Reinforced Concrete Buildings," by Y.S. Chung, C. Meyer and M. Shinozuka, 7/5/88, (PB89-122170/AS). This report is available only through NTIS (see address given above).

NCEER-88-0025 "Experimental Study of Active Control of MDOF Structures Under Seismic Excitations," by L.L. Chung, R.C. Lin, T.T. Soong and A.M. Reinhorn, 7/10/88, (PB89-122600/AS).

NCEER-88-0026 "Earthquake Simulation Tests of a Low-Rise Metal Structure," by J.S. Hwang, K.C. Chang, G.C. Lee and R.L. Ketter, 8/1/88, (PB89-102917/AS).

NCEER-88-0027 "Systems Study of Urban Response and Reconstruction Due to Catastrophic Earthquakes," by F. Kozin and H.K. Zhou, 9/22/88, (PB90-162348/AS).

NCEER-88-0028 "Seismic Fragility Analysis of Plane Frame Structures," by H.H-M. Hwang and Y.K. Low, 7/31/88, (PB89-131445/AS).

NCEER-88-0029 "Response Analysis of Stochastic Structures," by A. Kardara, C. Bucher and M. Shinozuka, 9/22/88, (PB89-174429/AS).

NCEER-88-0030 "Nonnormal Accelerations Due to Yielding in a Primary Structure," by D.C.K. Chen and L.D. Lutes, 9/19/88, (PB89-131437/AS).

NCEER-88-0031 "Design Approaches for Soil-Structure Interaction," by A.S. Veletsos, A.M. Prasad and Y. Tang, 12/30/88, (PB89-174437/AS). This report is available only through NTIS (see address given above).

NCEER-88-0032 "A Re-evaluation of Design Spectra for Seismic Damage Control," by C.J. Turkstra and A.G. Tallin, 11/7/88, (PB89-145221/AS).

NCEER-88-0033 "The Behavior and Design of Noncontact Lap Splices Subjected to Repeated Inelastic Tensile Loading," by V.E. Sagan, P. Gergely and R.N. White, 12/8/88, (PB89-163737/AS).

NCEER-88-0034 "Seismic Response of Pile Foundations," by S.M. Mamoon, P.K. Banerjee and S. Ahmad, 11/1/88, (PB89-145239/AS).

NCEER-88-0035 "Modeling of R/C Building Structures With Flexible Floor Diaphragms (IDARC2)," by A.M. Reinhorn, S.K. Kunnath and N. Panahshahi, 9/7/88, (PB89-207153/AS).

NCEER-88-0036 "Solution of the Dam-Reservoir Interaction Problem Using a Combination of FEM, BEM with Particular Integrals, Modal Analysis, and Substructuring," by C-S. Tsai, G.C. Lee and R.L. Ketter, 12/31/88, (PB89-207146/AS).

NCEER-88-0037 "Optimal Placement of Actuators for Structural Control," by F.Y. Cheng and C.P. Pantelides, 8/15/88, (PB89-162846/AS).

NCEER-88-0038 "Teflon Bearings in Aseismic Base Isolation: Experimental Studies and Mathematical Modeling," by A. Mokha, M.C. Constantinou and A.M. Reinhorn, 12/5/88, (PB89-218457/AS). This report is available only through NTIS (see address given above).

NCEER-88-0039 "Seismic Behavior of Flat Slab High-Rise Buildings in the New York City Area," by P. Weidlinger and M. Ettouney, 10/15/88, (PB90-145681/AS).

NCEER-88-0040 "Evaluation of the Earthquake Resistance of Existing Buildings in New York City," by P. Weidlinger and M. Ettouney, 10/15/88, to be published.

NCEER-88-0041 "Small-Scale Modeling Techniques for Reinforced Concrete Structures Subjected to Seismic Loads," by W. Kim, A. El-Attar and R.N. White, 11/22/88, (PB89-189625/AS).

NCEER-88-0042 "Modeling Strong Ground Motion from Multiple Event Earthquakes," by G.W. Ellis and A.S. Cakmak, 10/15/88, (PB89-174445/AS).

NCEER-88-0043 "Nonstationary Models of Seismic Ground Acceleration," by M. Grigoriu, S.E. Ruiz and E. Rosenblueth, 7/15/88, (PB89-189617/AS).

NCEER-88-0044 "SARCF User's Guide: Seismic Analysis of Reinforced Concrete Frames," by Y.S. Chung, C. Meyer and M. Shinozuka, 11/9/88, (PB89-174452/AS).

NCEER-88-0045 "First Expert Panel Meeting on Disaster Research and Planning," edited by J. Pantelic and J. Stoyle, 9/15/88, (PB89-174460/AS).

NCEER-88-0046 "Preliminary Studies of the Effect of Degrading Infill Walls on the Nonlinear Seismic Response of Steel Frames," by C.Z. Chrysostomou, P. Gergely and J.F. Abel, 12/19/88, (PB89-208383/AS).

NCEER-88-0047 "Reinforced Concrete Frame Component Testing Facility - Design, Construction, Instrumentation and Operation," by S.P. Pessiki, C. Conley, T. Bond, P. Gergely and R.N. White, 12/16/88, (PB89-174478/AS).

NCEER-89-0001 "Effects of Protective Cushion and Soil Compliancy on the Response of Equipment Within a Seismically Excited Building," by J.A. HoLung, 2/16/89, (PB89-207179/AS).

NCEER-89-0002 "Statistical Evaluation of Response Modification Factors for Reinforced Concrete Structures," by H.H-M. Hwang and J-W. Jaw, 2/17/89, (PB89-207187/AS).

NCEER-89-0003 "Hysteretic Columns Under Random Excitation," by G-Q. Cai and Y.K. Lin, 1/9/89, (PB89-196513/AS).

NCEER-89-0004 "Experimental Study of 'Elephant Foot Bulge' Instability of Thin-Walled Metal Tanks," by Z-H. Jia and R.L. Ketter, 2/22/89, (PB89-207195/AS).

NCEER-89-0005 "Experiment on Performance of Buried Pipelines Across San Andreas Fault," by J. Isenberg, E. Richardson and T.D. O'Rourke, 3/10/89, (PB89-218440/AS).

NCEER-89-0006 "A Knowledge-Based Approach to Structural Design of Earthquake-Resistant Buildings," by M. Subramani, P. Gergely, C.H. Conley, J.F. Abel and A.H. Zaghw, 1/15/89, (PB89-218465/AS).

NCEER-89-0007 "Liquefaction Hazards and Their Effects on Buried Pipelines," by T.D. O'Rourke and P.A. Lane, 2/1/89, (PB89-218481).

NCEER-89-0008 "Fundamentals of System Identification in Structural Dynamics," by H. Imai, C-B. Yun, O. Maruyama and M. Shinozuka, 1/26/89, (PB89-207211/AS).

NCEER-89-0009 "Effects of the 1985 Michoacan Earthquake on Water Systems and Other Buried Lifelines in Mexico," by A.G. Ayala and M.J. O'Rourke, 3/8/89, (PB89-207229/AS).

NCEER-89-R010 "NCEER Bibliography of Earthquake Education Materials," by K.E.K. Ross, Second Revision, 9/1/89, (PB90-125352/AS).

NCEER-89-0011 "Inelastic Three-Dimensional Response Analysis of Reinforced Concrete Building Structures (IDARC-3D), Part I - Modeling," by S.K. Kunnath and A.M. Reinhorn, 4/17/89, (PB90-114612/AS).

NCEER-89-0012 "Recommended Modifications to ATC-14," by C.D. Poland and J.O. Malley, 4/12/89, (PB90-108648/AS).

NCEER-89-0013 "Repair and Strengthening of Beam-to-Column Connections Subjected to Earthquake Loading," by M. Corazao and A.J. Durrani, 2/28/89, (PB90-109885/AS).

NCEER-89-0014 "Program EXKAL2 for Identification of Structural Dynamic Systems," by O. Maruyama, C-B. Yun, M. Hoshiya and M. Shinozuka, 5/19/89, (PB90-109877/AS).

NCEER-89-0015 "Response of Frames With Bolted Semi-Rigid Connections, Part I - Experimental Study and Analytical Predictions," by P.J. DiCorso, A.M. Reinhorn, J.R. Dickerson, J.B. Radziminski and W.L. Harper, 6/1/89, to be published.

NCEER-89-0016 "ARMA Monte Carlo Simulation in Probabilistic Structural Analysis," by P.D. Spanos and M.P. Mignolet, 7/10/89, (PB90-109893/AS).

NCEER-89-P017 "Preliminary Proceedings from the Conference on Disaster Preparedness - The Place of Earthquake Education in Our Schools," Edited by K.E.K. Ross, 6/23/89.

NCEER-89-0017 "Proceedings from the Conference on Disaster Preparedness - The Place of Earthquake Education in Our Schools," Edited by K.E.K. Ross, 12/31/89, (PB90-207895). This report is available only through NTIS (see address given above).

NCEER-89-0018 "Multidimensional Models of Hysteretic Material Behavior for Vibration Analysis of Shape Memory Energy Absorbing Devices, by E.J. Graesser and F.A. Cozzarelli, 6/7/89, (PB90-164146/AS).

NCEER-89-0019 "Nonlinear Dynamic Analysis of Three-Dimensional Base Isolated Structures (3D-BASIS)," by S. Nagarajaiah, A.M. Reinhorn and M.C. Constantinou, 8/3/89, (PB90-161936/AS). This report is available only through NTIS (see address given above).

NCEER-89-0020 "Structural Control Considering Time-Rate of Control Forces and Control Rate Constraints," by F.Y. Cheng and C.P. Pantelides, 8/3/89, (PB90-120445/AS).

NCEER-89-0021 "Subsurface Conditions of Memphis and Shelby County," by K.W. Ng, T-S. Chang and H-H.M. Hwang, 7/26/89, (PB90-120437/AS).

NCEER-89-0022 "Seismic Wave Propagation Effects on Straight Jointed Buried Pipelines," by K. Elhmadi and M.J. O'Rourke, 8/24/89, (PB90-162322/AS).

NCEER-89-0023 "Workshop on Serviceability Analysis of Water Delivery Systems," edited by M. Grigoriu, 3/6/89, (PB90-127424/AS).

NCEER-89-0024 "Shaking Table Study of a 1/5 Scale Steel Frame Composed of Tapered Members," by K.C. Chang, J.S. Hwang and G.C. Lee, 9/18/89, (PB90-160169/AS).

NCEER-89-0025 "DYNA1D: A Computer Program for Nonlinear Seismic Site Response Analysis - Technical Documentation," by Jean H. Prevost, 9/14/89, (PB90-161944/AS). This report is available only through NTIS (see address given above).

NCEER-89-0026 "1:4 Scale Model Studies of Active Tendon Systems and Active Mass Dampers for Aseismic Protection," by A.M. Reinhorn, T.T. Soong, R.C. Lin, Y.P. Yang, Y. Fukao, H. Abe and M. Nakai, 9/15/89, (PB90-173246/AS).

NCEER-89-0027 "Scattering of Waves by Inclusions in a Nonhomogeneous Elastic Half Space Solved by Boundary Element Methods," by P.K. Hadley, A. Askar and A.S. Cakmak, 6/15/89, (PB90-145699/AS).

NCEER-89-0028 "Statistical Evaluation of Deflection Amplification Factors for Reinforced Concrete Structures," by H.H.M. Hwang, J-W. Jaw and A.L. Ch'ng, 8/31/89, (PB90-164633/AS).

NCEER-89-0029 "Bedrock Accelerations in Memphis Area Due to Large New Madrid Earthquakes," by H.H.M. Hwang, C.H.S. Chen and G. Yu, 11/7/89, (PB90-162330/AS).

NCEER-89-0030 "Seismic Behavior and Response Sensitivity of Secondary Structural Systems," by Y.Q. Chen and T.T. Soong, 10/23/89, (PB90-164658/AS).

NCEER-89-0031 "Random Vibration and Reliability Analysis of Primary-Secondary Structural Systems," by Y. Ibrahim, M. Grigoriu and T.T. Soong, 11/10/89, (PB90-161951/AS).

NCEER-89-0032 "Proceedings from the Second U.S. - Japan Workshop on Liquefaction, Large Ground Deformation and Their Effects on Lifelines, September 26-29, 1989," Edited by T.D. O'Rourke and M. Hamada, 12/1/89, (PB90-209388/AS).

NCEER-89-0033 "Deterministic Model for Seismic Damage Evaluation of Reinforced Concrete Structures," by J.M. Bracci, A.M. Reinhorn, J.B. Mander and S.K. Kunnath, 9/27/89.

NCEER-89-0034 "On the Relation Between Local and Global Damage Indices," by E. DiPasquale and A.S. Cakmak, 8/15/89, (PB90-173865).

NCEER-89-0035 "Cyclic Undrained Behavior of Nonplastic and Low Plasticity Silts," by A.J. Walker and H.E. Stewart, 7/26/89, (PB90-183518/AS).

NCEER-89-0036 "Liquefaction Potential of Surficial Deposits in the City of Buffalo, New York," by M. Budhu, R. Giese and L. Baumgrass, 1/17/89, (PB90-208455/AS).

NCEER-89-0037 "A Deterministic Assessment of Effects of Ground Motion Incoherence," by A.S. Veletsos and Y. Tang, 7/15/89, (PB90-164294/AS).

NCEER-89-0038 "Workshop on Ground Motion Parameters for Seismic Hazard Mapping," July 17-18, 1989, edited by R.V. Whitman, 12/1/89, (PB90-173923/AS).

NCEER-89-0039 "Seismic Effects on Elevated Transit Lines of the New York City Transit Authority," by C.J. Costantino, C.A. Miller and E. Heymsfield, 12/26/89, (PB90-207887/AS).

NCEER-89-0040 "Centrifugal Modeling of Dynamic Soil-Structure Interaction," by K. Weissman, Supervised by J.H. Prevost, 5/10/89, (PB90-207879/AS).

NCEER-89-0041 "Linearized Identification of Buildings With Cores for Seismic Vulnerability Assessment," by I-K. Ho and A.E. Aktan, 11/1/89, (PB90-251943/AS).

NCEER-90-0001 "Geotechnical and Lifeline Aspects of the October 17, 1989 Loma Prieta Earthquake in San Francisco," by T.D. O'Rourke, H.E. Stewart, F.T. Blackburn and T.S. Dickerman, 1/90, (PB90-208596/AS).

NCEER-90-0002 "Nonnormal Secondary Response Due to Yielding in a Primary Structure," by D.C.K. Chen and L.D. Lutes, 2/28/90, (PB90-251976/AS).

NCEER-90-0003 "Earthquake Education Materials for Grades K-12," by K.E.K. Ross, 4/16/90, (PB91-113415/AS).

NCEER-90-0004 "Catalog of Strong Motion Stations in Eastern North America," by R.W. Busby, 4/3/90, (PB90-251984)/AS.

NCEER-90-0005 "NCEER Strong-Motion Data Base: A User Manual for the GeoBase Release (Version 1.0 for the Sun3)," by P. Friberg and K. Jacob, 3/31/90 (PB90-258062/AS).

NCEER-90-0006 "Seismic Hazard Along a Crude Oil Pipeline in the Event of an 1811-1812 Type New Madrid Earthquake," by H.H.M. Hwang and C-H.S. Chen, 4/16/90(PB90-258054).

NCEER-90-0007 "Site-Specific Response Spectra for Memphis Sheahan Pumping Station," by H.H.M. Hwang and C.S. Lee, 5/15/90, (PB91-108811/AS).

NCEER-90-0008 "Pilot Study on Seismic Vulnerability of Crude Oil Transmission Systems," by T. Ariman, R. Dobry, M. Grigoriu, F. Kozin, M. O'Rourke, T. O'Rourke and M. Shinozuka, 5/25/90, (PB91-108837/AS).

NCEER-90-0009 "A Program to Generate Site Dependent Time Histories: EQGEN," by G.W. Ellis, M. Srinivasan and A.S. Cakmak, 1/30/90, (PB91-108829/AS).

NCEER-90-0010 "Active Isolation for Seismic Protection of Operating Rooms," by M.E. Talbott, Supervised by M. Shinozuka, 6/8/9, (PB91-110205/AS).

NCEER-90-0011 "Program LINEARID for Identification of Linear Structural Dynamic Systems," by C-B. Yun and M. Shinozuka, 6/25/90, (PB91-110312/AS).

NCEER-90-0012 "Two-Dimensional Two-Phase Elasto-Plastic Seismic Response of Earth Dams," by A.N. Yiagos, Supervised by J.H. Prevost, 6/20/90, (PB91-110197/AS).

NCEER-90-0013 "Secondary Systems in Base-Isolated Structures: Experimental Investigation, Stochastic Response and Stochastic Sensitivity," by G.D. Manolis, G. Juhn, M.C. Constantinou and A.M. Reinhorn, 7/1/90, (PB91-110320/AS).

NCEER-90-0014 "Seismic Behavior of Lightly-Reinforced Concrete Column and Beam-Column Joint Details," by S.P. Pessiki, C.H. Conley, P. Gergely and R.N. White, 8/22/90, (PB91-108795/AS).

NCEER-90-0015 "Two Hybrid Control Systems for Building Structures Under Strong Earthquakes," by J.N. Yang and A. Danielians, 6/29/90, (PB91-125393/AS).

NCEER-90-0016 "Instantaneous Optimal Control with Acceleration and Velocity Feedback," by J.N. Yang and Z. Li, 6/29/90, (PB91-125401/AS).

NCEER-90-0017 "Reconnaissance Report on the Northern Iran Earthquake of June 21, 1990," by M. Mehrain, 10/4/90, (PB91-125377/AS).

NCEER-90-0018 "Evaluation of Liquefaction Potential in Memphis and Shelby County," by T.S. Chang, P.S. Tang, C.S. Lee and H. Hwang, 8/10/90, (PB91-125427/AS).

NCEER-90-0019 "Experimental and Analytical Study of a Combined Sliding Disc Bearing and Helical Steel Spring Isolation System," by M.C. Constantinou, A.S. Mokha and A.M. Reinhorn, 10/4/90, (PB91-125385/AS).

NCEER-90-0020 "Experimental Study and Analytical Prediction of Earthquake Response of a Sliding Isolation System with a Spherical Surface," by A.S. Mokha, M.C. Constantinou and A.M. Reinhorn, 10/11/90, (PB91-125419/AS).

NCEER-90-0021 "Dynamic Interaction Factors for Floating Pile Groups," by G. Gazetas, K. Fan, A. Kaynia and E. Kausel, 9/10/90, (PB91-170381/AS).

NCEER-90-0022 "Evaluation of Seismic Damage Indices for Reinforced Concrete Structures," by S. Rodriguez-Gomez and A.S. Cakmak, 9/30/90, PB91-171322/AS).

NCEER-90-0023 "Study of Site Response at a Selected Memphis Site," by H. Desai, S. Ahmad, E.S. Gazetas and M.R. Oh, 10/11/90, (PB91-196857/AS).

NCEER-90-0024 "A User's Guide to Strongmo: Version 1.0 of NCEER's Strong-Motion Data Access Tool for PCs and Terminals," by P.A. Friberg and C.A.T. Susch, 11/15/90, (PB91-171272/AS).

NCEER-90-0025 "A Three-Dimensional Analytical Study of Spatial Variability of Seismic Ground Motions," by L-L. Hong and A.H.-S. Ang, 10/30/90, (PB91-170399/AS).

NCEER-90-0026 "MUMOID User's Guide - A Program for the Identification of Modal Parameters," by S. Rodriguez-Gomez and E. DiPasquale, 9/30/90, (PB91-171298/AS).

NCEER-90-0027 "SARCF-II User's Guide - Seismic Analysis of Reinforced Concrete Frames," by S. Rodriguez-Gomez, Y.S. Chung and C. Meyer, 9/30/90, (PB91-171280/AS).

NCEER-90-0028 "Viscous Dampers: Testing, Modeling and Application in Vibration and Seismic Isolation," by N. Makris and M.C. Constantinou, 12/20/90 (PB91-190561/AS).

NCEER-90-0029 "Soil Effects on Earthquake Ground Motions in the Memphis Area," by H. Hwang, C.S. Lee, K.W. Ng and T.S. Chang, 8/2/90, (PB91-190751/AS).

NCEER-91-0001 "Proceedings from the Third Japan-U.S. Workshop on Earthquake Resistant Design of Lifeline Facilities and Countermeasures for Soil Liquefaction, December 17-19, 1990," edited by T.D. O'Rourke and M. Hamada, 2/1/91, (PB91-179259/AS).

NCEER-91-0002 "Physical Space Solutions of Non-Proportionally Damped Systems," by M. Tong, Z. Liang and G.C. Lee, 1/15/91, (PB91-179242/AS).

NCEER-91-0003 "Seismic Response of Single Piles and Pile Groups," by K. Fan and G. Gazetas, 1/10/91, (PB92-174994/AS).

NCEER-91-0004 "Damping of Structures: Part 1 - Theory of Complex Damping," by Z. Liang and G. Lee, 10/10/91, (PB92-197235/AS).

NCEER-91-0005 "3D-BASIS - Nonlinear Dynamic Analysis of Three Dimensional Base Isolated Structures: Part II," by S. Nagarajaiah, A.M. Reinhorn and M.C. Constantinou, 2/28/91, (PB91-190553/AS).

NCEER-91-0006 "A Multidimensional Hysteretic Model for Plasticity Deforming Metals in Energy Absorbing Devices," by E.J. Graesser and F.A. Cozzarelli, 4/9/91, (PB92-108364/AS).

NCEER-91-0007 "A Framework for Customizable Knowledge-Based Expert Systems with an Application to a KBES for Evaluating the Seismic Resistance of Existing Buildings," by E.G. Ibarra-Anaya and S.J. Fenves, 4/9/91, (PB91-210930/AS).

NCEER-91-0008 "Nonlinear Analysis of Steel Frames with Semi-Rigid Connections Using the Capacity Spectrum Method," by G.G. Deierlein, S-H. Hsieh, Y-J. Shen and J.F. Abel, 7/2/91, (PB92-113828/AS).

NCEER-91-0009 "Earthquake Education Materials for Grades K-12," by K.E.K. Ross, 4/30/91, (PB91-212142/AS).

NCEER-91-0010 "Phase Wave Velocities and Displacement Phase Differences in a Harmonically Oscillating Pile," by N. Makris and G. Gazetas, 7/8/91, (PB92-108356/AS).

NCEER-91-0011 "Dynamic Characteristics of a Full-Size Five-Story Steel Structure and a 2/5 Scale Model," by K.C. Chang, G.C. Yao, G.C. Lee, D.S. Hao and Y.C. Yeh," 7/2/91.

NCEER-91-0012 "Seismic Response of a 2/5 Scale Steel Structure with Added Viscoelastic Dampers," by K.C. Chang, T.T. Soong, S-T. Oh and M.L. Lai, 5/17/91 (PB92-110816/AS).

NCEER-91-0013 "Earthquake Response of Retaining Walls; Full-Scale Testing and Computational Modeling," by S. Alampalli and A-W.M. Elgamal, 6/20/91, to be published.

NCEER-91-0014 "3D-BASIS-M: Nonlinear Dynamic Analysis of Multiple Building Base Isolated Structures," by P.C. Tsopelas, S. Nagarajaiah, M.C. Constantinou and A.M. Reinhorn, 5/28/91, (PB92-113885/AS).

NCEER-91-0015 "Evaluation of SEAOC Design Requirements for Sliding Isolated Structures," by D. Theodossiou and M.C. Constantinou, 6/10/91, (PB92-114602/AS).

NCEER-91-0016 "Closed-Loop Modal Testing of a 27-Story Reinforced Concrete Flat Plate-Core Building," by H.R. Somaprasad, T. Toksoy, H. Yoshiyuki and A.E. Aktan, 7/15/91, (PB92-129980/AS).

NCEER-91-0017 "Shake Table Test of a 1/6 Scale Two-Story Lightly Reinforced Concrete Building," by A.G. El-Attar, R.N. White and P. Gergely, 2/28/91, (PB92-222447/AS).

NCEER-91-0018 "Shake Table Test of a 1/8 Scale Three-Story Lightly Reinforced Concrete Building," by A.G. El-Attar, R.N. White and P. Gergely, 2/28/91.

NCEER-91-0019 "Transfer Functions for Rigid Rectangular Foundations," by A.S. Veletsos, A.M. Prasad and W.H. Wu, 7/31/91.

NCEER-91-0020 "Hybrid Control of Seismic-Excited Nonlinear and Inelastic Structural Systems," by J.N. Yang, Z. Li and A. Danielians, 8/1/91, (PB92-143171/AS).

NCEER-91-0021 "The NCEER-91 Earthquake Catalog: Improved Intensity-Based Magnitudes and Recurrence Relations for U.S. Earthquakes East of New Madrid," by L. Seeber and J.G. Armbruster, 8/28/91, (PB92-176742/AS).

NCEER-91-0022 "Proceedings from the Implementation of Earthquake Planning and Education in Schools: The Need for Change - The Roles of the Changemakers," by K.E.K. Ross and F. Winslow, 7/23/91, (PB92-129998/AS).

NCEER-91-0023 "A Study of Reliability-Based Criteria for Seismic Design of Reinforced Concrete Frame Buildings," by H.H.M. Hwang and H-M. Hsu, 8/10/91, (PB92-140235/AS).

NCEER-91-0024 "Experimental Verification of a Number of Structural System Identification Algorithms," by R.G. Ghanem, H. Gavin and M. Shinozuka, 9/18/91, (PB92-176577/AS).

NCEER-91-0025 "Probabilistic Evaluation of Liquefaction Potential," by H.H.M. Hwang and C.S. Lee," 11/25/91, (PB92-143429/AS).

NCEER-91-0026 "Instantaneous Optimal Control for Linear, Nonlinear and Hysteretic Structures - Stable Controllers," by J.N. Yang and Z. Li, 11/15/91, (PB92-163807/AS).

NCEER-91-0027 "Experimental and Theoretical Study of a Sliding Isolation System for Bridges," by M.C. Constantinou, A. Kartoum, A.M. Reinhorn and P. Bradford, 11/15/91, (PB92-176973/AS).

NCEER-92-0001 "Case Studies of Liquefaction and Lifeline Performance During Past Earthquakes, Volume 1: Japanese Case Studies," Edited by M. Hamada and T. O'Rourke, 2/17/92, (PB92-197243/AS).

NCEER-92-0002 "Case Studies of Liquefaction and Lifeline Performance During Past Earthquakes, Volume 2: United States Case Studies," Edited by T. O'Rourke and M. Hamada, 2/17/92, (PB92-197250/AS).

NCEER-92-0003 "Issues in Earthquake Education," Edited by K. Ross, 2/3/92, (PB92-222389/AS).

NCEER-92-0004 "Proceedings from the First U.S. - Japan Workshop on Earthquake Protective Systems for Bridges," 2/4/92, to be published.

NCEER-92-0005 "Seismic Ground Motion from a Haskell-Type Source in a Multiple-Layered Half-Space," A.P. Theoharis, G. Deodatis and M. Shinozuka, 1/2/92, to be published.

NCEER-92-0006 "Proceedings from the Site Effects Workshop," Edited by R. Whitman, 2/29/92, (PB92-197201/AS).

NCEER-92-0007 "Engineering Evaluation of Permanent Ground Deformations Due to Seismically-Induced Liquefaction," by M.H. Baziar, R. Dobry and A-W.M. Elgamal, 3/24/92, (PB92-222421/AS).

NCEER-92-0008 "A Procedure for the Seismic Evaluation of Buildings in the Central and Eastern United States," by C.D. Poland and J.O. Malley, 4/2/92, (PB92-222439/AS).

NCEER-92-0009 "Experimental and Analytical Study of a Hybrid Isolation System Using Friction Controllable Sliding Bearings," by M.Q. Feng, S. Fujii and M. Shinozuka, 5/15/92, (PB93-150282/AS).

NCEER-92-0010 "Seismic Resistance of Slab-Column Connections in Existing Non-Ductile Flat-Plate Buildings," by A.J. Durrani and Y. Du, 5/18/92.

NCEER-92-0011 "The Hysteretic and Dynamic Behavior of Brick Masonry Walls Upgraded by Ferrocement Coatings Under Cyclic Loading and Strong Simulated Ground Motion," by H. Lee and S.P. Prawel, 5/11/92, to be published.

NCEER-92-0012 "Study of Wire Rope Systems for Seismic Protection of Equipment in Buildings," by G.F. Demetriades, M.C. Constantinou and A.M. Reinhorn, 5/20/92.

NCEER-92-0013 "Shape Memory Structural Dampers: Material Properties, Design and Seismic Testing," by P.R. Witting and F.A. Cozzarelli, 5/26/92.

NCEER-92-0014 "Longitudinal Permanent Ground Deformation Effects on Buried Continuous Pipelines," by M.J. O'Rourke, and C. Nordberg, 6/15/92.

NCEER-92-0015 "A Simulation Method for Stationary Gaussian Random Functions Based on the Sampling Theorem," by M. Grigoriu and S. Balopoulou, 6/11/92, (PB93-127496/AS).

NCEER-92-0016 "Gravity-Load-Designed Reinforced Concrete Buildings: Seismic Evaluation of Existing Construction and Detailing Strategies for Improved Seismic Resistance," by G.W. Hoffmann, S.K. Kunnath, J.B. Mander and A.M. Reinhorn, 7/15/92, to be published.

NCEER-92-0017 "Observations on Water System and Pipeline Performance in the Limón Area of Costa Rica Due to the April 22, 1991 Earthquake," by M. O'Rourke and D. Ballantyne, 6/30/92, (PB93-126811/AS).

NCEER-92-0018 "Fourth Edition of Earthquake Education Materials for Grades K-12," Edited by K.E.K. Ross, 8/10/92.

NCEER-92-0019 "Proceedings from the Fourth Japan-U.S. Workshop on Earthquake Resistant Design of Lifeline Facilities and Countermeasures for Soil Liquefaction," Edited by M. Hamada and T.D. O'Rourke, 8/12/92, (PB93-163939/AS).

NCEER-92-0020 "Active Bracing System: A Full Scale Implementation of Active Control," by A.M. Reinhorn, T.T. Soong, R.C. Lin, M.A. Riley, Y.P. Wang, S. Aizawa and M. Higashino, 8/14/92, (PB93-127512/AS).

NCEER-92-0021 "Empirical Analysis of Horizontal Ground Displacement Generated by Liquefaction-Induced Lateral Spreads," by S.F. Bartlett and T.L. Youd, 8/17/92.

NCEER-92-0022 "IDARC Version 3.0: Inelastic Damage Analysis of Reinforced Concrete Structures," by S.K. Kunnath, A.M. Reinhorn and R.F. Lobo, 8/31/92, to be published.

NCEER-92-0023 "A Semi-Empirical Analysis of Strong-Motion Peaks in Terms of Seismic Source, Propagation Path and Local Site Conditions, by M. Kamiyama, M.J. O'Rourke and R. Flores-Berrones, 9/9/92, (PB93-150266/AS).

NCEER-92-0024 "Seismic Behavior of Reinforced Concrete Frame Structures with Nonductile Details, Part I: Summary of Experimental Findings of Full Scale Beam-Column Joint Tests," by A. Beres, R.N. White and P. Gergely, 9/30/92, to be published.

NCEER-92-0025 "Experimental Results of Repaired and Retrofitted Beam-Column Joint Tests in Lightly Reinforced Concrete Frame Buildings," by A. Beres, S. El-Borgi, R.N. White and P. Gergely, 10/29/92, to be published.

NCEER-92-0026 "A Generalization of Optimal Control Theory: Linear and Nonlinear Structures," by J.N. Yang, Z. Li and S. Vongchavalitkul, 11/2/92.

NCEER-92-0027 "Seismic Resistance of Reinforced Concrete Frame Structures Designed Only for Gravity Loads: Part I - Design and Properties of a One-Third Scale Model Structure," by J.M. Bracci, A.M. Reinhorn and J.B. Mander, 12/1/92, to be published.

NCEER-92-0028 "Seismic Resistance of Reinforced Concrete Frame Structures Designed Only for Gravity Loads: Part II - Experimental Performance of Subassemblages," by L.E. Aycardi, J.B. Mander and A.M. Reinhorn, 12/1/92.

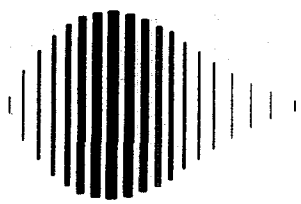

National Center for Earthquake Engineering Research
State University of New York at Buffalo